Defects of micropolar continua in Riemann-Cartan manifolds and its applications

Yongjo Lee

A thesis submitted in conformity with the requirements

for the degree of Doctor of Philosophy

Department of Mathematics

University College London

April 2021

Declaration

I, Yongjo Lee confirm, that the work presented in this thesis is my own. Where information has been derived from other sources, I confirm that this has been indicated in the thesis.

Abstract

We derive equations of motion and its solutions in the form of solitons from deformational energy functionals of a coupled system of microscopic and macroscopic deformations. Then criteria in constructing the chiral energy functional is specified to be included to obtain soliton-like solutions.

We show various deformational measures, used in deriving the soliton solutions, can be written when both curvature and torsion are allowed, especially by means of microrotations and its derivatives. Classical compatibility conditions are re-interpreted leading to a universal process to derive a distinct set of compatibility conditions signifying a geometrical role of the Einstein tensor in Riemann-Cartan manifolds.

Then we consider position-dependent axial configurations of the microrotations to construct intrinsically conserved currents. We show that associated charges can be written as integers under a finite energy requirement in connection with homotopic considerations. This further leads to a notion of topologically stable defects determined by invariant winding numbers for a given solution classification.

Nematic liquid crystals are identified as a projective plane from a sphere hinted by the discrete symmetry in its directors. Order parameters are carefully defined to be used both in homotopic considerations and free energy expansion in the language of microcontinua. Micropolar continua are shown to be the general case of nematic liquid crystals in projective geometry, and in formulations of the order parameter, which is also the generalisation of the Higgs isovectors.

Lastly we show that defect measures of pion fields description of the Skyrmions are related to the defect measures of the micropolar continua via correspondences between its underlying symmetries and compatibility conditions of vanishing curvature.

Impact Statement

Descriptions of deformational propagations in coupled systems of microscopic and macroscopic continua are shown to be the form of solitons. This further can be extended to a quantised soliton system which can be seen in the Euclidean Yang-Mills theory under the non-relativistic limit.

A notion of zero curvature in the Einstein-Cartan theory is explicitly related to elasticity in the context of compatibility conditions. And homotopy groups are used to classify these compatibility conditions. This can be related to the theories in understanding the microscopic gravitation when one considers the elasticity in the curved space.

A construction of position-dependent axial microrotational fields as field configurations for conserved currents is discussed. Associated total charges of the conserved currents are shown to be topologically and geometrically invariant integers. In constructing field configurations, chiral structures on the given manifold is highly dependent on integers that embedded in axial fields. Hence, it can be useful to consider the origin of the chirality especially using projective geometry, for example in magnetic monopoles as seen as projected defects from higher dimensions.

Nematic liquid crystals are confirmed to be a special case of micropolar continua in terms of order parameters and its projective geometrical properties. Further, micropolar continua are identified as projective space of the Skyrmions of the spin-isospin system, sharing an identical form of the compatibility condition for vanishing curvature. A number of phases of superfluid liquid helium of ^{3}He are known to exhibit similar symmetries of the spin-orbit system accompanied by the well-established order parameter formalism, which is much similar to that of nematic liquid crystals. Hence it is applicable to extend our generalisation of micropolar continua in those phases of ^{3}He.

Acknowledgement

I would like to thank my supervisor Dr. Christian Böhmer for his kindness, patience, and invitation into this wonderland of microcontinua. I would like to thank Dr. Franco Fiorini and Dr. Santiago Hernández for their warm hospitality during my visit to Centro Atómico Bariloche, Departamento de Ingeniería en Telecomunicaciones and Instituto Balseiro, Argentina. Especially Dr. Franco Fiorini for stimulating discussions about "locally" invariant microrotations. I received enormous support from members of Department of Mathematics UCL during my Ph.D, and without them, this work would be impossible to finish.

Notations

$\boldsymbol{a}$	: 3-vector and 3-component quantity
$\boldsymbol{n}_{\mathrm{v}}$	: normalised 2-component vortex field
$\boldsymbol{n}_3$	: normalised 3-component field
$\boldsymbol{n}_{\mathrm{N}}$	: normalised nematic liquid crystal field
$\boldsymbol{n}_{\mathrm{h}}$	: normalised 3-component hedgehog field
$\boldsymbol{n}_4$	: normalised 4-component field
$\boldsymbol{A}$	: 3×3 matrix of $M_3(\mathbb{R})$
$\mathbb{1}$	: 3×3 identity matrix
a	: arbitrary n-component tensor
A	: general $n \times n$ matrix of $M_n(\mathbb{R}, \mathbb{C})$
I	: general $n \times n$ identity matrix
$\bar{z}$	: complex conjugate of $z \in \mathbb{C}$
A^*	: complex conjugate of $A \in M_n(\mathbb{C})$
$A^\dagger$	: transpose of complex conjugate of $A \in M_n(\mathbb{C})$
A^T	: transpose of $A \in M_n(\mathbb{R}, \mathbb{C})$
u_i	: displacement vector $\boldsymbol{u}$
u_{ij}	: distortion tensor, $\operatorname{grad} \boldsymbol{u} = \partial_j u_i$
ϵ_{ijk}	: Levi-Civita symbol, $\epsilon_{123} = 1 = -\epsilon_{213}$
Γ	: Nye's tensor
$F = \nabla\psi = \mathbb{1} + \nabla\boldsymbol{u}$	: deformation gradient tensor
$F = RU = \operatorname{polar}(F)U$	: classical polar decomposition
$\overline{\overline{U}} = \overline{R}^T F$	: first Cosserat deformation tensor
$\overline{R}^T \operatorname{Grad} \overline{R}$	: second Cosserat deformation tensor
$(\operatorname{Div} A)_i = \partial_j A_{ij}$	: divergence on the tensor A
$(\operatorname{Curl} A)_{ij} = \epsilon_{jkl}\partial_k A_{il}$	: curl on the tensor A
$(\operatorname{Grad} A)_{ijk} = \partial_k A_{ij}$	: gradient on the tensor A
$(\operatorname{Div}(\operatorname{grad} \boldsymbol{A}))_i = \partial_j\partial_j A_i$	: divergence on the tensor $(\operatorname{grad} \boldsymbol{A})_{ij} = \partial_j A_i$
$(\operatorname{div} \boldsymbol{A}) = \partial_i A_i$	: divergence on the vector $\boldsymbol{A}$
$(\operatorname{grad} \boldsymbol{A})_{ij} = \partial_j A_i$	: gradient on the vector $\boldsymbol{A}$
$(\operatorname{curl} \boldsymbol{A})_i = \epsilon_{ijk}\partial_j A_k$	: curl on the vector $\boldsymbol{A}$
$\operatorname{sym} M = (M + M^T)/2$	: symmetric part of matrix M
$\operatorname{skew\ sym} M = (M - M^T)/2$	: skew-symmetric part of M
$\operatorname{dev} M = M - \operatorname{tr}(M)\mathbb{1}/3$	: deviatoric or trace-free part of M
$A : B = \langle A, B\rangle = \operatorname{tr}(AB^T) = \operatorname{tr}(A^T B)$	: Frobenius product of matrices A and B
$\|X\|^2 = \langle X, X\rangle = \operatorname{tr}(XX^T)$	: Frobenius norm of X

Contents

Part I

Defects in microstructures

Chapter 1

Microcontinuum

It all started from a question. What does microscopic deformation look like when a large body undergoes elastic deformation? Then a following question arises. Can it be the same description that we know from the classical elasticity or something completely different? The same questions may have occurred to the brothers, François Cosserat (1852–1914) and Eugéne Cosserat (1866–1931), when they started to explore the theory of microscopic deformable body. In Part I, we would like to present solutions for deformational propagations in deformable media, based on the variational principle in attempting to understand deformations in coupled systems of microscopic and macroscopic continua. Part I is mainly based on our published works [1, 2].

1.1 Introduction

Classical elasticity is based on considering materials whose idealised material points are structureless. Any possible internal properties are neglected in the classical theory.

A microcontinuum, on the other hand, is a continuous collection of deformable material points. The characteristic aspect of the theory with a microstructure is that we assume a microelement to exhibit an inner structure attached to vectors called **directors**, which span internal three-dimensional space. Directors can rotate, compress and shear, independently of macroscopic deformations, to describe interior deformations of the microstructure.

The first ideas along those lines go back to the Cosserat brothers who pioneered such theories [3] back in 1909, fully in its geometrically nonlinear setting. In some ways, their work was ahead of their time and its significance had been overlooked for many decades. Starting from the 1950s, interests in this theory increased and many advances were made since then [4–7, 7–13].

The most general elasticity theories with microstructure contain nine additional degrees of freedom which consist of three microrotations, one microvolume expansion, and five microshear deformations. A comprehensive account of microcontinuum theories can be found in [9, 14, 15]. A material structure of this generalised theory is called micromorphic and if we disregard the microshear deformations from the micromorphic, the theory is called microstretch in which the directors can change its microvolume element and orientations under the microrotations. Some example of micromorphic continua include turbulent fluids, blood cell and some models of liquid crystals. Recent developments of nonlinear problems in generalised continua can be found in [16–20].

If we restrict these microdeformations to be rigid, so we further disregard the microshear, one deals with three degrees of freedom of the microrotations, in addition to the classical translational deformation field. The resulting model is often referred to as Cosserat elasticity or micropolar theory. A few example of materials exhibiting the micropolar structure are ferromagnetic fluids, and fluids of rigid microelements. Animal bone structures are particularly

good example of micropolar media, with pores in the bone are filled with micropolar materials which can undergo rigid microrotations.

We would like to consider the nature of microdeformation in micropolar models in which the rotation play a central role of the microscopic defects. If these deformations are time dependent, we wish to consider dynamic evolution of the microdeformations which may or may not be coupled to the macroscopic deformational measures. To do so, we would like to start from total energy functions regarding microscopic and macroscopic deformations with a set of appropriate classical and micropolar parameters. All other microscopic version of continuity equations, constitutive equations and balance laws can be found in the literatures introduced above, especially in [3].

Once one can identify and collect the relevant energy functionals for the micropolar elasticity, equations of motion for the system can be found by the variational principle. Due to the highly nonlinear nature of the system, various attempts were made to simplify the process under relatively weak restrictions and a simple ansatz. Spinor methods were used in [21] to simplify the Euler-Lagrange equation and subsequent works appeared in [22, 23], with an intrinsically two-dimensional model studied in [24]. In [25], polarity of ferromagnets gave rise to descriptions of the defects in order parameters as solitary waves under external magnetic stimuli, followed by the study in the elastic crystals as a micropolar continuum in [26], again with descriptions of soliton solutions for topological defects.

Variants of the geometrically nonlinear Cosserat model are also used to describe lattice rotations in metal plasticity in [27]. Further recent developments in the theory including nonlinear problems in generalised continua were studied rigorously for instance in [16–20, 28–31].

1.2 Deformational measures in classical and microcontinuum mechanics

In a usual rectangular Cartesian coordinate system with the origin O, suppose we have a fixed region of space R_0 occupied by continuously distributed matter. After a subsequent time t, an original body B_0 is moved or deformed to a new body B in the region R. One of critical assumptions in continuum mechanics is that we are able to identify individual particle element of the body so that we can track a point P in a body B_0 at time $t = 0$ to a point p in B at an arbitrary time t.

Then the motion of B can be written as a function of the new position vector $\boldsymbol{x}$ dependent on the original position $\boldsymbol{X}$ and time t.

$$\boldsymbol{x} = \boldsymbol{x}(\boldsymbol{X}, t) \tag{1.2.1}$$

for all $\boldsymbol{X} \in R_0$ and $\boldsymbol{x} \in R$. In practice, we can solve this for $\boldsymbol{X}$ to obtain

$$\boldsymbol{X} = \boldsymbol{X}(\boldsymbol{x}, t). \tag{1.2.2}$$

The configuration of B_0 occupied by the position of particles at $t = 0$ is called the reference (or material) configuration and we denote any quantity in the reference configuration by a capital letter. The configuration of B with position of particles at $\boldsymbol{x}$ is called the spatial configuration and we denote quantities in this reference by a lower case. And we call the expression (1.2.2) as a spatial description in which we regard the spatial coordinate $\boldsymbol{x}$ as independent variables and the expression (1.2.1) as the material description treating $\boldsymbol{X}$ as independent variables.

A displacement vector $\boldsymbol{u}$ describes macroscopic translations of a point particle at P with a vector $\boldsymbol{X}$ to the point p with $\boldsymbol{x}$ and this can be written in the spatial description as

$$\boldsymbol{u}(\boldsymbol{x}, t) = \boldsymbol{x} - \boldsymbol{X}(\boldsymbol{x}, t). \tag{1.2.3}$$

In this way, we can write quantities such as velocity $\boldsymbol{v}$, acceleration $\boldsymbol{a}$, etc. in terms of either material or spatial description, defined by

$$\boldsymbol{v}(\boldsymbol{X},t)=\frac{\partial \boldsymbol{u}(\boldsymbol{X},t)}{\partial t}\ , \qquad \boldsymbol{a}=\frac{\partial \boldsymbol{v}(\boldsymbol{X},t)}{\partial t}. \tag{1.2.4}$$

One of most important tensors describing deformations is a deformation gradient tensor F defined by

$$F_{kK}=\frac{\partial x_k}{\partial X_K}\ , \tag{1.2.5}$$

which can be defined in a same way for the classical and microcontinuum theory. In the classical continuum theory, this tensor can be decomposed using the polar decomposition as

$$F=RU=VR \tag{1.2.6}$$

with a right stretch U and a left stretch tensor V satisfy, respectively,

$$U^2=F^TF \qquad \text{and} \qquad V^2=FF^T\ . \tag{1.2.7}$$

We assume that $\det F\neq 0$ and it is obvious that F^T is also second-order tensor and so is F^{-1}, where

$$F^{-1}_{Kk}=\frac{\partial X_K}{\partial x_k}\ . \tag{1.2.8}$$

A displacement gradient tensor is defined by $F_{iR}-\delta_{iR}$, which is

$$F_{iR}-\delta_{iR}=\frac{\partial x_i}{\partial X_R}-\delta_{iR}=\frac{\partial u_i}{\partial X_R}\ . \tag{1.2.9}$$

A strain tensor is defined by the symmetric part of the displacement gradient tensor

$$u_{ij}=\frac{1}{2}\left(\frac{\partial u_i}{\partial x_j}+\frac{\partial u_j}{\partial x_i}\right), \qquad u_{ij}=u_{ji}\ , \tag{1.2.10}$$

where we made an approximation $x_i\approx X_R$ for small deformations.

Next, we consider forces acting in an interior of continuous body. Suppose that a part of a body B occupies a region R which has a surface S. Let P be a point on the surface S, $\boldsymbol{n}$ a unit vector directed along the outward normal to S at P and δS an area of an element of S which contains P. We assume that S and R possess any necessary smoothness and continuity properties (e.g. it is assumed that the normal to S is uniquely defined at P).

It is also assumed that on the surface element with area δS, the material outside R exerts force on the material inside R.

$$\delta \boldsymbol{f}=\boldsymbol{t}^{(n)}\delta S. \tag{1.2.11}$$

Force $\delta \boldsymbol{f}$ is called surface force, and $\boldsymbol{t}^{(n)}$ mean surface traction transmitted across the element of area δS from the outside to the inside of R.

We can approximate that the surface traction $\boldsymbol{t}^{(n)}$ becomes a quantity that is independent of the shape of the infinitesimal area as $\delta S\to 0$ to write

$$\boldsymbol{t}^{(n)}=\lim_{\delta S\to 0}\frac{\delta \boldsymbol{f}}{\delta S}\ . \tag{1.2.12}$$

In a system of rectangular Cartesian coordinates, we can write $\boldsymbol{t}^{(n)}$ with respect to the usual orthonormal base vectors $\boldsymbol{e}_i$ by

$$\boldsymbol{t}_i=t_{ij}\boldsymbol{e}_j\ , \tag{1.2.13}$$

for $i, j = 1, 2, 3$. Using $\boldsymbol{e}_i \cdot \boldsymbol{e}_j = \delta_{ij}$, this becomes

$$t_{ij} = \boldsymbol{t}_i \cdot \boldsymbol{e}_j \ . \tag{1.2.14}$$

Projection of the traction $\boldsymbol{t}_i$ in the direction of $\boldsymbol{e}_j$ will define a tensor t_{ij} called the stress tensor. For example, t_{11} is the component of $\boldsymbol{t}_1$ in the direction of $\boldsymbol{e}_1$. And t_{11} is positive if the material on the x-positive side of the surface on which $\boldsymbol{t}_1$ acts is pulling the material on the x-negative side. In particular, diagonal components $\{t_{11}, t_{22}, t_{33}\}$ are called direct stress components and remaining components are called shearing stress components.

As an immediate application of the definition of the stress tensor, suppose the body in the region R is in equilibrium so that resultant force and resultant couple about O on the continuum in the region is zero. These give a set of statements that

$$\begin{aligned} \int_S \boldsymbol{t}^{(n)} \, dS + \int_R \rho \boldsymbol{g} \, dV = 0 \ , \\ \int_S \boldsymbol{x} \times \boldsymbol{t}^{(n)} \, dS + \int_R \rho \boldsymbol{x} \times \boldsymbol{g} \, dV = 0 \end{aligned} \tag{1.2.15}$$

where $\rho \boldsymbol{g}$ is the body force (e.g. gravitational, electromagnetic forces) per unit volume.

Using divergence theorem, (1.2.15) can be written in components

$$\int_R \left(\frac{\partial t_{ij}}{\partial x_i} + \rho g_j \right) dV = 0 \ , \tag{1.2.16a}$$

$$\int_R \epsilon_{jpq} \left(\frac{\partial}{\partial x_r} (x_p t_{rq}) + \rho x_p g_q \right) dV = 0 \ . \tag{1.2.16b}$$

The equation (1.2.16a) will give the equation of equilibrium,

$$\frac{\partial t_{ij}}{\partial x_i} + \rho g_j = 0 \tag{1.2.17}$$

and (1.2.16b) will be reduced to $\epsilon_{jpq} t_{pq} = 0$, which characterises the symmetric property of the stress tensor,

$$t_{pq} = t_{qp} \ . \tag{1.2.18}$$

A microcontinuum, on the other hand, is a continuous collections of deformable and stable (i.e. indestructible) material points [15]. We call these stable and deformable structures as particles and a typical example of a particle in the microcontinuum is illustrated in Fig.1.1 (right). A cesium chloride (CsCl) is often used to illustrate the inner structure of the microcontinuum [15] with Cs^+ ion located at the centre of the cube and Cl^- ions at eight corners of the cube. This model can be constructed from alternating layers of equally spaced cesium layers and chloride layers in bulk. The cubane of chemical formula C_8H_8 with its genuine individual cubic molecular structure provides good model of micropolar medium with eight hydrogen molecules are attached in the conners of the cubic. In cesium chloride model, we can assign a position of Cs^+ a vector $\boldsymbol{X}$ at P in the material configuration but at this time, we need an additional set of vectors for Cl^- to describe the inner structure of the cubic crystalline solid and its deformations.

In other words, the particles are assumed as point particles with infinitesimal size in the classical theory. But since they are deformable by definition in the microcontinuum theory, it is clear that we need an extra set of degrees of freedom to describe the theory of these particle's deformability, in addition to the vectors assigned to P in the classical theory as being treated as a point particle. This means, in addition to the classical translational deformation field, the body as a collection of point particle P can be deformable in a classical (macroscopic scale) way and the inner structure of the particle can only experience microdeformations.

The inner microdeformation and macroscopic displacement are illustrated in Fig.1.1. For the inner structure, we assign a new set of vectors, the directors, $\boldsymbol{\Xi}$ in the reference configuration and $\boldsymbol{\xi}$ in the spatial configuration, so that after time t,

$$\boldsymbol{X} \xrightarrow{t} \boldsymbol{x} \qquad \text{and} \qquad \boldsymbol{\Xi} \xrightarrow{\boldsymbol{X},t} \boldsymbol{\xi} \,. \tag{1.2.19}$$

A micromorphic continuum is the most general deformable inner structure with its macroscopic motions are described by $\boldsymbol{X} \to \boldsymbol{x}$ of (1.2.1), while the microelement undergoes transformations described by its directors $\boldsymbol{\Xi} \to \boldsymbol{\xi}$. And the transformations are uniquely invertible, so there exist χ_{kK} and $\mathfrak{X}_{Kk}$ such that

$$\begin{array}{lcl} x_k = x_k(X_K, t) & \overset{\text{inverse}}{\longrightarrow} & X_K = X_K(x_k, t) \\ \boldsymbol{\xi}_k = \chi_{kK}(X_K, t)\boldsymbol{\Xi}_K & \overset{\text{inverse}}{\longrightarrow} & \boldsymbol{\Xi}_K = \mathfrak{X}_{Kk}(x_k, t)\boldsymbol{\xi}_k \end{array} \tag{1.2.20}$$

where rank-two tensors $\chi_{kK} \in GL(3;\mathbb{R})$ and its inverse $\mathfrak{X}$ are called microdeformation tensors.

In addition, the condition of indestructible microdeformation implies that the microelement and its infinitesimal volume element cannot shrink or explode. This condition is ensured by imposing the *Implicit Functions Theorem*, which states the existence of inverse relation of (1.2.20) by non-negative volume measures of J and j, defined by determinants,

$$J \equiv \det\left(\frac{\partial x_k}{\partial X_K}\right) \qquad \text{and} \qquad j \equiv \det\left(\frac{\partial \boldsymbol{\xi}_k}{\partial \boldsymbol{\Xi}_K}\right) = \det \chi_{kK} = \frac{1}{\det \mathfrak{X}_{Kk}} \,. \tag{1.2.21}$$

Now, the deformation gradient tensor satisfy

$$\frac{\partial x_k}{\partial X_K}\frac{\partial X_K}{\partial x_l} = \delta_{kl} \qquad \text{and} \qquad \frac{\partial x_k}{\partial X_K}\frac{\partial X_L}{\partial x_k} = \delta_{KL} \,, \tag{1.2.22}$$

and similarly, for the microdeformation tensor we have

$$\frac{\partial \boldsymbol{\xi}_k}{\partial \boldsymbol{\Xi}_K}\frac{\partial \boldsymbol{\Xi}_K}{\partial \boldsymbol{\xi}_l} = \delta_{kl} \qquad \text{and} \qquad \frac{\partial \boldsymbol{\xi}_k}{\partial \boldsymbol{\Xi}_K}\frac{\partial \boldsymbol{\Xi}_L}{\partial \boldsymbol{\xi}_k} = \delta_{KL} \tag{1.2.23}$$

which is

$$\chi_{kK}\mathfrak{X}_{Kl} = \delta_{kl} \qquad \text{and} \qquad \chi_{kK}\mathfrak{X}_{Lk} = \delta_{KL} \,. \tag{1.2.24}$$

When we need to distinguish macrodeformations from microdeformations, we will put a bar over the micro-deformational measures. For example, if we define

$$\overline{F}_{kK} = \frac{\partial \boldsymbol{\xi}_k}{\partial \boldsymbol{\Xi}_K} = \chi_{kK} \,, \tag{1.2.25}$$

we may apply the polar decomposition to write (1.2.25 in terms of some microrotation $\overline{R}$ and microstretches $\overline{U}$ and $\overline{V}$

$$\overline{F} = \overline{R}\,\overline{U} = \overline{V}\,\overline{R} \,. \tag{1.2.26}$$

Then

$$\overline{U}^2 = \boldsymbol{\chi}^T\boldsymbol{\chi}, \qquad\qquad \overline{V}^2 = \boldsymbol{\chi}\boldsymbol{\chi}^T \,. \tag{1.2.27}$$

A special case arises when $\overline{U}^2 = \overline{V}^2 = \mathbb{1}$ which yields $\boldsymbol{\chi}^{-1} = \boldsymbol{\chi}^T$. This means

$$\boldsymbol{\chi}^T = \boldsymbol{\mathfrak{X}} \qquad \text{and} \qquad \boldsymbol{\chi}\boldsymbol{\mathfrak{X}} = \mathbb{1} \,. \tag{1.2.28}$$

From (1.2.21) we have $j = 1$ and we can see this is the precise condition for the rigid microdeformation and the deformation is described by the microrotation only. And $\overline{R} \in SO(3)$, provided

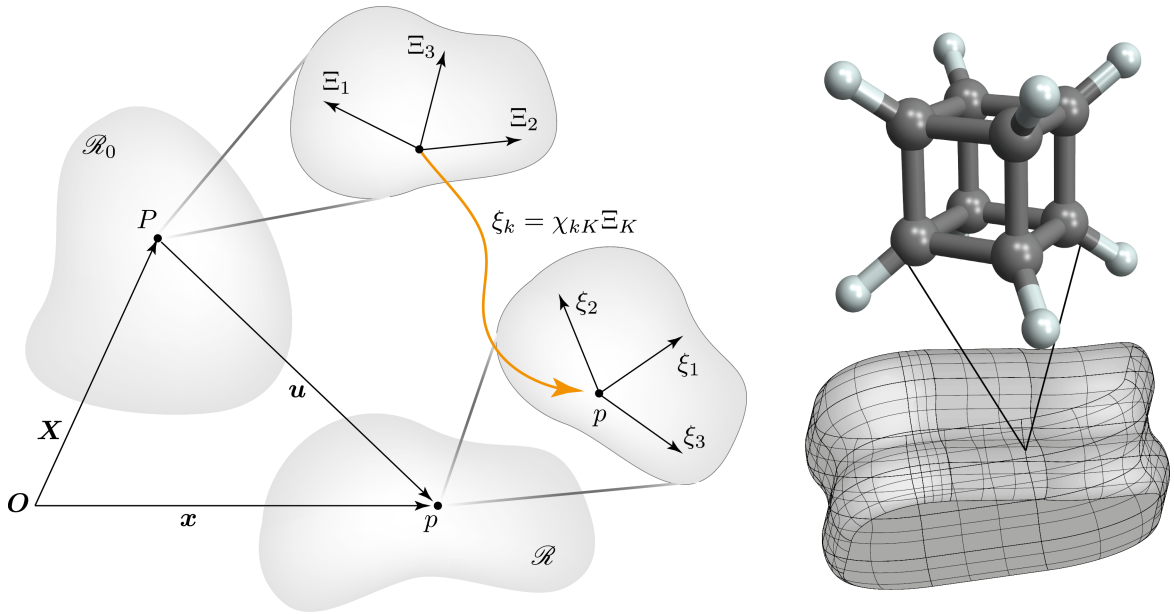

Figure 1.1: On the left, the transformation of the inner structure of the microelement with centroids positioned at P and p in the reference configuration and the spatial configuration, respectively, is illustrated. This shows how the directors $\boldsymbol{\Xi}$ in the original body B_0 undergoes microdeformation under χ_{kK} transform to $\boldsymbol{\xi}$, while the original body B_0 experiences displacement to become a deformed configuration body B in three-dimensional space under the macroscopic displacement $\boldsymbol{u}$. The typical *particle* modelled by cubane as a micropolar continuum is shown in its microscopic cubic molecular structure in the bulk body on the right.

we can rescale the magnitude of the directors $\{\boldsymbol{\Xi}, \boldsymbol{\xi}\}$ to unity to retain the rigidity of the inner structure.

A microstretch continuum is characterised by the property

$$\mathfrak{X}_{Kk} = \frac{1}{j^2}\chi_{kK} \ . \tag{1.2.29}$$

As illustrated in Fig.1.1, the microrotations $\overline{R}$ are responsible for the inner rotations of the directors such that

$$\boldsymbol{\xi}_k = \overline{R}_{kK}\boldsymbol{\Xi}_K \qquad \text{and} \qquad \boldsymbol{\Xi}_K = \overline{R}_{Kk}\boldsymbol{\xi}_k \ . \tag{1.2.30}$$

The finite microrotation of an angle ϕ about a normalised axis $\boldsymbol{n}$ is represented by $\overline{R}_{kl}$,

$$\overline{R}_{kl} = \cos\phi\ \delta_{kl} - \sin\phi\ \epsilon_{klm}n_m + (1-\cos\phi)n_k n_l \tag{1.2.31}$$

where

$$\phi = (\phi_k\phi_k)^{1/2}, \qquad n_k = \frac{\phi_k}{\phi}, \qquad \overline{R}_{kl} = \overline{R}_{kL}\delta_{Ll} \tag{1.2.32}$$

For small rotations, the expression (1.2.31) becomes

$$\overline{R}_{kl} \approx \delta_{kl} - \epsilon_{klm}\phi_m \ . \tag{1.2.33}$$

i.e. the rotation tensor can be represented by a vector ϕ_k, and this limit becomes apparent when one represents the rotation by an exponential of an antisymmetric matrix as in (8.4.13). In classical continuum mechanics, the macrorotation tensor due to a change of line elements is

$$R_{kK} = \frac{\partial x_k}{\partial X_L}C_{LK}^{-1/2} \ . \tag{1.2.34}$$

This follows from the polar decomposition (1.2.6), where C_{LK} is the classical deformation tensor known as the right Cauchy-Green tensor, defined by

$$C_{LK} = \frac{\partial x_k}{\partial X_L}\frac{\partial x_k}{\partial X_K}, \qquad C = F^T F. \tag{1.2.35}$$

In the linear theory, the macrorotation (1.2.34) reduces to an infinitesimal rotation tensor in classical continuum mechanics,

$$\tilde{R}_{km} \equiv R_{km} - \delta_{km} = \frac{1}{2}\left(\frac{\partial u_k}{\partial x_m} - \frac{\partial u_m}{\partial x_k}\right) , \tag{1.2.36}$$

where u_k is the displacement vector. For small angle consideration, from (1.2.33) and (1.2.36), we can identify the difference between macrorotation R and microrotation $\overline{R}$.

We introduce some useful deformational measures as follows.

$$\begin{aligned}
\mathfrak{C}_{KL} &\equiv \frac{\partial x_k}{\partial X_K}\frac{\partial \Xi_L}{\partial \xi_k} = \frac{\partial x_k}{\partial X_K}\mathfrak{X}_{Lk} = \frac{\partial x_k}{\partial X_K}\chi_{kL} \\
\mathcal{C}_{KL} &\equiv \frac{\partial \xi_k}{\partial \Xi_K}\frac{\partial \xi_k}{\partial \Xi_L} = \chi_{kK}\chi_{kL} = \mathcal{C}_{LK} \\
\Gamma_{KLM} &\equiv \frac{\partial \Xi_K}{\partial \xi_k}\frac{\partial \chi_{kL}}{\partial X_M} = \mathfrak{X}_{Kk}\frac{\partial \chi_{kL}}{\partial X_M}
\end{aligned} \tag{1.2.37}$$

where $\mathfrak{C}_{KL}$ is called the deformation tensor, $\mathcal{C}_{KL}$ the microdeformation tensor, and Γ_{KLM} the wryness tensor. In case of micropolar continua, the deformation tensor $\mathfrak{C}_{KL}$ is known as the first Cosserat deformation tensor and the wryness tensor reduces to

$$\Gamma_{KL} = \frac{1}{2}\epsilon_{KMN}\frac{\partial \chi_{kM}}{\partial X_L}\chi_{kN} , \tag{1.2.38}$$

from which we recognise $\chi_{kN} \in SO(3)$.

1.3 Deformational energy

We would like to look at formulation of an energy function $V_{\text{elastic}}(F, \overline{R})$ in a coupled form of the displacement gradient tensor F and the microrotation $\overline{R}$, and an energy function $V_{\text{curvature}}(\overline{R})$ due to the microrotation entirely and its implications briefly. More comprehensive treatments in deriving general energy functionals can be found in [21, 23].

In constructing energy functions, we must note that the energy function must be a function of the strain tensor (classical or microcontinuum), as emphasised in [32]. In addition, we would like to have each term in the energy functionals remains invariant under the rotation, if the rigidity in the microelement is imposed. These conditions in formulating the energy functionals suggest that we need a set of independent scalars of second-order tensors to form the energy functional. For this purpose, we introduce the Cartan-Lie decomposition for any 3×3 matrix M,

$$M = \text{dev sym } M + \text{skew } M + \frac{1}{3}\text{tr}M \cdot \mathbb{1} , \tag{1.3.1}$$

where dev sym M is the traceless symmetric part of M and skew M is the skew-symmetric part of M.

The most general form of the energy function, in the classical theory, $V_{\text{classical}}$ satisfying above mentioned conditions is

$$V_{\text{classical}} = \mu\|u_{ij}\|^2 + \frac{\lambda}{2}\|u_{ii}\|^2 , \tag{1.3.2}$$

where μ and λ are called Lamé coefficients. The first term on the right-hand side represents the energy associated to the pure shear and the second term represents the energy associated to the volumetric expansion (or compression). These can be seen if one calculate and compare a undeformed volume element dV and a deformed volume element dV'.

The energy function (1.3.2) indeed leads to the classical Hooke's law and the force f is defined by

$$f_i = \frac{\partial t_{ij}}{\partial x_j} \, . \tag{1.3.3}$$

By Newton's third law, interaction between two forces f_i and f_j $(i \neq j)$ is cancelled internally. Hence the total force per unit volume $\boldsymbol{f}$ is a sum of the individual f_i for a given internal surface element of the body, so that we can write

$$\sum_i \int_R f_i \, dV = \int_R \boldsymbol{f} \, dV \, . \tag{1.3.4}$$

The resultant integral on the right-hand side of (1.3.4) represents the sum of all forces acting on all surface element for a given body volume. In other words, the sum of integral over a given volume element is transformed into the integral over the surface elements, and all the internal stresses can be transformed into integral over the surface. This agrees with the definition of force given in (1.3.3) and (1.2.11) in terms of the stress tensor, hence we can write

$$\int_R f_i \, dV = \int_R \partial_j t_{ij} \, dV = \int_S t_{ij} \, dS_j \, . \tag{1.3.5}$$

We can generalise this idea in formulating the elastic energy functionals for the microcontinuum theory. Using the decomposition (1.3.1), we can write

$$V_{\text{elastic}}(F, \overline{R}) = \mu \left\| \text{sym}(\overline{R}^T F - \mathbb{1}) \right\|^2 + \frac{\lambda}{2} \left[\text{tr} \left(\text{sym}(\overline{R}^T F - \mathbb{1}) \right) \right]^2 \tag{1.3.6}$$

where the term $\overline{R}^T F$ is the first Cosserat deformation tensor in the coupled system of microrotation $\overline{R}$ and the classical displacement gradient tensor F. Analogous to (1.3.2), the first term on the right-hand side of (1.3.6) represents energy for the pure shear and the quantity $\overline{R}^T F - \mathbb{1}$ is symmetrised in accordance with the symmetric classical strain tensor u_{ij}, which can be seen directly from (1.2.9) under the limit $\overline{R} \to \mathbb{1}$. The second term of (1.3.6) represents energy associated to the volumetric expansion. Hence, we can see that the elastic energy functional (1.3.6) is a natural generalisation of the classical expression (1.3.2).

Chapter 2

Dynamical Cosserat media

In Section 2.1, we present the full treatment for solutions of elastic and rotational propagations of deformations in the complete dynamical Cosserat problem. This involves a total energy functional given by

$$V = V_{\text{elastic}}(F, \overline{R}) + V_{\text{curvature}}(\overline{R}) + V_{\text{interaction}}(F, \overline{R}) + V_{\text{coupling}}(F, \overline{R}) \ .$$

We will obtain equations of motion, from variations of

$$\frac{\delta V_{\text{total}}}{\delta F} \qquad \text{and} \qquad \frac{\delta V_{\text{total}}}{\delta \overline{R}} \tag{2.0.1}$$

where V_{total} is energy function including kinetic terms.

Primary mathematical interests in finding the equations of motion using the variational calculus come from the fact that many terms in the energy functionals contain quantities such as

$$\overline{R}^T \text{Curl}\, \overline{R} \ , \qquad \overline{R}^T \text{polar}(F) \ , \qquad \overline{R}^T F$$

throughout the calculations. Since, in general, the elements in $SO(3)$ do not commute, the variations require careful treatment in the calculations. There are two approaches we can take in varying those quantities. One way is to put a Lagrangian multiplier λ in a Lagrangian $\mathcal{L}$ in a form of $\lambda(R^T R - \mathbb{1})$ to obtain the Euler-Lagrangian equation, and another is to use the exponential representation of the rotational matrix $R = e^A$ under certain condition such as the small rotational angle assumption.

In Section 2.2, after stating each energy functional in terms of F and $\overline{R}$, we use the variation of the total energy functional including kinetic energy terms. We collect terms from variational field expressions with respect to F and $\overline{R}$, to obtain a complete coupled system of equations of motion. It turns out that if we impose certain set of restrictions (e.g. small displacements), newly generated nonlinear coupling terms in the complete description are indeed responsible for the contribution in additional terms of the sine-Gordon type equation.

This observation reduces the problem to solving the double sine-Gordon equation [33] of a function of $\phi = \phi(z, t)$. In the final part, we illustrate effects of rotational and displacement propagations in a simple model of microcontinua with additional features of a kink-antikink form of solutions, and profiles of a wave number k and a wave velocity v.

2.1 Energy functions

If we assign a set of time-dependent functions to a microrotational measure $\overline{R}$ and a macroscopic displacement gradient F, the field equations will be descriptions of propagating defects in a certain direction.

We introduce each energy functional for the full treatment of the geometrically nonlinear Cosserat problem in three-dimensional space. We will include kinetic energy terms to appropriate energy functionals before deriving the equations of motion. First, the energy functional for elastic deformations is

$$V_{\text{elastic}}(F,\overline{R}) = \mu \left\|\text{sym}(\overline{R}^T F - \mathbb{1})\right\|^2 + \frac{\lambda}{2}\left[\text{tr}\left(\text{sym}(\overline{R}^T F - \mathbb{1})\right)\right]^2 \tag{2.1.1}$$

where λ and μ are the standard Lamé parameters. The microrotations are governed by $V_{\text{curvature}}(\overline{R})$,

$$\begin{aligned} V_{\text{curvature}}(\overline{R}) = \kappa_1 \left\|\text{dev sym}(\overline{R}^T \text{Curl}\, \overline{R})\right\|^2 + \kappa_2 \left\|\text{skew}(\overline{R}^T \text{Curl}\, \overline{R})\right\|^2 \\ + \kappa_3 \Big[\text{tr}(\overline{R}^T \text{Curl}\, \overline{R})\Big]^2 \end{aligned} \tag{2.1.2}$$

where κ_i are the elastic constants for the microrotations. The operation of Curl on any 3×3 matrix M is defined by

$$\text{Curl}\, M = \begin{pmatrix} \partial_y M_{13} - \partial_z M_{12} & \partial_z M_{11} - \partial_x M_{13} & \partial_x M_{12} - \partial_y M_{11} \\ \partial_y M_{23} - \partial_z M_{22} & \partial_z M_{21} - \partial_x M_{23} & \partial_x M_{22} - \partial_y M_{21} \\ \partial_y M_{33} - \partial_z M_{32} & \partial_z M_{31} - \partial_x M_{33} & \partial_x M_{32} - \partial_y M_{31} \end{pmatrix} \tag{2.1.3}$$

or in components, this is

$$(\text{Curl}\, M)_{ij} = \epsilon_{jkl}\partial_k M_{il}\ . \tag{2.1.4}$$

Formulation of this energy functional follows immediately from the decomposition of (1.3.1) with the required conditions mentioned before. The quantity

$$\overline{R}^T \text{Curl}\, \overline{R} \tag{2.1.5}$$

is called a dislocation density tensor and it originates back in Nye's pioneering work [34]. A fairly straightforward explanation of this quantity can be found in [35], in developing a total displacement known as Burgers vector, caused by continuous distribution of dislocations (hence the name). We will find that this rank-two tensor (2.1.5) will be one of our central ingredients in understanding both in microscopic and macroscopic deformations especially when we regard the notion of torsion, accompanied by more formal definition and its use in Part II.

Interaction between elastic displacements and microrotations is described by irreducible parts of the elastic deformations and microrotations, such as $\overline{R}^T F - \mathbb{1}$ and $\overline{R}^T \text{Curl}\, \overline{R}$ respectively, to form a energy functional $V_{\text{interaction}}(F,\overline{R})$, defined by

$$\begin{aligned} V_{\text{interaction}}(F,\overline{R}) = \chi_1 \text{tr}(\overline{R}^T \text{Curl}\, \overline{R})\text{tr}(\overline{R}^T F) \\ + \chi_3 \langle \text{dev sym}(\overline{R}^T \text{Curl}\, \overline{R}),\ \text{dev sym}(\overline{R}^T F - \mathbb{1})\rangle. \end{aligned} \tag{2.1.6}$$

where χ_1 and χ_3 are coupling constants, while the vanishing χ_2 term can be seen from the absence of $\text{skew}(\overline{R}^T F - \mathbb{1})$ term in (2.1.1). We denote the Frobenius product of matrices A and B by

$$\langle A, B\rangle = A : B = \text{tr}(AB^T) = \text{tr}(A^T B)\ .$$

Lastly, we will consider the Cosserat coupling term which is given by

$$V_{\text{coupling}}(F,\overline{R}) = \mu_c \left\|\overline{R}^T\ \text{polar}(F) - \mathbb{1}\right\|^2 \tag{2.1.7}$$

where μ_c is the Cosserat couple modulus, and $\text{polar}(F)$ is the polar part in the classical decomposition of $F = RU$. This energy function explicitly distinguishes the microrotation $\overline{R}$ and

the macrorotation defined by polar(F), but express non-trivial coupled energy between them. This can be easily seen from the fact that $V_{\text{coupling}}(F,\overline{R})$ vanishes when $\overline{R}\to\text{polar}(F)$. Couple modulus in the classical elastic theory can be found in [6, 36], and various limiting cases of the Cosserat couple modulus are studied in [37, 38].

Variations of the energy functionals, in the following expression, are quite technically involved.

$$\delta V(F,\overline{R}) = \delta V_{\text{coupling}}(F,\overline{R}) + \delta V_{\text{interaction}}(F,\overline{R}) + \delta V_{\text{elastic}}(F,\overline{R}) + \delta V_{\text{curvature}}(\overline{R})\ . \tag{2.1.8}$$

All detailed results are stated explicitly in Appendix A, but the principle idea is to vary term by term according to the basic variational calculus such as

$$\delta V(F,\overline{R}) = \frac{\partial V}{\partial F} : \delta F + \frac{\partial V}{\partial \overline{R}} : \delta\overline{R}$$

with the help of chain rules in varying the matrices summarised in Appendix A.

Now, we gather all the variational terms (A.0.5), (A.0.13), (A.0.15) and (A.0.19), we will obtain the complete variational functional of the theory for the dynamical case as follows.

$$\begin{aligned}
\delta V_{\text{elastic}}(F,\overline{R}) &= \Big[\mu(\overline{R}F^T\overline{R}+F) - (2\mu+3\lambda)\overline{R} + \lambda\text{tr}(\overline{R}^TF)\overline{R}\Big] : \delta F \\
&\quad + \Big[\mu F\overline{R}^TF - (2\mu+3\lambda)F + \lambda\text{tr}(\overline{R}^TF)F\Big] : \delta\overline{R} + \rho\ddot{u}\ \delta u \qquad (2.1.9a)\\
\delta V_{\text{curvature}}(\overline{R}) &= \Big[(\kappa_1-\kappa_2)\Big((\text{Curl}\,\overline{R})\overline{R}^T(\text{Curl}\,(\overline{R})) + \text{Curl}\Big[\overline{R}(\text{Curl}\,\overline{R})^T\overline{R}\Big]\Big) + (\kappa_1+\kappa_2)\text{Curl}\Big[\text{Curl}\,\overline{R}\Big] \\
&\quad - \Big(\frac{\kappa_1}{3}-\kappa_3\Big)\Big(4\text{tr}(\overline{R}^T\text{Curl}\,\overline{R})\text{Curl}\,(\overline{R}) - 2\overline{R}\Big(\text{grad}\Big(\text{tr}[\overline{R}^T\text{Curl}\,\overline{R}]\Big)\Big)^\star + 2\rho_{\text{rot}}\ddot{\overline{R}}\Big] : \delta\overline{R} \qquad (2.1.9b)\\
\delta V_{\text{interaction}}(F,\overline{R}) &= \Big\{\Big(\chi_1-\frac{\chi_3}{3}\Big)\Big(2\text{tr}(\overline{R}^TF)\text{Curl}\,(\overline{R}) + \text{tr}(\overline{R}^T\text{Curl}\,\overline{R})F - \overline{R}\Big[\text{grad}\Big(\text{tr}[\overline{R}^TF]\Big)\Big]^\star\Big) \\
&\quad + \frac{\chi_3}{2}\Big(\text{Curl}\,(F) + (\text{Curl}\,(\overline{R}))\overline{R}^TF + F\overline{R}^T(\text{Curl}\,(\overline{R})) + \text{Curl}\,(\overline{R}F^T\overline{R})\Big)\Big\} : \delta\overline{R} \qquad (2.1.9c)\\
&\quad + \Big\{\chi_1\text{tr}(\overline{R}^T\text{Curl}\,\overline{R})\overline{R} + \frac{\chi_3}{2}\Big(\text{Curl}\,(\overline{R}) + \overline{R}(\text{Curl}\,(\overline{R}))^T\overline{R}\Big) - \frac{\chi_3}{3}\text{tr}(\overline{R}^T\text{Curl}\,(\overline{R}))\overline{R}\Big\} : \delta F \\
\delta V_{\text{coupling}}(F,\overline{R}) &= -2\mu_c\overline{R} : \delta\overline{R} - \frac{2\mu_c}{\det(Y)}\Big[RY(R^T\overline{R}-\overline{R}^TR)Y\Big] : \delta F \qquad (2.1.9d)
\end{aligned}$$

where dots imply the time derivatives for the variation in the kinetic terms $\rho\ddot{u}\ \delta u = \rho\partial_{tt}\psi\ \delta\psi$. We defined $Y = \text{tr}(U)\mathbb{1} - U$, and the kinetic term for $V_{\text{curvature}}$ by

$$V_{\text{curvature,kinetic}} = \rho_{\text{rot}}\|\dot{\overline{R}}\|^2 = \rho_{\text{rot}}\text{tr}(\dot{\overline{R}}\ \dot{\overline{R}}^T)\ .$$

The next step will be collecting various expressions with respect to F and $\overline{R}$ to construct the field equations.

2.2 Equations of motion and solutions

In the recent paper [39], the dynamical Cosserat model was investigated by analysing the geometrically nonlinear and coupled nature of the system, in which linearised energy functionals are considered to simplify the problem. It allowed reduction of the coupled system of partial differential equations to a sine-Gordon equation, which in turn yielded soliton solutions both in

microrotational and displacement deformations under the assumption that displacements are small while microrotations can be arbitrarily large.

By the nature of micropolar continua, the microrotation can be represented by an arbitrary rotational angle $\phi = \phi(x, y, z, t)$ about an arbitrary axis $\boldsymbol{n} = \boldsymbol{n}(x, y, z, t)$ in three spatial dimensions. In other words, every individual point in the micropolar continua can have independent rigid rotational degrees of freedom. Moreover, since we are dealing with the dynamic problem, an elastic wave (if there is any) of microrotation ϕ and macrodeformation ψ can propagate independently with different velocities which may propagate in the form of either longitudinal or transverse through the given media in each case, hence four different combinations are possible. This means, if we consider a general case, the equations of motion would be highly nonlinear by nature, and it might not be possible to solve them analytically. Therefore, we would like to make following assumptions.

1. We assume that points in our microcontinuum can only experience rotations about a fixed axis, say the z-axis, which allows us to write

$$\overline{R} = \begin{pmatrix} \cos\phi & -\sin\phi & 0 \\ \sin\phi & \cos\phi & 0 \\ 0 & 0 & 1 \end{pmatrix} . \tag{2.2.1}$$

   In this case, the variation of microrotation is simply

$$\delta\overline{R} = \begin{pmatrix} -\sin\phi\ \delta\phi & -\cos\phi\ \delta\phi & 0 \\ \cos\phi\ \delta\phi & -\sin\phi\ \delta\phi & 0 \\ 0 & 0 & 0 \end{pmatrix} . \tag{2.2.2}$$

2. We will look for solutions of ϕ and ψ, or coupled system, in which both microrotational and macro-displacement waves are longitudinal about the same axis, the z-axis in this case, so that we can write forms of wave equations by

$$\begin{aligned} \text{Microrotation: } \phi &= \phi(z, t) \\ \text{Macro displacement: } \psi &= \psi(z, t) \ . \end{aligned} \tag{2.2.3}$$

   Hence the displacement vector, in $F = \mathbb{1} + \nabla\boldsymbol{u}$, is just

$$\boldsymbol{u} = \begin{pmatrix} 0 \\ 0 \\ \psi(z,t) \end{pmatrix} \qquad \text{and} \qquad \nabla\boldsymbol{u} = \begin{pmatrix} 0 & 0 & 0 \\ 0 & 0 & 0 \\ 0 & 0 & \partial_z\psi(z,t) \end{pmatrix} . \tag{2.2.4}$$

Under these assumptions, we might expect that the dynamic problem will be simplified significantly while the central properties of Cosserat problem are retained, but even with these simplified situation, the equations to be solved can be quite challenging.

We are ready to collect relevant terms with respect to F and $\overline{R}$ separately. Unlike the case of $\delta\overline{R}$, in which the variational kinetic term is readily written with respect to $\overline{R}$, the variational kinetic term from the interaction energy functional is written with respect to $\delta\boldsymbol{u}$. But the variation with respect to F can be restated as the variation with respect to $\boldsymbol{u}$, hence with respect to ψ as we will see shortly.

Collecting terms for δF from (2.1.9) gives

$$\begin{pmatrix} A_{11} & A_{12} & 0 \\ -A_{12} & A_{11} & 0 \\ 0 & 0 & A_{33} \end{pmatrix} = \Big[\mu\left(\overline{R}F^T\overline{R}+F\right)-(2\mu+3\lambda)\overline{R}+\lambda\mathrm{tr}(\overline{R}^TF)\overline{R}\Big] + \left[\chi_1\mathrm{tr}\left(\overline{R}^T\mathrm{Curl}\,\overline{R}\right)\overline{R}+\frac{\chi_3}{2}\left(\mathrm{Curl}\,\overline{R}+\overline{R}(\mathrm{Curl}\,\overline{R})^T\overline{R}\right)-\frac{\chi_3}{3}\mathrm{tr}\left(\overline{R}^T\mathrm{Curl}\,\overline{R}\right)\overline{R}\right] + \frac{2\mu_c}{\det Y}\left[RY\left(\overline{R}^TR-R^T\overline{R}\right)Y\right], \quad (2.2.5)$$

where

$$\begin{aligned} A_{11} &= \frac{1}{3}\cos\phi\Big[6(\lambda+\mu)(-1+\cos\phi)+(6\chi_1+\chi_3)\partial_z\phi+3\lambda\partial_z\psi\Big] \\ A_{12} &= -\frac{1}{3}\sin\phi\Big[-6\lambda-6\mu+6\lambda\cos\phi+6\mu\cos\phi-6\mu_c+(6\chi_1+\chi_3)\partial_z\phi+3\lambda\partial_z\psi\Big] \\ A_{33} &= 2\lambda(-1+\cos\phi)+\left(2\chi_1-\frac{2\chi_3}{3}\right)\partial_z\phi+(\lambda+2\mu)\partial_z\psi\,. \end{aligned} \quad (2.2.6)$$

Now, the terms which appear in the variation with respect to F can be transformed into the variation with respect to $\nabla\boldsymbol{u}$, for any matrix $\boldsymbol{A}$, as shown below.

$$\boldsymbol{A}:\delta F = A_{ij}\delta F_{ij} \longrightarrow -\partial_j A_{ij}\delta u_i = -(\partial_1 A_{31}+\partial_2 A_{32}+\partial_3 A_{33})\delta\psi\,, \quad (2.2.7)$$

up to a boundary term. In this case, the contribution comes only from A_{33} ,and we are left with

$$\left[2\lambda\sin\phi\,\partial_z\phi-\left(2\chi_1-\frac{2\chi_3}{3}\right)\partial_{zz}\phi-(\lambda+2\mu)\partial_{zz}\psi\right]\delta\psi\,. \quad (2.2.8)$$

We now include the kinetic variational term $\rho\ddot{u}\;\delta u=\rho\partial_{tt}\psi\;\delta\psi$ to obtain the equation of motion for F,

$$-\lambda\left(\partial_{zz}\psi-2\partial_z\phi\sin\phi\right)-2\mu\partial_{zz}\psi+\rho\partial_{tt}\psi+\frac{2}{3}(\chi_3-3\chi_1)\partial_{zz}\phi=0\,. \quad (2.2.9)$$

In the same way, we collect terms for $\delta\overline{R}$ to obtain

$$\begin{pmatrix} B_{11} & B_{12} & 0 \\ -B_{12} & B_{11} & 0 \\ 0 & 0 & B_{33} \end{pmatrix} = 2\rho_{\mathrm{rot}}\ddot{\overline{R}}+\mu F\overline{R}^TF-(2\mu+3\lambda)F+\lambda\mathrm{tr}(\overline{R}^TF)F-2\mu_cR + (\kappa_1-\kappa_2)\Big[(\mathrm{Curl}\,\overline{R})\overline{R}^T(\mathrm{Curl}\,\overline{R})+\mathrm{Curl}\left(\overline{R}(\mathrm{Curl}\,\overline{R})^T\overline{R}\right)\Big]+(\kappa_1+\kappa_2)\Big[\mathrm{Curl}\,(\mathrm{Curl}\,\overline{R})\Big] - \left(\frac{\kappa_1}{3}-\kappa_3\right)\Big[4\mathrm{tr}(\overline{R}^T\mathrm{Curl}\,\overline{R})\mathrm{Curl}\,\overline{R}-2\overline{R}\Big(\mathrm{grad}\Big[\mathrm{tr}(\overline{R}^T\mathrm{Curl}\,\overline{R})\Big]\Big)^\star\Big] + \left(\chi_1-\frac{\chi_3}{3}\right)\left(2\mathrm{tr}(\overline{R}^TF)\mathrm{Curl}\,\overline{R}+\mathrm{tr}(\overline{R}^T\mathrm{Curl}\,\overline{R})F-\overline{R}\Big[\mathrm{grad}(\mathrm{tr}(F\overline{R}^T))\Big]^\star\right) + \frac{\chi_3}{2}\left(\mathrm{Curl}\,F+(\mathrm{Curl}\,\overline{R})\overline{R}^TF+F\overline{R}^T(\mathrm{Curl}\,\overline{R})+\mathrm{Curl}\,(\overline{R}F^T\overline{R})\right) \quad (2.2.10)$$

where

$$
\begin{aligned}
B_{11} =& -2(\lambda+\mu+\mu_c)+6\chi_1\cos^2\phi\,\partial_z\phi+\lambda\partial_z\psi \\
&+\frac{1}{3}\cos\phi\Big[3(2\lambda+\mu)-6\rho_{\rm rot}(\partial_t\phi)^2+(\kappa_1-3\kappa_2+24\kappa_3)(\partial_z\phi)^2+2(3\chi_1-\chi_3)\partial_z\phi(1+\partial_z\psi)\Big] \\
&+\frac{1}{3}\sin\phi\Big[-6\rho_{\rm rot}\partial_{tt}\phi+2(\kappa_1+6\kappa_3)\partial_{zz}\phi+(3\chi_1-\chi_3)\partial_{zz}\psi\Big] \\
B_{12} =& \frac{1}{3}\sin\phi\Big[3\mu+6\rho_{\rm rot}(\partial_t\phi)^2-(\kappa_1-3\kappa_2+24\kappa_3)(\partial_z\phi)^2-2(3\chi_1-\chi_3)\partial_z\phi(1+\partial_z\psi)\Big] \\
&+\cos\phi\Big[-6\chi_1\sin\phi\,\partial_z\phi+\frac{1}{3}\left(-6\rho_{\rm rot}\partial_{tt}\phi+2(\kappa_1+6\kappa_3)\partial_{zz}\phi+(3\chi_1-\chi_3)\partial_{zz}\psi\right)\Big] \\
B_{33} =& -2\mu_c+2\lambda\cos\phi(1+\partial_z\psi)+\frac{1}{3}(1+\partial_z\psi)\Big[(6\chi_1-2\chi_3)\partial_z\phi+3(-2\lambda-\mu+(\lambda+\mu)\partial_z\psi)\Big]\,.
\end{aligned}
\tag{2.2.11}
$$

Applying $B:\delta\overline{R}$ gives

$$
B:\delta\overline{R}=\mathrm{tr}\left[B^T\delta\overline{R}\right]=-(2B_{11}\sin\phi+2B_{12}\cos\phi)\delta\phi\,, \tag{2.2.12}
$$

which is

$$
\begin{aligned}
\Big[&4(\lambda+\mu+\mu_c)\sin\phi-2(\lambda+\mu)\sin 2\phi-2\lambda\sin\phi\,\partial_z\psi+4\rho_{\rm rot}\partial_{tt}\phi \\
&-4\left(\frac{\kappa_1}{3}+2\kappa_3\right)\partial_{zz}\phi-2\left(\chi_1-\frac{\chi_3}{3}\right)\partial_{zz}\psi\Big]\delta\phi\,.
\end{aligned}
\tag{2.2.13}
$$

Therefore, from (2.2.9) and (2.2.13), we obtain two equations of motion by varying the total energy functional with respect to F and $\overline{R}$, respectively, as follows

$$
\begin{aligned}
&-(\lambda+\mu+\mu_c)\sin\phi+\frac{1}{2}(\lambda+\mu)\sin 2\phi+\frac{1}{2}\lambda\sin\phi\partial_z\psi-\rho_{\rm rot}\partial_{tt}\phi \\
&\qquad+\left(\frac{\kappa_1}{3}+2\kappa_3\right)\partial_{zz}\phi+\left(\frac{\chi_1}{2}-\frac{\chi_3}{6}\right)\partial_{zz}\psi=0\,, \qquad (2.2.14a)\\
&-\lambda\left(\partial_{zz}\psi-2\partial_z\phi\sin\phi\right)-2\mu\partial_{zz}\psi+\rho\partial_{tt}\psi+\frac{2}{3}(\chi_3-3\chi_1)\partial_{zz}\phi=0\,. \qquad (2.2.14b)
\end{aligned}
$$

These can be written in components form by

$$
\begin{pmatrix}\partial_{tt}\phi\\ \partial_{tt}\psi\end{pmatrix}=\boldsymbol{M}\begin{pmatrix}\partial_{zz}\phi\\ \partial_{zz}\psi\end{pmatrix}+\begin{pmatrix}0 & \frac{\lambda\sin\phi}{2\rho_{\rm rot}}\\ -\frac{2\lambda\sin\phi}{\rho} & 0\end{pmatrix}\begin{pmatrix}\partial_z\phi\\ \partial_z\psi\end{pmatrix}-\frac{(\lambda+\mu+\mu_c)}{\rho_{\rm rot}}\begin{pmatrix}\sin\phi\\ 0\end{pmatrix}+\frac{\lambda+\mu}{2\rho_{\rm rot}}\begin{pmatrix}\sin 2\phi\\ 0\end{pmatrix} \tag{2.2.15}
$$

where

$$
\boldsymbol{M}=\begin{pmatrix}(\kappa_1+6\kappa_3)/3\rho_{\rm rot} & (3\chi_1-\chi_3)/6\rho_{\rm rot}\\ 2(3\chi_1-\chi_3)/3\rho & (\lambda+2\mu)/\rho\end{pmatrix}\,. \tag{2.2.16}
$$

From this, we can see immediately that the off-diagonal entries of $\boldsymbol{M}$ are responsible for the coupled system, and due to the remaining nonlinear terms, it is difficult to diagonalise the whole system to uncouple the variables. Also, we note that we will recover the result obtained in [39] if we assume the linearised energy functionals which lead to the approximations such as $\lambda\phi\ll 1$ and $\mu\phi\ll 1$, while the matrix elements $\boldsymbol{M}$ remain unchanged.

A similar problem was investigated in [26], and its revised results were stated in [15], in which case the longitudinal wave is expressed as the displacement vector $u(x,t)$ along the x-axis with the rotational deformation $\phi(x,t)$ about x-axis. The equations of motion are described

as a system of coupled expressions,

$$\begin{pmatrix}\partial_{tt}\phi\\ \partial_{tt}u\end{pmatrix}=\boldsymbol{N}\begin{pmatrix}\partial_{xx}\phi\\ \partial_{xx}u\end{pmatrix}+\begin{pmatrix}0 & \frac{2\lambda'\sin\phi}{\rho_0 J}\\ -\frac{2(\lambda'+2\mu'+\kappa')\sin\phi}{\rho_0} & 0\end{pmatrix}\begin{pmatrix}\partial_x\phi\\ \partial_x u\end{pmatrix}+\frac{2\lambda'}{\rho_0 J}\begin{pmatrix}\sin\phi\\ 0\end{pmatrix}+\frac{2\lambda'+\mu'}{\rho_0 J}\begin{pmatrix}\sin 2\phi\\ 0\end{pmatrix} \tag{2.2.17}$$

where $\alpha, \lambda', \mu', \kappa'$ are isotropic material moduli used in [15], and

$$\boldsymbol{N}=\begin{pmatrix}\frac{\alpha}{\rho_0 J} & 0\\ 0 & \frac{\lambda'+2\mu'+\kappa'}{\rho_0}\end{pmatrix}\ . \tag{2.2.18}$$

Since the matrix $\boldsymbol{N}$ is diagonal, we do not have second order coupling terms in the equations of motion. Unlike our current case, the system (2.2.17) is readily solvable under the small displacement limit, using the conventional method for the one-dimensional d'Alembert's solution subject to appropriate boundary conditions.

2.3 Solution for the double sine-Gordon equation

What we obtained so far is a system of nonlinear coupled partial differential equations (2.2.14) and a non-diagonal matrix representation of $\boldsymbol{M}$ in (2.2.16). We note that we cannot make any assumptions for the parameters in $\boldsymbol{M}$ unless any specific physical system is assumed to simplify the problem significantly.

We will generalise the previously considered deformations in [39] of limited case to include the fully nonlinear model with arbitrarily large rotations and displacements. This discussion will give us further insights into the nature of the nonlinear geometry of Cosserat micropolar elasticity.

Now, before we solve the equations, we make an additional assumption that the elastic and rotational waves propagate with the same constant wave speed v, and $\psi = g(z - vt)$, so that ψ satisfies

$$\partial_{tt}\psi = v^2\partial_{zz}\psi\ . \tag{2.3.1}$$

First, we denote the diagonal entries of $\boldsymbol{M}$ by $v_{\text{rot}}^2 = M_{11}$ and $v_{\text{elas}}^2 = M_{22}$. Then (2.2.14b) becomes

$$g''(z-vt) = \partial_{zz}\psi = \frac{M_{21}}{v^2 - v_{\text{elas}}^2}\partial_{zz}\phi - \frac{2\lambda}{\rho(v^2 - v_{\text{elas}}^2)}\sin\phi\ \partial_z\phi\ . \tag{2.3.2}$$

Integrating with respect to z once gives

$$g'(z-vt) = \partial_z\psi = \frac{M_{21}}{v^2 - v_{\text{elas}}^2}\partial_z\phi + \frac{2\lambda}{\rho(v^2 - v_{\text{elas}}^2)}\cos\phi \tag{2.3.3}$$

in which we set the constant of integration to zero by imposing following boundary conditions for $\psi = g(z - vt)$,

$$\psi(\pm\infty, t) = 0 \qquad \text{and} \qquad \partial_z\psi(\pm\infty, t) = 0\ . \tag{2.3.4}$$

The first asymptotic condition for $\psi(z, t)$ is reasonable in a sense that the elastic macrodeformation will not affect the point located far away from the place where the deformation currently occurs, and the material point should return to its original configuration as we approach spatial infinity $z \to \pm\infty$. The second condition follows from the finite energy requirement when one integrate over the region for the continuum.

Substituting (2.3.2) and (2.3.3) into the remaining equation of motion (2.2.14a) gives

$$\partial_{tt}\phi - \left[v_{\rm rot}^2 + \frac{M_{12}M_{21}}{v^2 - v_{\rm elas}^2}\right]\partial_{zz}\phi - \frac{\lambda}{2(v^2 - v_{\rm elas}^2)}\left[\frac{M_{21}}{\rho_{\rm rot}} - \frac{4M_{12}}{\rho}\right]\sin\phi\,\partial_z\phi + \frac{(\lambda+\mu+\mu_c)}{\rho_{\rm rot}}\sin\phi - \left[\frac{\lambda^2}{2\rho_{\rm rot}\rho(v^2 - v_{\rm elas}^2)} + \frac{\lambda+\mu}{2\rho_{\rm rot}}\right]\sin 2\phi = 0\ . \tag{2.3.5}$$

Moreover, if we rescale z by

$$z = \left(v_{\rm rot}^2 + \frac{M_{12}M_{21}}{v^2 - v_{\rm elas}^2}\right)^{1/2}\hat{z} \tag{2.3.6}$$

then (2.3.5) reduces to, the double sine-Gordon equation

$$\partial_{tt}\phi - \partial_{\hat{z}\hat{z}}\phi + m^2\sin\phi + \frac{b}{2}\sin 2\phi = 0\ , \tag{2.3.7}$$

where

$$m^2 = \frac{(\lambda+\mu+\mu_c)}{\rho_{\rm rot}} \qquad \text{and} \qquad b = -\frac{1}{\rho_{\rm rot}}\left[\frac{\lambda^2}{\rho(v^2 - v_{\rm elas}^2)} + (\lambda+\mu)\right]\ . \tag{2.3.8}$$

The apparent singularity in b as v^2 approaches $v_{\rm elas}^2$ can be removed if we make a further transformation on v by

$$v \longrightarrow \left(v_{\rm rot}^2 + \frac{M_{12}M_{21}}{v^2 - v_{\rm elas}^2}\right)^{1/2}\hat{v}\ . \tag{2.3.9}$$

We note that this transformation on v would not change our assumption on ψ along with the rescaling on z, since $\partial_{tt}\psi = v^2\partial_{zz}\psi$ implies $\partial_{tt}\psi = \hat{v}^2\partial_{\hat{z}\hat{z}}\psi$.

The general solution of (2.3.7) is given in [33] as

$$\phi(\hat{z},t) = 2\,\arcsin(X(\hat{z},t)) \tag{2.3.10}$$

where

$$X(\hat{z},t) = \frac{u}{\sqrt{1 + \frac{1}{2}u^2\left(1 + \frac{b}{m^2+b}\right) + \frac{1}{16}u^4\left(1 - \frac{b}{m^2+b}\right)^2}}\ , \tag{2.3.11}$$

in which $u = u(\hat{z},t)$ must satisfy following two conditions

$$\begin{aligned} \partial_{tt}u - \partial_{\hat{z}\hat{z}}u + (m^2+b)u &= 0\ , \\ (\partial_t u)^2 - (\partial_{\hat{z}}u)^2 + (m^2+b)u^2 &= 0\ . \end{aligned} \tag{2.3.12}$$

The simplest form of solution satisfying these conditions would be

$$u(\hat{z},t) = \exp\left[\sqrt{\frac{m^2+b}{1-\hat{v}^2}}\,(\hat{z} - \hat{v}t) \pm \delta\right] \tag{2.3.13}$$

for some constant δ.

Now, we can write the solution ϕ using the identity $\arcsin(x) = 2\arctan\left(\frac{x}{1+\sqrt{1-x^2}}\right)$. After some straightforward calculations, one obtains

$$\phi(\hat{z},t) = \begin{cases} 4\arctan\left[\frac{1}{2}e^{+\sqrt{\frac{m^2+b}{1-\hat{v}^2}}(\hat{z}-\hat{v}t)}\right] & \text{if} \quad e^{2\sqrt{\frac{m^2+b}{1-\hat{v}^2}}(\hat{z}-\hat{v}t)} < 4\ , \\ 4\arctan\left[2e^{-\sqrt{\frac{m^2+b}{1-\hat{v}^2}}(\hat{z}-\hat{v}t)}\right] & \text{if} \quad e^{2\sqrt{\frac{m^2+b}{1-\hat{v}^2}}(\hat{z}-\hat{v}t)} > 4\ . \end{cases} \tag{2.3.14}$$

This solution corresponds to the **kink** and **antikink** solution of ϕ, and the bifurcation into these two branches from the original solution (2.3.10) arises quite naturally in translating the solution in terms of arcsin into arctan functions, see Fig. 2.1.

For the next step, we would like to put the rescaled variables $\{\hat{z}, \hat{v}\}$ back to the original variables $\{z, v\}$. This can be done if we apply inverse transformations of (2.3.6) and (2.3.9), but we would like to consider a simpler method by comparing the previously obtained result in [39]. The microrotational propagation solution ϕ_0, based on the linearised energy functionals, is obtained

$$\phi_0 = 4 \arctan e^{\pm k_0(z-vt)\pm\delta} \tag{2.3.15}$$

with corresponding k_0 and m_0 are given by

$$k_0^2 = \frac{v_{\text{elas}}^2 - v^2}{v^4 - \text{tr}(\boldsymbol{M})v^2 + \det(\boldsymbol{M})} m_0^2 \,, \qquad\qquad m_0^2 = \frac{\mu_c}{\rho_{\text{rot}}}. \tag{2.3.16}$$

Now, consider the term which enters into the exponential of (2.3.13)

$$\pm \sqrt{\frac{m_0^2}{1-\hat{v}^2}}\, (\hat{z} - \hat{v}t) \pm \delta \tag{2.3.17}$$

where we see now that $\delta = \ln \frac{1}{2}$. We would like to see if this agrees with the argument of the exponential in (2.3.15). This can be done if we apply a reverse operation (2.3.6) of z, and an inverse transformation (2.3.9) of v. After some calculations, we obtain

$$\pm \sqrt{\frac{m_0^2}{1-\hat{v}^2}}\, (\hat{z} - \hat{v}t) \pm \delta \longrightarrow \pm k_0(z - vt) \pm \delta \,. \tag{2.3.18}$$

Hence, we can express the solution of ϕ_0 in terms of rescaled variables $\{\hat{z}, \hat{v}\}$ or the original variables $\{z, v\}$ with k_0 of (2.3.16), and find

$$\phi_0 = 4 \arctan e^{\pm k_0(z-vt)\pm\delta} = 4 \arctan e^{\pm \sqrt{\frac{m_0^2}{1-\hat{v}^2}}\, (\hat{z}-\hat{v}t)\pm\delta} \,. \tag{2.3.19}$$

For the current case, by following the same reasoning, we find that the rescaled variables and original variables are interchangeable, by the following relation,

$$\pm \sqrt{\frac{m^2 + b}{1-\hat{v}^2}}\, (\hat{z} - \hat{v}t) \pm \delta \longrightarrow \pm k(z - vt) \pm \delta \tag{2.3.20}$$

in which k_0^2 and m_0^2 are now replaced by k^2 and m^2, which are

$$k^2 = \frac{v_{\text{elas}}^2 - v^2}{v^4 - \text{tr}(\boldsymbol{M})v^2 + \det(\boldsymbol{M})} (m^2 + b) \,, \qquad\qquad m^2 = \frac{\lambda + \mu + \mu_c}{\rho_{\text{rot}}} \,. \tag{2.3.21}$$

Therefore, we can write the solution (2.3.14) of ϕ in terms of z and v by

$$\phi = 4 \arctan e^{\pm k(z-vt)\pm\delta} \tag{2.3.22}$$

with $\delta = \ln \frac{1}{2}$.

- We note that the matrix $\boldsymbol{M}$ used in (2.3.21) and (2.3.16) are identical to that of (2.2.16).
- The Lamé parameters λ and μ are brought into play in the fully nonlinear case through the quantity m^2, while those parameters are missing in m_0^2 when considering the approximations $\lambda\phi \ll 1$ and $\mu\phi \ll 1$, which effectively lead to the results $b = 0$ and $m \to m_0$.

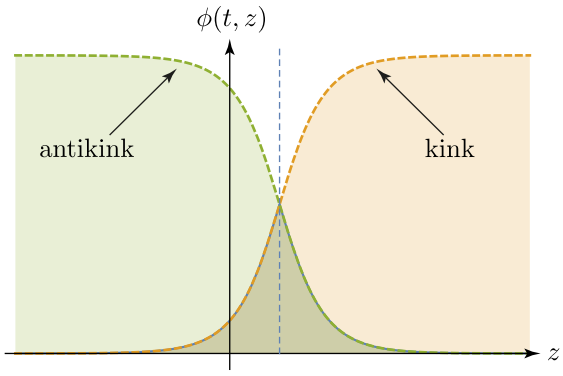

Figure 2.1: Two branches of solution $\phi = 4\arctan e^{\pm k(z-vt)\pm\delta}$ of (2.3.14) are plotted where the orange solution is for $+k$ and the green solution is for $-k$ case, corresponding to a kink and an antikink solution respectively. These two branches meet at $z = \ln 4/(2k) + vt$ as indicated by the blue vertical dashed line. The overlap is essentially the solution of the form $\phi = 2\arcsin(X)$ as in (2.3.10). We set $k = 1.5$, $v = 0.1$ at $t = 7.0$.

- Consequently, we have to treat a more complicated form of k replacing k_0^2 with an additional contribution from b.

For the solution of ψ, first we write X (hence u) in terms of $\{z, v\}$ instead of $\{\hat{z}, \hat{v}\}$.

$$X = \frac{u}{\sqrt{1 + \frac{1}{2}u^2\left(1 + \frac{b}{m^2+b}\right) + \frac{1}{16}u^4\left(1 - \frac{b}{m^2+b}\right)^2}}\,, \qquad u = e^{\pm k_(z-vt)\pm\delta}\,. \tag{2.3.23}$$

Now, since we obtain the solution ϕ of (2.3.22), we use this to find ψ. This can be done if we put the solution (2.3.22) into (2.3.2) to obtain

$$\begin{aligned} g''(z-vt) = {} & \frac{4M_{21}k^2}{v_{\text{elas}}^2 - v^2}\frac{e^{\pm k(z-vt)\pm\delta}(e^{2(\pm k(z-vt)\pm\delta)} - 1)}{(e^{2(\pm k(z-vt)\pm\delta)} + 1)^2} \\ & + \frac{2\lambda}{\rho(v^2 - v_{\text{elas}}^2)}\frac{\pm k(m^2+b)^2\left(64e^{6(\pm k(z-vt)\pm\delta)}m^4 - 1024e^{2(\pm k(z-vt)\pm\delta)}(m^2+b)^2\right)}{\left(e^{4(\pm k(z-vt)\pm\delta)}m^4 + 16(m^2+b)^2 + 8e^{2(\pm k(z-vt)\pm\delta)}(m^2+b)(m^2+2b)\right)^2}\,. \end{aligned} \tag{2.3.24}$$

If we put $s = z - vt$, then this becomes a second-order ordinary differential equation for $g(s)$. We integrate twice with respect to s using the boundary conditions (2.3.4) to obtain

$$\psi(t,z) = \frac{4M_{21}}{v^2 - v_{\text{elas}}^2}\arctan e^{\pm k(z-vt)\pm\delta} + \frac{4\lambda}{\rho k(v^2 - v_{\text{elas}}^2)}\sqrt{1 + \frac{m^2}{b}}\,\text{acrtanh}(Y) + C\,, \tag{2.3.25}$$

where

$$Y = \begin{cases} \dfrac{8b^2 + 12bm^2 + m^4(\frac{1}{4}e^{2k(z-vt)} + 4)}{8\sqrt{b}\,(m^2+b)^{3/2}} & \text{if} \quad e^{2k(z-vt)} < 4\,, \\ \dfrac{8b^2 + 12bm^2 + m^4(4e^{-2k(z-vt)} + 4)}{8\sqrt{b}\,(m^2+b)^{3/2}} & \text{if} \quad e^{2k(z-vt)} > 4\,. \end{cases} \tag{2.3.26}$$

The boundary conditions (2.3.4) fix the value for the constant C by

$$C = -\frac{4\lambda}{\rho k(v^2 - v_{\text{elas}}^2)}\sqrt{1 + \frac{m^2}{b}}\,\text{acrtanh}\left(\frac{8b^2 + 12bm^2 + 4m^4}{8\sqrt{b}\,(m^2+b)^{3/2}}\right)\,. \tag{2.3.27}$$

Using the restriction $\lambda\phi \ll 1$ and $\mu\phi \ll 1$, the solutions (2.3.22) and (2.3.25) reduce to the solutions we obtained in [39]

$$\begin{aligned} \phi_0 &= 4 \arctan e^{\pm k_0(z-vt)\pm\delta} \\ \psi_0 &= \frac{4M_{21}}{v^2 - v_{\text{elas}}^2} \arctan e^{\pm k_0(z-vt)\pm\delta} \ . \end{aligned} \tag{2.3.28}$$

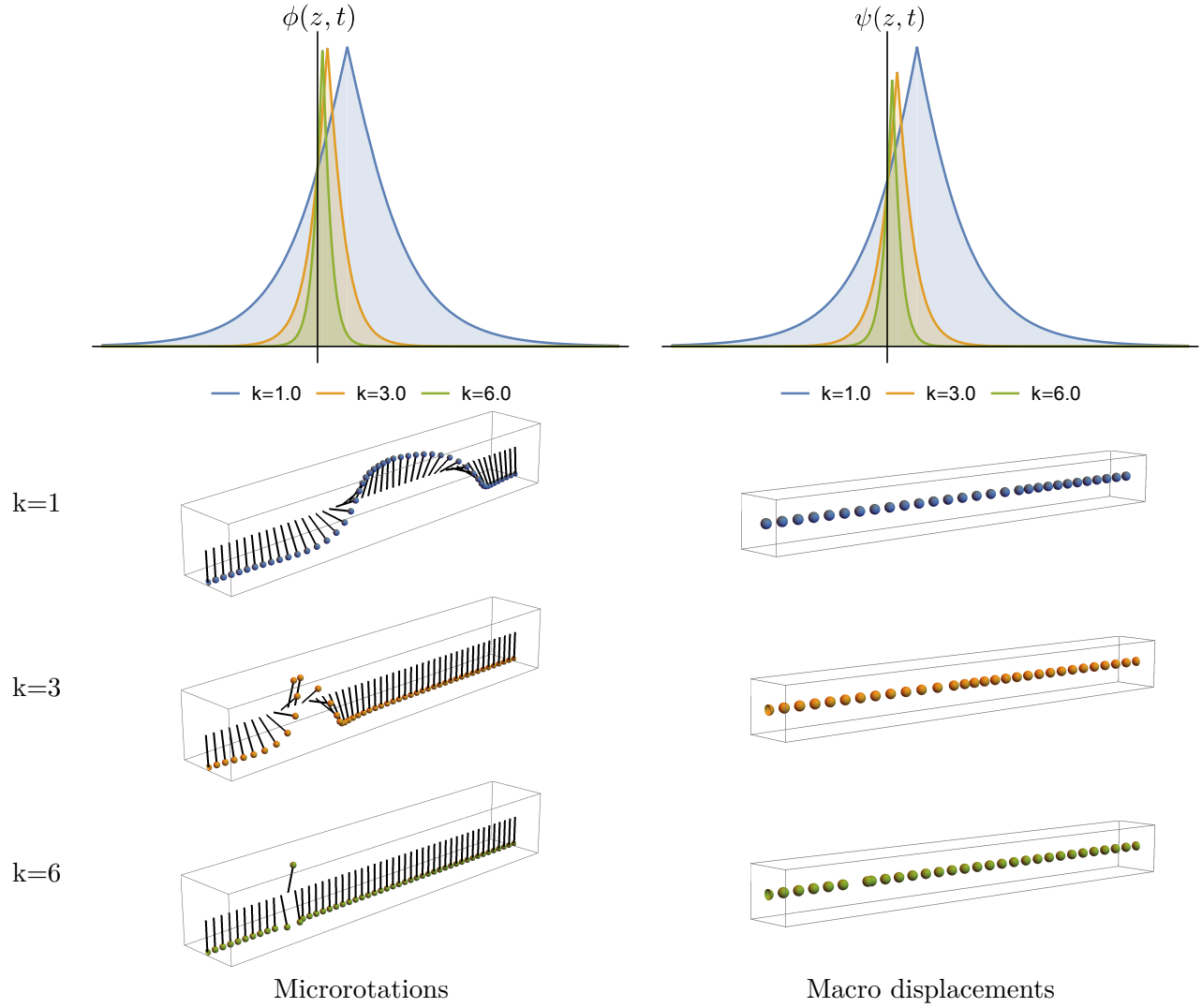

Figure 2.2: For small values of k (the blue shaded wave, pendulums and beads), we observe the width of microrotational/displacement deformation is broad, while we observe narrow microrotational/displacement deformations for large values of k (the green shaded wave, pendulums and beads).

In Fig. 2.2, the soliton solutions for $\phi(z,t)$ and $\psi(z,t)$ are given at $t = 0$ with corresponding values of k. As the rotational wave $\phi(z,t)$ propagates with a speed v along the z-axis, the points of microcontinuum (displayed as pendulums along the z-axis) experience microrotational deformations perpendicular to the axis. In the same way, the longitudinal solution $\psi(z,t)$ gives rise to the compressional deformation wave propagating with the same speed v, on the points of macroscopic continuum (shown as beads) along the same axis. As we vary the values of k, the widths of the soliton solutions are changed, and this affects overall deformational behaviours both in microrotations and macrodisplacements.

The soliton solutions for both rotations and displacements were obtained from the equations of motion, and these allowed us to understand the geometric interpretation of the deformation waves. Physically dominant parameters of the complete model in determining the overall behaviour of deformational soliton wave are the Lamé parameters $\{\lambda, \mu\}$ and the Cosserat couple modulus μ_c. This fact becomes evident by looking at the k dependency, or equivalently m dependency, of the soliton solutions on these parameters.

The various values for k in the soliton solutions for ϕ and ψ give different overall behaviours while other values of parameters are fixed. Regarding the microrotations, the effect becomes apparent for large values of k, which induces high-frequency of localised energy distribution on the narrow-width affected cross section both for the microrotational and displacement deformations, whereas small values of k induce gradual and broad energy distribution for the deformations over the microcontinuum media. The role of k can be understood using a simple model of beads and pendulums as shown in Fig. 2.2.

In the remaining part of this Chapter, we would like to consider some properties of the solution and its behaviours in limiting cases.

2.4 Properties of solutions

We notice that there might be possible singularity issues in the amplitude of $\psi(z,t)$ in (2.3.25) as v^2 approaches v_{elas}^2. Similar situation arose in case of $\phi(z,t)$ in the value of b, but this has been resolved by a simple transformation (2.3.9). In order to resolve the current problem, we would like to look closely at k as a function of v taking account of all nine parameters, $\{\kappa_1, \kappa_3, \chi_1, \chi_3, \rho, \rho_{\text{rot}}, \mu_c, \lambda, \mu\}$. We will see that the values for v are restricted to certain ranges for a given k, so we might expect that this would resolve the singularity problem. This is to specify a profile of v in terms of k which is often seen in dispersion relations.

We consider only positive roots of k^2 of (2.3.21) to understand the possible range of k for a given v. After putting all relevant parameters in (2.3.21), we obtain

$$\begin{aligned} k &= 3\left(\frac{\lambda^2+(\lambda+2\mu-v^2\rho)\mu_c}{3(\lambda+2\mu-v^2\rho)(\kappa_1+6\kappa_3)-9v^2\rho_{\text{rot}}(\lambda+2\mu-v^2\rho)-(3\chi_1-\chi_3)^2}\right)^{1/2} \\ &= \frac{3}{\sqrt{\rho\rho_{\text{rot}}}}\left(\frac{\lambda^2+\mu_c\rho(v_{\text{elas}}^2-v^2)}{v^4-(v_{\text{elas}}^2+v_{\text{rot}}^2)v^2+(v_{\text{elas}}^2v_{\text{rot}}^2-M_{12}M_{21})}\right)^{1/2}. \end{aligned} \tag{2.4.1}$$

Now, to determine whether k possesses any singularity, we compute the discriminant of the quartic of v in the denominator regarding it as a quadratic equation for v^2.

$$(v_{\text{elas}}^2+v_{\text{rot}}^2)^2-4(v_{\text{elas}}^2v_{\text{rot}}^2-M_{12}M_{21}) = (v_{\text{elas}}^2-v_{\text{rot}}^2)^2+\frac{16\rho_{\text{rot}}}{\rho}v_\chi^4\,, \tag{2.4.2}$$

where we put $v_\chi^2 \equiv M_{12}$. The expression (2.4.2) is strictly non-negative, so that we can have four possible roots of v in the denominator of (2.3.28), which will cause the singularity of k. We denote four distinct roots as v_i, $i = 1,2,3,4$, and assume that $v_1 < v_2 < 0 < v_3 < v_4$. In particular, we write explicitly

$$v^2 = \frac{1}{2}\left((v_{\text{elas}}^2+v_{\text{rot}}^2) \pm \sqrt{(v_{\text{elas}}^2-v_{\text{rot}}^2)^2+\frac{16\rho_{\text{rot}}}{\rho}v_\chi^4}\right)\,. \tag{2.4.3}$$

The square root of this gives the four roots of v_i where two positive roots v_3 and v_4 are related to two negative roots v_1 and v_2 by $v_3 = -v_2$ and $v_4 = -v_1$.

It can be recognised immediately that the values of $v_{\rm elas}$ and $v_{\rm rot}$ are restricted by

$$v_1 \leq -v_{\rm elas}, -v_{\rm rot} \leq v_2 \qquad \text{and} \qquad v_3 \leq v_{\rm elas}, v_{\rm rot} \leq v_4 \ .$$

Also, we will have $k = 0$ if v becomes

$$v_0^2 \equiv (\lambda^2/\rho\mu_c) + v_{\rm elas}^2 \ . \tag{2.4.4}$$

Now, we plot the profiles of v as a function of k and we consider only the positive values of v for the sake of simplicity. At this time, we only have two asymptotic lines of v_3 and v_4 (again we assume $v_3 < v_4$). And we assume that $v_{\rm elas} > v_{\rm rot}$.

Two characteristic types of parameter ranges for v with various values for a set of parameters with relevant asymptotic lines, and the locations of v_0, $v_{\rm elas}$ and $v_{\rm rot}$ are given in Fig. 2.3. If $v_0 > v_4$ we will have the type (a) and if $v_0 < v_4$ then the type (b).

- The threshold in transition from the type (a) to (b) is evidently the relative positions between v_0 and v_4. The values of $v_{\rm elas}$ and $v_{\rm rot}$ are located inside (or on the boundary of) the shaded region surrounded by asymptotic lines, which can be shown directly from (2.4.3).

- The dominating set of parameters in determining the characteristics is the set of constants $\{\lambda, \mu, \mu_c\}$ of the energy functional $V_{\rm elastic}$. Notably, we observe that we only alter the value of the parameter μ_c to obtain the type (b) solution from the type (a) solution, while keeping all remaining parameters unchanged.

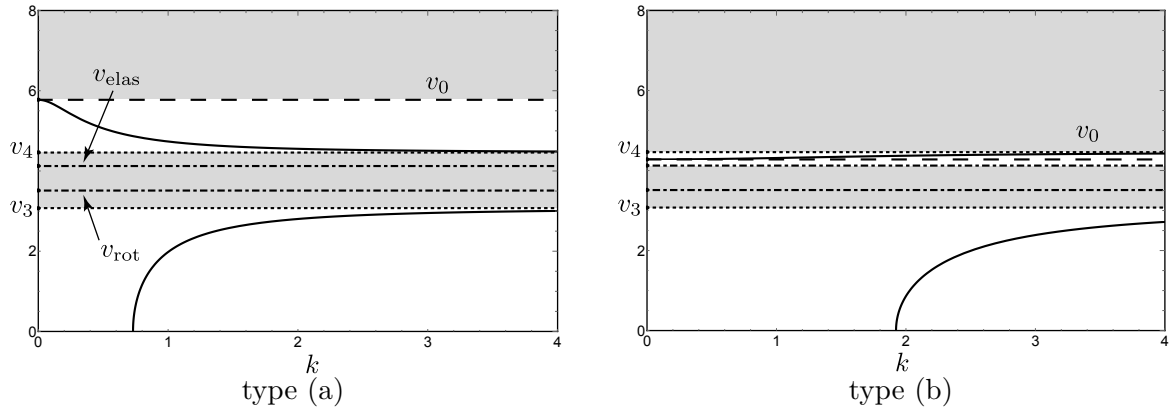

Figure 2.3: The dashed lines indicate the position of v_0, the dot-dashed lines are for $v_{\rm elas}$ and $v_{\rm rot}$. The positions of asymptotic lines v_3, v_4 are shown in dotted lines. We put the values of parameters $(\kappa_1, \kappa_3, \chi_1, \chi_3, \rho, \rho_{\rm rot}, \mu_c, \lambda, \mu) = (0.7, 0.5, 0.5, 0.1, 0.1, 0.1, 0.3, 1.0, 0.5)$ for type (a). For type (b), we alter one value of parameters $\mu_c = 1.2$. In this way, we obtain two distinct types of behaviours of v and k. This again determines two characteristic overall behaviours of the soliton solution of Fig. 2.2.

In both types (a) and (b) solutions, there exist regions (the shaded regions) in which v cannot be defined for a given k, solutions with such parameter choices do not exist. In case of type (a), the values of v are defined in $v \in [0, v_3)$ and $v \in (v_4, v_0]$. The upper limit of v is bounded by v_0 and we can see that $v_0 \to \infty$ as $\mu_c \to 0$, which is evident from (2.4.4), see Fig. 2.4.

On the other hand, for the type (b), the position of v_0 is $v_3 < v_{\rm elas} < v_0 < v_4$. Now, the line of v_0 acts the role of the boundary line along with v_3 in (b). So v takes the values in the region $v \in [0, v_3)$ and $v \in [v_0, v_4)$. We must notice that for type (b) solutions, the value of v_0 cannot be exactly $v_{\rm elas}$ due to the restriction (2.4.4), as long as we have a nonzero λ. We observe that

v_0 approaches $v_{\rm elas}$ as $\mu_c \to \infty$, but the lower profile of v in (b) will be shifted to the right indefinitely, i.e. $k \to \infty$, see Fig. 2.4.

In the limit $\mu_c \to \infty$, it is clear that we will have a profile of type (b). Also we can see from (2.3.21) that $m^2 \to m_0^2$, hence $k^2 \to k_0^2$. This agrees with the observation we made earlier that b becomes negligible, and we will be left with the soliton solution $\phi \to \phi_0$ of the form (2.3.15).

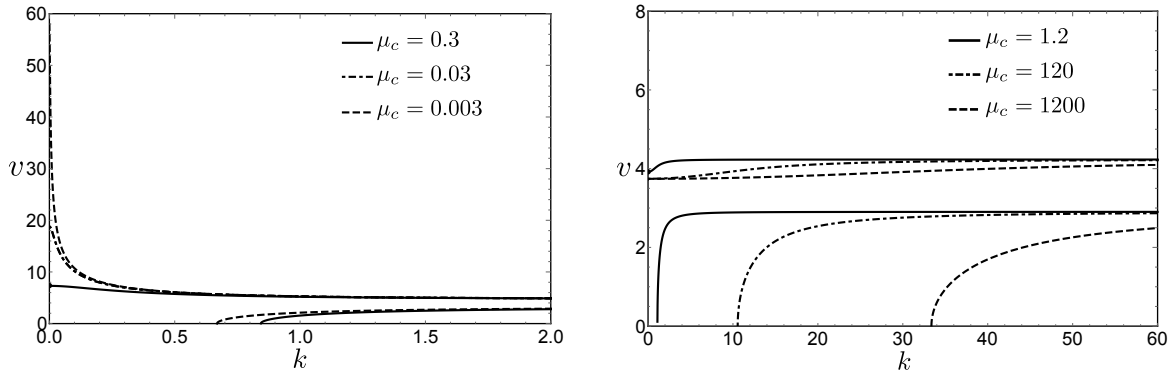

Figure 2.4: We indicate the modified profiles of the type (a) and (b) solutions as dot-dashed and dotted lines in the two limits of $\mu_c \to 0$ and $\mu_c \to \infty$. As $\mu_c \to 0$, the upper boundary v_0, in the type (a) of Fig. 2.3, is pushed up to the infinity (left). In the limit $\mu_c \to \infty$ the lower profile of type (b) will shift to infinity along the k axis (right).

Next, we consider the limit

$$\frac{\rho_{\rm rot}}{\rho}\frac{v_\chi^4}{(v_{\rm elas}^2 - v_{\rm rot}^2)^2} \ll 1 \ . \tag{2.4.5}$$

In this limit, we can approximate the expressions of v_3 and v_4 given by (2.4.3) as follows

$$v_4 \approx v_{\rm elas}\left(1 + \frac{2\rho_{\rm rot} v_\chi^4}{\rho(v_{\rm elas}^2 - v_{\rm rot}^2)v_{\rm elas}^2}\right) , \qquad v_3 \approx v_{\rm rot}\left(1 - \frac{2\rho_{\rm rot} v_\chi^4}{\rho(v_{\rm elas}^2 - v_{\rm rot}^2)v_{\rm rot}^2}\right) . \tag{2.4.6}$$

Hence we can see that $v_{\rm elas}$ approaches v_4 and $v_{\rm rot}$ approaches v_3 for the type (a) parameter choice. In case of type (c) of Fig. 2.5, we set $v_\chi = 0$ (i.e., $3\chi_1 - \chi_3 = 0$) to illustrate that $v_{\rm elas} = v_4$ and $v_{\rm rot} = v_3$, and that lines of $v_{\rm elas}$ and $v_{\rm rot}$ play the role of asymptotic lines. In this case, the matrix $\boldsymbol{M}$ of (2.2.16) becomes diagonal and the system looks similar to (2.2.17). Of course, if we had assumed that $v_{\rm elas} < v_{\rm rot}$, then we would have $v_{\rm rot} = v_4$ and $v_{\rm elas} = v_3$. We may obtain the similar observation in type (b) diagram by adjusting μ_c, but $v_{\rm elas}, v_{\rm rot} \to v_3$. Furthermore, in the same limit of $v_\chi = 0$, if we set an additional condition that $v_{\rm elas} = v_{\rm rot}$, then we will have one asymptotic line $v_{\rm elas}$ as shown in the diagram, type (d) of Fig. 2.5 and the matrix $\boldsymbol{M}$ will simply become the identity matrix (up to the rescaling).

Now, we return to the singularity problem of the amplitude ψ in (2.3.25) affected by two coefficients (the matrix element M_{21} can be written in terms of $v_\chi^2 \equiv M_{12}$),

$$\frac{16\rho_{\rm rot} v_\chi^2}{\rho(v^2 - v_{\rm elas}^2)} \qquad \text{and} \qquad \frac{4\lambda}{\rho k(v^2 - v_{\rm elas}^2)} \ . \tag{2.4.7}$$

The analytic investigation on the profiles of v as a function of k provides us the clue that the amplitude of ψ cannot be arbitrarily large. To see this, as $k \to \infty$, we know $v^2 \to v_{\rm elas}^2$. But the statement that the value of $v_{\rm elas}^2$ approaches v_4^2 is equivalent to say that $v_\chi^2 \to 0$, as we can see directly from (2.4.6). Hence the first coefficient of (2.4.7) is assumed to remain finite in this limit. Similarly, the second coefficient cannot be arbitrarily large. In other words, k and $(v^2 - v_{\rm elas}^2)$ will compensate each other as $k \to \infty$. This is shown in the type (c), or more extreme case, the type (d) in Fig. 2.5.

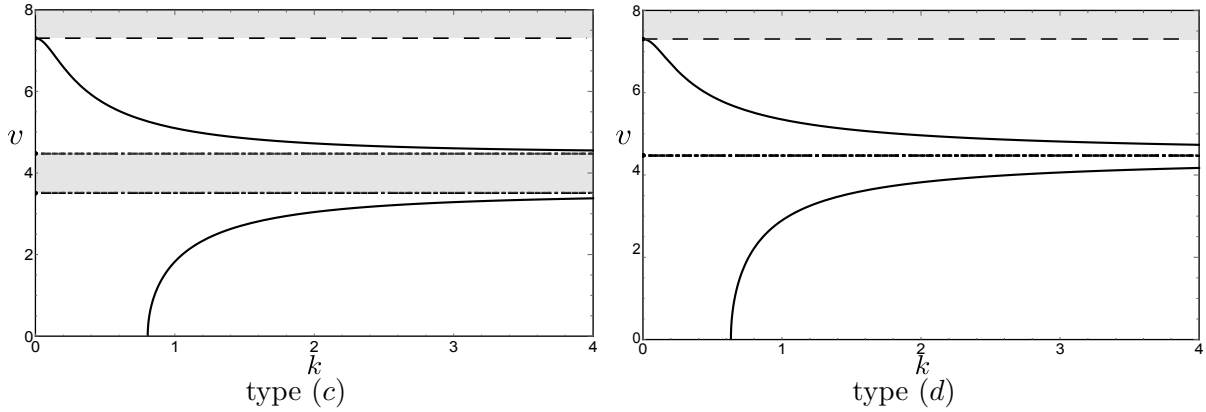

type (c) type (d)

Figure 2.5: For (c), we put $(\kappa_1, \kappa_3, \chi_1, \chi_3, \rho, \rho_{\rm rot}, \mu_c, \lambda, \mu) = (0.7, 0.5, 0.5, 1.5, 0.1, 0.1, 0.3, 1.0, 0.5)$ so that $3\chi_1 - \chi_3 = 0$ and we obtain $v_4 = v_{\rm elas} = 4.47214$ and $v_3 = v_{\rm rot} = 3.51188$. For (d), we only altered value of parameter $\kappa_1 = 3.0$ so that $v_{\rm elas} = v_{\rm rot} = v_3 = v_4 = 4.47214$.

2.5 Galilean transformations and Lorentzian transformations

If a given system is invariant under certain symmetry, then we can apply the same symmetry to a solution of the Euler-Lagrangian equation from the system to see whether the symmetry remain valid or not. This gives us a clue about the nature of solution space. For example, suppose we have a system of scalar field $\phi(z,t)$ with a Lagrangian

$$\mathcal{L} = \frac{1}{2}\left(\frac{\partial\phi}{\partial t}\right)^2 - \frac{1}{2}\left(\frac{\partial\phi}{\partial z}\right)^2 - U(\phi) \tag{2.5.1}$$

for some potential $U(\phi)$. The equation of motion can be obtained by

$$\left(\frac{\partial^2}{\partial t^2} - \frac{\partial^2}{\partial z^2}\right)\phi = -\frac{\partial U}{\partial \phi}\ . \tag{2.5.2}$$

We can write total energy H defined by an integration of energy density $\mathcal{H}$ over all space,

$$\begin{aligned} H &= \int dz\, \mathcal{H} \\ &= \int dz \left[\frac{1}{2}\left(\frac{\partial\phi}{\partial t}\right)^2 + \frac{1}{2}\left(\frac{\partial\phi}{\partial z}\right)^2 + U(\phi)\right]\ , \end{aligned} \tag{2.5.3}$$

where energy density $\mathcal{H}$ in terms of conjugate momentum $\pi = \partial\mathcal{L}/\partial\dot{\phi}$ is defined by

$$\mathcal{H} = \pi\dot{\phi} - \mathcal{L}\ . \tag{2.5.4}$$

Now, if we consider a static case in evaluating the solution, we have

$$\frac{\partial^2\phi}{\partial z^2} = \frac{\partial U}{\partial\phi}\ . \tag{2.5.5}$$

In particular, if we have the potential U given by

$$U(\phi) = \frac{1}{4}\left(\phi^2 - 2m^2\right)^2\ ,$$

then the solution is the well-known form of a pair of kink and antikink soliton solutions subject to boundary conditions similar to (2.3.4),

$$\phi(z) = \pm\sqrt{2}m\tanh\left(\sqrt{m^2}\ z\right)\ . \tag{2.5.6}$$

Further, we impose that the Lagrangian is invariant under the Lorentz transformation. This means that if we apply the same transformation to the wave equation we obtained, it will still remain as a valid solution to the given system. This is a widely known technique in solving a time-dependent partial differential equation from its static case [40], when a certain symmetry group for the Lagrangian is identified, and applicable to the static solution. We would like to emphasise here that the same method can be applied in our solution, by noting that the Galilean transformation is a limiting case of the Lorentz transformation.

Now, if we apply the Lorentz boost (the Lorentz transformation in one direction) to the static wave solution (2.5.6) along, say the z-axis, then what we can expect is that the wave packet starts moving in the direction along the transformation applied with a nonzero velocity. Hence a time-dependent wave solution for (2.5.2) is simply

$$\phi(z,t) = \pm\sqrt{2}m \tanh\left(\sqrt{\frac{m^2}{1-v^2}}\,(z-vt)\right)\,, \tag{2.5.7}$$

in which z is replaced by $(z-vt)/\sqrt{1-v^2}$, according to the Lorentz boost along the z-axis (we put the speed of light $c=1$),

$$t' = \frac{t - v/c^2 z}{\sqrt{1-v^2/c^2}}\,, \qquad z' = \frac{z-vt}{\sqrt{1-v^2/c^2}}\,, \qquad x' = x\,, \qquad y' = y\,. \tag{2.5.8}$$

For our case of the soliton solution for the microrotation governed by ϕ, suppose we have started with a static case with an equation of motion, instead of the full dynamic case (2.3.7),

$$-\frac{\partial^2\phi}{\partial z^2} + m^2\sin\phi + \frac{b}{2}\sin 2\phi = 0\,, \tag{2.5.9}$$

in which we dropped the hat for the rescaled quantities for now. It is easy to check that the solution for this is of the form,

$$\phi(z) = 2\,\arcsin(X(z)) \tag{2.5.10}$$

with the identical form X of (2.3.11), but now the static function u in X is

$$u(z) = \exp\left[\sqrt{m^2+b}\,z\right]\,. \tag{2.5.11}$$

If we apply the Lorentz boost in the z-axis to this static solution, then the time-dependent soliton solution would be (2.3.10) with

$$u(z,t) = \exp\left[\sqrt{\frac{m^2+b}{1-v^2}}\,(z-vt) \pm \delta\right]\,, \tag{2.5.12}$$

which agrees with the solution we obtained in (2.3.10).

Of course, the key ingredient in facilitating the analysis we used in solving the coupled system given in (2.2.15) is strictly based on the dynamic assumption that the displacement wave propagation satisfies (2.3.1),

$$\partial_{tt}\psi = v^2\partial_{zz}\psi\,,$$

and the underlying symmetry in the energy functional is the global Galilean transformation with the speed of light is taken to be $c\to\infty$ in (2.5.8)

$$t' = t\,, \qquad z' = z - vt\,, \qquad x' = x\,, \qquad y' = y\,. \tag{2.5.13}$$

However, we would like to emphasise the fact that the equation of motion and its soliton solution for the microrotation we obtained is well compatible with the system which contains the Lorentz transformation as its fundamental symmetry group, once one identifies the equation of motion can be derived to the form of (2.3.7).

This also signifies the effect and its validity of applying the Lorentz boost to the static solution to obtain the time-dependent solution, when the soliton solution describes the particle-like isolated behaviour prevented from any possible interference from undesired interaction to lose its solitonic character, in particular when one considers the multi-soliton system. This is exactly the case when we have $k \to \infty$ in (2.3.21), see Fig. 2.2, in our soliton solution ϕ of (2.3.22).

Chapter 3

Chiral energy

3.1 Chiralities in continua

A group of geometric symmetries which keeps at least one point fixed is called a point group. A point group in N-dimensional Euclidean space is a subgroup of the orthogonal group $O(N)$. Naturally this leads to the distinction of rotations and improper rotations. Centrosymmetry corresponds to a point group which contains an inversion centre as one of its symmetry elements. Chiral symmetry is one example of non-centrosymmetry which is characterised by the fact that a geometric figure cannot be mapped into its mirror image by an element of the Euclidean group, proper rotations $SO(N)$ and translations. We denote this property as chirality, and quantities responsible for this property by chiral terms.

This non-superimposability (i.e. chirality) to its mirror image is best illustrated by the left and right hands. There is no way to map the left hand onto the right by simply rotating the left hand in the plane. And there is no mirror symmetry line within one hand to map into another. This geometrical feature of chirality can be found in many molecules which can have distinct chemical properties. A fairly stable or harmless substance can have an unstable or noxious substance as its chiral counterpart [41].

If one applies the Lorentz boost discussed in Section 2.5 to a spinning particle in its momentum direction in one frame of reference, while retaining its spin orientation, this will cause an opposite direction of momentum to another frame of reference. This discrete symmetry is known as parity and leads to the notion of left or right-handedness in particle physics.

In continuum mechanics, it is often observed that chiral materials in three-dimensional space lose their chirality [42–44] when projected into a two-dimensional plane. A linear energy function (quadratic energy in small strains) for an isotropic material in the centrosymmetric case was studied in [10], and the absence of odd-rank isotropic tensors implicitly implied the lack of material parameters for the non-centrosymmetric case. Similar works [42, 45] considered an energy function which contains a fourth order isotropic tensor with chiral coupling terms by identifying axial tensors as being asymmetric under the inversion. When one attempts to apply these ideas to the planar case, the chiral coupling term turns out to vanish [43, 44], and one arrives at an isotropic (and centrosymmetric) model without chirality.

A rank-five isotropic tensor is introduced in [46] to impose chirality on the energy containing a single chiral material parameter. This type of chirality is related to the gradient of rotation, which led to the existence of torsion. Based on the assertion that hyperelastic Cosserat materials are hemitropic, invariant under the right action of $SO(3)$, if and only if the strain energy is hemitropic, a set of hemitropic strain invariants can be found in [47]. Many attempts were made to understand the mechanism behind the loss of chirality, and in constructing a generic two-dimensional chiral configuration without referring to higher dimensions. A chiral rank-four

isotropic tensor is used in [44] to derive a chiral material constant in the equations of motion, and in subsequent works [48,49] the two-dimensional chirality problem is further considered. A planar micropolar model is proposed in [50] with the help of the irreducible decomposition of group representation.

Recent growing interests of planar chirality [51–55] concerns the polarised propagation of electromagnetic waves. The optical behaviour indicates that planar chirality behaves differently from its three-dimensional counterpart. In [56] a two-dimensional chiral optical effect in nanostructure is studied in comparison with three-dimensional chirality. The two-dimensional micropolar continuum model of a chiral auxetic lattice structure in connection with negative Poisson's ratio is discussed in [43,50,57,58]. The theoretical analysis of planar chiral lattices is compared with experimental results in [59].

A schematic description of chiral transformations and changes of the number of symmetry groups from higher dimensions (macroscale chiral layers) to lower dimensions (molecules of chiral line structure) is outlined in [60], backed by various experimental results. Further developments in three-dimensional chiral structures can be found in [61–63].

Let us begin with an immediate observation regarding the rotational field in line of our interests. In three-dimensional space it is in general non-Abelian, while it may become Abelian group structure in lower dimensions. So, a certain loss of information is expected when projecting to lower dimensional space.

In this Chapter, we will construct a new geometrically nonlinear energy term which is explicitly chiral in three dimensions, and which does not lose this character when applied to the planar problem. This will shed light in understanding the genuine property of energy terms which gives rise to chirality in various models.

We would like to introduce the so-called first planar Cosserat problem briefly here. The displacement vector is given by $\boldsymbol{u} = (u_1, u_2, 0)$ while planar rotations are described by a rotation axis $\boldsymbol{n} = (0, 0, n_3)$. Then the dislocation density tensor (2.1.5) defined by

$$\overline{K} = \overline{R}^T \operatorname{Curl} \overline{R}$$

is nonzero. Since the microrotations are described by the orthogonal matrix $\overline{R} \in SO(3)$, it does contain a 2×2 zero block matrix in the planar indices. This induces several orthogonal relations, for example, with the first Cosserat deformation tensor $\tilde{U} = \overline{R}^T F$, which makes it impossible to construct coupling terms in the energy which do not vanish identically in the plane, see the detailed discussions in [24,64].

Let us illustrate a simple example regarding chirality in three dimensions which can be translated into two dimensions. In Fig. 3.1, two chiral dice are given which cannot be $SO(3)$-rotated to superimpose onto each other in three dimensions on the top, and two chiral hexagons are given which again cannot be $SO(2)$-rotated to superimpose onto each other in two dimensions on the bottom. In the middle, there are two specific procedures to preserve the chirality from three dimensions when projected to two dimensions. One of them is the way of labelling the number of dots on the chiral dice to be projected to the chiral hexagon, and another is to specify the choice of perspective.

This example suggests, at least at an intuitive level, that one can construct a three-dimensional chiral structure and a projection, such that the resulting two-dimensional structure inherits the chirality in a certain way. However we must note that if we had a different way of labelling dots on the chiral dice or with a different choice of perspective, we would not find a chiral hexagon on the plane. In other words, the chirality preservation through the projection into the lower-dimensional space depends critically on its construction.

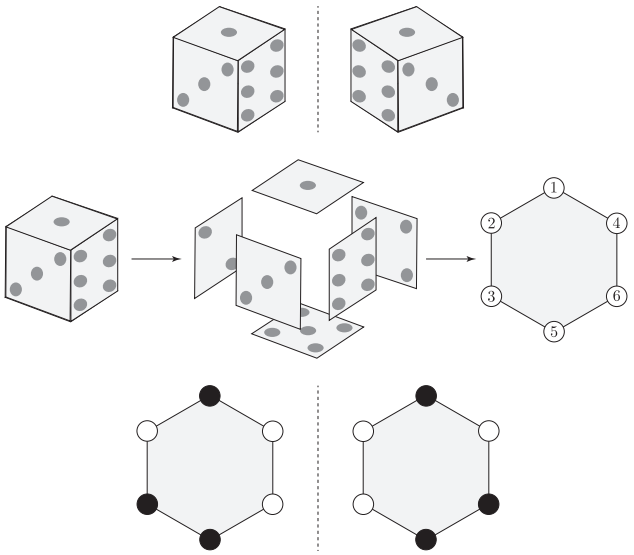

Figure 3.1: We project the image of a chiral dice into a two-dimensional plane along with a particular point of view to obtain a regular hexagon with numbered balls on its vertices, where the numbers are exactly in the order as printed on the given die. Further, we map even numbers into white balls and odd numbers into black balls. We get a chiral hexagonal two-dimensional structure.

3.2 Construction of chirality in deformational measures

We state our definition of chirality formally, and its application to the deformation gradient tensor and the dislocation density tensor. First, we define a coordinate-inversion operator # that acts on a function $\varphi = \varphi(x, y, z)$,

$$\varphi^{\#}(x, y, z) = \varphi(-x, -y, -z) \; . \tag{3.2.1}$$

This means we evaluate the function φ at the inverted coordinates $(-x, -y, -z)$. On the deformation gradient tensor this operator acts as

$$F^{\#} = (\nabla\varphi)^{\#} = -\nabla\varphi(-x, -y, -z) = -F(-x, -y, -z) \; . \tag{3.2.2}$$

i.e. under the operator #, F picks up the negative sign at the inverted coordinates.

The stretch part of F defined by $U = \sqrt{F^T F}$, in the polar decomposition, is invariant under # since

$$U^{\#} = \sqrt{(F^T F)^{\#}} = \sqrt{(F^T)^{\#} \, F^{\#}} = \sqrt{F^T F} = U \; . \tag{3.2.3}$$

We note that the operation #, when acting on a product of matrices, does not reverse the order of the multiplication, unlike for example the transpose operation $(AB)^T = B^T A^T$.

On the other hand, to see the action of the operator # on the polar part of F, $\mathrm{polar}(F) = R$, we consider the action on the polar decomposition of F,

$$F^{\#} = (R\,U)^{\#} = R^{\#}\, U^{\#} = R^{\#}\, U = -F(-x, -y, -z) \; . \tag{3.2.4}$$

This implies that the orthogonal matrix $R = \mathrm{polar}(F)$ transforms under # as

$$R^{\#}(x, y, z) = -R(-x, -y, -z) \tag{3.2.5}$$

in complete analogy to the transformation of F. Consequently,

$$(R^{\#})^T = -R^T(-x, -y, -z) = (R^T)^{\#} \; , \tag{3.2.6}$$

which means that F (or F^T) and its polar part R (or R^T) transform in the same way under $\#$.

There is a deep meaning of acquiring the additional minus sign when one applies the inversion $\#$ to the rotation, in particular, if one takes the rotation R such as (2.2.1) with a fixed rotational axis. For example, if we consider the general rotational representation (1.2.31), the transformation properties of a general rotational matrix under inversion can be understood quite naturally. Consider the transformation from the reference configuration X_L to the spatial configuration $x_i = R_{iL}X_L$ by a rotation

$$R_{iL} = \delta_{iL}\cos\phi + \epsilon_{ijL}n_j\sin\phi + (1-\cos\phi)n_i n_L \tag{3.2.7}$$

where n_i is an axis of rotation and ϕ is a rotational angle in spatial configuration. n_L is an axial vector in the reference configuration. Then applying the inversion operator $\#$ gives

$$R^{\#}_{iL} = -\delta_{iL}\cos\phi - \epsilon_{ijL}n_j\sin\phi - (1-\cos\phi)n_i n_L \ , \tag{3.2.8}$$

in which δ_{iL} acquires a negative sign in the spatial configuration, and n_i changes its direction under the inverted coordinates but n_L remains unaffected in the reference configuration. This agrees with result (3.2.5). More generally speaking, for $R \in O(3)$, we have $\det R = \pm 1$ and we can write

$$R = s\, e^A \ , \qquad \det R = \begin{cases} +1 & \text{if } s = +1 \ , \\ -1 & \text{if } s = -1 \ , \end{cases} \tag{3.2.9}$$

where A is a 3×3 skew-symmetric matrix. This classification identifies the relation between $R \in SO(3)$ and its chiral counterpart $R^{\#}$. If $\det R = +1$ we have $\det R^{\#} = -1$, and vice versa. We note that these arguments are valid not only in case of macrorotations, but also in microrotations in which the relations are defined by (1.2.25) in terms of directors.

On an equal footing, the deformation gradient tensor is defined by $F_{iR} = \frac{\partial x_i}{\partial X_R}$ for $x_i = X_i + u_i(X_k)$, and applying the operator $\#$ gives

$$F^{\#}_{iR} = \frac{\partial(-x_i)}{\partial X_R} = -F_{iR} \ , \tag{3.2.10}$$

also in agreement with (3.2.4).

Now, consider the operation Curl of (2.1.4) on $R^{\#}$,

$$(\mathrm{Curl}\, R^{\#})_{ij} = \epsilon_{jkl}\partial_k R^{\#}_{il} \ . \tag{3.2.11}$$

It is easy to observe that each partial derivative gives additional minus signs to the matrix elements of $R^{\#}$ using the chain rule, for instance

$$\partial_y R^{\#} = -\partial_y R(-x,-y,-z) = \partial_{-y} R(-x,-y,-z) = (\partial_y R)(-x,-y,-z) \tag{3.2.12}$$

so that the partial derivative of R with respect to y is evaluated in the usual Cartesian coordinates, but the quantity $\partial_y R$ is viewed in the inverted coordinate system $(-x,-y,-z)$. Then

$$\mathrm{Curl}\,(R^{\#})(x,y,z) = (\mathrm{Curl}\, R)(-x,-y,-z) \ . \tag{3.2.13}$$

Hence, we see that the operator Curl negates the minus sign obtained when $\#$ is acted on R. But we can easily construct a deformational measure which transforms like (3.2.4). The dislocation density tensor is such an example, satisfying

$$(R^T \mathrm{Curl}\, R)^{\#} = (R^{\#})^T \mathrm{Curl}\, R^{\#} = -(R^T \mathrm{Curl}\, R)(-x,-y,-z) \ . \tag{3.2.14}$$

It is no coincidence that the dislocation density tensor is exactly of this form. Clearly, we will arrive at the same conclusions for $\overline{R} = \mathrm{polar}(\overline{F})$ and $\overline{F} \in GL(3;\mathbb{R})$

$$\overline{F}^{\#}(x,y,z) = -\overline{F}(-x,-y,-z)\ , \tag{3.2.15a}$$

$$\overline{R}^{\#}(x,y,z) = -\overline{R}(-x,-y,-z)\ , \tag{3.2.15b}$$

$$\overline{K}^{\#} = (\overline{R}^T \operatorname{Curl} \overline{R})^{\#}(x,y,z) = -(\overline{R}^T \operatorname{Curl} \overline{R})(-x,-y,-z) = -\overline{K}\ . \tag{3.2.15c}$$

In this way, we would like to investigate some frequently appearing matrix quantities in the Cosserat elasticity energy functional, accompanied by conventional matrix operations such as transpose, trace or Frobenius scalar product. We will see whether they are chiral or not. This will lead to a simple combination of products which yields a chiral energy functional.

3.3 Constructing chiral energy functionals

We show the construction of one possible chiral term which can form the building blocks in constructing a multitude of other chiral terms. In searching for a generic objective [65] and chiral term for a chiral energy functional, we begin by recalling objectivity.

We call an energy functional objective if it is invariant under the left-action of global rotations Q with $\det Q = +1$, here $Q \in SO(3)$ is a constant position-independent orthogonal matrix. Under the global rotation of Q on F and $\overline{R}$, respectively, we have

$$F = RU \longrightarrow QF = QRU \qquad \text{and} \qquad \overline{R} \longrightarrow Q\overline{R}\ . \tag{3.3.1}$$

It is easy to verify that the dislocation density tensor $\overline{K}$ is objective, under the global rotation Q acting on $\overline{R}$

$$\overline{K} = \overline{R}^T \operatorname{Curl} \overline{R} \longrightarrow (Q\overline{R})^T \operatorname{Curl} (Q\overline{R}) = \overline{R}^T Q^T Q \operatorname{Curl} \overline{R} = \overline{K}\ . \tag{3.3.2}$$

Therefore, $\overline{K}$ is objective and also chiral quantity due to (3.2.15c).

These observations allow us to construct two additional terms which are both objective and chiral quantities from which we wish to use in constructing the chiral energy term, namely

$$L = R^T \operatorname{Curl} \overline{R} \qquad \text{and} \qquad M = \overline{R}^T \operatorname{Curl} R\ . \tag{3.3.3}$$

Here, again, R is the orthogonal part of the polar decomposition, while $\overline{R}$ is the microrotation. In principle one could also consider the term $K = R^T \operatorname{Curl} R$.

Now, we have a set of chiral and objective terms at our disposal

$$\{\overline{K}, K, L, M, \overline{K}^T, K^T, L^T, M^T, \cdots\}\ , \tag{3.3.4}$$

from which we can construct a chiral energy functional. We note that a product of an odd number of chiral terms is required to preserve chirality.

In addition to the notion of objectivity, an energy functional is hemitropic if it is invariant under right-action of global rotations excluding inversions, i.e. right-invariant under the elements of $SO(3)$ [65]. In particular, the invariance under the right-action of $O(3)$ is called isotropy. Considering the (right) rotation $Q_2 \in SO(3)$, we find that F and $\overline{R}$ transform as

$$F = RU \longrightarrow RQ_2U \qquad \text{and} \qquad \overline{R} \longrightarrow \overline{R}Q_2\ . \tag{3.3.5}$$

This implies the following property

$$\overline{K} = \overline{R}^T \operatorname{Curl} \overline{R} \longrightarrow (\overline{R}Q_2)^T \operatorname{Curl} (\overline{R}Q_2) = Q_2^T \overline{R}^T \operatorname{Curl} \overline{R}Q_2 = Q_2^T \overline{K} Q_2\ . \tag{3.3.6}$$

Likewise, we find

$$\begin{aligned} L = R^T \operatorname{Curl} \overline{R} &\longrightarrow (RQ_2)^T \operatorname{Curl} \overline{R} Q_2 = Q_2^T L Q_2 \ , \\ M = \overline{R}^T \operatorname{Curl} R &\longrightarrow (\overline{R}Q_2)^T \operatorname{Curl} R Q_2 = Q_2^T M Q_2 \ . \end{aligned} \tag{3.3.7}$$

Finally, we consider the energy functional

$$V_\chi = \chi \operatorname{tr}\left(\overline{K}\ \overline{K}\ \overline{K}\right) \ , \qquad \chi \in \mathbb{R} \ . \tag{3.3.8}$$

We note its three main properties as follows.

1. $\overline{K}$ is invariant under the left action of $SO(3)$, hence V_χ is invariant under the left action of $SO(3)$, thus it is objective.
2. $\overline{K}$ is chiral, V_χ is odd in $\overline{K}$ and hence V_χ is chiral, $V_\chi^\# = -V_\chi$.
3. V_χ is invariant under the right action of $SO(3)$, so it is hemitropic. This is because

   $$V_\chi = \chi \operatorname{tr}\left(\overline{K}\ \overline{K}\ \overline{K}\right) \longrightarrow \chi \operatorname{tr}\left(Q_2^T \overline{K} Q_2 Q_2^T \overline{K} Q_2 Q_2^T \overline{K} Q_2\right) = \chi \operatorname{tr}\left(Q_2^T \overline{K}\ \overline{K}\ \overline{K} Q_2\right) = V_\chi \ ,$$

   due to the cyclic property of the trace.

This means V_χ is objective, hemitropic and chiral. Clearly, following the same approach, one can consider similarly structured terms based on cubic combinations of $\overline{K}$, L and M. For the sake of simplicity, we will focus on the easiest of these terms.

3.4 Variations of a chiral equation

The chiral energy term V_χ is by no means guaranteed to lead to a non-vanishing contribution to the equations of motion when the planar problem is considered. However, it will turn out to produce the necessary terms to preserve planar chirality. In the following we will define an energy functional from which we will derive equations of motions. After constructing an explicit solution, we will discuss the chiral properties of the solution.

Let us begin by defining the total energy functional now including a chiral term V_χ of the form (3.3.8) for the Cosserat material which is given by

$$V = V_{\text{elastic}}(F, \overline{R}) + V_{\text{curvature}}(\overline{R}) + V_\chi(\overline{R}) - V_{\text{kinetic}}(\mathbf{u}, \overline{R}) \ , \tag{3.4.1}$$

where the individual terms are

$$V_{\text{elastic}}(F, \overline{R}) = \mu \left\| \operatorname{sym}(\overline{R}^T F - \mathbb{1}) \right\|^2 + \frac{\lambda}{2} \left[\operatorname{tr}\left(\operatorname{sym}(\overline{R}^T F - \mathbb{1}) \right) \right]^2 \tag{3.4.2a}$$

$$V_{\text{curvature}}(\overline{R}) = \kappa_1 \left\| \operatorname{dev} \operatorname{sym}(\overline{R}^T \operatorname{Curl} \overline{R}) \right\|^2 + \kappa_2 \left\| \operatorname{skew}(\overline{R}^T \operatorname{Curl} \overline{R}) \right\|^2 + \kappa_3 \left[\operatorname{tr}(\overline{R}^T \operatorname{Curl} \overline{R}) \right]^2 \tag{3.4.2b}$$

$$V_\chi(\overline{R}) = \chi \operatorname{tr}\left(\overline{K}\ \overline{K}\ \overline{K}\right) \tag{3.4.2c}$$

$$V_{\text{kinetic}} = \frac{1}{2} \rho \|\dot{\mathbf{u}}\|^2 + \rho_{\text{rot}} \|\dot{\overline{R}}\|^2 \ . \tag{3.4.2d}$$

Following the results from Chapter 2, the variation of the total energy functional

$$\delta V = \delta V_{\text{elastic}}(F, \overline{R}) + \delta V_{\text{curvature}}(\overline{R}) + \delta V_\chi(\overline{R}) - \delta V_{\text{kinetic}}(\mathbf{u}, \overline{R}) \tag{3.4.3}$$

will lead to the equations of motion by collecting corresponding terms of $\delta\overline{R}$ and δF separately. The detailed calculations for varying functionals V_{elastic} and $V_{\text{curvature}}$ are given in Appendix A. The variation of V_χ can also be found in Appendix A and we write these variational terms,

$$\delta V_{\text{elastic}}(F,\overline{R}) = \Big[\mu(\overline{R}F^T\overline{R}+F) - (2\mu+3\lambda)\overline{R} + \lambda\text{tr}(\overline{R}^TF)\overline{R}\Big] : \delta F + \Big[\mu F\overline{R}^TF - (2\mu+3\lambda)F + \lambda\text{tr}(\overline{R}^TF)F\Big] : \delta\overline{R} + \rho\ddot{u}\,\delta u \tag{3.4.4a}$$

$$\delta V_{\text{curvature}}(\overline{R}) = \Big[(\kappa_1-\kappa_2)\Big((\text{Curl}\,\overline{R})\overline{R}^T(\text{Curl}\,(\overline{R})) + \text{Curl}\,\Big[\overline{R}(\text{Curl}\,\overline{R})^T\overline{R}\Big]\Big) + (\kappa_1+\kappa_2)\text{Curl}\,\Big[\text{Curl}\,\overline{R}\Big] - \Big(\frac{\kappa_1}{3}-\kappa_3\Big)\Big(4\text{tr}(\overline{R}^T\text{Curl}\,\overline{R})\text{Curl}\,(\overline{R}) - 2\overline{R}\Big(\text{grad}\,\Big(\text{tr}[\overline{R}^T\text{Curl}\,\overline{R}]\Big)\Big)^\star + 2\rho_{\text{rot}}\ddot{\overline{R}}\Big] : \delta\overline{R} \tag{3.4.4b}$$

$$\delta V_\chi = 3\chi\Big[(\text{Curl}\,\overline{R})(\overline{K}^2) + \text{Curl}\,[\overline{R}(\overline{K}^2)^T]\Big] : \delta\overline{R}\,. \tag{3.4.4c}$$

Collecting δF terms gives 3×3 matrix $\boldsymbol{A}$

$$\mu(\overline{R}F^T\overline{R}+F) - (2\mu+3\lambda)\overline{R} + \lambda\text{tr}(\overline{R}^TF)\overline{R} = \boldsymbol{A}\,. \tag{3.4.5}$$

As we did in Chapter 2, the δF terms are evaluated using the fact

$$\boldsymbol{A} : \delta F = A_{ij}\delta F_{ij} \longrightarrow -\partial_j A_{ij}\delta u_i = -\left(\partial_1 A_{31} + \partial_2 A_{32} + \partial_3 A_{33}\right)\delta\psi\,,$$

for any matrix $\boldsymbol{A}$, where a total derivative term was neglected.

Likewise, collecting $\delta\overline{R}$ terms from these variations can be summarised to a single matrix $\boldsymbol{B}$ as shown in the following

$$\begin{aligned}3\chi\Big[(\text{Curl}\,\overline{R})(\overline{K}^2) + \text{Curl}\,[\overline{R}(\overline{K}^2)^T]\Big] + \mu F\overline{R}^TF - \Big(2\mu+3\lambda\Big)F + \lambda\text{tr}(\overline{R}^TF)F \\ + (\kappa_1-\kappa_2)\Big((\text{Curl}\,\overline{R})\overline{R}^T(\text{Curl}\,(\overline{R})) + \text{Curl}\,\Big[\overline{R}(\text{Curl}\,\overline{R})^T\overline{R}\Big]\Big) \\ + (\kappa_1+\kappa_2)\text{Curl}\,\Big[\text{Curl}\,\overline{R}\Big] - \Big(\frac{\kappa_1}{3}-\kappa_3\Big)\Big(4\text{tr}(\overline{R}^T\text{Curl}\,\overline{R})\text{Curl}\,(\overline{R}) \\ - 2\overline{R}\Big[\text{grad}\Big(\text{tr}[\overline{R}^T\text{Curl}\,\overline{R}]\Big)\Big]^\star\Big) + 2\rho_{\text{rot}}\ddot{\overline{R}} = \boldsymbol{B}\,.\end{aligned} \tag{3.4.6}$$

3.5 Equations of motion and solutions

Now we are in position to state explicitly the dynamic equations of motion in the plane, and show that chirality does not vanish. We then solve those equations and explain their chiral structure. In order to study the equations of motion in the plane, we will make the following identical assumptions we used in Chapter 2. These are

1. Material points can only experience rotations about one axis, say the z-axis.
2. Displacements occur along this axis of rotation.
3. Elastic displacement waves and microrotational waves are both longitudinal, and propagate with the same constant wave speed v.

Consequently, the microrotation matrix, the displacement vector and deformation gradient tensor are exactly identical to (2.2.1) and (2.2.4). This implies $F = U$ and $\text{polar}(F) = R = \mathbb{1}$.

And from these, we can write the explicit forms of the dislocation density tensor $\overline{K}$ defined by $\overline{K} = \overline{R}^T \operatorname{Curl} \overline{R}$,

$$\overline{K} = \begin{pmatrix} \partial_z\phi & 0 & 0 \\ 0 & \partial_z\phi & 0 \\ 0 & 0 & 0 \end{pmatrix} . \tag{3.5.1}$$

Now, under these assumptions, only the A_{33} contributes in the δF term, which is given by

$$A_{33} = 2\lambda(\cos\phi - 1) + (\lambda + 2\mu)\partial_z\psi \, . \tag{3.5.2}$$

This gives the equation of motion of ψ,

$$\rho\partial_{tt}\psi + 2\lambda \sin\phi \, \partial_z\phi - (\lambda + 2\mu)\partial_{zz}\psi = 0 \, . \tag{3.5.3}$$

On the other hand, the quantity $\mathbf{B} : \delta\overline{R}$ becomes

$$\begin{aligned} \mathbf{B} : \delta\overline{R} = \operatorname{tr}[B^T\delta\overline{R}] &= \operatorname{tr}\left[\begin{pmatrix} B_{11} & -B_{12} & 0 \\ B_{12} & B_{11} & 0 \\ 0 & 0 & B_{33} \end{pmatrix}\begin{pmatrix} -\sin\phi & -\cos\phi & 0 \\ \cos\phi & -\sin\phi & 0 \\ 0 & 0 & 0 \end{pmatrix}\right]\delta\phi \\ &= -(2B_{11}\sin\phi + 2B_{12}\cos\phi)\delta\phi \, . \end{aligned} \tag{3.5.4}$$

The required components of $\boldsymbol{B}$ are given by

$$\begin{aligned} B_{11} = -2(\lambda+\mu) + \frac{1}{3}\cos\phi\Big[3(2\lambda+\mu) - 6\rho_{\mathrm{rot}}(\partial_t\phi)^2 + (\partial_z\phi)^2(\kappa_1 - 3\kappa_2 + 24\kappa_3 + 18\chi\partial_z\phi)\Big] \\ + \lambda\partial_z\psi + \frac{2}{3}\sin\phi\Big[-3\rho_{\mathrm{rot}}\partial_{tt}\phi + (\kappa_1 + 6\kappa_3 + 9\chi\partial_z\phi)\partial_{zz}\phi\Big] \, , \end{aligned} \tag{3.5.5a}$$

$$\begin{aligned} B_{12} = \frac{1}{3}\sin\phi\Big[(3\mu + 6\rho_{\mathrm{rot}}(\partial_t\phi)^2 - (\partial_z\phi)^2(\kappa_1 - 3\kappa_2 + 24\kappa_3 + 18\chi\partial_z\phi)\Big] \\ + \frac{2}{3}\cos\phi\Big[-3\rho_{\mathrm{rot}}\partial_{tt}\phi + (\kappa_1 + 6\kappa_3 + 9\chi\partial_z\phi)\partial_{zz}\phi\Big] \, . \end{aligned} \tag{3.5.5b}$$

Putting everything together gives the equation of motion for ϕ, together with the previous equation for ψ of (3.5.3). This coupled system of equations is given by

$$\rho_{\mathrm{rot}}\,\partial_{tt}\phi - \left(\frac{\kappa_1 + 6\kappa_3}{3}\right)\partial_{zz}\phi - 3\chi\partial_z\phi\,\partial_{zz}\phi + (\lambda+\mu)(1-\cos\phi)\sin\phi - \frac{\lambda}{2}\sin\phi\,\partial_z\psi = 0 \, , \tag{3.5.6a}$$

$$\rho\,\partial_{tt}\psi + 2\lambda\sin\phi\,\partial_z\phi - (\lambda+2\mu)\partial_{zz}\psi = 0 \, . \tag{3.5.6b}$$

Now, we seek solutions of the form $\phi = f(z - vt)$ and $\psi = g(z - vt)$, where v is the same wave speed for both the elastic and the rotational wave propagation according to our assumptions. This means they both satisfy the wave equations

$$\partial_{tt}f = v^2\partial_{zz}f \qquad \text{and} \qquad \partial_{tt}g = v^2\partial_{zz}g \, .$$

We introduce a new variable $s = z - vt$, and denote the differentiation with respect to s by a prime. Putting this ansatz into the equation of motion of ψ (3.5.5b) gives

$$\rho v^2 g'' + 2\lambda\sin(f)f' - (\lambda+2\mu)g'' = 0 \, ,$$

which can be rewritten by

$$(\rho v^2 - (\lambda+2\mu))g'' - 2\lambda\sin(f)f' = 2\lambda\frac{d}{ds}(\cos(f)) \, . \tag{3.5.7}$$

Since it is reduced to a second-order ordinary differential equation, we can now integrate with respect to s which gives

$$g' = \frac{2\lambda}{\rho v^2 - (\lambda + 2\mu)} \cos(f) + C_1 \ , \tag{3.5.8}$$

for some constant of integration C_1. Since $\partial_z \psi = g'$ we can now eliminate this term from the equation of motion (3.5.6a) which becomes

$$\begin{aligned} \rho_{\text{rot}} v^2 f'' - \left(\frac{\kappa_1 + 6\kappa_3}{3}\right) f'' - 3\chi f' f'' + (\lambda + \mu)(1 - \cos\phi)\sin\phi \\ - \frac{\lambda}{2}\sin(f)\left(\frac{2\lambda}{\rho v^2 - (\lambda + 2\mu)}\cos(f) + C_1\right) = 0 \ . \end{aligned} \tag{3.5.9}$$

After rearranging terms, this can be rewritten as follows

$$\begin{aligned} \rho_{\text{rot}} v^2 f'' - \left(\frac{\kappa_1 + 6\kappa_3}{3}\right) f'' - 3\chi f' f'' + \left[(\lambda + \mu) - \frac{\lambda}{2} C_1\right]\sin(f) \\ - \frac{1}{2}\left[(\lambda + \mu) + \frac{\lambda^2}{\rho v^2 - (\lambda + 2\mu)}\right]\sin(2f) = 0 \ . \end{aligned} \tag{3.5.10}$$

When setting $\chi = 0$, this becomes the double sine-Gordon equation, we saw in Chapter 2 for the soliton solution we constructed with the line of symmetry passes through the peak of the wave packet, hence non-chiral. However, with a nonzero chiral parameter χ, there is an additional contribution from the non-linearity of the form $\chi f' f''$, and this might give the desired result for the chirality in the solution.

3.6 Constructing approximate solutions

Inspection of equation (3.5.10) shows that each of these five terms can be integrated after the entire equation is multiplied by f'. This yields

$$\begin{aligned} \frac{1}{2}\left[\rho_{\text{rot}} v^2 - \left(\frac{\kappa_1 + 6\kappa_3}{3}\right)\right](f')^2 - \chi (f')^3 - \left[(\lambda + \mu) - \frac{\lambda}{2} C_1\right]\cos(f) \\ + \frac{1}{4}\left[(\lambda + \mu) + \frac{\lambda^2}{\rho v^2 - (\lambda + 2\mu)}\right]\cos(2f) = C_2 \ , \end{aligned} \tag{3.6.1}$$

where C_2 is another constant of integration. Formally, this is a cubic equation in f' (quadratic in f' if $\chi = 0$) which can, in principle, be solved for f' and will give three different solutions in general. The resulting equation is always of the general form $f' = H(f)$ and is hence separable.

- This means we have reduced finding a solution to our system of nonlinear wave equations (3.5.6a) and (3.5.6b) to an integration problem. Note that this solution depends on the eight parameters $\{v, \lambda, \mu, \rho, \kappa_1, \kappa_3, \rho_{\text{rot}}, \chi\}$ and two constants of integration C_1 and C_2. In general, these solutions will involve special functions if an explicit solution can be found.
- With nonzero chiral parameter χ, we cannot approach with the analytic method used in the double sine-Gordon equation. But we will construct an approximated solution to (3.6.1), using a suitable choice of the constants of integration.

The chiral parameter χ is assumed to be small so that a series expansion in this parameter can be made. We choose $C_1 = 2(\lambda + \mu)/\lambda$, put $\mathcal{F}(s) = 2f(s)$ and choose C_2 such that one can write

$$(\mathcal{F}')^2 - \tilde{\chi}(\mathcal{F}')^3 = 2\tilde{m}^2(1 - \cos(\mathcal{F})) \tag{3.6.2}$$

where the following constants are introduced

$$\tilde{\chi} = \frac{3\chi}{\rho_{\rm rot} v^2 - (\kappa_1 + 6\kappa_3)} \qquad \text{and} \qquad \tilde{m}^2 = \frac{3v^2\rho(\lambda+\mu) - 3\mu(3\lambda+2\mu)}{(\lambda+2\mu-v^2\rho)(\kappa_1+6\kappa_3-3v^2\rho_{\rm rot})} \,. \tag{3.6.3}$$

Now, to solve this, we use regular perturbation methods. First we write the function $\mathcal{F}(s)$ as a series expansion

$$\mathcal{F}(s) = \mathcal{F}_0(s) + \tilde{\chi}\mathcal{F}_1(s) + \tilde{\chi}^2\mathcal{F}_2(s) + \cdots \tag{3.6.4}$$

in the chiral parameter $\tilde{\chi}$ which we assume to be small $\tilde{\chi} \ll 1$. Further, we impose initial conditions followed by the periodicity of $\mathcal{F}(s) = 2f(s)$, and the resemblance from the previously obtained solution in (2.3.22), and the assumption of the dominant term in the expansion is the first term $\mathcal{F}_0(s)$,

$$\mathcal{F}(0) = \mathcal{F}_0(0) = \pi \qquad \text{and} \qquad \mathcal{F}_1(0) = \mathcal{F}_2(0) = \cdots = 0 \,. \tag{3.6.5}$$

Let us begin with the function $\mathcal{F}_0(s)$ which satisfies

$$\frac{d\mathcal{F}_0}{ds} = \pm\tilde{m}\sqrt{2[1-\cos(\mathcal{F}_0)]} \,, \tag{3.6.6}$$

the solution of which is well known

$$\mathcal{F}_0(s) = 4\arctan(e^{\pm\tilde{m}s}) \,. \tag{3.6.7}$$

Again, this is a pair of kink/antikink solutions. The deviation from this solution comes from the nonzero $\tilde{\chi}$ term, when we substitute $\mathcal{F}(s)$ into the equation of motion (3.6.2), and make a series expansion in $\tilde{\chi}$ up to the first order to obtain

$$-(\mathcal{F}_0')^3 - 2\tilde{m}^2\sin(\mathcal{F}_0)\,\mathcal{F}_1 + 2\,\mathcal{F}_0'\,\mathcal{F}_1' = 0 \,, \tag{3.6.8}$$

where

$$\mathcal{F}_0' = 2\tilde{m}\,\mathrm{sech}(\tilde{m}s) = 2\,\frac{\tilde{m}}{\cosh(\tilde{m}s)} = 4\,\frac{\tilde{m}}{e^{\tilde{m}s}+e^{-\tilde{m}s}}$$

follows from (3.6.7). With the initial condition $\mathcal{F}_1(0) = 0$, we obtain

$$\mathcal{F}_1(s) = \tilde{m}\,\mathrm{sech}(\tilde{m}s)\Big(4\arctan(e^{\tilde{m}s}) - \pi\Big) = \frac{1}{2}\mathcal{F}_0'(\mathcal{F}_0 - \pi) \,, \tag{3.6.9}$$

which gives the first order solution

$$\mathcal{F}(s) = 4\arctan(e^{\tilde{m}s}) + \tilde{\chi}\tilde{m}\,\mathrm{sech}(\tilde{m}s)\Big(4\arctan(e^{\tilde{m}s}) - \pi\Big) \,. \tag{3.6.10}$$

Using similar perturbative expansion, one can obtain the second order $\mathcal{F}_2(s)$ satisfying

$$-\tilde{m}^2\cos(\mathcal{F}_0)(\mathcal{F}_1)^2 - 2\tilde{m}^2\sin(\mathcal{F}_0)\mathcal{F}_2 - 3(\mathcal{F}_0')^2\mathcal{F}_1' + (\mathcal{F}_1')^2 + 2\mathcal{F}_0'\,\mathcal{F}_2' = 0 \,. \tag{3.6.11}$$

This depends on the lower order solutions $\mathcal{F}_0$ and $\mathcal{F}_1$. We can solve this by using the already obtained results for $\mathcal{F}_0$ and $\mathcal{F}_1$, with the initial condition $\mathcal{F}_2(0) = 0$. The solution is given by

$$\mathcal{F}_2(s) = \frac{1}{8}\mathcal{F}_0''\left[\left(\mathcal{F}_0 + \frac{(\mathcal{F}_0')^2}{\mathcal{F}_0''} - \pi\right)^2 - \left(\frac{(\mathcal{F}_0')^2}{\mathcal{F}_0''}\right)^2 - 12\right] \,. \tag{3.6.12}$$

Following the identical boundary condition under the elastic base (2.3.4), for all time t we have

$$\phi(\pm\infty, t) = 0 \qquad \text{and} \qquad \partial_z\phi(\pm\infty, t) = 0 \,.$$

To incorporate these boundary conditions, the kink and antikink solutions (3.6.7) are readily applicable. So, we can redefine $\mathcal{F}_0(s)$ as follows

$$\mathcal{F}_0(s) = \begin{cases} 4\arctan(e^{+\tilde{m}s}) & \text{if } s < 0\,, \\ 4\arctan(e^{-\tilde{m}s}) & \text{if } s > 0\,. \end{cases} \tag{3.6.13}$$

Next, we can apply the same reasoning to the first order contribution (3.6.9). We note that the solution $\mathcal{F}_1(s)$ is invariant under the change $\tilde{m} \to -\tilde{m}$, which is the equivalent to $s \to -s$ in this case. This is clear from (3.6.9) using the identity $\arctan(x^{-1}) = \pi/2 - \arctan(x)$.

Now, putting back $s = z - vt$ and $\phi(z,t) = f(z-vt) = \mathcal{F}/2$, and using (3.6.10), the first order solution for $\phi(z,t)$ becomes

$$\phi(z,t) = \begin{cases} 2\arctan(e^{+\tilde{m}(z-vt)}) + \frac{\tilde{\chi}\tilde{m}}{2}\mathrm{sech}(\tilde{m}(z-vt))(4\arctan(e^{\tilde{m}(z-vt)}) - \pi) & \text{if } z < v\,t\,, \\ 2\arctan(e^{-\tilde{m}(z-vt)}) + \frac{\tilde{\chi}\tilde{m}}{2}\mathrm{sech}(\tilde{m}(z-vt))(4\arctan(e^{\tilde{m}(z-vt)}) - \pi) & \text{if } z > v\,t\,. \end{cases} \tag{3.6.14}$$

The solution constructed in this way gives rise to a localised wave which propagates along the z-axis. The amplitude decreases exponentially such that the material recovers its original shape once the wave passes through, which is the boundary condition we imposed in Chapter 2 in the framework of the elasticity, see Fig. 3.2.

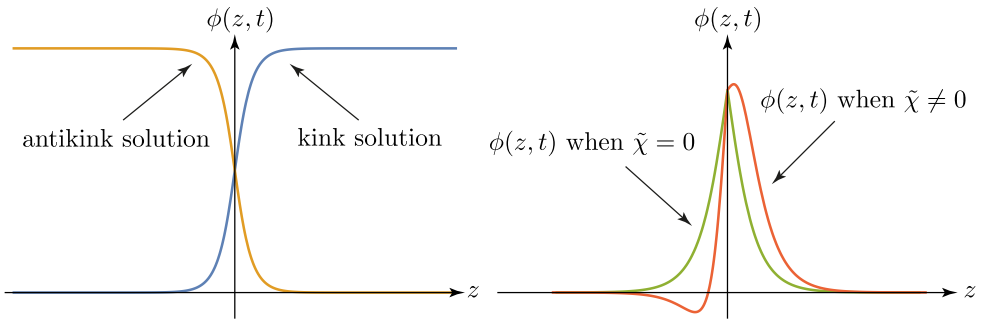

Figure 3.2: Left panel: The kink and antikink solutions obtained in (3.6.10) are shown at $t = 0$, indicating the asymptotic behaviours of $\phi_{\text{kink}}(+\infty, t)$ and $\phi_{\text{antikink}}(-\infty, t)$. Right panel: The piece-wise definition (3.6.14) of $\phi(z,t)$ is shown for $\tilde{\chi} = 0$ and $\tilde{\chi} \neq 0$.

If we apply the inversion operator to (3.5.10), it will yield a new equation of motion where $\phi(z,t)$ is replaced by $\phi^{\#}(z,t) = \phi(-z,t)$. Then the χ term in (3.5.10) acquires an additional minus sign due to the presence of three derivatives with respect to z, one second derivative and one first derivative. This results in

$$\begin{aligned} \left[\rho_{\text{rot}} v^2 - \left(\frac{\kappa_1 + 6\kappa_3}{3}\right)\right]\partial_{zz}\phi^{\#} + 3\chi\partial_z\phi^{\#}\partial_{zz}\phi^{\#} + \left[(\lambda+\mu) - \frac{\lambda}{2}C_1\right]\sin(\phi^{\#}) \\ - \frac{1}{2}\left[(\lambda+\mu) + \frac{\lambda^2}{\rho v^2 - (\lambda+2\mu)}\right]\sin(2\phi^{\#}) = 0\,. \end{aligned} \tag{3.6.15}$$

This is precisely the equation of motion we would have obtained if we have started with the total energy of $V_\chi^{\#}$. At first sight, it is not straightforward to see that (3.6.15) is the chiral counterpart of (3.5.10) other than the sign change of the χ term. However, first of all, the wave speeds for both wave equations are identical and, formally, we will arrive at the same solution, as it should be.

We know from $\phi^{\#}(z,t) = \phi(-z,t)$ that the solution to one equation gives the solution to the other by a reflection. In other words, the wave solution of (3.5.10) will be the right-moving

wave while the solution of (3.6.15) describes the left-moving wave. Also we note that $\phi(z,t)$ is an even function if $\chi = 0$ while this is not the case when $\chi \neq 0$ as expected.

Furthermore, the left-moving wave will be governed by the rotation matrix $\overline{R}^{\#} = -\overline{R}$ with respect to the inverted axis $-z$. Hence the orientations of left-moving wave and right-moving wave for the material elements, which experience microrotations in xy-plane, are identical but reflected. Therefore, we can conclude that two wave solutions are chiral to each other. The right-moving waves rotates anti-clockwise while the left-moving one rotates clockwise.

We emphasise that this inversion operation on $\overline{R}$ only takes effect on the terms coupled to the chiral part. Specifically, only the chiral energy $V_\chi(\overline{R})$ is responsible for generating the chiral counterpart $\overline{R}^{\#}$ while the other energy functional terms are invariant under this inversion operation. This is also evident from the variation with respect to $\delta\overline{R}$. Consequently, the chiral coupled term in the equation of motion and its solutions experience the effects of the inversion operation on the rotational matrix as the wave propagate along the axes. The travelling wave solutions are shown in Fig. 3.3.

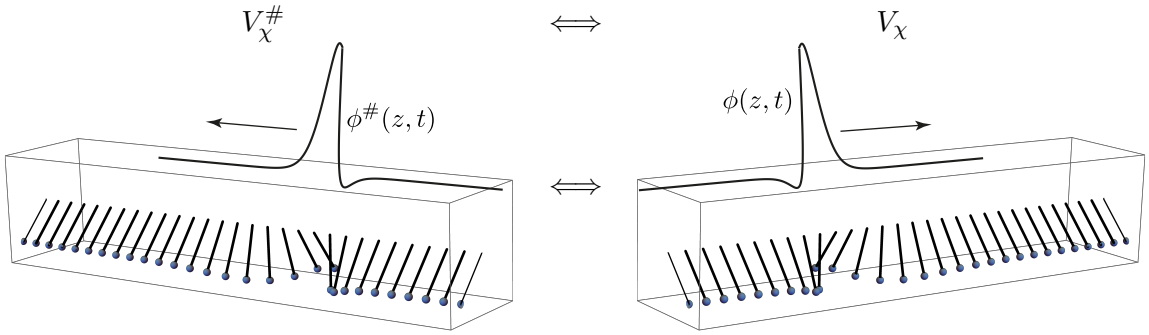

Figure 3.3: In analogy with Fig. 2.2, this shows the rotational deformations governed by the micro-rotation occurring on the xy-plane the material elements, modelled by pendulums as the deformational waves propagate. The right-moving wave along the z-axis corresponds to the chiral energy V_χ (right panel). On the other hand, the left-moving wave gives the same rotational defects resulted from $V_\chi^{\#}$ as it propagates to the left (left panel). We set $\tilde{\chi} = 0.6$ and $\tilde{m} = 2$.

We started by defining the inversion operator # in three-dimensional space to define what is meant by chirality. In words, an energy term which acquires an additional minus sign when evaluated in the inverted coordinates. By recognising the fact that it is possible to construct chiral terms, which are objective and hemitropic, we suggested various chiral energy functionals and formulated a total energy functional. This consisted of elastic energy functionals accompanied by a chiral term. This chiral term will appear again in Section 8.4 when we consider the theory of defects of liquid crystals under the free energy expansion formalism.

An interesting question to consider in general is whether the chiral energy V_χ should change its sign under inversions or not. If it does, as we assumed in the above, one of the two chiral states has a lower energy state than the other. Consequently one of the two chiral states is favoured energetically. This is somewhat at odds with the fact that simple chiral molecules appear in equal proportion in chemical experiments. On the other hand, there are also known examples [41] where the chiral counterpart is unstable, hence justifying a lower energy for one of the two states.

Our proposed model is able to take into account both setups by simply setting either $\chi^{\#} = \chi$ or $\chi^{\#} = -\chi$. The case $\chi^{\#} = \chi$ corresponds to the chiral counterparts having a different energy states, hence it will be useful in modelling a system where one of chiral states is favoured in terms of energy stability. When working with $\chi^{\#} = -\chi$, the energy of both chiral states is

identical. Our solution is suitable for both types of models as the value of the chiral parameter only affects the shape of the localised solution, but does not change any of the interpretation.

Part II

Defects in Riemann-Cartan manifolds

Chapter 4

Background and motivation

4.1 Differential geometry and elasticity

In continuum physics, there are two distinct measures of defects, called disclination and dislocation. In this Chaper, we will see that these measures are related to curvature and torsion, respectively. These defect measures can be detected due to the broken symmetries, for example, in Bravais lattices, the idealised approximation of crystalline. When defects are detected, these can be explained by the broken rotational symmetries caused by the disclination, and the broken translational symmetries caused by the dislocation [66–69].

In general relativity, the notion of curvature has been the main ingredient in describing deformed spacetime, and the notion of torsion is largely omitted. Nonetheless, in developing the theory for generalised local symmetry under the Poincaré group, the theory similar to those of Yang-Mills theory [70] in the curved spacetime, the notion of torsion has essentially become evident in completing the theory with the spinning particles coupled to torsion [71–75] under the minimal prescription by promoting ordinary partial derivatives to covariant derivatives with appearances of new local gauge fields. Hence, the needs for the non-Riemann manifold arises naturally which can contain the Cartan's torsion tensor.

Riemann-Cartan manifolds contain both curvature and torsion, and provide a suitable background when one brings concepts of curvature and torsion to a given manifold at the same time, using the method of differential geometry in describing the intrinsic nature of defects and its classifications. Pioneering works using this mathematical framework were explored in [66,76–79]. Inspired from similarities and its applicabilities, links between the theories of the continuum physics and the Einstein-Cartan theory in describing the defects were made in [80–84]. It is worth noting that these geometrical considerations are commonly used in the Einstein-Cartan theory [74, 85, 86], teleparallel gravity [87], gauge theories of gravity [88–90] and the condensed matter system [91–93]. In a microscopic point of view, microrotations and torsion were explored in [21–23, 82, 94]. Recent developments in incorporating the elasticity theory and spinning particles using the tetrad formalism can be found in [95, 96].

Since the Riemann curvature tensor satisfies various geometrical identities such as Bianchi's identities, it is natural to expect that these identities also play a role in continuum mechanics, if one considers the possibility that the Riemann curvature tensor can contain both measures of pure curvature originated from the metric tensor and torsion which can arise independently of the metric field. In particular, we will see that the vanishing Riemann curvature and its related measures imply the theory is in the regime of elasticity, and a set of partial differential equations may lead to an integrability condition which is commonly called the compatibility condition in some cases.

This will be our starting point in connecting the theories of defects in continuum physics

to those of the gravitational theory via the Riemann-Cartan geometry to see how torsion and curvature can be conceived in both settings. For example, in [97], the notion of metric elasticity in the Riemann manifold is introduced, hence it is essentially required to bring the notion of force in the formalism which is one of distinct features from the conventional theory of gravitation [85].

It is well known that the vanishing Riemann curvature tensor in the deformed body yields the compatibility conditions equivalent to the Saint-Venant compatibility conditions [98–103] in the classical elasticity theory, which are otherwise derived by considering higher order partial derivatives, that have to necessarily commute. After revisiting these basic results in the classical theory of continuum, we will show that one of compatibility conditions known as the Vallée's compatibility condition, is in fact equivalent to the vanishing of the three-dimensional Einstein tensor using tools of differential geometry and we will develop its further implications. In Part II, we will follow closely the results obtained in [104].

4.2 Compatibility conditions

Compatibility conditions in continuum mechanics form a set of partial differential equations which are not completely independent of each other. They may impose certain conditions among unknown number of functions which are often derived by applying higher-order mixed partial derivatives to given system of equations. They are closely related to integrability conditions.

In 1992 Vallée [105] showed that the standard Saint-Venant compatibility condition of linear elasticity, known since the mid-19th century, can be written in the convenient form

$$\mathrm{Curl}\,\Lambda + \mathrm{Cof}\,\Lambda = 0\ , \tag{4.2.1}$$

where the operators Curl and Cof in (4.2.1), for 3×3 matrices, are defined by

$$(\mathrm{Curl}\,\Lambda)_{ij} = \epsilon_{jmn}\partial_m\Lambda_{in}\ , \qquad \text{and} \qquad (\mathrm{Cof}\,\Lambda)_{ij} = \frac{1}{2}\epsilon_{ims}\epsilon_{jnt}\Lambda_{mn}\Lambda_{st}\ , \tag{4.2.2}$$

and ϵ_{ijk} is the totally antisymmetric Levi-Civita symbol for $i,j,k=1,2,3$. The 3×3 matrix Λ is given by

$$\Lambda = \frac{1}{\det U}\left[U(\mathrm{Curl}\,U)^T U - \frac{1}{2}\mathrm{tr}\left[(\mathrm{Curl}\,U)^T U\right]U\right]\ . \tag{4.2.3}$$

This formulation is based on Riemannian geometry where the metric tensor is written as $g_{\mu\nu} = U^a_\mu U^b_\nu \delta_{ab}$. Here U is the right stretch tensor of the polar decomposition of the deformation gradient tensor $F = RU$ of (1.2.6), and R is an orthogonal matrix which is the polar part.

Condition (4.2.1) is derived by finding the integrability condition of the system for the right Cauchy-Green deformation tensor C defined in (1.2.35),

$$C = (\nabla\Theta)^T(\nabla\Theta)\ . \tag{4.2.4}$$

The deformation of the continuum is expressed by a diffeomorphism $\Theta : M \to \mathbb{R}^3$ in the classical theory, such that $\boldsymbol{x} = \boldsymbol{X} + \boldsymbol{u}$ with u being the displacement vector. Hence, the tensor C assumes the role of a metric tensor in the given smooth manifold M. Later [106], the existence of such an immersion Θ is proved which maps an open subset of $\mathbb{R}^3$ into $\mathbb{R}^3$ in which the metric tensor field defined by C with U in the polar decomposition $\nabla\Theta = RU$. The expression (4.2.1) will be shown to be equivalent to the vanishing of the Riemann curvature tensor in this setting and the zero curvature characterises the differential equation (4.2.4) to be integrable. For a small displacement field $\boldsymbol{u}$, the notion of zero curvature reduced to the classical *Saint-Venant integrability conditions*.

Much earlier, in 1953 Nye [34] showed that there exists a curvature related rank-two tensor Γ of the form

$$\Gamma = \frac{1}{2}\mathrm{tr}\left(R^T \mathrm{Curl}\, R\right)\mathbb{1} - (R^T \mathrm{Curl}\, R)^T \,, \tag{4.2.5}$$

satisfying the identical form of compatibility condition

$$\mathrm{Curl}\,\Gamma + \mathrm{Cof}\,\Gamma = 0 \,. \tag{4.2.6}$$

The object Γ is often called Nye's tensor, and is written in terms of the dislocation density tensor $K = R^T \mathrm{Curl}\, R$ we used in constructing the energy functional $V_{\mathrm{curvature}}$ and V_χ in Part I, for example (3.2.14) and (3.3.8). We note that the dislocation density tensor here only depends on the orthogonal matrix R.

We would like to show that these two compatibility conditions (4.2.2) and (4.2.6), seemingly arose from different and incomparable settings, are in fact special cases of a much broader compatibility condition which can be formulated in Riemann-Cartan geometry.

Chapter 5

Deformational measures in Riemann-Cartan manifold

We introduce frame basis and co-frame basis, also called tangent and co-tangent basis respectively, together with its polar decompositions. Then we define various quantities including a general affine connection, a spin connection, and torsion formally. We decompose these tensors into two parts, one which is torsion-free and one that contains torsion. The Riemann tensor will be expressed in various ways using above mentioned tensors. We then introduce the Einstein tensor in terms of Riemann curvature tensor in three dimensions.

5.1 Frame fields and non-frame fields

Let us begin with a three-dimensional Riemannian manifold M with coordinates x, and let us introduce a set of bases for the tangent space and co-vectors (or 1-forms) for the co-tangent space, respectively, at some point $x \in M$

$$E_b^\mu(x) \qquad \text{and} \qquad e_\mu^a(x) \tag{5.1.1}$$

where the Latin indices $a, b, \cdots = 1, 2, 3$ are tangent space indices, and Greek letters $\mu, \nu, \cdots = 1, 2, 3$ denote coordinate indices. This basis is often called a (co-)tetrad field. For the frame field, we define the tangent basis

$$E_a = E_a^\mu \frac{\partial}{\partial x^\mu} \ , \tag{5.1.2}$$

where E_a^μ is an element of 3×3 real general linear group $GL(3; \mathbb{R})$. So we can say that E_a is obtained by the transformation of the frame fields $\{\partial/\partial x^\mu\}$ by some element E_a^μ. Similarly, we define the co-frame field (or co-tangent field), the dual fields of frame field,

$$e^a = e_\mu^a dx^\mu \ , \tag{5.1.3}$$

where e_μ^a is also an element of $GL(3; \mathbb{R})$. These satisfy orthogonal relations

$$e_\mu^a E_a^\nu = \delta_\mu^\nu \qquad \text{and} \qquad e_\mu^a E_b^\mu = \delta_b^a \ . \tag{5.1.4}$$

Here δ_μ^ν and δ_b^a are the Kronecker deltas in their respective spaces. We emphasise that for a given manifold, we can find these tangent bases locally so that we can relate different sets of tangent bases in different points by simple transformations defined by an element $GL(3; \mathbb{R})$.

However, it is impossible to find a single frame field which is nowhere vanishing globally, unless the manifold is completely parallelisable. For example, the *hairy ball theorem* [107]

illustrates that we cannot comb the hair on a 2-sphere S^2, embedded in three dimensions, smoothly everywhere. Hence this justifies the use of the locally defined diffeomorphism as the immersion of $\Theta : M \to \mathbb{R}^3$ used in (4.2.4).

In the framework of tetrad formalism, the metric tensor emerges as a secondary quantity defined in terms of tetrad fields. We have

$$g_{\mu\nu}(x) = e^a_\mu(x) e^b_\nu(x) \delta_{ab} \ , \tag{5.1.5}$$

where δ_{ab} is the globally flat Euclidean metric with the signature $(+1, +1, +1)$ in three dimensions. And it is easy to see that its inverse is $g^{\mu\nu}$, defined by

$$g^{\mu\nu}(x) = E^\mu_a(x) E^\nu_b(x) \delta^{ab} \ .$$

Using these, we can raise and lower indices of the (co-)tangent frame objects by applying $g_{\mu\nu}$, δ_{ab}, and its corresponding inverses. In Riemannian geometry, the metric (5.1.5) gives rise to an invariant length element under a general diffeomorphism and a tangent space transformation,

$$(ds)^2 = g_{\mu\nu} dx^\mu dx^\nu = e^a_\mu e^b_\nu \delta_{ab} dx^\mu dx^\nu = e^a e^b \delta_{ab} \ , \tag{5.1.6}$$

and similarly for the E^μ_a field.

This means we can use the co-tangent basis e^a_μ to describe the local deformation given by the metric tensor $g_{\mu\nu}$ from the flat space δ_{ab} written in the coordinate basis. As a result, the metric tensor $g_{\mu\nu}$ is obtained from the flat Euclidean metric δ_{ab} by a set of deformational informations, encoded in $e^a_\mu(x) \in GL(3;\mathbb{R})$ at each point $x \in M$. Since any deformation can be regarded as a combination of rotation, shear and compression, the common terms in (micro)continuum physics, we can apply the polar decomposition to e^a_μ as we did in Part I,

$$e^a_\mu(x) = R^a{}_b(x) U^b_\mu(x) \ , \tag{5.1.7}$$

where $R^a{}_b$ is an orthogonal matrix (a pure tangent space object with Latin indices) while the field U^b_μ is a symmetric and positive-definite matrix. Whenever we need to distinguish the microdeformations from the macrodeformations, we will put a bar over the corresponding tensor. When this decomposition is applied to (5.1.5) one arrives at

$$g_{\mu\nu} = R^a{}_c R_{ad} U^c_\mu U^d_\nu = \delta_{cd} U^c_\mu U^d_\nu \ , \tag{5.1.8}$$

which shows that the metric is completely independent of $R^a{}_b$ and only depends on U^b_μ. This is a well-known result in differential geometry, namely, the metric field is independent of tangent space rotations. The polar decomposition for the inverse frame can be similarly written by

$$E^\mu_a = R_a{}^b U^\mu_b \ , \tag{5.1.9}$$

so that U^μ_b is the inverse of U^a_μ, both of which are positive-definite and symmetric. Consequently, the co-tangent basis given by a specific metric tensor (5.1.5) is not uniquely determined. This can be seen by counting the number of required independent parameters in the expression of the symmetric metric tensor (5.1.5). Hence, the additional number of degrees of freedom on the tetrad fields implies that any two (co-)tetrads $\tilde{e}^a_\mu$ and e^a_μ will yield the same metric provided they are related by a rotation

$$\tilde{e}^a_\mu = Q^a{}_b e^b_\mu \ , \qquad Q^a{}_b \in SO(3) \ . \tag{5.1.10}$$

A metric compatible covariant derivative is introduced in differential geometry through the condition

$$\nabla_\lambda g_{\mu\nu} = 0 \ . \tag{5.1.11}$$

This introduces the Christoffel symbol components $\Gamma^{\lambda}_{\mu\nu}$ as the general affine connection. From (5.1.5), it is natural to assume that in the tetrad formalism,

$$\nabla_\mu e^a_\nu = 0 \ . \tag{5.1.12}$$

This, in turn, will uniquely determine the **spin connection** coefficients $\omega_\mu{}^a{}_b(x)$,

$$0 = \nabla_\mu e^a_\nu = \partial_\mu e^a_\nu - \Gamma^{\lambda}_{\mu\nu} e^a_\lambda + \omega_\mu{}^a{}_b e^b_\nu \ , \tag{5.1.13}$$

where $\Gamma^{\mu}_{\lambda\nu}$ is a general affine connection, and the lower indices in this connection are not necessarily symmetric. Using the orthogonality (5.1.4), we can rewrite (5.1.13) by

$$\omega_\mu{}^a{}_b = e^a_\lambda \Gamma^{\lambda}_{\mu\nu} E^\nu_b + e^a_\nu \partial_\mu E^\nu_b \ . \tag{5.1.14}$$

Note that the spin connection is invariant under global rotations but not under local rotations. And the derivative terms will pick up additional terms, this is of course expected when working with connections.

The covariant derivative for a general vector V^μ in coordinate space is defined by

$$\nabla_\lambda V^\mu = \partial_\nu V^\mu + \Gamma^{\mu}_{\lambda\nu} V^\nu \ . \tag{5.1.15}$$

Being equipped with the frame (and co-frame) field, we might introduce a quantity,

$$V^a = e^a_\mu V^\mu \tag{5.1.16}$$

which denotes the tangent space components of a general vector V^μ. We can see that the vector V^μ is rotated by the tetrad e^a_μ to become V^a in the tangent field. It is easy to see that its inverse relation is simply $V^\mu = E^\mu_a V^a$. Naturally, the covariant derivative of V^a can be described using the spin connection, in view of (5.1.15). This gives

$$\nabla_\mu V^a = \partial_\mu V^a + \omega_\mu{}^a{}_b V^b \ , \tag{5.1.17}$$

and can be extended to higher-rank objects in the same way.

For completeness, we state the inverse of (5.1.14), so that the general affine connection is expressed in terms of the spin connection

$$\Gamma^{\lambda}_{\mu\nu} = E^\lambda_a \omega_\mu{}^a{}_b e^b_\nu + E^\lambda_a \partial_\mu e^a_\nu \ . \tag{5.1.18}$$

Equations (5.1.14) and (5.1.18) together with the (co-)frame allow us to express geometrical identities in either the tangent space or the coordinate space.

In general, unlike the coordinate bases $\partial/\partial x^\mu$, the non-coordinate bases $E_a = E^\mu_a \partial_\mu$ do not commute, and one introduces the object of anholonomity as follows. Let u be a smooth differentiable function, then a direct and straightforward calculation gives

$$[E_a, E_b]\, u = E^\mu_a E^\nu_b (\partial_\nu e^c_\mu - \partial_\mu e^c_\nu) E_c u \ . \tag{5.1.19}$$

This must be valid for the arbitrary u, so we can write

$$[E_a, E_b] = f^c{}_{ab} E_c \ , \tag{5.1.20}$$

where the $f^c{}_{ab}$ are the structure constants, which are given by

$$f^c{}_{ab} = E^\mu_a E^\nu_b (\partial_\nu e^c_\mu - \partial_\mu e^c_\nu) \ . \tag{5.1.21}$$

5.2 Torsion and curvature

Given a general affine connection, the **torsion** tensor is defined by

$$T^{\lambda}{}_{\mu\nu} = \Gamma^{\lambda}_{\mu\nu} - \Gamma^{\lambda}_{\nu\mu} \,, \tag{5.2.1}$$

which is the antisymmetric part of the connection.

Throughout this paper, we will use the decomposition of the various tensor quantities into a torsion-free part and a separate torsion part. These correspond to the quantities in Riemann space and the quantities in non-Riemann space. Also we will use the notation " $\circ$ " specifically indicating the torsion-free quantities, or equivalently the quantities written in terms of the metric compatible connection which is generally referred to as the Christoffel symbol.

The main reason for this process is that by applying these decompositions to various deformational measures both in Riemann and non-Riemann space, we might hope to see the relations between the compatibility conditions, introduced in Section 4.2, originated from the distinct space connected by some additional fields.

First we decompose the general affine connection

$$\Gamma^{\rho}_{\nu\sigma} = \mathring{\Gamma}^{\rho}_{\nu\sigma} + K^{\rho}{}_{\nu\sigma} \,, \tag{5.2.2}$$

which introduces the **contortion** tensor $K^{\rho}{}_{\nu\sigma}$. Using the definition of torsion (5.2.1), we immediately have

$$T^{\lambda}{}_{\mu\nu} = K^{\lambda}{}_{\mu\nu} - K^{\lambda}{}_{\nu\mu} \,, \tag{5.2.3}$$

which one can also solve for the contortion tensor. This yields

$$K^{\lambda}{}_{\mu\nu} = \frac{1}{2}\left(T^{\lambda}{}_{\mu\nu} + T_{\nu}{}^{\lambda}{}_{\mu} - T_{\mu\nu}{}^{\lambda}\right) \,, \tag{5.2.4}$$

which in turn implies the antisymmetric property $K^{\lambda}{}_{\mu\nu} = -K_{\nu\mu}{}^{\lambda}$.

The Riemann curvature tensor is defined by

$$R^{\rho}{}_{\sigma\mu\nu} = \partial_{\mu}\Gamma^{\rho}_{\nu\sigma} - \partial_{\nu}\Gamma^{\rho}_{\mu\sigma} + \Gamma^{\rho}_{\mu\lambda}\Gamma^{\lambda}_{\nu\sigma} - \Gamma^{\rho}_{\nu\lambda}\Gamma^{\lambda}_{\mu\sigma} \tag{5.2.5}$$

where $\Gamma^{\rho}_{\nu\sigma}$ are the general affine connections.

Using the frame fields, we can introduce those tensors with mixed components (indices for coordinate space and tangent space), which will turn out to be useful for our subsequent discussion. We define a $GL(3;\mathbb{R})$-rotated torsion tensor by

$$T^{a}{}_{\mu\nu} = e^{a}_{\lambda} T^{\lambda}{}_{\mu\nu} \,, \tag{5.2.6}$$

Using (5.1.18), or the expression $\nabla_{\mu} e^{a}_{\nu} - \nabla_{\nu} e^{a}_{\mu} = 0$, we can write the torsion tensor in the following equivalent way,

$$T^{a}{}_{\mu\nu} = \partial_{\mu} e^{a}_{\nu} - \partial_{\nu} e^{a}_{\mu} + \omega_{\mu}{}^{a}{}_{b} e^{b}_{\nu} - \omega_{\nu}{}^{a}{}_{b} e^{b}_{\mu} \,. \tag{5.2.7}$$

Similarly, we can rewrite the Riemann tensor with mixed indices

$$R^{a}{}_{b\mu\nu} = e^{a}_{\rho} R^{\rho}{}_{\sigma\mu\nu} E^{\sigma}_{b} \,, \tag{5.2.8}$$

which allow us to write the Riemann tensor entirely in terms of the spin connections

$$R^{a}{}_{b\mu\nu} = \partial_{\mu}\omega_{\nu}{}^{a}{}_{b} - \partial_{\nu}\omega_{\mu}{}^{a}{}_{b} + \omega_{\mu}{}^{a}{}_{e}\omega_{\nu}{}^{e}{}_{b} - \omega_{\nu}{}^{a}{}_{e}\omega_{\mu}{}^{e}{}_{b} \,. \tag{5.2.9}$$

In addition to the antisymmetry in the last two indices in the Riemann tensor, this satisfies

$$R_{ab\mu\nu} = -R_{ba\mu\nu} \ . \tag{5.2.10}$$

In this way, we can recognise the torsion and Riemann curvature tensors of (5.2.7) and (5.2.9) are two-forms in the language of differential geometry, written conveniently

$$\boldsymbol{T}^a = d\boldsymbol{e}^a + \boldsymbol{\omega}^a{}_b \wedge \boldsymbol{e}^b \ , \tag{5.2.11a}$$

$$\boldsymbol{R}^a{}_b = d\boldsymbol{\omega}^a{}_b + \boldsymbol{\omega}^a{}_e \wedge \boldsymbol{\omega}^e{}_b \ . \tag{5.2.11b}$$

These are known as the *Cartan's structure equations*.

As a consequence of the decomposition (5.2.2), we apply the same concept to the spin connection to write its decomposition

$$\omega_\mu{}^a{}_b = \mathring{\omega}_\mu{}^a{}_b + K^a{}_{\mu b} \ , \tag{5.2.12}$$

where we used $K^a{}_{\mu b} = e^a_\nu K^\nu{}_{\mu\sigma} E^\sigma_b$. Inserting the relation (5.2.12) into (5.2.9) gives the decomposition of the Riemann tensor,

$$R^\rho{}_{\sigma\mu\nu} = \mathring{R}^\rho{}_{\sigma\mu\nu} + \left[\mathring{\nabla}_\mu K^\rho{}_{\nu\sigma} - \mathring{\nabla}_\nu K^\rho{}_{\mu\sigma} + K^\rho{}_{\mu\lambda} K^\lambda{}_{\nu\sigma} - K^\rho{}_{\nu\lambda} K^\lambda{}_{\mu\sigma}\right] \ , \tag{5.2.13}$$

where the Riemann tensor $\mathring{R}^\rho{}_{\sigma\mu\nu}$ is computed using the metric compatible connection $\mathring{\Gamma}^\rho_{\mu\nu}$ entirely.

We note that, for a general vector V^ρ, in the coordinate basis, the covariant derivative can be rewritten using (5.2.2) such that

$$\nabla_\mu V^\rho = \mathring{\nabla}_\mu V^\rho + K^\rho{}_{\mu\nu} V^\nu \ . \tag{5.2.14}$$

This relates the general covariant derivative ∇_μ and the torsion-free, metric compatible covariant derivative $\mathring{\nabla}_\mu$ used in (5.2.13). In addition to (5.2.2) and (5.2.12), we can regard the contortion tensor on the right-hand side as the connection between these two distinct covariant derivatives.

5.3 Einstein tensor in three-dimensional space

We define a rank-two quantity based on the spin connection by

$$\Omega_{c\mu} = -\frac{1}{2}\epsilon_{abc}\omega_\mu{}^{ab} \ , \tag{5.3.1}$$

which is equivalent to

$$\omega_\mu{}^{ab} = -\epsilon^{abc}\Omega_{c\mu} \ . \tag{5.3.2}$$

This is somewhat similar to extracting information of an axial field from a generator of a rotational matrix. A three-dimensional rotational matrix can be written in the exponential representation $R = e^A$ with its antisymmetric generator $A_{ij} = \theta a_{ij}$ and the rotation of an angle θ about the axis $n_i = -\frac{1}{2}\epsilon_{ijk}a_{jk}$.

We note that this construction is only valid in three dimensions to arrive at a rank-two object in (5.3.1). In the following, it will turn out that $\Omega_{c\mu}$ plays a crucial role in establishing our compatibility conditions. The same approach was applied to the torsion tensor in [21] where the setting was also $\mathbb{R}^3$.

We substitute (5.3.2) into the Riemann tensor (5.2.9), and find

$$R^a{}_{b\mu\nu} = \epsilon^{sa}{}_b\left(-\partial_\mu\Omega_{s\nu} + \partial_\nu\Omega_{s\mu}\right) + \epsilon^{sa}{}_e\epsilon^{te}{}_b\left(\Omega_{s\mu}\Omega_{t\nu} - \Omega_{s\nu}\Omega_{t\mu}\right) \ . \tag{5.3.3}$$

Next, we define another rank-two tensor, constructed from the Riemann tensor,

$$G^{\sigma c} = -\frac{1}{4}\epsilon^{abc}R_{ab\mu\nu}\epsilon^{\mu\nu\sigma} \ , \tag{5.3.4}$$

in which the Riemann curvature tensor on the left-hand side is antisymmetric in the first and second pairs of indices. Let us emphasise again that this construction is only possible in three dimensions, otherwise we would need to introduce a different rank in the Levi-Civita symbol.

Inserting (5.3.3) into (5.3.4), using the facts $\epsilon^{abc}\epsilon_{sab} = 2\delta^c_s$ and $\epsilon_{sae}\epsilon^{abc}\epsilon^{te}{}_b = -\epsilon^{tc}{}_s$, we obtain

$$G^{\sigma c} = \epsilon^{\mu\nu\sigma}\partial_\mu\Omega^c{}_\nu + \frac{1}{2}\epsilon^{cst}\epsilon^{\sigma\mu\nu}\Omega_{s\mu}\Omega_{t\nu} \ , \tag{5.3.5}$$

which can be written in the convenient form

$$G^{\sigma c} = (\mathrm{Curl}\,\Omega)^{c\sigma} + (\mathrm{Cof}\,\Omega)^{c\sigma} \ . \tag{5.3.6}$$

The quantity $G_{\sigma c}$ is, in fact, the Einstein tensor in three-dimensional space. This can be shown using (5.3.5) and (5.2.8) explicitly to obtain the familiar expression for the Einstein tensor,

$$G_{\tau\lambda} = R_{\tau\lambda} - \frac{1}{2}\delta_{\tau\lambda}R \ . \tag{5.3.7}$$

Here $R_{\tau\lambda}$ is the Ricci tensor defined by $R_{\tau\lambda} = R^\sigma{}_{\tau\sigma\lambda}$, and the trace of Ricci tensor is the Ricci scalar R. It is well known that in three dimensions, the Riemann tensor, the Ricci tensor, and the Einstein tensor have the same number of independent components, namely nine, provided torsion is included. Therefore, unlike the conventional theory of gravitation, the symmetric Ricci tensor and Einstein tensor are not assumed. One can readily verify that following three relations are equivalent to each other.

$$R^a{}_{b\mu\nu} = 0 \quad \Longleftrightarrow \quad R_{\tau\lambda} = 0 \quad \Longleftrightarrow \quad G_{\tau\lambda} = 0 \ . \tag{5.3.8}$$

In other words, the vanishing curvature means vanishing Einstein tensor in three dimensions.

Chapter 6

Compatibility conditions

We are in position to use the tools of differential geometry, various deformational measures, and its decompositions. We will derive compatibility conditions in various physical settings using a universal process. Firstly, Vallée's result will be re-derived, followed by Nye's condition. We carefully explain the connection between these two compatibility conditions, all explanations are originated from the vanishing Einstein tensor. We will show an extension of this result to the microcontinuum theories, and lastly we will derive a general compatibility condition, which is applicable to the case of nonzero curvature.

6.1 Vallée's classical result

We consider the torsion-free spin connection $\mathring{\Omega}_{c\mu} = -\frac{1}{2}\epsilon_{abc}\mathring{\omega}_{\mu}{}^{ab}$ with the metric tensor (5.1.5). The affine connection in torsion-free space is conventionally expressed by the metric compatible Levi-Civita connection which enters into the decomposition of (5.2.2),

$$\mathring{\Gamma}^{\lambda}_{\mu\nu} = \frac{1}{2}g^{\lambda\sigma}\left(\partial_\nu g_{\sigma\mu} + \partial_\mu g_{\sigma\nu} - \partial_\sigma g_{\mu\nu}\right) \ . \tag{6.1.1}$$

The torsion-free spin connection in terms of the Levi-Civita connection is simply

$$\begin{aligned}\mathring{\omega}_{\mu}{}^{a}{}_{b} &= e^a_\lambda \mathring{\Gamma}^{\lambda}_{\mu\nu}E^\nu_b + e^a_\nu \partial_\mu E^\nu_b \\ &= \frac{1}{2}e^a_\lambda g^{\lambda\tau}\left(\partial_\nu g_{\tau\mu} + \partial_\mu g_{\tau\nu} - \partial_\tau g_{\mu\nu}\right)E^\nu_b + e^a_\nu\partial_\mu E^\nu_b \ ,\end{aligned}$$

where we used (5.1.14). Inserting the explicit expression for the metric tensor (5.1.5) will give, after a lengthy but straightforward calculation,

$$\mathring{\omega}_{\mu}{}^{a}{}_{b} = \frac{1}{2}E^\sigma_b\left(\partial_\sigma e^a_\mu - \partial_\mu e^a_\sigma\right) - \frac{1}{2}\delta^{ad}\delta_{fb}E^\sigma_d\left(\partial_\sigma e^f_\mu - \partial_\mu e^f_\sigma\right) + \frac{1}{2}\delta^{ad}g_{\mu\sigma}\left(\partial_d E^\sigma_b - \partial_b E^\sigma_d\right) \tag{6.1.2}$$

in which we defined $\partial_a = E^\sigma_a\partial_\sigma$. This expression for the torsion-free spin connection is particularly useful in such a way that we can write the spin connection in terms of polar decomposition of co-frame field basis $e^a_\mu = R^a{}_b U^b_\mu$ to write $\mathring{\omega}_{\mu}{}^{ab}$ entirely in terms of $R^a{}_b$ and U^b_μ, and its derivatives. By doing so, we can split deformational measures in terms of the metric-dependent part, which only sees the stretches U^b_μ, and the metric-independent part depending only on the rotations $R^a{}_b$. The resulting expressions will be further simplified if we consider the cases $R^a{}_b = \delta^a_b$ and $U^b_\mu = \delta^b_\mu$ separately, to see whether these will lead to the desired compatibility conditions.

First, when $R^a{}_b = \delta^a_b$, after multiplying ϵ_{abc} to both sides of (6.1.2), we have

$$\epsilon_{abc}\mathring{\omega}_{\mu}{}^{ab} = \epsilon_{abc}\epsilon_{\sigma\mu\nu}U^{a\nu}(\mathrm{Curl}\,U)^{b\sigma} - \frac{1}{2}\epsilon_{abc}\epsilon_{\sigma\tau\rho}U^{a\rho}U^{b\sigma}(\mathrm{Curl}\,U)_f{}^{\tau}U^f_\mu \ . \tag{6.1.3}$$

We can extract the determinant of U from the first and the second term in the right-hand side of this,

$$\begin{aligned}\epsilon_{abc}\epsilon_{\sigma\mu\nu}U^{a\nu}(\mathrm{Curl}\,U)^{b\sigma} &= \frac{6}{\det U}\,\Big[U(\mathrm{Curl}\,U)^T U\Big]_{c\mu}\ ,\\ \epsilon_{abc}\epsilon_{\sigma\tau\rho}U^{a\rho}U^{b\sigma}(\mathrm{Curl}\,U)_f{}^{\tau}U^f_{\mu} &= \frac{6}{\det U}\,U_{c\mu}\mathrm{tr}\left[(\mathrm{Curl}\,U)^T U\right]\ .\end{aligned} \tag{6.1.4}$$

Therefore, we find

$$\mathring{\Omega}_{c\mu} = -3\frac{1}{\det U}\left[U(\mathrm{Curl}\,U)^T U - \frac{1}{2}\mathrm{tr}\left[(\mathrm{Curl}\,U)^T U\right]U\right]_{c\mu}\ . \tag{6.1.5}$$

The vanishing Riemann tensor in three-dimensional space ensures the vanishing Ricci tensor, hence the vanishing Einstein tensor $\mathring{G}_{\mu c} = 0$, as stated in (5.3.8). This leads to the compatibility condition in the torsion-free space of vanishing Riemann curvature, with the help of (5.3.6),

$$\mathrm{Curl}\,\mathring{\Omega} + \mathrm{Cof}\,\mathring{\Omega} = 0\ . \tag{6.1.6}$$

Of course, we can rescale $-\frac{1}{3}\mathring{\Omega} = \Lambda_U$ to match the Vallée's result [105] exactly

$$\Lambda_U = \frac{1}{\det U}\left[U(\mathrm{Curl}\,U)^T U - \frac{1}{2}\mathrm{tr}\left[(\mathrm{Curl}\,U)^T U\right]U\right]\ , \tag{6.1.7}$$

which reads

$$\mathrm{Curl}\,\Lambda_U + \mathrm{Cof}\,\Lambda_U = 0\ . \tag{6.1.8}$$

This result indicates that, as long as Λ_U satisfies the compatibility condition (6.1.8), the deformation can be compatible to that of trivial case $U^a_\mu = \delta^a_\mu$ regardless of the details of the stretch U^a_μ, where the deformational description of U^a_μ itself undergoes the transformation by the metric tensor $g_{\mu\nu}$. This implicitly suggests that the compatibility condition (6.1.8) is invariant under the diffeomorphism in a given manifold. Therefore, we can conclude that the larger class of solution space for the expression (4.2.4), which depends on U^a_μ, can be classified as the distinct set of equivalent classes.

This means that the elastic deformation is nothing but the diffeomorphism described by a metric tensor with an associated metric compatible connection $\mathring{\Gamma}^\lambda_{\mu\nu}$ as the fundamental measure of the deformation. Then, the prescription of elastic deformations requires vanishing curvature and torsion, hence the compatibility conditions (6.1.8) in the absence of the torsion or equivalently $R^a{}_b = \delta^a_b$ in this case, is precisely the statement of the elasticity.

We should also note the results of Edelen [108] where compatibility conditions were derived using Poincaré's lemma. This resulted in the vanishing Riemann curvature two-form, Eq. (3.3) in [108] while assuming the metric compatible connection, Eq. (3.4) in [108]. These conditions explicitly contained torsion due to the affine connection being non-trivial but curvature free.

6.2 Nye's tensor and its compatibility condition

Next, we set $U^b_\mu = \delta^b_\mu$ but assume a non-trivial rotation matrix $R^a{}_b$. This will give the expressions completely independent of metric tensor. And we might hope to see how the rotational fields contribute to the deformational expressions. To do so, we notice that the setting is already given in (6.1.2) and we put the non-trivial rotations $R^a{}_b$ but the trivial stretches $U^a_\mu = \delta^a_\mu$, hence we are still in the regime of zero curvature. This space is often referred as Weitzenböck space especially in the field of *Teleparallel Gravity*.

The calculation is identical if we replace the stretch parts by the rotation parts in deriving (6.1.8), starting from the torsion-free spin connection (6.1.2) after applying the decomposition $e^a_\mu = R^a{}_b U^b_\mu$. The final compatibility condition is then

$$\operatorname{Curl}\Lambda_R + \operatorname{Cof}\Lambda_R = 0\ , \tag{6.2.1}$$

where the quantity Λ_R is given by

$$\Lambda_R = R(\operatorname{Curl} R)^T R - \frac{1}{2}\operatorname{tr}\left[(\operatorname{Curl} R)^T R\right] R\ . \tag{6.2.2}$$

This confirms the replacing U^c_μ with $R^a{}_b$ in (6.1.7) and using $\det R^a{}_b = +1$.

It turns out that the quantity Λ_R is (up to a minus sign) Nye's tensor Γ which is known to satisfy the compatibility condition (6.2.1). This is quite a remarkable result which follows immediately from our geometrical approach to the problem.

- We emphasise that the metric tensor is independent of the rotations which implies that $U^c_\mu = \delta^c_\mu$ yields a vanishing (torsion-free) Levi-Civita connection $\overset{\circ}{\Gamma}{}^\lambda_{\mu\nu}$. Consequently the Levi-Civita part of the curvature tensor vanishes identically, $\overset{\circ}{R}{}^\rho{}_{\sigma\mu\nu} = 0$.

- The compatibility condition simply ensures that the micropolar deformations governed by $R^a{}_b$ do not induce curvature in the deformed body. We will see the mathematical justification of this fact shortly, but most importantly, nonzero torsion do not contribute the Riemann curvature tensor (hence the Einstein tensor), and we obtain the compatibility condition by simply replacing U^a_μ by $R^a{}_b$ from the previously obtained result.

Now, one of most significant consequences of the decomposition (5.2.2) we started with is the following. In the space where $\overset{\circ}{\Gamma}{}^\lambda_{\mu\nu} = 0$, or equivalently $U^c_\mu = \delta^c_\mu$ but with non-vanishing torsion, the general affine connection reduces to the contortion. Moreover, in the manifold of vanishing curvature, the Cartan's structure equation (5.2.11b) of the Riemann curvature two-form becomes

$$d\boldsymbol{\omega} = -\boldsymbol{\omega}\wedge\boldsymbol{\omega}\ .$$

It is known that the spin connection depends purely on the symmetry group of an inertial frame [87] (e.g the Lorentz transformation, or the Galilean transformation in the non-relativistic limit). Then one can choose such a frame so that $d\boldsymbol{\omega} = 0$. In other words, the curvature two-form now induces an integrable expression for the spin connection. Further, with the use of *Frobenius theorem* as introduced in [109], the spin connection becomes trivial, and one can put $\omega_\mu{}^a{}_b = 0$ in (5.1.18) without loss of generality. Then we have

$$\Gamma^\lambda_{\mu\nu} = (R_a{}^b\delta^\lambda_b)\partial_\mu(R^a{}_c\delta^c_\nu) = \delta^\lambda_b\delta^c_\nu(R_a{}^b\partial_\mu R^a{}_c) = \delta^\lambda_b\delta^c_\nu\delta^d_\mu(R_a{}^b\partial_d R^a{}_c)\ . \tag{6.2.3}$$

The final term in the brackets is recognised to be the second Cosserat tensor when written in index free notation $R^T\operatorname{Grad} R$, see for instance [110].

In the following, we will briefly discuss how the compatibility condition for Nye's tensor can also be derived directly without referring to the general result we will see in Section 6.4. In order to have completely vanishing curvature tensor (5.2.13) with $U^c_\mu = \delta^c_\mu$, we note another observation in addition to above mentioned consequences. That is, we can replace $\overset{\circ}{\nabla}_\mu$ with ∂_μ in (5.2.13). Under these circumstances, the Riemann curvature tensor (2.3.7) reduces to

$$R^\rho{}_{\sigma\mu\nu} = \partial_\mu K^\rho{}_{\nu\sigma} - \partial_\nu K^\rho{}_{\mu\sigma} + K^\rho{}_{\mu\lambda}K^\lambda{}_{\nu\sigma} - K^\rho{}_{\nu\lambda}K^\lambda{}_{\mu\sigma}\ . \tag{6.2.4}$$

Now, we would like to formally define a rank-two tensor $K_{\lambda\sigma}$ which is the **dislocation density tensor** [21, 31, 111], by contracting the contortion tensor with $\epsilon_{\sigma\mu\nu}$, in a similar way we did in (5.3.1),

$$K_{\lambda\sigma} = \epsilon_{\sigma}{}^{\mu\nu} K_{\lambda\mu\nu} \, . \tag{6.2.5}$$

This also gives a relation between the torsion tensor and the dislocation density tensor by

$$K^{\lambda\sigma}\epsilon_{\sigma\mu\nu} = T^{\lambda}{}_{\alpha\beta} \, . \tag{6.2.6}$$

For our explicit choice of the contortion tensor in (6.2.3), we can write the dislocation density tensor by

$$K_{\lambda\sigma} = \epsilon_{\sigma}{}^{\mu\nu}\delta_{\lambda b} R_a{}^b \partial_\mu R^a{}_c \delta^c_\nu = \Big(R^T \mathrm{Curl}\, R\Big)_{\lambda\sigma} \, . \tag{6.2.7}$$

This is nothing but the dislocation density tensor (2.1.5), we used throughout Part I, as appeared in the formulation of the energy functionals (2.1.2) (we dropped the bar here).

For Nye's tensor, we contract the first and third index of the contortion tensor

$$\Gamma_{\lambda\nu} = -\frac{1}{2}\epsilon_{\lambda}{}^{\rho\sigma} K_{\rho\nu\sigma} \, . \tag{6.2.8}$$

In turn, the relation between Nye's tensor and the contortion tensor becomes $\Gamma_{\lambda\nu}\epsilon^{\lambda}{}_{\mu\rho} = -K_{\mu\nu\rho}$. From this, the contortions can be substituted into (6.2.4) to write the Riemann curvature in terms of Nye's tensor entirely. This immediately yields

$$\mathrm{Curl}\,\Gamma + \mathrm{Cof}\,\Gamma = 0 \, . \tag{6.2.9}$$

This is our second compatibility condition written in terms of Nye's tensor, for the vanishing curvature and nonzero torsion tensor.

We note that combining the definitions of (6.2.5) and (6.2.8) together leads to the usual expression of Nye's tensor, originally introduced in [34]

$$\Gamma_{\lambda\nu} = \frac{1}{2}\mathrm{tr}\left(R^T \mathrm{Curl}\, R\right)\delta_{\lambda\nu} - \left(R^T \mathrm{Curl}\, R\right)^T{}_{\lambda\nu} \, . \tag{6.2.10}$$

Inversely, we can express the dislocation density tensor in terms of Nye's tensor

$$K_{\lambda\sigma} = \Gamma^{\mu}{}_{\mu}\delta_{\lambda\sigma} - (\Gamma^T)_{\lambda\sigma} \, . \tag{6.2.11}$$

One might get an impression from (6.2.4) that non-vanishing curvature might be induced by the non-vanishing contortion or torsion. However, this is not the case. As indicated in Section 10.3, the contortion tensor is of Maurer-Cartan form $\boldsymbol{K} = \boldsymbol{R}^T d\boldsymbol{R}$ which satisfies the Maurer-Cartan equation

$$d\boldsymbol{K} = -\boldsymbol{K} \wedge \boldsymbol{K} \, , \tag{6.2.12}$$

which is equivalent to the expression of the vanishing Riemann curvature tensor entirely in the form of (6.2.4).

6.3 Eringen's compatibility conditions

Now we would like to see how we can apply the results we obtained so far to the theory of microcontinuum, especially to the micropolar case. We will follow the notations used by Eringen in [15]. Strain measures introduced in (1.2.37) and (1.2.38) are

$$\begin{aligned} \mathfrak{C}_{KL} &= \frac{\partial x_k}{\partial X_K}\mathfrak{X}_{Lk} & \mathcal{C}_{KL} &= \chi_{kK}\chi_{kL} = \mathcal{C}_{LK} \\ \Gamma_{KLM} &= \mathfrak{X}_{Kk}\frac{\partial \chi_{kL}}{\partial X_M} & \Gamma_{KL} &= \frac{1}{2}\epsilon_{KMN}\Gamma_{NML} \end{aligned} \tag{6.3.1}$$

with the directors $\boldsymbol{\Xi}_K$ and $\boldsymbol{\xi}_k$ in material coordinate X_K, and spatial coordinate x_k, respectively. Now we recognise that the symmetric microdeformation tensor $\mathcal{C}_{KL}$ is analogous to the metric tensor in the form of (5.1.5).

In case of micropolar continua, it is easy to see the existence of the compatibility conditions by counting and comparing the total number of independent variables and the number of partial differential equations in the definitions of (6.3.1), for a given dimension. Specifically, with the possible symmetric property in mind, we note that the variables $\{x_k, \chi_{kX}\}$ are not independent, but these are related to each other. So, the simplest form of integrability conditions for these variables can be constructed from first-order partial differential equations $\partial_K x_k = 0$ and $\partial_L \chi_{kK} = 0$, where $\partial_K = \partial/\partial X_K$. And the necessary and sufficient condition for these integrability conditions are

$$\frac{\partial^2 x_k}{\partial X_P \partial X_Q} = \frac{\partial^2 x_k}{\partial X_Q \partial X_P} \qquad \text{and} \qquad \frac{\partial^2 \chi_{kK}}{\partial X_P \partial X_Q} = \frac{\partial^2 \chi_{kK}}{\partial X_Q \partial X_P} \,. \tag{6.3.2}$$

The deformational tensors of (6.3.1) can be decomposed into rotation and stretch parts, again the polar decomposition, as we did in the tetrad bases e^a_μ and E^ν_a. For example, after changing indices in accordance with the current use, we can rewrite the transformations between directors, $\boldsymbol{\chi}$ and $\boldsymbol{\mathfrak{X}}$, with the above mentioned deformational tensors,

$$\chi^a{}_c = \overline{R}^a{}_b \overline{U}^b_c \tag{6.3.3a}$$

$$\mathfrak{X}_a{}^c = \overline{R}_a{}^b \overline{U}^c_b \tag{6.3.3b}$$

$$\mathfrak{C}^\mu_a = \mathfrak{X}_a{}^c F_c{}^\mu = \overline{R}_a{}^b \overline{U}^c_b R_c{}^d U^\mu_d \tag{6.3.3c}$$

$$\mathcal{C}_{bc} = \chi^a{}_b \chi_{ac} = \overline{R}^a{}_e \overline{U}^e_b \overline{R}_{ad} \overline{U}^d_c \tag{6.3.3d}$$

$$\Gamma_{klm} = \chi^a{}_k \partial_m \chi_{al} = \overline{R}^a{}_b \overline{U}^b_k \partial_m (\overline{R}_{ac} \overline{U}^c_l) \,, \tag{6.3.3e}$$

in which we used bars over the the micro-deformations and used definition for the (macro)deformation gradient tensor F, with its polar decomposition into macrorotation and macrostretch.

The compatibility conditions for the micromorphic body [15] are given by

$$\epsilon_{KPQ} \left(\partial_Q \mathfrak{C}_{PL} + \mathfrak{C}_{PR} \Gamma_{LRQ} \right) = 0 \,, \tag{6.3.4a}$$

$$\epsilon_{KPQ} \left(\partial_Q \Gamma_{LMP} + \Gamma_{LRQ} \Gamma_{RMP} \right) = 0 \,, \tag{6.3.4b}$$

$$\partial_M \mathcal{C}_{KL} - \left(\Gamma_{PKM} \mathcal{C}_{LP} + \Gamma_{PLM} \mathcal{C}_{KP} \right) = 0 \,. \tag{6.3.4c}$$

It is evident from (6.3.3e) that the wryness tensor Γ_{KLM} can be viewed as the contortion tensor in differential geometry, so we can make a replacement $\Gamma_{PKM} \to K^P{}_{MK}$, hence the compatibility condition (6.3.4c) now becomes

$$\partial_M \mathcal{C}_{KL} - K^P{}_{MK} \mathcal{C}_{PL} - K^P{}_{ML} \mathcal{C}_{KP} = 0 \,. \tag{6.3.5}$$

Using the decomposition (5.2.2) with $\mathring{\Gamma}^P_{MK} = 0$, this will further reduce to

$$\nabla_M \mathcal{C}_{KL} = 0 \,. \tag{6.3.6}$$

This condition is now equivalent to the assumption (5.1.11) on the metric tensor, one of our assumptions of the geometrical approach, which is not derived from the integrability condition (6.3.2).

Next, we consider condition (6.3.4b). Using the replacement of $\Gamma_{PKM} \to K^P{}_{MK}$ gives

$$\partial_Q K^L{}_{PM} - \partial_P K^L{}_{QM} + K^L{}_{QR} K^R{}_{PM} - K^L{}_{PR} K^R{}_{QM} = 0 \,. \tag{6.3.7}$$

The left-hand side of this is precisely in the form of the Riemann curvature tensor (5.2.5), hence this condition is equivalent to $R^L{}_{MQP} = 0$. The same result can be derived if one expands the expression using the definitions of (6.3.1) and the conditions (6.3.2), in which the symmetry in P and Q, and antisymmetry in ϵ_{KPQ} yield the zero.

Lastly, for (6.3.4a) one writes

$$\epsilon_{KPQ}\left(\partial_Q \mathfrak{C}_{PL} + K^L{}_{QR}\mathfrak{C}_{PR}\right) = 0\,, \tag{6.3.8}$$

which is known as the compatibility condition for the disclination density tensor. After some algebraic manipulation ,(6.3.8) can be rewritten as

$$\nabla_Q \mathfrak{C}^L_P - \nabla_P \mathfrak{C}^L_Q + T^R{}_{PQ}\mathfrak{C}^L_R = 0\,, \tag{6.3.9}$$

and can be seen as the definition of torsion on the manifold, equivalent to (5.2.7).

For the micropolar case, by setting the the change of microvolume element (1.2.21) to the unity

$$j \equiv \det\left(\frac{\partial \xi_k}{\partial \Xi_K}\right) = \det \chi_{kK} = \frac{1}{\det \mathfrak{X}_{Kk}} = 1\,, \tag{6.3.10}$$

i.e. $\chi_{kK} \in SO(3)$, the rigid microrotation, the compatibility conditions of (6.3.4) are reduced to

$$\epsilon_{KPQ}\left(\frac{\partial \mathfrak{C}_{PL}}{\partial X_Q} + \epsilon_{MLN}\Gamma_{NQ}\mathfrak{C}_{PM}\right) = 0\,, \tag{6.3.11a}$$

$$\epsilon_{KPQ}\left(\frac{\partial \Gamma_{LQ}}{\partial X_P} + \frac{1}{2}\epsilon_{LMN}\Gamma_{MP}\Gamma_{NQ}\right) = 0\,, \tag{6.3.11b}$$

where

$$\Gamma_{KL} = \frac{1}{2}\epsilon_{KMN}\frac{\partial \chi_{kM}}{\partial X_L}\mathfrak{X}_{Nk} = \frac{1}{2}\epsilon_{KMN}\Gamma_{NML} = -\frac{1}{2}\epsilon_{KNM}K^N{}_{LM} \tag{6.3.12}$$

which agrees with our definition for the Nye's tensor (6.2.8). Now, in the micropolar case, we put microstretch and macrorotation to be identities in (6.3.3) so that

$$\chi^a{}_c = \overline{R}^a{}_c\,, \qquad \mathfrak{C}^\mu_c = E^\mu_c\,, \qquad \mathcal{C}_{bc} = \delta_{bc}\,. \tag{6.3.13}$$

Then the condition (6.3.11b) remains as the statement of vanishing Riemann curvature tensor, and the condition (6.3.6) of the micromorphic case disappears. This is because we have now the trivial expression $\mathcal{C}_{KL} = \delta_{KL}$ for the micropolar, hence the metric tensors do not see the microrotations, as expected.

6.4 Geometrical compatibility conditions for the general case

We considered the compatibility conditions under two settings so far, namely the implications of $U^a_\mu = \delta^a_\mu$ and $R^a{}_b = \delta^a_b$ separately,

$$\begin{array}{lllll} U^c_\mu = \delta^c_\mu & \Longrightarrow & \mathring{\Gamma}^\lambda_{\mu\nu} = \mathring{\Omega}_{c\mu} = \mathring{\omega}_\mu{}^a{}_b = 0 & \Longrightarrow & \mathring{R}^\rho{}_{\sigma\mu\nu} = 0 \text{ and } R^\rho{}_{\sigma\mu\nu} = 0\,, \\ R^a{}_b = \delta^a_b & \Longrightarrow & K_{\lambda\nu} = \Gamma_{\lambda\nu} = K_{\alpha\nu\beta} = 0 & \Longrightarrow & T^\lambda{}_{\mu\nu} = 0\,. \end{array} \tag{6.4.1}$$

However, the converses of these statements are not true in general, as will be shown shortly, when deriving the general form of the compatibility conditions.

The geometrical starting point for all compatibility conditions is the Bianchi identity which is satisfied by the curvature tensor, and is given by, see for instance [112]

$$\nabla_\rho R^{ab}{}_{\mu\nu} + \nabla_\nu R^{ab}{}_{\rho\mu} + \nabla_\mu R^{ab}{}_{\nu\rho} = R^{ab}{}_{\tau\nu}T^\tau{}_{\mu\rho} + R^{ab}{}_{\tau\mu}T^\tau{}_{\rho\nu} + R^{ab}{}_{\tau\rho}T^\tau{}_{\nu\mu}\,. \tag{6.4.2}$$

For completeness, we also state the well-known identity

$$R^{\rho}{}_{\sigma\mu\nu}+R^{\rho}{}_{\mu\nu\sigma}+R^{\rho}{}_{\nu\sigma\mu}=\nabla_{\sigma}T^{\rho}{}_{\mu\nu}+\nabla_{\mu}T^{\rho}{}_{\nu\sigma}+\nabla_{\nu}T^{\rho}{}_{\sigma\mu}-T^{\rho}{}_{\sigma\lambda}T^{\lambda}{}_{\mu\nu}-T^{\rho}{}_{\mu\lambda}T^{\lambda}{}_{\nu\sigma}-T^{\rho}{}_{\nu\lambda}T^{\lambda}{}_{\sigma\mu}\ , \tag{6.4.3}$$

for the Riemann curvature tensor which will also be required. Using $R^{ab}{}_{\mu\nu}=R^{\lambda\sigma}{}_{\mu\nu}e^{a}_{\lambda}e^{b}_{\sigma}$, and contracting twice over indices λ and ρ, and σ and ν, gives the well-known doubly contracted Bianchi identity,

$$\nabla_{\rho}\left(R^{\rho}{}_{\mu}-\frac{1}{2}\delta^{\rho}_{\mu}R\right)=R^{\lambda}{}_{\tau}T^{\tau}{}_{\mu\lambda}+\frac{1}{2}R^{\lambda\sigma}{}_{\tau\mu}T^{\tau}{}_{\lambda\sigma}\ . \tag{6.4.4}$$

The term in the first bracket on the left-hand side is the Einstein tensor, so that the most general compatibility condition can be written as

$$\nabla_{\rho}G^{\rho}{}_{\mu}=R^{\rho}{}_{\tau}T^{\tau}{}_{\mu\rho}+\frac{1}{2}R^{\rho\sigma}{}_{\tau\mu}T^{\tau}{}_{\rho\sigma}\ . \tag{6.4.5}$$

Equation (6.4.5) can be seen as a compatibility or integrability condition in the following sense. One cannot choose the curvature tensor and the torsion tensor fully independently as the above equations need to be satisfied for a consistent geometrical approach. Hence we might expect there is some relation between the torsion and curvature related measures.

Let us now recall (5.3.6), the Einstein tensor in terms of Ω, which is $G=\mathrm{Curl}\,\Omega+\mathrm{Cof}\,\Omega$. Next, we use the decomposition of the spin connection (5.2.12) into the definition of Ω of (5.3.1) to obtain

$$\Omega_{c\mu}=-\frac{1}{2}\omega_{\mu}{}^{ab}\epsilon_{abc}=-\frac{1}{2}\left(\mathring{\omega}_{\mu}{}^{ab}+K^{a}{}_{\mu}{}^{b}\right)\epsilon_{abc}=\mathring{\Omega}_{c\mu}+\Gamma_{c\mu}\ . \tag{6.4.6}$$

When this decomposition is put into the expression of the explicit Einstein tensor, a straightforward calculation yields,

$$\begin{aligned}
G^{\lambda c}&=(\mathrm{Curl}\,\Omega)^{c\lambda}+(\mathrm{Cof}\,\Omega)^{c\lambda}\\
&=\mathrm{Curl}\,(\mathring{\Omega}+\Gamma)^{c\lambda}+\mathrm{Cof}\,(\mathring{\Omega}+\Gamma)^{c\lambda}\\
&=(\mathrm{Curl}\,\mathring{\Omega})^{c\lambda}+(\mathrm{Curl}\,\Gamma)^{c\lambda}+\frac{1}{2}\epsilon^{cab}\epsilon^{\lambda\mu\nu}\left(\mathring{\Omega}_{a\mu}+\Gamma_{a\mu}\right)\left(\mathring{\Omega}_{b\nu}+\Gamma_{b\nu}\right)\\
&=\left\{(\mathrm{Curl}\,\mathring{\Omega})^{c\lambda}+(\mathrm{Cof}\,\mathring{\Omega})^{c\lambda}\right\}+\left\{(\mathrm{Curl}\,\Gamma)^{c\lambda}+(\mathrm{Cof}\,\Gamma)^{c\lambda}\right\}+\epsilon^{cab}\epsilon^{\lambda\mu\nu}\mathring{\Omega}_{a\mu}\Gamma_{b\nu}\ .
\end{aligned} \tag{6.4.7}$$

The final term is a cross-term which mixes the curvature and the torsion parts of the connection. Without this term one of the compatibility conditions would necessarily implies the other, hence it is precisely the presence of this term which gives the general condition a much richer structure.

Using (6.4.5) and (6.4.7), we are now ready to present a universal process in deriving the complete description of compatibility conditions encountered so far

Case I: No curvature and no torsion

Let us set $R^{\rho}{}_{\sigma\mu\nu}=0$ and $T^{\lambda}{}_{\mu\nu}=0$ in (6.4.7). Then we must also have $K_{b\nu}=\Gamma_{b\nu}=0$ by the definitions, and we find the compatibility condition

$$\mathring{G}^{\lambda c}=(\mathrm{Curl}\,\mathring{\Omega})^{c\lambda}+(\mathrm{Cof}\,\mathring{\Omega})^{c\lambda}=0\ , \tag{6.4.8}$$

which is Vallée's result (6.1.6) discussed earlier.

Case II: No curvature and nonzero torsion

Let us set $R^{\rho}{}_{\sigma\mu\nu} = 0$ and $T^{\lambda}{}_{\mu\nu} \neq 0$ in (6.4.7) which becomes

$$G^{\lambda c} = \Big\{(\mathrm{Curl}\,\Gamma)^{c\lambda} + (\mathrm{Cof}\,\Gamma)^{c\lambda}\Big\} + \epsilon^{cab}\epsilon^{\lambda\mu\nu}\mathring{\Omega}_{a\mu}\Gamma_{b\nu} = 0\ . \tag{6.4.9}$$

Furthermore if we impose the condition $U^a_\mu = \delta^a_\mu$, then as observed in (6.4.1), $\mathring{\Omega}_{a\mu} = 0$ the compatibility condition reduces to

$$G^{\lambda c} = (\mathrm{Curl}\,\Gamma)^{c\lambda} + (\mathrm{Cof}\,\Gamma)^{c\lambda} = 0 \tag{6.4.10}$$

which is the Nye's result (6.2.9) and the micromorphic case (6.3.7).

Case III: No torsion and nonzero curvature

The nonzero Einstein tensor alone cannot constitute any of compatibility conditions. But using $R^{\rho}{}_{\sigma\mu\nu} \neq 0$ and $T^{\lambda}{}_{\mu\nu} = 0$ in (6.4.5) we have the compatibility condition

$$\mathring{\nabla}_\mu \mathring{G}^{\mu\sigma} = 0\ , \tag{6.4.11}$$

where $\mathring{G}^{\mu\sigma}$ is now a symmetric tensor. These equations are well known in the context of General Relativity (in this case one works on the four dimensional Lorentzian manifold) where they imply the conservation equations for the stress-energy-momentum tensor.

In four-dimensional case, along with the correspondence between matter and geometry [113, 114], the Einstein tensor can be related to the stress-energy-momentum tensor $T_{\mu\sigma}$ by

$$\mathring{G}_{\mu\sigma} = kT_{\mu\sigma}\ , \tag{6.4.12}$$

where $k = 8\pi G/c^4$ with the constant of gravitation G. The stress-energy-momentum tensor $T_{\mu\sigma}$ is symmetric and it contains the symmetric stress tensor t_{ij} of (1.2.14) for $i, j = 1, 2, 3$ as its subcomponents. The condition (6.4.11) suggests that the conservation equation for the stress-energy-momentum tensor reduces to the continuity equation similar to that of (1.2.17).

Case IV: Both nonzero curvature and torsion

In this case, the Einstein equation is related to the canonical stress-energy-momentum tensor $\Sigma_{\mu\sigma}$, [74]

$$G_{\mu\sigma} = k\Sigma_{\mu\sigma}\ . \tag{6.4.13}$$

The symmetry in the indices is not guaranteed when one brings the torsion in the equation, but the symmetric part of $\Sigma_{\mu\sigma}$ is $T_{\mu\sigma}$ in four dimensions.

There are no compatibility equations as such to satisfy. However, one should read (6.4.5) as integrability or consistency condition in the following sense. In deriving (6.4.2) and (6.4.3), as (6.4.5) is the consequence of these two expressions, we cannot expect that an arbitrary torsion field can arise in a manner that completely independent of the arbitrary curvature tensor, but there must be a relation between curvature and torsion tensor. A simple example of such a relation between curvature and torsion tensors will be given in Section 7.1, in the form of a continuity equation, after we define density tensors for both in curvature and torsion tensors, followed by brief consideration on homotopic classifications of the compatibility conditions.

Chapter 7

Manifold structures and the compatibility conditions

7.1 Burgers vector and Frank's vector

In this Section, we would like to see various integral forms of Burgers vector and Frank's vector that originated from the broken translational and rotational symmetries, due to the non-trivial torsion and curvature respectively.

For a n-dimensional manifold M, its interior and boundary, $\text{int}(M)$ and ∂M, are submanifolds of M with dimensions n and $n-1$, respectively. An $(n-1)$-form $\boldsymbol{\alpha} = \alpha_{\mu_1 \cdots \mu_{n-1}}$ defined on ∂M, and an n-form $d\boldsymbol{\alpha}$ defined in $\text{int}(M)$ for some differential operator d, are related by

$$\int_{\partial M} \boldsymbol{\alpha} = \int_{\text{int}(M)} d\boldsymbol{\alpha} \, . \tag{7.1.1}$$

This is a generalisation of the Stoke's theorem for a vector field $\boldsymbol{A}$

$$\oint_C \boldsymbol{A} \cdot d\boldsymbol{r} = \int_S (\nabla \times \boldsymbol{A}) \cdot d\boldsymbol{S} \tag{7.1.2}$$

where C is the boundary (a closed contour) for the interior (a surface) S.

The integral forms of Burgers and Frank's vectors, using the similar settings of Chapter 6 and Chapter 7, are given in [81]. Nonetheless, we would like to use the results we obtained so far and the above generalised Stoke's theorem, to identify and interpret the classical terms of dislocation density and disclination density tensors following the precise manner we have developed in torsion and curvature tensors.

Before we proceed, we would like to note that there are two scenarios when the spin connection vanishes. The first possibility is, as mentioned before, when the curvature is zero the spin connection is trivial [109] and becomes pure gauge. This is somewhat similar asymptotic behaviour to that is known in Euclidean Yang-Mills configuration and General Relativity. The second one is when we choose the normal coordinate system, we can put the spin connection to be zero but with nonzero derivative terms, which is also well-known in General Relativity.

Now, in the classical theory [68, 115], the Burgers vector is the sum of total changes in displacement vector $\delta \boldsymbol{u}$, caused by the dislocation when one measures the defects around a closed simple contour C. The dislocation line will be deformed in a way that an initially closed small loop might not be closed due to the broken translational symmetry. This breaking of the closed loop is analogous to the analysis of the torsion in general relativity [116], if we start with an infinitesimal parallelogram that is initially closed before the deformation.

In the manifold with zero curvature and nonzero torsion, by following the construction of the metric tensor given in Section 5.1, we can define the Burgers vector $\boldsymbol{b}$ by the integration of the total defects caused by the non-trivial tetrad field in analogous with the classical definition $\boldsymbol{u} = \Delta\boldsymbol{x}$ along the contour C

$$\oint_C e^a_\mu \, dx^\mu = -b^a \, . \tag{7.1.3}$$

The nonzero dislocation density tensor implies a nonzero torsion tensor. Hence the above definition can be written using the generalised Stoke's theorem by

$$\oint_C e^a_\mu \, dx^\mu = \int_S \left(\partial_\mu e^a_\nu - \partial_\nu e^a_\mu\right) dx^\mu \wedge dx^\nu = -b^a \, . \tag{7.1.4}$$

We recognise the term $\left(\partial_\mu e^a_\nu - \partial_\nu e^a_\mu\right)$ acts the role of dislocation density tensor. But this is indeed the form of the torsion tensor (5.2.7) where we used the fact that the spin connection $\omega_\mu{}^a{}_b$ vanishes when we have the zero curvature. Also this fact agrees with the previous relation of the dislocation density tensor $K^a{}_\rho$ and the torsion tensor $T^a{}_{\mu\nu}$ in (6.2.6). So we can write further

$$\oint_C e^a_\mu \, dx^\mu = \int_S T^a{}_{\mu\nu} \, dx^\mu \wedge dx^\nu = \int_S K^a{}_\rho \epsilon^\rho{}_{\mu\nu} \, dx^\mu \wedge dx^\nu = -b^a \, . \tag{7.1.5}$$

In addition, non-vanishing term of $\left(\partial_\mu e^a_\nu - \partial_\nu e^a_\mu\right)$ implies the anholonomic property (5.1.21), which is exactly the current case.

On the other hand, in the space of the nonzero curvature tensor and the zero torsion tensor, the Frank vector $\boldsymbol{F}$ can be defined by

$$F^c = \frac{1}{2}\epsilon^{abc} F_{ab} \tag{7.1.6}$$

where the quantity F^{ab} is defined by

$$\oint_C \mathring{\omega}_\mu{}^{ab} \, dx^\mu = F^{ab} \, . \tag{7.1.7}$$

Again, using the Stoke's theorem, we can write

$$\oint_C \frac{1}{2}\mathring{\omega}_\mu{}^{ab}\epsilon_{ab}{}^c \, dx^\mu = \int_S \frac{1}{2}\left(\partial_\mu \mathring{\omega}_\nu{}^{ab} - \partial_\nu \mathring{\omega}_\mu{}^{ab}\right)\epsilon_{ab}{}^c \, dx^\mu \wedge dx^\nu = F^c \, . \tag{7.1.8}$$

We see that the terms in the brackets of (7.1.8) is the Riemann curvature tensor $\mathring{R}^{ab}{}_{\mu\nu}$ of (5.2.9) where the quadratic terms vanish if we choose the normal coordinate system. This agrees with the classical definition of the disclination density tensor [115, 117] which measures the disclination of planar defects with a given uniaxial system. Then

$$\oint_C \frac{1}{2}\mathring{\omega}_\mu{}^{ab}\epsilon_{ab}{}^c \, dx^\mu = \int_S \frac{1}{2}\mathring{R}^{ab}{}_{\mu\nu}\epsilon_{ab}{}^c \, dx^\mu \wedge dx^\nu = F^c \, . \tag{7.1.9}$$

Furthermore, from the definition of the Einstein tensor (5.3.4) we can write

$$\mathring{G}^{\sigma c} = -\frac{1}{4}\epsilon_{ab}{}^c \epsilon^{\sigma\mu\nu}\mathring{R}^{ab}{}_{\mu\nu} = -\frac{1}{2}\epsilon_{ab}{}^c \epsilon^{\mu\nu\sigma}\partial_\mu \mathring{\omega}_\nu{}^{ab} \tag{7.1.10}$$

and

$$\mathring{G}^{\sigma c}\epsilon_{\sigma\mu\nu} = -\frac{1}{2}\epsilon_{ab}{}^c \mathring{R}^{ab}{}_{\mu\nu} \quad . \tag{7.1.11}$$

A similar analysis can be found in [81] as we mentioned, but here we emphasise the identifications that the Einstein tensor acts as the disclination density tensor. Then we can rewrite the Burgers

and the Frank's vectors in terms of various forms of dislocation and disclination density tensors,

$$\oint_C e^a_\mu \, dx^\mu = \int_S T^a{}_{\mu\nu} \, dx^\mu \wedge dx^\nu = \int_S K^a{}_\rho \epsilon^\rho{}_{\mu\nu} \, dx^\mu \wedge dx^\nu = -b^a \, , \tag{7.1.12a}$$

$$\oint_C \frac{1}{2} \mathring{\omega}_\mu{}^{ab} \epsilon_{ab}{}^c \, dx^\mu = \int_S \frac{1}{2} \mathring{R}^{ab}{}_{\mu\nu} \epsilon_{ab}{}^c \, dx^\mu \wedge dx^\nu = \int_S -\mathring{G}^{\sigma c} \epsilon_{\sigma\mu\nu} \, dx^\mu \wedge dx^\nu = F^c \, . \tag{7.1.12b}$$

Now, we go back to the general case of manifold in which both curvature and torsion tensors are nonzero. The contracted form of $G_{\sigma c}$ with $\epsilon_a{}^{\sigma c}$ followed by the decomposition (5.2.12) gives

$$\begin{aligned} \epsilon_a{}^{\sigma c} G_{\sigma c} &= -\frac{1}{2} \epsilon_a{}^{\sigma c} \epsilon_{lbc} \epsilon^{\mu\nu}{}_\sigma \partial_\mu \left(\mathring{\omega}_\nu{}^{lb} + K^l{}_\nu{}^b \right) \\ &= \frac{1}{2} \epsilon_a{}^{c\sigma} \epsilon_{lbc} \epsilon^{\mu\nu}{}_\sigma \partial_\mu K^l{}_\nu{}^b + \epsilon_a{}^{\sigma c} \mathring{G}_{\sigma c} \, , \end{aligned} \tag{7.1.13}$$

in which we have now the symmetric Einstein tensor $\mathring{G}_{\sigma c}$ on the right-hand side, hence it vanishes. Using the definition of Nye's tensor (6.2.8) and its relation with the dislocation density tensor (6.2.11), we obtain

$$\partial_\mu K_a{}^\mu + \epsilon_a{}^{c\sigma} G_{c\sigma} = 0 \, . \tag{7.1.14}$$

This continuity equation signifies the fact that the disclination density tensor (i.e. the Einstein tensor) acts as the source or the sink of the dislocation density tensor. Also this supports our statement given in the end of Section 6.4 that the torsion and curvature cannot be determined arbitrarily at the same time. Similar continuity equations in the classical theory linking the dislocation and disclination density tensors can be found, for example, in [67, 115] without identifying the Einstein tensor as the disclination density tensor in general.

7.2 Homotopy for the compatibility conditions

In [118], it is shown that the existence of the metric tensor field (4.2.4) for a given immersion $\Theta : \Omega \to \mathbb{E}^3$ requires the condition $R^\rho{}_{\sigma\mu\nu} = 0$ in $\Omega \subset \mathbb{R}^3$ and Ω to be simply-connected. It is further shown to be necessary and sufficient. If the subset of the given manifold is just connected subset, then Θ is unique up to isometry of Euclidean space $\mathbb{E}^3$ to ensure the existence of the metric field

$$C = (\nabla \tilde{\Theta})^T (\nabla \tilde{\Theta}) \, , \tag{7.2.1}$$

where $\Theta = Q\tilde{\Theta} + T$ for $Q \in SO(3)$ and T is translation.

We saw in Section 6.3 that the integrability for the partial differential equation $\partial_K x_k = 0$ requires the condition

$$\frac{\partial^2 x_k}{\partial X_P \partial X_Q} = \frac{\partial^2 x_k}{\partial X_Q \partial X_P} \, ,$$

which in turn implies the vanishing curvature tensor $\mathring{R}^\rho{}_{\sigma\mu\nu} = 0$. But this formalism is highly dependent on the symmetric property of the metric tensor under the diffeomorphism. The nonzero torsion and the existence of the non-trivial Burgers vector, as we saw in Section 7.1, implies the anholonomy (5.1.21). This signals the departure from the compatibility condition based on the diffeomorphism such as the classical Vallée's result.

Now, we wish to establish how many compatibility conditions, or more precisely, how many classifications of such compatibility conditions are derivable from the condition $R^\rho{}_{\sigma\mu\nu} = 0$. One possible approach to answer this question would be the consideration of homotopy classification

$\pi_n(M)$, where n is a dimension of an n-sphere S^n, a probe of defects in the space M, in which an *order parameter* is defined. We can take the order parameter as a measure for degrees of ordered state for now, but we will see more details in Part III. For example, in a completely random state in a high temperature, the order parameter becomes zero in some physical model. In our case, we can put the order parameter to simply be the tetrad field e^a_μ so that $M = SO(3)$, a measure for the rotational fields hence a measure for the nonzero torsion tensor.

It is well-known that the dislocation tensor or equivalently the torsion tensor can be measured by following a small closed path in the crystal lattice structure, and the curvature tensor can be computed in a similar manner as we mentioned in the previous Section. For this purpose, we can put $n = 1$ to consider the fundamental group for $SO(3)$, which is a homotopy group for the line defects in three dimensions

$$\pi_1(SO(3)) \cong \mathbb{Z}_2 \, . \tag{7.2.2}$$

This suggests that we can have two distinct classifications for the compatibility conditions under $R^\rho{}_{\sigma\mu\nu} = 0$. One of them is the trivial class, the elastic regime so that all elastic deformations belong to the same compatible condition. And the non-trivial classification is for the microstructure description where one is only dealing with microdeformations. Similar group theoretical analysis can be found in [68, 119, 120].

Interestingly, in some simplified Skyrme models [121], the homotopy class $\pi_4(SO(3))$ is identified with $\pi_1(SO(3))$. Since $SO(3)$ is not simply connected, it is straightforward to see that its fundamental group is isomorphic to $\mathbb{Z}_2$. Further, using J-homomorphism (see Appendix B), we can state

$$\pi_4(SO(3)) \cong \pi_1(SO(3)) \cong \mathbb{Z}_2 \, . \tag{7.2.3}$$

This characterises the equivalent classes of the compatibility conditions, hence the possible solution space for the system in describing the deformations, as below.

$$\begin{aligned} &\{0\} : \text{Configurations that can be continuously deformed uniformly via diffeomorphisms.} \\ &\{1\} : \text{Configurations that cannot be continuously deformed in a way of } \{0\}. \end{aligned} \tag{7.2.4}$$

The elastic compatibility condition including the Vallée's result (6.1.8) falls into the classification $\{0\}$, vanishing curvature and torsion. The conditions of Nye (6.2.9) and the micropolar case (6.3.11b) belong to $\{1\}$, vanishing curvature and nonzero torsion. These classifications are particularly significant if one interprets that every description of deformations within one class, say $\{0\}$, must remain in that class while further smooth and small deformations are admissible. This is equivalent to say that all deformational descriptions can be classified by its discrete equivalent classes, in which different configurations of system can be continuously deformed from one to other without violating any physically sensible requirements such as the finite energy condition.

We will see more of the formal homotopy classification, and the group theoretical treatment of soliton solutions, the deformational description of Part I, with the help of physical systems of condensed crystal models and systems with a spinor structure in Part III.

Part III

Defects in director fields

Chapter 8

Theories of directors

We review some of topological properties in the projective space, and the well-known fact that the real projective space $\mathbb{R}P^2$ can be viewed as a manifold for the nematic liquid crystals [32, 69, 122–124]. The relation between the projective space $\mathbb{R}P^2$ and the sphere S^2 will essentially allow us to view the micropolar continua as the projective space but this shall wait until Chapter 10. After we define the order parameter, we will take the nematic liquid crystals as our model to investigate the role of order parameters on the projected subspace. Then we consider the free energy formalism to understand the nematic liquid crystals in the framework of the micropolar continua, by comparing with the deformational measures we developed in Part II. The deformational measures used in Part II, notably the quantity $\partial_\mu R$, would be meaningless if the rotational axis and angles are constant. In Part I, we based on the assumptions such as a constant axis of the rotation to simplify the problem and to obtain the overall picture for the microrotational deformations. In Part III, along with arbitrary angular fields, we would like consider position-dependent axial configurations for the microrotations. Part III is mainly based on the work [125].

8.1 Projective space and homotopy classification

Suppose we have a system which lies on a two-dimensional sphere S^2 in $\mathbb{R}^3$. We would like to find the correspondence between the projected space on $\mathbb{R}^2$ from the unit sphere S^2, using the stereographic projection. For S^2, we denote $\boldsymbol{n}_\infty = (0, 0, 1)$ the north pole, and for a given point $\boldsymbol{s} \in S^2$, an intersecting point of line connecting $\overline{\boldsymbol{n}_\infty \boldsymbol{s}}$ and xy-plane be p. For this purpose, the stereographic projection is most instructive to illustrate the projective space. In three dimensions, the stereographic projection is defined by

$$\begin{aligned} &\pi : S^2 \backslash \{\boldsymbol{n}_\infty\} \longrightarrow \mathbb{R}^2 \\ &\pi(s_1, s_2, s_3) = \left(\frac{s_1}{1 - s_3}, \frac{s_2}{1 - s_3} \right) = (x, y) \end{aligned} \tag{8.1.1}$$

for a point $\boldsymbol{s} = (s_1, s_2, s_3) \in S^2$ such that $s_1^2 + s_2^2 + s_3^2 = 1$ and $(x, y) \in \mathbb{R}^2$. Inversely, we can express a point on S^2 in terms of (x, y) on $\mathbb{R}^2$ with $r^2 = x^2 + y^2$ by

$$\boldsymbol{s} = \left(\frac{2x}{r^2 + 1}, \frac{2y}{r^2 + 1}, \frac{r^2 - 1}{r^2 + 1} \right) \tag{8.1.2}$$

and we can see that $\boldsymbol{s} \to \boldsymbol{n}_\infty = (0, 0, 1)$ as $r \to \infty$. If we identify the point on the xy-plane in the limit of $r \to \infty$ as a north pole of S^2, then we have a bijection between the extended complex

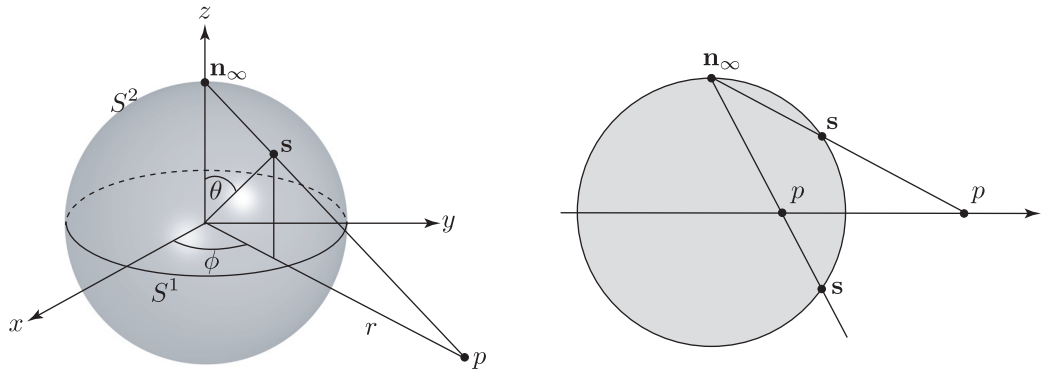

Figure 8.1: Left: A unit sphere in polar coordinate system with its centre located at the origin. The great circle (the equator) corresponds to the unit disk S^1 lying on the xy-plane. Right: The extended line segment $\boldsymbol{n}_\infty \boldsymbol{s}$ will intersect the xy-plane in the point p located outside the sphere if $\boldsymbol{s}$ is on the northern hemisphere, and p will locate on the interior of S^1 if $\boldsymbol{s}$ is on the southern hemisphere. The south pole with the coordinate $(0, 0, -1) \in S^2$ corresponds to the origin by the projection.

plane $\mathbb{C}_\infty$ and S^2. Under this identification, S^2 is the **Riemann sphere**, the compactification of an infinite radius of the plane into a sphere.

Next, we would like to review briefly the real and the complex projective space. These two spaces will play significant roles in developing connections between two topological spaces by recognising antipodals on the given unit sphere as a hypersurface for a given manifold.

8.1.1 Real projective space

The n-dimensional real projective space $\mathbb{R}P^n$ is the space of all lines through the origin in $\mathbb{R}^{n+1}$. And this space is obtained from $S^n \subset \mathbb{R}^{n+1}$

$$S^n = \{x \in \mathbb{R}^{n+1} \mid |x| = 1\}$$

by taking the quotient of $\mathbb{R}^{n+1}\backslash\{0\}$ under the equivalence classes

$$x \sim \lambda x \qquad \text{for} \qquad \lambda \in \mathbb{R},\ \lambda \neq 0\ .$$

We can always find a λ such that $|\lambda| = 1$ for all $x \in \mathbb{R}^{n+1}\backslash\{0\}$. Hence there are two such λ, namely $\lambda = +1, -1$. This implies that the real projective space $\mathbb{R}P^n$ can be recognised as the quotient space

$$\mathbb{R}P^n \cong S^n/\{\text{antipodal}\}\ , \tag{8.1.3}$$

by identifying a pair of antipodals $\{x, -x\}$ on the surface of S^n. This allows us to view $\mathbb{R}P^n$ as the quotient space of a hemisphere of S^n with antipodals on the boundary of ∂S^n are identified. Since the boundary, with antipodal points identified, is again $\mathbb{R}P^{n-1}$ we see that $\mathbb{R}P^n$ can be constructed from $\mathbb{R}P^{n-1}$ by attaching an n-cell with the quotient projection $S^{n-1} \to \mathbb{R}P^{n-1}$ as the attaching map [126]. And it is well-known that the n-sphere S^n is a covering space $\mathbb{R}P^n$ for $n \geq 2$.

We consider $\mathbb{R}P^2$ to illustrate the real projective space both in geometrical and topological points of view. From a geometrical point of view, we can represent $\mathbb{R}P^2$ as a subset of $\mathbb{R}^2$ plane with *ideal points* as equivalence classes $x \sim \lambda x$ passing through the origin. These lines will meet at infinity, and point the opposite directions. But these lines are merely the projection of *rays* passing through the origin of $\mathbb{R}^3$, from which we can recognise that the horizontal rays are ideal points in $\mathbb{R}P^2$ when they are projected on the plane. See Fig. 8.2.

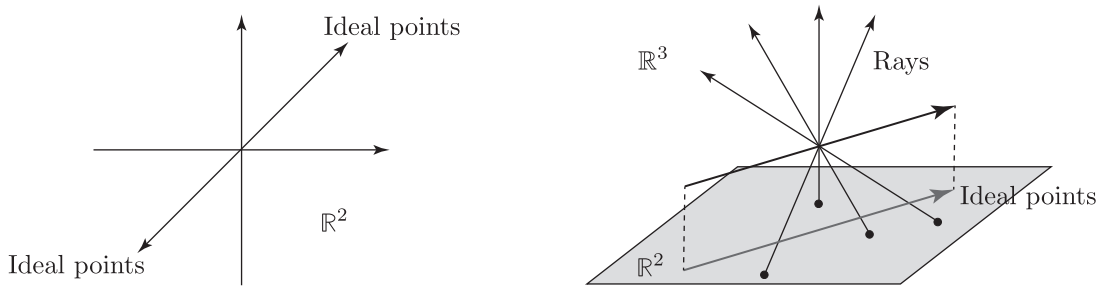

Figure 8.2: Left: Ideal points passing through the origin on $\mathbb{R}^2$. Right: Equivalent rays passing through the origin in $\mathbb{R}^3$ are shown. One special class of rays are those lie on the disk S^1, which are projected to be ideal points on the plane.

If we construct curved space which intersects all rays in $\mathbb{R}^3$, this will effectively reduce the number of equivalence classes. So, we can identify two points $\boldsymbol{n} = -\boldsymbol{n}$ on the sphere S^2 for $\boldsymbol{n} = (n_1, n_2)$ satisfying $n_1^2 + n_2^2 = 1$. Hence, we have $\mathbb{R}P^2 \cong S^2/\{\text{antipodal}\}$. This identification of the antipodals allows us to remove the redundancy by removing the upper hemisphere (equally we can remove the lower half). And we recognise that rays are only ideal points which meet at two points on the equator of the hemisphere of S^2. Using the definition of the projective space with antipodals and rays on the sphere, and ideal points on the projected plane, a schematic process of removing the redundancy on S^2 is shown in Fig. 8.3.

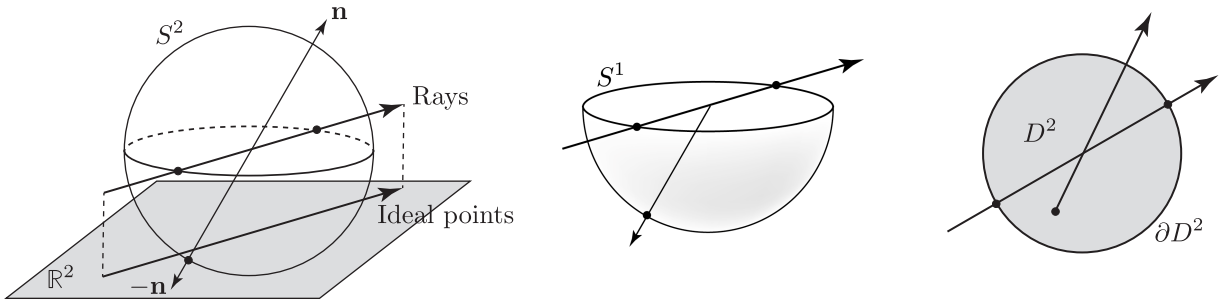

Figure 8.3: Left: We start from identifying rays and antipodals on S^2. Middle:We remove the upper hemisphere by identifying $\boldsymbol{n} = -\boldsymbol{n}$ but keep the points of the rays on the equator. Right: We flatten the hemisphere to obtain a disk with its interior filled with the projection from S^2, and the boundary consists of the ideal points of rays.

In order to get the better idea, we flatten the hemisphere to obtain a disk D^2 with ideal points on the boundary. In this way, we can construct $\mathbb{R}P^2$ in the interior of D^2 with ideal points on its boundary ∂D^2. In general, we can regard $\mathbb{R}P^n$ as an n-dimensional disk D^n with the ideal points on the boundary $\partial D^n \cong S^{n-1}$, so that

$$\mathbb{R}P^n \cong D^n \cup \partial D^n \cong D^n \cup S^{n-1} \,. \tag{8.1.4}$$

There is an additional important feature in the projective plane that the projective plane can be *non-orientable*. In other words, it may contain a Möbius band. To see this, we go back to the sphere with rays, and consider the cylindrical portion on S^2 with equivalent antipodal points represented by the same colours as shown in Fig. 8.4.

We know there are two identifiable points on the edge of the band. This means we can cut the band half, and glue it after half twist to match antipodal points $\boldsymbol{n} = -\boldsymbol{n}$. By gluing we really

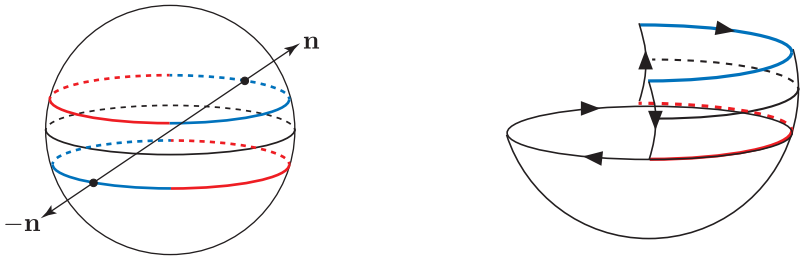

Figure 8.4: Left: Antipodals can be shown as a pair of outward vectors $\{-\boldsymbol{n}, \boldsymbol{n}\}$ on the edge of cylindric portion of the sphere with the same colour. Right: We can assign a direction following on the boundary of the disk D^2 to the edge of the Möbius band with antipodals identified on S^2 after obtaining the most compact representation of $\mathbb{R}P^2$ after removing all possible redundancies.

mean that we identify the space topologically and, on the other hand, identifying antipodals emphasises the geometrical sense. This geometrical recognition will reveal its physicaly relevant system in Section 8.3. As a result, we will obtain the Möbius band M^2. Further, we combine the remaining part of the hemisphere which is topologically equivalent to the flattened disk D^2 with its boundary ∂D^2 representing the set of all ideal points. We finally obtain the most compact topological representation of the real projective space $\mathbb{R}P^2$, after removing all the redundancies as much as possible, by a union of a Möbius band and a disk D^2. See Fig. 8.5.

$$\mathbb{R}P^2 \cong M^2 \cup D^2 \ . \tag{8.1.5}$$

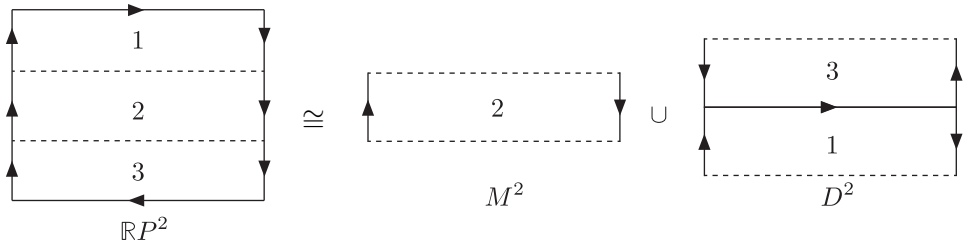

Figure 8.5: We can follow the arrows on the hemisphere and a bisected cylindrical portion on the sphere illustrated in Fig. 8.4 to represent the fundamental polygon of $\mathbb{R}P^2$. This further reduces to a union of Möbius band and a disk with its corresponding representations. The dotted lines are free, and the directed solid lines are identifiable. i.e. it can be glued together if the direction of arrows are identical, if not, we can twist them to identify the directions as in the case of the Möbius band.

8.1.2 Complex projective space

In analogy to the real case, the complex projective space $\mathbb{C}P^n$ is the space of complex lines through the origin in $\mathbb{C}^{n+1}$. This space is constructed by considering a complex manifold of nonzero $(n+1)$ complex coordinates

$$z = (z_1, \cdots, z_{n+1}) \in \mathbb{C}^{n+1} \backslash \{0\} \ .$$

As the case of the real projective space, the equivalence classes are defined by

$$z \sim \zeta z \qquad \text{for} \qquad \zeta \in \mathbb{C}, \zeta \neq 0 \ .$$

Again, we can always find a $\zeta \in \mathbb{C}$ such that $|\zeta| = 1$. Hence, this equivalent class is the quotient of the unit sphere

$$S^{2n+1} \subset \mathbb{C}^{n+1} \ ,$$

which can be seen from the fact that

$$S^{2n+1} \subset \mathbb{R}^{2(n+1)} \cong \mathbb{C}^{n+1} \ .$$

But vectors in $S^{2n+1} \subset \mathbb{C}^{n+1}$, with its last component is real and non-negative, are precisely vectors of the form

$$(\omega, \sqrt{1-|\omega|^2}) \in \mathbb{C}^n \times \mathbb{C}, \qquad |\omega| \leq 1 \ .$$

In particular, we can regard this as a disk D^{2n} bounded by the sphere S^{2n+1} if it consists of vectors

$$(\omega, 0) \in \mathbb{C}^n \times \mathbb{C}, \qquad |\omega| = 1 \ ,$$

where we used the identifications of spheres, disks and its boundaries for a given $\mathbb{R}^{n+1}$ by

$$S^n \subset \mathbb{R}^{n+1}, \qquad D^n \subset \mathbb{R}^n, \qquad \partial D^n = S^{n-1} \ .$$

Hence, each vector in S^{2n+1} is equivalent under the identifications $z \sim \zeta z$ to a vector in D^{2n} and the vectors are unique if its last component is nonzero. If the last coordinate is zero, we can always have the identifications $z \sim \zeta z$ for $z \in S^{2n-1}$. In other words, every line in $\mathbb{C}^{n+1}$ intersects the unit sphere in a circle and we can write

$$\mathbb{C}P^n \cong S^{2n+1}/S^1 \ . \tag{8.1.6}$$

This is analogous to the real projective space (8.1.3) in which the quotient space is taken by the set of antipodals. So, the difference between the real and the complex projective space arises by identifying the equivalence classes in each space of $\mathbb{R}^{n+1}$ and $\mathbb{C}^{n+1}$, in such a way that

$$\begin{array}{lllll} \mathbb{R}P^n \subset \mathbb{R}^{n+1}: & x \sim \lambda x & |\lambda| = 1, \ \lambda \in \mathbb{R} & \{\text{antipodals}\} \\ \mathbb{C}P^n \subset \mathbb{C}^{n+1}: & z \sim \zeta z & |\zeta| = 1, \ \lambda \in \mathbb{C} & S^1 \ . \end{array} \tag{8.1.7}$$

Moreover, a pair of antipodals in the real and the complex projective spaces are invariant under discrete symmetry $x \to -x$ and under $SO(2)$, respectively.

8.1.3 Homotopy and projective space

The principal fibre bundle structure $\{E, M, G, \pi, \psi\}$ consists of total space E and its projected base space M by a map π. The action of the group G is defined on the total space by a map $\psi : E \times G \longrightarrow E$. With a notion of fibre bundle F, it is conveniently expressed by a sequential expression

$$F \hookrightarrow E \to M \ . \tag{8.1.8}$$

We note that the complex projective space $\mathbb{C}P^n$ carries the structure of a complex manifold of $\mathbb{C}^n$ and the structure of a real manifold $\mathbb{R}^{2n}$. In particular, if $n = 1$ the complex projective space $\mathbb{C}P^1$ is identified with the Riemann sphere. This is known as the **Hopf fibration**, and its fibre bundle structure is conventionally written by

$$S^1 \hookrightarrow S^3 \to \mathbb{C}P^1 \ . \tag{8.1.9}$$

In general, we summarise some important fibrations as follows.

$$SO(n-1) \hookrightarrow SO(n) \to S^{n-1} \ , \tag{8.1.10a}$$

$$SU(n-1) \hookrightarrow SU(n) \to S^{2n-1} \ , \tag{8.1.10b}$$

$$S^0 (= \mathbb{Z}_2) \hookrightarrow S^n \to \mathbb{R}P^n \ , \tag{8.1.10c}$$

$$S^1 \hookrightarrow S^{2n+1} \to \mathbb{C}P^n \ . \tag{8.1.10d}$$

In addition, we summarise fundamental group properties of some well-known compact groups in Table 8.1 with the simply-connected group structure for the later use. And, if the given group is not simply-connected, the relation with its universal covering group can be given. For example, suppose the given manifold M (and its isomorphic group structure) is simply-connected, then any simple closed loop contained in the given manifold can be continuously deformed into another loop and eventually can be deformed to a point. Then, by definition of the first homotopy or the fundamental group, we will have a trivial homotopy

$$\pi_1(M) \cong \{e\} \tag{8.1.11}$$

On the other hand, if the manifold is not simply-connected, its fundamental group will be non-trivial. We denote the identity element of a given group by $\{e\}$. When the group operation is defined by the addition, we simply denote the identity element by $\{0\}$. Some of useful and well-known higher homotopy groups are listed in Appendix B, with a number of generalisations and corresponding theorems [126–128].

Compact group	Simply connected	Fundamental group
$SO(2)$	No	$\mathbb{Z}$
$SO(n),\ n \geq 3$	No	$\mathbb{Z}_2$
$U(n)$	No	$\mathbb{Z}$
$SU(n)$	Yes	e
S^1	No	$\mathbb{Z}$
$S^n,\ n \geq 2$	Yes	e
$\mathbb{R}P^1$	No	$\mathbb{Z}$
$\mathbb{R}P^n,\ n \geq 2$	No	$\mathbb{Z}_2$
$\mathbb{C}P^n$	Yes	e

Table 8.1:

Since all S^n, for $n \geq 2$, are simply-connected, we have $\pi_1(S^n) \cong \{e\}$ for $n \geq 2$. Hence S^n is the universal covering space of $\mathbb{R}P^n$. By the *Lifting Properties* of the fundamental group [126], this recognition further gives isomorphisms

$$\pi_n(S^n) \cong \pi_n(\mathbb{R}P^n) \cong \mathbb{Z}, \qquad n \geq 2\ . \tag{8.1.12}$$

8.2 Order parameter and homotopy

In general, when a physical system undergoes a phase transition, the symmetry of the system will be altered, and this reduction in the symmetry is described by degrees of order of the system defined in the **order parameter space** M [122, 129, 130]. If the system is in the completely random state, say in a high temperature, we can regard that there is no meaningful measure of ordered state, and we say the order parameter is zero.

As the system undergoes the phase transition, for example as the temperature decreases, there may be points, lines or surfaces in the medium on which the degrees of order are not uniquely defined. They are called the **defects**, and the names of defect with respective dimensions are given in Table 8.2. These defects can be understood in connection with topological invariant quantities, and can be found in diverse physical systems with order parameters describing the defects of distinct nature [131, 132].

For example, the three-dimensional *Ising model* takes its degrees of alignment of the spin direction in the order parameter space M of two different spin states S, namely spin-up $|\uparrow\rangle$ and spin-down $|\downarrow\rangle$, so that we can put $M = |\uparrow\rangle \cup |\downarrow\rangle$. If the system is not completely isotropic, then

Dimensions	Names	
0	Point defects:	Monopoles
1	Line defects:	Vortices
2	Surface defects:	Domain walls

Table 8.2:

there might be a region in which the degrees of alignment of the spin are not well defined but with the mixed states of the spins. In other words, if $S = |\uparrow\rangle$ for $x < 0$ and $S = |\downarrow\rangle$ for $x > 0$, there is a defected region called *domain wall* in the yz-plane at $x = 0$. i.e. the region in which the order parameter is not uniquely determined. A similar analysis can be done in Heisenberg ferromagnet system with the spontaneous magnetisation.

In this way, a uniform system takes its value in a certain region M, the *order parameter space* and degrees of order are called the **order parameters**. The mixed uses of these terminologies are often seen in the literature. The order parameter space can be viewed as an internal space, and generally differs from the physical space where the medium resides. The order parameter space can be characterised by its dimension (again may differ from the physical dimension) and topological properties such as simply connectedness and compactness. See Table 8.1.

If the system is in an inhomogeneous state through the phase transition, when one considers the energy required in the phase transformation, the derivatives of the order parameter cannot be negligible and the degrees of order parameter may not be in M as we noted.

The defects are classified by the homotopy groups according to their dimensions. To see this, let E be space which is filled with the medium under consideration. Apart from the notion as a measure of some state of the system, it is more appropriate to regard the order parameter as a function $\Psi(x)$ depends on the point $x \in E$ that maps E to M in which the order parameter is defined,

$$\Psi : E \longrightarrow M \ . \tag{8.2.1}$$

This assignment emphasises that the order parameter $\Psi(x)$ is a subset of order parameter space M, in general.

Now, we consider the reduction of symmetry group in the system in terms of order parameter space M. Suppose there is a group G under which a homogeneous configuration remains invariant when the system exhibits completely random degrees of order, for example, in a high temperature. As the temperature decreases, the state of randomness may decrease and the group G will be no longer valid but it will be altered to its subgroup H, ideally its normal subgroup, see Fig. 8.6. This means we have a **spontaneous symmetry breaking**, and this can be represented by a group R which is isomorphic to a coset group structure defined by

$$R \cong G/H \ . \tag{8.2.2}$$

Consequently, the modified order parameter space M will be acted by the reduced group structure, and if there is an isomorphism between them we can assign

$$M \cong G/H \ . \tag{8.2.3}$$

Now, we establish the connection between order parameter and homotopy classification. Suppose there is a defect in the medium, for example, a line defect (i.e. vortices) in the three-dimensional medium. Imagine a unit circle S^1, as the order parameter encircles the line defect. If each part of S^1 is far from the line defect, much further than the coherence length scale of molecules at the stable energy level, we may assume the order parameter along S^1 to take its value in the order parameter space $M = U(1)$. This is how the fundamental group can be put

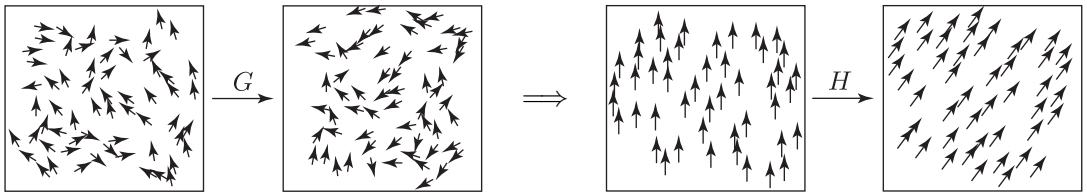

Figure 8.6: On the left, the system is in its homogeneous state, and shows zero degrees of order where the arrows represent the direction of spin or simply director of the internal molecular structure. This state is invariant under the group G, a composite of local rotations and local translations. After the phase transition, as shown on the right, the state starts to show the nonzero degrees of order of alignment and the local rotation is no longer valid but only the global rotation and the translation are valid symmetries, represented by the subgroup H. Hence there exists a certain spontaneously broken symmetries in the system.

into action, and we can classify the defect for a given dimensionality. In this case, we have loops in topological space $U(1)$ and the map

$$S^1 \longrightarrow U(1) \tag{8.2.4}$$

is classified by the homotopy group. We can regard the map (8.2.1) for the general case of the correspondence between the n-dimensional sphere surrounding the possible defect of the physical space and the d-dimensional internal space where the order parameter is defined. We may write this correspondence simply by

$$S^n_{\text{phy}} \longrightarrow S^d_{\text{int}} \ . \tag{8.2.5}$$

For the map (8.2.4), since (see Appendix B)

$$\pi_1(U(1)) \cong \mathbb{Z} \ ,$$

we may assign an integer to classify the line defect (we will see shortly why we took this particular homotopy group). This integer is called the **winding number**, since it literally counts how many times the image of S^1 winds the space $U(1)$. See Fig. 8.7.

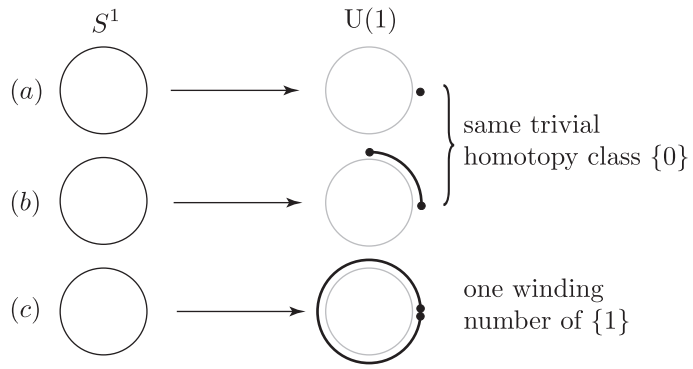

Figure 8.7: The map (a) and (b) show no complete winding, and the map (b) can be continuously deformed to the map (a) so that both belong to the trivial homotopy class $\{0\}$. The map (c) describes a complete winding and this cannot be continuously deformed into the class $\{0\}$ but it belongs to the class $\{1\}$. By counting the winding numbers, we can assign a distinct set of integer-valued classification.

- If two defects have the same winding number, it can be continuously deformed to the other. This means that two defects belong to the same homotopy group, and they are regarded equivalent.

- If two defects l_1 and l_2 merge together, the new defect belongs to the homotopy class of the product of the homotopy classes to which l_1 and l_2 belonged before coalescence.

- Since the group operation of $\mathbb{Z}$ (in this particular example) is an addition, the new winding number is a sum of the individual winding numbers. In particular, a uniform distribution of the order parameter corresponds to the constant map $\Psi(x) = x_0 \in M$, belongs to the unit element $\{0\} \in \mathbb{Z}$.

- If two defects of opposite winding numbers merge together, this will lead to the defect-free configuration of $\{0\}$. For example, the collision of vortex and anti-vortex with corresponding winding numbers $+1$ and -1 will annihilate each other.

In practice, in order to determine the homotopy groups we will proceed according to the following steps.

i) We identify the dimension of the manifold m where the medium is defined. This can be different from the dimension of physical space where the medium is located.

ii) We take account of the dimensionality d of the physically possible defect.

iii) We identify the n-sphere S^n which surrounds the region of defects.

In general [133] , the dimension of S^n is restricted by the d-dimensional defect in a m-dimensional medium and is classified by the homotopy group

$$\pi_n(M), \qquad n = m - d - 1 \; . \tag{8.2.6}$$

This expression can be seen as the defects with dimension d is being measured by a *probe* with dimension n of S^n separated by a line of dimension 1, and all of them are in the manifold of interest with dimension m. We can assign the degrees of defect from the measure with a ruler S^n a point in the manifold M. This will show the continuous deformation from one description of the defect to other in the form of equivalent classes, hence the homotopy group representation.

For example, a point defect can be investigated in a three-dimensional medium surrounded by S^2 $(2 = 3 - 0 - 1)$ and the defect is classified by

$$\pi_2(M) \; .$$

Then, what we are left with is to identify the topological nature of the order parameter space to determine the dimension of M. Particularly intuitive case is that if there is an isomorphism between the order parameter M and m-sphere S^m. This allows us to investigate the possible class of defects by relatively simple homotopic consideration of counting the number of winding of S^n over S^m

$$\pi_n(M) \cong \pi_n(S^m) \; . \tag{8.2.7}$$

This will give us the clue whether the defects classified in Table 8.2 are trivial $\{0\}$ so that we cannot expect to see any of these defects for the given system, or something else.

8.3 Nematic liquid crystals

Certain organic crystals exhibit quite interesting optical properties when they are in the isotropic fluid phases in which orientations and positions of directors are randomly distributed. They are called liquid crystals, characterized by their optical features. We are particularly interested in the so-called **nematic liquid crystals**. These are characterised by its long axes oriented along a certain direction while the positions of the centre of individual molecule are isotropic. An example of this is would be Octyloxy-Cyanobiphenyl. See Fig. 8.8.

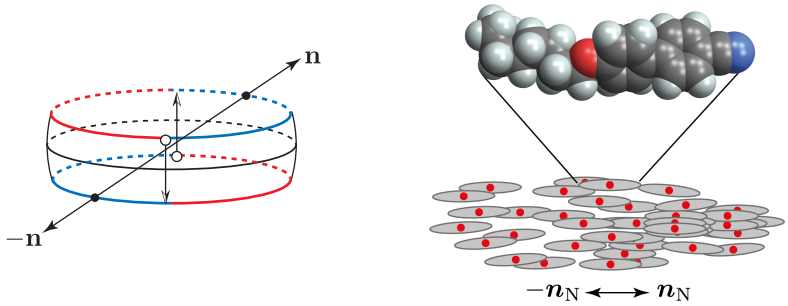

Figure 8.8: Left: By following a pair of antipodals on the cylindrical portion in constructing the Möbius band on S^2, it is easy to associate opposite signed directors $\boldsymbol{n}$ and $-\boldsymbol{n}$ on the sphere. Right: A molecule model of rod-like shaped Octyloxy-Cyanobiphenyl with chemical formula $C_{21}H_{25}NO$ is shown with one oxygen atom in the middle (red) and one nitrogen atom attached in the end (blue) among the compound of hydrogen and carbon molecules in the aligned bulk along the direction of vector $\boldsymbol{n}_{\mathrm{N}}$.

In this case, we can take the order parameter M as the measure of the *degree of alignment* among the molecules, and is proportional to the **director** aligned to a vector $\boldsymbol{n}_{\mathrm{N}}$. And it is given by the average direction of the rigid rod-like molecular structure. This suggests the rotational symmetry is broken while the translational symmetry still holds through the symmetry reduction process from the completely random state. Although the molecule possesses the apparently distinguishable head and tail feature, we do not distinguish the directors. i.e. If the molecules are aligned in one direction, then it possesses the discrete symmetry, $\boldsymbol{n}_{\mathrm{N}} \to -\boldsymbol{n}_{\mathrm{N}}$. We might assume that this vector is normalised, so that

$$\boldsymbol{n}_{\mathrm{N}} \cdot \boldsymbol{n}_{\mathrm{N}} = 1 \, . \tag{8.3.1}$$

Further, if we assign a point of the nematic liquid crystal $x \in \mathbb{R}^3$, we can express a pair of identifiable directors in the polar coordinate system,

$$\boldsymbol{n}_{\mathrm{N}} = (\theta, \phi) \qquad \text{and} \qquad -\boldsymbol{n}_{\mathrm{N}} = (\pi - \theta, \pi + \phi) \, . \tag{8.3.2}$$

From (8.2.7) and (8.3.2), we can see these constitute a point on $S^2 \subset \mathbb{R}^3$ representing the same state. We see that the identification of $\boldsymbol{n}_{\mathrm{N}} = -\boldsymbol{n}_{\mathrm{N}}$ is nothing but the identification of the antipodals on S^2. Therefore the order parameter space of the nematic liquid crystals is the projective plane $\mathbb{R}P^2$.

In general, the director field depends on the position $x \in S^2 \subset \mathbb{R}^3$ and we may define a map following (8.2.1),

$$\Psi : S^2 \longrightarrow \mathbb{R}P^2 \, . \tag{8.3.3}$$

This particular example emphasises the difference between the space S^2 where the medium exists and the order parameter space $\mathbb{R}P^2$ due to the identification $\boldsymbol{n}_{\mathrm{N}} = -\boldsymbol{n}_{\mathrm{N}}$. This map is called the *texture*. Sometimes, the actual order parameter configuration in $\mathbb{R}^3$ is also called the texture.

If we bring back the construction of the Möbius band in Section 8.1, we recognise the topological identification of antipodals directly corresponds to the identification of the geometrical and physical identification of directors $\boldsymbol{n}_{\rm N} = -\boldsymbol{n}_{\rm N}$. See Fig. 8.8. Therefore, using (8.1.12), we can write an expression for the general homotopy group, now the order parameter space M is recognised,

$$\pi_n(S^2/\{\text{antipodal}\}) \cong \pi_n(\mathbb{R}P^2) \ . \tag{8.3.4}$$

Let us investigate various possible defects whether (8.3.4) gives us any meaningful indication. For the line defects, we have the dimension $d = 1$ and the dimension of media is $m = 3$. So that $n = 3 - 1 - 1 = 1$, and this gives the first homotopy group we can work with,

$$\pi_1(\mathbb{R}P^2) \cong \mathbb{Z}_2 = \{0, 1\} \ . \tag{8.3.5}$$

This implies that there exist two kinds of line defect in nematic liquid crystals [69,123,124,133],

$$\begin{aligned} &\{0\} : \text{one can be continuously deformed into a uniform configuration,} \\ &\{1\} : \text{one cannot be continuously deformed into a uniform configuration.} \end{aligned} \tag{8.3.6}$$

The latter represents non-trivial defect, a stable vortex, and we can see how the loop is mapped to $\mathbb{R}P^2$ by this texture.

For the point defect, we can consider the case for $m = 3$, $d = 0$ and $n = 3 - 0 - 1 = 2$, so that the corresponding homotopy group is now

$$\pi_2(S^2) \cong \pi_2(\mathbb{R}P^2) \cong \mathbb{Z} \ . \tag{8.3.7}$$

where we used (8.1.12). This indicates that there are stable point defects in the nematic liquid crystals classified by some integers, and this classification can be equally applied to the field configuration defined on S^2. This idea of linking an integer with homotopy group is a central ingredient to represent the topological invariants that we will see in Section 9.2.

In this way, in principle we can investigate the classifications of defects in various physical models, after defining i) the order parameters and ii) the order parameter space by recognising the underlying symmetries in the system in each case. In particular, we would like to consider the homotopy and the physical meaning of $\mathbb{R}P^3$ with its topological implication. This is essentially the generalisation of the nematic liquid crystals case. Before that, we shall go back to the notion of directors in micropolar theory and its characteristic deformational measures to consider the energy functions within the framework of the free energy formalism.

8.4 Free energy formalism and its expansion

8.4.1 Order parameters in the energy expansion

External factors such as a temperature, chemical interaction, an electromagnetic field or a gravitational field can induce the phase transition and the order parameter acquires nonzero values, if one started from the completely random state, defined in certain order parameter space. Then it is natural to expect that some of symmetric properties in the isotropic state are broken during the phase transition, and the energy density can be expressed as a function of the field of the order parameter.

The **free energy formalism** for the liquid crystals was established by Oseen [134] and Frank [135]. Later the theory was further developed by Ericksen and Leslie [136–138], incorporating inequalities in the nematic liquid crystals within the framework of the continuum theory. The free energy formalism is based on the notion of the energy required for deviations from the

isotropic state in which the order parameter is taken to be zero [139]. This immediately suggests that we can take the director $\boldsymbol{\xi}_a$ as the order parameter to investigate potential deformations (or deviations from the initial state). Therefore, the energy density must be proportional to the derivative of the order parameter,

$$\mathcal{F} \propto (\nabla \boldsymbol{\xi}_a)^2 \, . \tag{8.4.1}$$

The free energy density can be written in terms of the power expansion of the order parameter and its derivatives, under the assumption that the spatial variations are slow relative to the characteristic length scale, for example, the range of interaction or the coherent length in the lattice space for a given system. This form of expansion is highly dependent on the nature of the order parameter itself in the given physical system. It can be a single real scalar parameter or an n-component complex field. But we are particularly interested in its simple form of free energy expansion in the case of nematic liquid crystals given in terms of the directors.

For the nematic liquid crystals, the energy expansion is written by the linear expansion of the polynomial of the order parameter $\boldsymbol{Q}$ up to finite powers to ensure the stability of the system and its derivative combinations [32, 140]. In each expansion of the energy function, the 3×3 matrix $\boldsymbol{Q}$ is known as traceless and symmetric written in such a way that each term in the expansion of $\mathcal{F}$ is invariant individually under the global rotation. Terms containing derivative operator of $\boldsymbol{Q}$ are called the *gradient free energy*, and it is written up to second order. And terms without the derivative operator are known as the *bulk free energy* up to fourth order, so that the free energy density is written as

$$\mathcal{F} = \mathcal{F}_{\text{bulk}} + \mathcal{F}_{\text{grad}} \, . \tag{8.4.2}$$

Specifically, we can write the expansion [141] with some elastic moduli k_i

$$\mathcal{F}_{\text{bulk}} = k_1 \text{tr}\, \boldsymbol{Q}^2 + k_2 \text{tr}\, \boldsymbol{Q}^3 + k_3 [\text{tr}\, \boldsymbol{Q}^2]^2 \, , \tag{8.4.3a}$$

$$\mathcal{F}_{\text{grad}} = k_4 \left(\nabla \times \boldsymbol{Q} + k_5 \boldsymbol{Q}\right)^2 + k_6 \left(\nabla \cdot \boldsymbol{Q}\right)^2 \, . \tag{8.4.3b}$$

where we can rewrite the fourth power term in (8.4.3a) by $\text{tr}\, \boldsymbol{Q}^4 = \frac{1}{2}[\text{tr}\, \boldsymbol{Q}^2]^2$, for $\boldsymbol{Q}$ is 3×3 traceless matrix.

Now, we would like to specify the form of the order parameter $\boldsymbol{Q}$ which must be a function of the director $\boldsymbol{n}_{\text{N}}$, and it must be zero when the system is in the completely random state losing all its degrees of alignment, so that it is no longer the nematic but in an isotropic configuration. There are number of approaches in the literature to determine the order parameter $\boldsymbol{Q}$, but we would like to take one that can encompass the theory of the microcontinuum.

The relation of vanishing order parameter and the resulting isotropic configuration can be found in consideration of the so-called *microinertia* defined by Eringen [142]. The microinertia for micropolar continua is defined by

$$j_{ij} = \chi_{iA} \chi_{jB} J_{AB} \, , \tag{8.4.4}$$

where j_{ij} and J_{AB} are microinertia described by the directors $\boldsymbol{\xi}_k$ and $\boldsymbol{\Xi}_K$ in the spatial frame and reference frame respectively, and we identify χ_{iA} as the microrotation of $SO(3)$ following the discussion in Section 6.3. A special case arises when we have $j_{ij} = J_{AB}$. Then this means the microinertia is conserved regardless of the choice of the local microrotational axis, and the system is in the isotropic configuration. Further, since $\boldsymbol{\chi}\boldsymbol{\chi}^T = \mathbb{1}$, the expression (8.4.4) becomes

$$\boldsymbol{j}\boldsymbol{\chi} = \boldsymbol{\chi}\boldsymbol{j} \, .$$

Using the *Schur's Lemma* [143], we can regard the microinertia as the map of the finite-dimensional vector space V to itself. So that for a nonzero eigenvector $\boldsymbol{v} \in V$ with a nonzero

eigenvalue $\lambda \in \mathbb{R}$, $\boldsymbol{j}\boldsymbol{v} = \lambda\boldsymbol{v}$ implies $\boldsymbol{j}(\boldsymbol{\chi}\boldsymbol{v}) = \boldsymbol{\chi}(\boldsymbol{j}\boldsymbol{v}) = \lambda\boldsymbol{\chi}\boldsymbol{v}$ for all $\boldsymbol{v} \in V$. Therefore the eigenspace is invariant under the microrotation as expected and $\boldsymbol{j}$ must be proportional to the identity. Hence, we can write the microinertia in the form

$$j_{ij} = \frac{2}{3} j_{kk}\delta_{ij} \, . \tag{8.4.5}$$

Now, in the nematic state, this microinertia will be modified to take the form, according to [142]

$$j_{ij} = \sigma(\delta_{ij} - n_{\mathrm{N}i}n_{\mathrm{N}j}) \tag{8.4.6}$$

where σ is some constant, and $n_{\mathrm{N}i}$ are normalised directors satisfying $\boldsymbol{n}_{\mathrm{N}} \cdot \boldsymbol{n}_{\mathrm{N}} = 1$. Then we can determine the form of the order parameter Q_{ij} as the measure of its *deviation from the isotropic state* by

$$\begin{aligned} Q_{ij} &= \frac{2}{3} j_{kk}\delta_{ij} - j_{ij} \\ &= \left(n_{\mathrm{N}i}n_{\mathrm{N}j} - \frac{1}{3}\delta_{ij} \right) \sigma \end{aligned} \tag{8.4.7}$$

which is traceless and symmetric. And we can confirm that $Q_{ij} \to 0$ when the system approaches the isotropic state $j_{ij} \to \frac{2}{3} j_{kk}\delta_{ij}$ as expected.

If we insert the form of the order parameter Q_{ij} of (8.4.7) into the free energy $\mathcal{F}$ (8.4.2), then the form of $\mathcal{F}$ will be written entirely in terms of the directors $\boldsymbol{n}_{\mathrm{N}}$ and its derivatives [141],

$$\mathcal{F} = \frac{1}{2} K_1 [\nabla \cdot \boldsymbol{n}_{\mathrm{N}}]^2 + \frac{1}{2} K_2 \left[\boldsymbol{n}_{\mathrm{N}} \cdot (\nabla \times \boldsymbol{n}_{\mathrm{N}})\right]^2 + \frac{1}{2} K_3 [\boldsymbol{n}_{\mathrm{N}} \times (\nabla \times \boldsymbol{n}_{\mathrm{N}})]^2 \, , \tag{8.4.8}$$

where K_i are some material constants relating k_i in (8.4.3), and the higher order terms are ignored. Also, we dropped the surface terms knowing that the total energy function is obtained after the volume integration accompanied by the density constant. Each term attributes forms of defects, namely, splay (divergence), bend (curvature) and twist (torsion) terms, respectively,

$$[\nabla \cdot \boldsymbol{n}_{\mathrm{N}}]^2, \qquad [\boldsymbol{n}_{\mathrm{N}} \times (\nabla \times \boldsymbol{n}_{\mathrm{N}})]^2, \qquad \left[\boldsymbol{n}_{\mathrm{N}} \cdot (\nabla \times \boldsymbol{n}_{\mathrm{N}})\right]^2 \, , \tag{8.4.9}$$

satisfying a set of required symmetries in the energy function. We can see that these satisfy the global rotation and the discrete symmetry $\boldsymbol{n}_{\mathrm{N}} \to -\boldsymbol{n}_{\mathrm{N}}$. In particular, it is widely known [140] that if the system requires the chirality such as cholesteric liquid crystals, we need an additional energy term

$$\boldsymbol{n}_{\mathrm{N}} \cdot (\nabla \times \boldsymbol{n}_{\mathrm{N}}) \, , \tag{8.4.10}$$

with an appropriate coupling parameter.

Similar form of the free energy formalism can be found in the general Ginzburg-Landau expansion [144], if the systems satisfying certain criteria, for example, when the order parameter is small and uniform near the critical temperature T_c during the phase transition.

Some useful identities in the expansion are

$$(\nabla \boldsymbol{n})^2 = (\nabla \cdot \boldsymbol{n})^2 + (\nabla \times \boldsymbol{n})^2 + \nabla \cdot \Big[(\boldsymbol{n} \cdot \nabla)\boldsymbol{n} - \boldsymbol{n}(\nabla \cdot \boldsymbol{n}) \Big] \, , \tag{8.4.11a}$$

$$[(\boldsymbol{n} \cdot \nabla)\boldsymbol{n}]^2 = [\boldsymbol{n} \times (\nabla \times \boldsymbol{n})]^2 \, , \tag{8.4.11b}$$

$$(\nabla \times \boldsymbol{n})^2 = [\boldsymbol{n} \cdot (\nabla \times \boldsymbol{n})]^2 + [\boldsymbol{n} \times (\nabla \times \boldsymbol{n})]^2 \, . \tag{8.4.11c}$$

8.4.2 Torsion terms in the energy expansion

Now, we are particularly interested in the twist term in connection with the term which played the central role in developing the torsion throughout Part I and Part II. This quantity is $R^T \mathrm{Curl}\, R$ which can be related to the term $\boldsymbol{n}_{\mathrm{N}} \cdot (\nabla \times \boldsymbol{n}_{\mathrm{N}})$ to investigate the torsion contribution to the given system with the energy configuration as the invariant linear combinations of those terms. For instance, we can derive the form of the free energy functional as discussed in [15] to compare the energy functionals we used in (2.1.1) and (3.4.2). So, the first step is to establish the relationship between

$$R^T \mathrm{Curl}\, R \qquad \text{and} \qquad \boldsymbol{n}_{\mathrm{N}} \cdot (\nabla \times \boldsymbol{n}_{\mathrm{N}}) \, . \tag{8.4.12}$$

We would like to look closely at the rotational matrix to investigate the role of its axis and the angle for our purpose. The matrix $R \in SO(3)$, describing the rotation of the angle θ about the normalised axis $\boldsymbol{n}$, can be expressed as the exponential of the antisymmetric matrix A,

$$R = e^A \qquad \text{for} \qquad A^T = -A \, . \tag{8.4.13}$$

where the matrix A can be written

$$A_{ij} = \theta(\boldsymbol{n} \cdot \boldsymbol{J}) \equiv \theta a_{ij} \tag{8.4.14}$$

and the generators $\boldsymbol{J} = (J_1, J_2, J_3)$ of $SO(3)$ are

$$J_1 = \begin{pmatrix} 0 & 0 & 0 \\ 0 & 0 & -1 \\ 0 & 1 & 0 \end{pmatrix} , \qquad J_2 = \begin{pmatrix} 0 & 0 & 1 \\ 0 & 0 & 0 \\ -1 & 0 & 0 \end{pmatrix} , \qquad J_3 = \begin{pmatrix} 0 & -1 & 0 \\ 1 & 0 & 0 \\ 0 & 0 & 0 \end{pmatrix} \tag{8.4.15}$$

satisfying the commutation relation,

$$[J_i, J_j] = \epsilon_{ijk} J_k \, . \tag{8.4.16}$$

The axial vector n_i for the rotation is defined by

$$n_i = -\frac{1}{2} \epsilon_{ijk} a_{jk} \qquad \text{and} \qquad a_{ij} = -\epsilon_{ijk} n_k \, . \tag{8.4.17}$$

Both variables of n_i and θ can be arbitrary functions of space $\boldsymbol{x} = (x, y, z)$ and time t, but we only consider the static case so that both axis and rotational angle are time-independent functions. We can write the rotational axis by

$$\boldsymbol{n} = (n_1(\boldsymbol{x}),\ n_2(\boldsymbol{x}),\ n_3(\boldsymbol{x})) \qquad \text{satisfying} \qquad \boldsymbol{n} \cdot \boldsymbol{n} = 1 \, . \tag{8.4.18}$$

There are number of known representations for the rotation R, and one of them is *Rodrigues' formula*

$$R_{ij} = \delta_{ij} + a_{ij} \sin\theta + (a^2)_{ij} (1 - \cos\theta) \, . \tag{8.4.19}$$

Using the fact that $(a^2)_{ij} = a_{ik} a_{kj} = -\delta_{ij} n_l n_l + n_i n_j$, we can write the equivalent expression,

$$R_{ij} = \cos\theta \cdot \delta_{ij} + n_i n_j (1 - \cos\theta) - \epsilon_{ijm} n_m \sin\theta \, . \tag{8.4.20}$$

We note that because of the normalisation constraint $n_1^2 + n_2^2 + n_3^2 = 1$, the total number of independent parameters required is three, which agrees with the number of generators $\boldsymbol{J}$ in (8.4.15). These representations of matrices A_{ij} and R_{ij} are particularly useful if one considers

an anisotropic system. For example, in the planar case, the axial vector $\boldsymbol{n}$ can be perpendicular to the director fields which might give rise to the solution that minimises the energy function.

Now, we return to the issue of relating $\boldsymbol{R}^T\partial\boldsymbol{R}$ and $\boldsymbol{n}_{\rm N}\cdot(\nabla\times\boldsymbol{n}_{\rm N})$. Intuitively, one might hope to write the contortion (6.2.3) by

$$K_{piq} = R_{dp}\partial_i R_{dq} = \boldsymbol{R}^{-1}\partial_i\boldsymbol{R} = \partial_i \log \boldsymbol{R} = \partial_i A_{pq} \ . \tag{8.4.21}$$

when the rotation is expressed by the exponential form of the antisymmetric matrix A of (8.4.13). This is not true in general, simply because in the matrix $A_{ij} = \theta a_{ij} = -\epsilon_{ijk}n_k\theta$, the rotational angle θ and the axis $\boldsymbol{n}$ are position-dependent functions. Nonetheless, if the angle θ is small, using the definition of contortion with the exponential representation of rotation $R = e^A$, we can show that

$$K_{piq} \approx \partial_i A_{pq} \ . \tag{8.4.22}$$

But, if the normalised rotational axis is constant in space, which is the case we have seen in Part I of (2.2.1), while the rotational angle can be an arbitrary function of space, then the contortion tensor can be written exactly as

$$K_{piq} = \partial_i A_{pq} \ . \tag{8.4.23}$$

To see this, first we write an N product of the generators A of $R\in SO(3)$

$$(A^N)_{ij} = \theta a_{il_1}\theta a_{l_1l_2}\cdots\theta a_{l_nn} = \theta^N a_{1l_1}\cdots a_{l_nj} \ ,$$

with its derivative

$$\partial_m(A^N)_{in} = a_{il_1}\cdots a_{l_nn}\partial_m\theta^N = N(A^{N-1}\partial_m A) \ .$$

Using this, the contortion $K = R^T\partial R$ becomes

$$\begin{aligned} K_{piq} &= (e^A)^T\left(\mathbb{1} + A + \frac{1}{2!}A^2 + \cdots\right)\partial_i A \\ &= (e^A)^T e^A\partial_i A \end{aligned} \tag{8.4.24}$$

which gives the result, for $R^TR = \mathbb{1}$. In particular, the dislocation density tensor (6.2.5) and Nye's tensor (6.2.8) simply become,

$$K_{pj} = \delta_{jp}\partial_i\theta n_i - \partial_p\theta n_j \ , \tag{8.4.25a}$$

$$\Gamma_{ji} = \partial_i\theta n_j \ . \tag{8.4.25b}$$

Further, the torsion tensor defined by $T_{ipq} = \Gamma_{ipq} - \Gamma_{iqp}$ in (5.2.1) can be written in terms of the contortion tensor under the assumption that $U^b_\mu = \delta^b_\mu$ in the decomposition (5.2.2),

$$T_{piq} = a_{pq}\partial_i\theta - a_{pi}\partial_q\theta \ . \tag{8.4.26}$$

In other words, the torsion tensor can be written as the gradient of the scalar field if the rotational axis do not change in space. Torsion as the gradient of the scalar field is discussed extensively in [75].

In Weitzenböck space (i.e. the space of zero curvature but nonzero torsion), the general affine connection is identified with the contortion tensor, so the Riemann curvature tensor can be written entirely with the contortion tensor. Then, a straightforward calculation using (8.4.23) and (8.4.14), gives the expression (6.2.4)

$$R_{\rho\sigma\mu\nu} = \partial_\mu K_{\rho\nu\sigma} - \partial_\nu K_{\rho\mu\sigma} + K_{\rho\mu\lambda}K_{\lambda\nu\sigma} - K_{\rho\nu\lambda}K_{\lambda\mu\sigma} \tag{8.4.27}$$

which again agrees with the result we obtained in Section 6.2.

Now, in the language of the micropolar deformation, we can relate the directors $\boldsymbol{\xi}_a$ and rotations R with respect to the orthonormal basis $\boldsymbol{e}_i$ in the Cartesian coordinate system, following similar reasoning used in [142, 145, 146]. We may assign the tetrad field $E^\mu_a \in GL(3;\mathbb{R})$ and its dual e^a_μ, the χ_{kK} and its inverse in (1.2.20), in describing the transformations of the directors in the spatial frame and the reference frame to write

$$\boldsymbol{\xi}_a = E^\mu_a \boldsymbol{\Xi}_\mu \qquad \text{and} \qquad \boldsymbol{\Xi}_\mu = e^a_\mu \boldsymbol{\xi}_a \ . \tag{8.4.28}$$

In the case of micropolar continua, according to the decompositions (6.3.3a) and (6.3.4b), the transformation can be described only by the microrotation so that $\boldsymbol{\xi}_a = R^a{}_\mu \boldsymbol{\Xi}_\mu$, or vice versa. The director $\boldsymbol{\Xi}_\mu$, as the description of the internal structure, is highly dependent on the individual molecular structure. However, if we have a model such as cubane as shown in Fig. 1.1, we may put the director in the reference frame to the usual orthonormal Cartesian basis to write

$$\boldsymbol{\xi}_c = R_{cb} \boldsymbol{e}_b \ . \tag{8.4.29}$$

i.e. we can regard that the director $\boldsymbol{\xi}_a$ is obtained after applying the rigid rotation to the standard orthonormal basis in three dimensions. Then the contortion becomes

$$K_{a\mu b} = R_{ca} \partial_\mu R_{cb} = \boldsymbol{\xi}_a \partial_\mu \boldsymbol{\xi}_b \ . \tag{8.4.30}$$

Consequently, the dislocation density tensor becomes

$$K_{ad} = \epsilon_{d\mu b} K_{a\mu b} = \boldsymbol{\xi}_a \epsilon_{d\mu b} \partial_\mu \boldsymbol{\xi}_b = \boldsymbol{\xi}_a (\mathrm{Curl}\, \boldsymbol{\xi})_d \ . \tag{8.4.31}$$

And Nye's tensor becomes

$$\Gamma_{ji} = -\frac{1}{2} \epsilon_{jpq} K_{piq} = -\frac{1}{2} \epsilon_{jpq} \boldsymbol{\xi}_p \partial_i \boldsymbol{\xi}_q \ . \tag{8.4.32}$$

Now, it becomes clear that the quantity corresponding to the twist in (8.4.8) $[\boldsymbol{\xi} \cdot (\mathrm{Curl}\, \boldsymbol{\xi})]$ is the trace of the dislocation density tensor

$$\mathrm{tr}\ \boldsymbol{K} = [\boldsymbol{\xi} \cdot (\mathrm{Curl}\, \boldsymbol{\xi})] \ . \tag{8.4.33}$$

Furthermore, from the relation between Nye's tensor and the dislocation density tensor (6.2.11), we obtain the explicit relation between Nye's tensor and the measure for the twist, as given in [142] and [145]

$$\mathrm{tr}\ \boldsymbol{\Gamma} = \frac{1}{2} \mathrm{tr}\ \boldsymbol{K} = \frac{1}{2} \boldsymbol{\xi} \cdot (\mathrm{Curl}\, \boldsymbol{\xi}) \ . \tag{8.4.34}$$

We also note that (8.4.33) and (8.4.34) are precisely the simplest form of the chiral energy form we discussed in Section 3.3,

$$V_\chi = \chi \mathrm{tr}(\boldsymbol{K}). \tag{8.4.35}$$

In words, a system with no mirror symmetry is defined by the chirality, and this system must accompanied by the chiral energy form V_χ which in turn induced by nonzero torsion in the form either by the dislocation density tensor or Nye's tensor via contortion tensor. Consequently, for such a system the parameter, now we can set $k_5 = \chi$, is nonzero in (8.4.3b).

In case of nematic liquid crystals [142, 146], the directors $\boldsymbol{n}_{\mathrm{N}}$ are obtained simply following the same reasoning of (8.4.29) but by fixing $\boldsymbol{e}_i$ to be $\boldsymbol{e}_3$,

$$n_{\mathrm{N}i} = R_{i3} \boldsymbol{e}_3 \ . \tag{8.4.36}$$

In this way, it is easy to see that the result we obtained so far can be translated into the forms such as

$$\boldsymbol{\xi} \cdot (\mathrm{Curl}\, \boldsymbol{\xi}) \longrightarrow \boldsymbol{n}_{\mathrm{N}} \cdot (\nabla \times \boldsymbol{n}_{\mathrm{N}}) \,. \tag{8.4.37}$$

Then it is straightforward to see that the nematic liquid crystals are in its homogeneous anisotropic configuration seen as the special case of micropolar theory, as claimed by Eringen in [142]. In particular, the term with K_2 on the right hand side of (8.4.8) is in its even power of (8.4.37). This manifests that the energy functional for the liquid nematic crystals is the non-chiral case, following the conclusion of Section 3.3. Therefore, we can set the constant $k_5 = 0$ in (8.4.3b).

8.4.3 Order parameter for the micropolar continua

Lastly, we would like to make some remarks on the equation of motion for the general micropolar continua obtained in Chapter 2 in connection with those in [15].

$$\begin{pmatrix} \partial_{tt}\phi \\ \partial_{tt}\psi \end{pmatrix} = \boldsymbol{M} \begin{pmatrix} \partial_{zz}\phi \\ \partial_{zz}\psi \end{pmatrix} + \begin{pmatrix} 0 & \frac{\lambda \sin\phi}{2\rho_{\mathrm{rot}}} \\ -\frac{2\lambda \sin\phi}{\rho} & 0 \end{pmatrix} \begin{pmatrix} \partial_z\phi \\ \partial_z\psi \end{pmatrix} - \frac{(\lambda+\mu+\mu_c)}{\rho_{\mathrm{rot}}} \begin{pmatrix} \sin\phi \\ 0 \end{pmatrix} + \frac{\lambda+\mu}{2\rho_{\mathrm{rot}}} \begin{pmatrix} \sin 2\phi \\ 0 \end{pmatrix} \tag{8.4.38a}$$

$$\begin{pmatrix} \partial_{tt}\phi \\ \partial_{tt}u \end{pmatrix} = \boldsymbol{N} \begin{pmatrix} \partial_{xx}\phi \\ \partial_{xx}u \end{pmatrix} + \begin{pmatrix} 0 & \frac{2\lambda' \sin\phi}{\rho_0 J} \\ -\frac{2(\lambda'+2\mu'+\kappa')\sin\phi}{\rho_0} & 0 \end{pmatrix} \begin{pmatrix} \partial_x\phi \\ \partial_x u \end{pmatrix} + \frac{2\lambda'}{\rho_0 J} \begin{pmatrix} \sin\phi \\ 0 \end{pmatrix} + \frac{2\lambda'+\mu'}{\rho_0 J} \begin{pmatrix} \sin 2\phi \\ 0 \end{pmatrix} \tag{8.4.38b}$$

where

$$\boldsymbol{M} = \begin{pmatrix} (\kappa_1 + 6\kappa_3)/3\rho_{\mathrm{rot}} & (3\chi_1 - \chi_3)/6\rho_{\mathrm{rot}} \\ 2(3\chi_1 - \chi_3)/3\rho & (\lambda + 2\mu)/\rho \end{pmatrix} , \qquad \boldsymbol{N} = \begin{pmatrix} \frac{\alpha}{\rho_0 J} & 0 \\ 0 & \frac{\lambda'+2\mu'+\kappa'}{\rho_0} \end{pmatrix} . \tag{8.4.39}$$

In our case, we obtained the equations of motion by collecting all relevant energy functionals in terms of the microrotation and the macro-displacement. And the variational principle led to (8.4.38a). For (8.4.39b), it is based on the different approach starting from the constitutive equations for the micropolar media and identifying two order parameters $\mathfrak{C}_{KL}$ and Γ_{KL} in the free energy density $\mathcal{F}$ given by

$$T_{Kl} = \frac{\partial \mathcal{F}}{\partial \mathfrak{C}_{KL}} \chi_{lL} \qquad \text{and} \qquad M_{Kl} = \frac{\partial \mathcal{F}}{\partial \Gamma_{LK}} \chi_{lL} \,, \tag{8.4.40}$$

where Piola-Kirchhoff tensors are defined by

$$T_{Kl} = J \frac{\partial X_K}{\partial x_k} t_{kl} \qquad \text{and} \qquad M_{Kl} = J \frac{\partial X_K}{\partial x_k} m_{kl}$$

for t_{kl} and m_{kl} are the stress tensor and the couple tensor, respectively, and the determinant J is given by (1.2.22). The free energy density (8.4.8) is then given by the simplified linear expansion of powers of two order parameters [146, 147], with the aids of identities (8.4.11), in the form

$$\mathcal{F} = \frac{1}{2}\lambda' I_1^2 + \mu' I_2 + (\mu' + \kappa') I_4 + \frac{1}{2}\alpha' I_{10} + \beta' I_{11} - \gamma' I_{13} \tag{8.4.41}$$

where $\{\lambda', \mu', \kappa', \alpha', \beta', \gamma'\}$ are some elastic parameters. The invariants in (8.4.41) are

$$\begin{array}{lll} I_1 = \mathrm{tr}\ \mathfrak{C}, & I_2 = \frac{1}{2}\mathrm{tr}\ \mathfrak{C}^2, & I_4 = \frac{1}{2}\mathrm{tr}\ (\mathfrak{C}\mathfrak{C}^T) \,, \\ I_{10} = \mathrm{tr}\ \boldsymbol{\Gamma}, & I_{11} = \frac{1}{2}\mathrm{tr}\ \boldsymbol{\Gamma}^2, & I_{13} = \frac{1}{2}\mathrm{tr}\ (\boldsymbol{\Gamma}\boldsymbol{\Gamma}^T) \,. \end{array} \tag{8.4.42}$$

The appearance of two different kinds of order parameters of the first Cosserat deformation tensor $\mathfrak{C}$ and Nye's tensor $\boldsymbol{\Gamma}$ in the expansion explains the setting we are dealing with. This is the coupled system of micro and macro-deformations leading to the two deformational wave propagations. Moreover, the constitutive equations (8.4.40) is of the form we used in (2.0.1), and the identification between the trace of Nye's tensor and the dislocation density tensor in terms of the twist measure of the director explains the similarity.

In a sense, our formalism (2.0.1) in varying the total energy functional in terms of the microrotation $\overline{R}$ and the deformation gradient tensor F, is equivalent to the formalism based on the constitutive equations (8.4.40). The chain rules introduced in Appendix A would be particularly useful in varying the first Cosserat deformation tensor ($\overline{\overline{U}} = \overline{R}^T F$ in our convention) and Nye's tensor (as the product of the microrotation and its derivative). This essentially leads to the close similarity in the final coupled set of equations of motion as shown in (8.4.38).

In principle, one may adjust the parameters in the matrix $\boldsymbol{M}$ to obtain a diagonalised matrix to match the entries of the matrix $\boldsymbol{N}$ under certain circumstances in evaluating the constitutive equations exactly. Then the simple ansatz, such as the microrotation with fixed axis (2.2.1), can be imposed to yield the identical set of equations of motion from the rather different approaches. We note that while Nye's tensor is extensively used as the order parameter in literature [15, 26, 142, 146], we can equally use the dislocation density tensor $\boldsymbol{K}$ as the order parameter according to (8.4.34).

Chapter 9

Topological invariants and conserved currents

We would like reconsider the soliton solutions we obtained in Part I through some simple cases to investigate the relationship with the homotopy to classify the solution space in describing the defects. This solution space can be arbitrarily large if there exist underlying symmetries of infinite order group structures.

Various systems which yield a soliton solution are introduced, and we will see that the finite energy requirement is the crucial feature in determining the asymptotic behaviour of the soliton solutions and this will further be related to the homotopic classifications.

These asymptotic conditions are responsible for the existence of topological invariant charges Q, and these topological invariants are different from the conventionally derived quantities, such as Noether's current, from the continuous symmetry in the Lagrangian of the system leading to the conservation of energy and momentum. Depending on the physical system, this total charge Q can be of the form of a mass, an electric charge or an intrinsic quantum number. Also this charge will turn out to be a unique topological invariant in classifying the defects introduced in Table 8.2.

The associated conserved current is used extensively throughout Skyrme's pioneering works. From a mathematical point of view, the theories of solitons are rigorously developed in various contexts in connection with the physical systems, and comprehensive discussions of the soliton theory can be found, for example, in [40].

9.1 Simple soliton solutions in low dimensions

In this Section, we will use the metric tensor with its signature $(+1, -1, \cdots -1)$ in n spatial dimensions with one time component of the tensors defined in an $(n+1)$-dimensional differentiable manifold. For example, the Lorentzian metric tensor $\eta_{\mu\nu}$ for $\mu, \nu = \{t, x, y, z\}$ in $(3+1)$ dimensions will give the invariant length element (5.1.6) (we put the speed of light $c = 1$)

$$(ds)^2 = \eta_{\mu\nu} dx^\mu dx^\nu = (dt)^2 - (dx)^2 - (dy)^2 - (dz)^2 \, ,$$

and the indices of vectors are naturally raised and the indices of derivatives are naturally lowered.

Let us start with a scalar field ϕ in a $(1+1)$-dimensional model without stating any specific form of the Lagrangian. The zero dimensional sphere S^0 is the set of two points which can be taken to be $x = \pm\infty$. The corresponding homotopy group for the order parameter, using (8.2.3), is therefore

$$\pi_0(M) \cong \pi_0(G/H) \, . \tag{9.1.1}$$

This particular homotopy group counts the number of components of the order parameter space M. So, $\pi_0(M)$ is nonzero if M is discrete, or equivalently G is discrete. We will see that this implies that the disconnected groups impose $(1+1)$-dimensional soliton solutions.

Let us start with the currents for the scalar field ϕ defined by

$$J^\mu = \epsilon^{\mu\nu}\partial_\nu\phi \tag{9.1.2}$$

where $\epsilon^{\mu\nu}$ is the totally antisymmetric Levi-Civita symbol in two dimensions with μ, ν for the spacetime indices in (1+1) dimensions. It is easy to see that this is conserved, by its construction

$$\partial_\mu J^\mu = 0 \ . \tag{9.1.3}$$

And the corresponding total charge is defined by the integration of the time component of the current J over all space,

$$Q = \int_{-\infty}^{\infty} dx \ J^t = \int_{-\infty}^{\infty} dx \ \frac{\partial\phi}{\partial x} = \phi(+\infty, t) - \phi(-\infty, t) \ . \tag{9.1.4}$$

under the assumption that J^t approaches zero as $|x| \to \infty$, hence (9.1.4) states that a conserved current implies a conserved charge in time. It is easy to show that the charge Q is a time-independent quantity, hence it possesses an intrinsic topological property.

For the finite energy requirement, the total charge must be localised. If the amplitude of $\phi(\pm\infty, t)$ increases (or decreases) indefinitely or oscillates arbitrarily, we cannot expect to have the finite-valued total charge. This will eventually violate the finite energy requirement for the given system, and it is required to set the asymptotic values for $\phi(x, t)$ to obtain the meaningful physical solution.

One solution for such condition would be the constant solution, but we can put this constant to be zero without loss of generality, so that the trivial solution is

$$\phi(\pm\infty, t) = 0 \ , \tag{9.1.5}$$

to give $Q = 0$. But for the non-trivial case, we will have the nonzero-valued Q and we might have a situation that

$$\phi(+\infty, t) \neq \phi(-\infty, t) \ , \tag{9.1.6}$$

where each $\phi(+\infty, t)$ and $\phi(-\infty, t)$ approaches distinct finite asymptotic values. This analysis agrees with the asymptotic condition we imposed in the case of elastic wave propagations in (2.3.4). The distinct asymptotic values for $\phi(+\infty, t)$ and $\phi(-\infty, t)$ can impose different interpretation when we consider the elastic deformation.

Soliton solutions are characterised by their solitary wave form with non-dissipative terms and its interference-free properties from the collision or long-ranged interaction between distinct waves. We would like to derive the soliton solutions similar to those we used in Part I, but through much simpler and familiar examples.

First, the Lagrangian for the ϕ^4 theory of the real scalar field in $(1+1)$ dimensions is

$$\mathcal{L} = \frac{1}{2}\partial_\mu\phi\partial^\mu\phi + \frac{1}{2}\mu^2\phi^2 - \frac{1}{4}\lambda\phi^4 \ , \tag{9.1.7}$$

where we understood that $\partial_\mu\phi\partial^\mu\phi = (\partial_t\phi)^2 - (\partial_x\phi)^2$ and μ, λ are real coupling constants. The only symmetry in this system is $O(1) \cong \mathbb{Z}_2$, which is simply the identity and its reflection,

$$\phi \longrightarrow -\phi \ . \tag{9.1.8}$$

The homotopy group in this case is a map between the physically allowed space and the internal space, therefore using (8.2.5) we have

$$\pi_0(\mathbb{Z}_2) \cong \mathbb{Z}_2 \ . \tag{9.1.9}$$

Hence, we can expect that there are two classes of solutions, namely

$$\phi(+\infty, t) = \phi(-\infty, t) \qquad \text{and} \qquad \phi(+\infty, t) \neq \phi(-\infty, t) \ .$$

This shows that by following a simple reasoning on the structure of order parameter space M and its associated symmetry, we can have some approximate ideas about the solution space well before we actually tackle the equation of motion to solve it.

Now, the equation of motion can be obtained by

$$\partial_\mu \partial^\mu \phi \equiv \frac{\partial^2 \phi}{\partial t^2} - \frac{\partial^2 \phi}{\partial x^2} = \mu^2 \phi - \lambda \phi^3 \tag{9.1.10}$$

with constant solutions for the first class of $\{0\} \in \mathbb{Z}_2$ yielding the zero charge Q, called a vacuum solution,

$$\phi_{\text{vac}} = 0 \qquad \text{and} \qquad \phi_{\text{vac}} = \pm \frac{\mu}{\sqrt{\lambda}} \ . \tag{9.1.11}$$

For the solution of the second class $\phi(+\infty, t) \neq \phi(-\infty, t)$, for the nonzero total charge, we consider the static solution of (9.1.10), and this can be done by integrating both sides with respect to x after multiplying by $\partial\phi/\partial x$, to obtain

$$x = \pm \int \frac{1}{\sqrt{\frac{1}{2}\lambda\phi^4 - \mu^2\phi^2 + k}} \, d\phi \ , \tag{9.1.12}$$

for some constant k, and we put the integration constant to be zero. This is in the form of an elliptic integral, hence the solution ϕ can be periodic in the complex plane. But if we have the repeated roots in the square, we can integrate exactly, and this is the case when $k = \mu^4/2\lambda$. Then (9.1.12) reduces to a simple integration and we obtain the *kink/antikink solution*,

$$\phi_{\text{kink}}(x) = \pm \frac{\mu}{\sqrt{\lambda}} \tanh\left[\frac{\mu}{\sqrt{2}} \, x\right] \ . \tag{9.1.13}$$

Using the result we obtained in Section 2.5, we can obtain the time-dependent wave solution propagating with the velocity v, by applying the Lorentz boost in the direction of x provided the Lagrangian is Lorentz invariant

$$\phi_{\text{kink}}(x, t) = \pm \frac{\mu}{\sqrt{\lambda}} \tanh\left[\frac{\mu}{\sqrt{2}} \frac{1}{\sqrt{1 - v^2}} (x - vt)\right] \ . \tag{9.1.14}$$

It is clear that these solutions belong to the classification of $\phi(+\infty, t) \neq \phi(-\infty, t)$, and their asymptotic behaviour indicates that

$$\phi_{\text{kink}}(x, t) \longrightarrow \phi_{\text{vac}} \quad \text{as} \quad x \to \pm\infty \ .$$

This solution leads to the finite energy with respect to the vacuum, if we insert the kink solution (9.1.14) into the Hamiltonian H defined by the integration over the energy density $\mathcal{H}(x)$ of (2.5.3),

$$H = \int dx \, \left(\frac{1}{2}\left[\left(\frac{\partial\phi}{\partial t}\right)^2 + \left(\frac{\partial\phi}{\partial x}\right)^2\right] - \frac{1}{2}\mu^2\phi^2 + \frac{\lambda}{4}\phi^4\right) \ . \tag{9.1.15}$$

From this, we obtain the finite-valued energy as shown in Fig. 9.1,

$$H_{\phi_{\rm kink}} - H_{\phi_{\rm vac}} = \frac{2\sqrt{2}}{3}\,\frac{\mu^3}{\lambda} \tag{9.1.16}$$

as expected, and the nonzero value for the charge Q is given by

$$Q = |\phi_{\rm kink}(+\infty) - \phi_{\rm kink}(-\infty)| = \frac{2\mu}{\sqrt{\lambda}}\ . \tag{9.1.17}$$

Therefore, the discrete order parameter space $M \cong \mathbb{Z}_2$ gives rise to the existence of the kink solution along with the constant solution prescribed by (9.1.11).

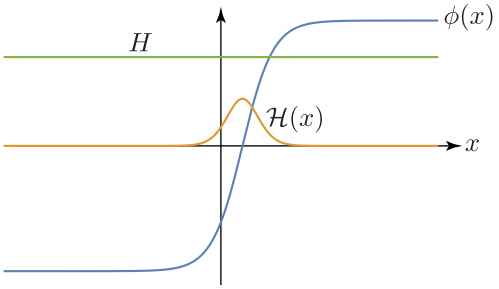

Figure 9.1: A static kink solution $\phi(x)$ by taking the positive sign in the solution (9.1.13) is shown, satisfying the asymptotic condition considered. The constant finite-valued energy H with the localised energy density $\mathcal{H}(x)$ are shown according to the result (9.1.15) and (9.1.16).

Our second example of the soliton solution in $(1+1)$ dimensions is the sine-Gordon equation

$$\partial_\mu\partial^\mu\phi + m^2 \sin\phi = 0\ , \tag{9.1.18}$$

which is the equation of motion of the system with the Lagrangian

$$\mathcal{L} = \frac{1}{2}\partial_\mu\phi\partial^\mu\phi - m^2(1-\cos\phi)\ . \tag{9.1.19}$$

In addition to the discrete symmetry (9.1.8), this is invariant under the transformations

$$\phi \longrightarrow \phi + 2\pi N, \qquad N \in \mathbb{Z} \tag{9.1.20}$$

i.e. the system is invariant under the infinite dihedral group $D_\infty = \mathbb{Z} \rtimes \mathbb{Z}_2$, semi direct product such that $\mathbb{Z} \cup \mathbb{Z}_2 = \{0\}$, and we have infinite solution space determined by integers N.

For the static solution, we follow the same steps, as we did in (9.1.14), to obtain the soliton solution

$$\phi_{\rm sol}(x) = 4\arctan e^{m(x-x_0)}\ . \tag{9.1.21}$$

As before, the time-dependent solution can be obtained to give the solution of the form (2.3.15) after applying the Lorentz boost. We obtain the static solution by recognising a degenerate elliptic function separating two infinite-energy regimes, and we find the energy difference is finite,

$$H_{\phi_{\rm sol}} - H_{\phi_{\rm vac}} = \int dx \left[\frac{1}{2}\left(\frac{\partial\phi_{\rm sol}}{\partial x}\right)^2 + m^2(1-\cos\phi_{\rm sol})\right] = 8m\ . \tag{9.1.22}$$

In this case, the internal invariance group is D_∞ and the stability group is $\mathbb{Z}_2$. Hence the order parameter space M is isomorphic to $D_\infty/\mathbb{Z}_2 \cong \mathbb{Z}$, and the homotopy classification is an infinite set of classifications

$$\pi_0(M) \cong \pi_0(D_\infty/\mathbb{Z}_2) \cong \pi_0(\mathbb{Z}) \cong \mathbb{Z}\ . \tag{9.1.23}$$

The solution (9.1.21) is the special static case when we put $b = 0$ in the double sine-Gordon system of (2.3.7) we considered in Part I,

$$\partial_{tt}\phi - \partial_{\hat{z}\hat{z}}\phi + m^2 \sin\phi + \frac{b}{2}\sin 2\phi = 0 \; .$$

And this will further reduce to the Klein-Gordon type system (9.2.3) when only small angle is allowed. This suggests there is a direct link between the solution space as the prescriptions of the deformable configuration and the topological invariant quantity N. In particular, we proposed the boundary conditions (2.3.4) based on the elasticity for the displacement propagation

$$\psi(\pm\infty, t) = 0 \qquad \text{and} \qquad \partial_z \psi(\pm\infty, t) = 0 \; ,$$

which in turn converted to the a set of boundary conditions for the microrotation propagation

$$\begin{array}{lll} \phi(\hat{z}, t) = 2\arcsin(X(\hat{z}, t)) \; , & \phi(\hat{z} = \pm\infty, t) = 0 \; , & \partial_{\hat{z}}\phi = 0 \; , \\ \phi(z, t) = 4\arctan e^{\pm k(z-vt)\pm\delta} \; , & \phi(-\infty, t) \neq \phi(+\infty, t) \; , & \end{array} \tag{9.1.24}$$

where the discrepancy in the forms of boundary conditions occurred in the process of converting the rescaled $\hat{z}$ to the original one as shown in Fig. 2.1. The condition $\partial_{\hat{z}}\phi = 0$ as $z \to \pm\infty$ is compatible to the condition $\partial_x \phi_{\rm sol} = 0$ to minimise the static energy H of (9.1.22). Therefore, our form of the solution (2.3.22) incorporates both type of boundary conditions as seen through the kink/antikink model and the sine-Gordon system of (9.1.5) and (9.1.6).

Also, in (7.2.4), the homotopy consideration is briefly mentioned in terms of classification of the compatibility conditions of the micropolar deformations in the manifold. In this manifold, both curvature and torsion are admissible with the explicit expression of the Einstein tensor, started from the polar decomposition of the tetrad basis e^a_μ. In the following Section, we will investigate these topological invariant numbers $N \in \mathbb{Z}$ of (9.1.23) from the topological and geometrical consideration.

9.2 Conserved current, soliton and homotopy

We would like to extend the observations obtained from the previous Section to the case of normalised multi-valued real fields of the nonlinear $O(N)$ model. We investigate the geometrical origin of the intuitive notion of the winding number. We start from the well-known form of the conserved current J^μ, with its associated charge Q, in two dimensions and we generalise the result up to the $d = n + 1$ dimensional configuration with the necessary requirement to retain the integer-valued charge Q. In particular, the current in $(3 + 1)$ dimensions is used throughout Skyrme's pioneering works representing its associated topological invariant charge by the baryon number as we will see in Section 10. Interesting and stimulating historic accounts on Skyrme's works can be found in [148].

9.2.1 Vortex field and winding number

The Lagrangian for the ϕ^4 theory (9.1.7) in (1+1)-dimensional space is related to the Lagrangian for the linear sigma model [149],

$$\mathcal{L} = \frac{1}{2}\partial_\mu \boldsymbol{n}_2 \partial^\mu \boldsymbol{n}_2 - \frac{1}{2}m^2(\boldsymbol{n}_2 \cdot \boldsymbol{n}_2 - 1) \tag{9.2.1}$$

where $\boldsymbol{n}_2 = (n_1(x,t), n_2(x,t))$ is a real-valued field satisfying the constraint

$$\boldsymbol{n}_2 \cdot \boldsymbol{n}_2 = n_1^2 + n_2^2 = 1 \; . \tag{9.2.2}$$

Here, the term m^2 in (9.2.1) can be regarded as the Lagrangian multiplier. This system is invariant under the global rotation $SO(2)$, and the associated equation of motion is the Klein-Gordon equation,

$$(\partial_\mu \partial^\mu + m^2)\boldsymbol{n}_2 = 0 \ . \tag{9.2.3}$$

The constraint (9.2.2) implies that the field $\boldsymbol{n}_2$ resides on S^1, and we can assign a new degree of freedom, using the polar coordinate system, $\phi = \phi(x,t)$ to write

$$\boldsymbol{n}_2(\phi) = (\cos N\phi, \sin N\phi) \ . \tag{9.2.4}$$

Now, there exists a conserved current (we will see more details of the origin of this current later)

$$J^\mu = \frac{1}{2\pi}\epsilon^{\mu\nu}\epsilon^{ab} n_a \partial_\nu n_b \tag{9.2.5}$$

where μ, ν are the spacetime indices, and $a, b = \{1, 2\}$ for the components of $\boldsymbol{n}_2 = (n_1, n_2)$ describing the internal degrees of freedom. This current is again conserved quantity by its construction,

$$\partial_\mu J^\mu \propto \frac{\partial(n_1, n_2)}{\partial(t, x)} \ . \tag{9.2.6}$$

The quantity $\partial_\mu J^\mu$ is proportional to the Jacobian matrix, recognised as the determinant of $\partial_\mu n_a$, between the set of spacetime variables and the newly generated coordinates $\boldsymbol{n}_2 = (\cos N\phi, \sin N\phi)$ under the constraint $\boldsymbol{n}_2 \cdot \boldsymbol{n}_2 = 1$, hence it vanishes. In this case, the homotopy group is

$$\pi_1(S^1) \cong \mathbb{Z} \ . \tag{9.2.7}$$

The associated conserved total charge is then obtained by the integration

$$Q = \int_{-\infty}^{+\infty} J^t \, dx = \frac{N}{2\pi}\int_{-\infty}^{+\infty} \frac{\partial \phi}{\partial x}\, dx = \frac{N}{2\pi}\left[\phi(+\infty, t) - \phi(-\infty, t)\right] \ . \tag{9.2.8}$$

Now, if we impose the asymptotic condition $\boldsymbol{n}_2(\pm\infty, t)$ approaches some finite values, as we did in evaluating the charge Q in (9.1.17), then we can assign the angular variable $\phi(x,t)$ to satisfy the condition

$$\phi(+\infty, t) = \phi(-\infty, t) + 2\pi \ . \tag{9.2.9}$$

This gives the identification that the total charge is nothing but the integer $N \in \mathbb{Z}$,

$$Q = N \ . \tag{9.2.10}$$

Since the classification of the solution space is characterised by the homotopy consideration (9.2.7), this identification gives a direct link between the topological invariants and the number of equivalent solution classification, as we will see more details in the next Section.

Geometrically, the nature of the invariant number $N \in \mathbb{Z}$, we call it the winding number without loss of generality henceforth, can be understood from the differential point of view for a two-dimensional static field in polar coordinates,

$$\boldsymbol{n}_2(\phi) = (\cos\phi, \ \sin\phi) \ , \tag{9.2.11}$$

where ϕ is a now time-independent function, $\phi(x,y) = \arctan y/x$. Now, we can write

$$d\phi = \frac{\partial \phi}{\partial y} dy + \frac{\partial \phi}{\partial x} dx = \frac{1}{r^2}\left(x dy - y dx\right) \ , \tag{9.2.12}$$

where $r^2 = x^2 + y^2$. Then the identical integer N can be obtained in the static two-dimensional case from the purely geometric interpretation that N is the integration of the total changes in the angular variable ϕ along the simple closed contour C divided by 2π, which is the genuine and intuitive notion of the counting the winding number,

$$N = \frac{1}{2\pi}\oint_C d\phi = \frac{1}{2\pi}\oint_C \frac{1}{r^2}\left(xdy - ydx\right) \ . \tag{9.2.13}$$

As shown in the above discussion, if we consider the spatial two-dimensional static configuration, we would have the same topological invariant N in the geometrical static space with the same homotopy group of the $(1+1)$-kink, but now S^0 is changed to S^1, on account of the two-dimensional spatial space (9.2.11). Therefore, the homotopy is a map from S^1 to S^1 so that

$$\pi_1(S^1) \cong \mathbb{Z} \ . \tag{9.2.14}$$

For the field configuration in static case which yields the integer N under the identical constraint, we used $\boldsymbol{n}_2 \cdot \boldsymbol{n}_2 = 1$, the natural candidate for this purpose would be the two-dimensional vortex field $\boldsymbol{n}_{\rm v}$ with an integer number N,

$$\boldsymbol{n}_{\rm v} = \left(\cos(N\phi),\ \sin(N\phi)\right) \ . \tag{9.2.15}$$

The form of the conserved current (9.2.5) is still valid with the indices are now $\{\mu, \nu\} = \{x, y\}$. Then in terms of its angular variable $\phi(x, y)$, this is explicitly

$$J^\mu = \frac{N}{2\pi r}\hat{\boldsymbol{r}} \ , \tag{9.2.16}$$

where $\hat{\boldsymbol{r}} = (x, y)/\sqrt{x^2 + y^2}$ and $r^2 = x^2 + y^2$. Now, a question arises. In the static vortex configuration, how one can evaluate the total charge $Q = \int_{\text{all space}} J^t$ without the time component of the current? The answer comes from the purely geometrical consideration of (9.2.13) where we can write the component of the current in terms of spatial derivatives of the angular variable ϕ. With the help of Green's theorem, we can rewrite (9.2.13) by

$$N = \int_R \nabla \cdot \boldsymbol{J}\ dxdy \tag{9.2.17}$$

where R is the region surrounded by the closed contour C. But we note that the integrand is the expression of the conserved current $\partial_\mu J^\mu = \nabla \cdot \boldsymbol{J} = 0$. The clue for this problem comes from the fact that the form of the current (9.2.16) is not defined in the origin, but elsewhere. Hence, it will lead to the conclusion that it is the Dirac delta function in two dimensions [150]

$$\nabla \cdot \boldsymbol{J} = \frac{N}{2\pi}\nabla \cdot \frac{\hat{\boldsymbol{r}}}{r} = \frac{N}{2\pi}\delta^2(\boldsymbol{r}) \ . \tag{9.2.18}$$

The configuration of (9.2.11) is a trivial case of $N = 1$, and any other vortex (or antivortex with negative integers) configuration with the same topological number N can be obtained by smooth deformations from the vortex field configuration (9.2.15) ensured by the topological invariant total charge $Q = N$, hence belongs to the equivalent solution space.

Now, in order to understand the geometrical meaning of the winding number N better, we would like to consider a physical system of nematic liquid crystals of Section 8.3. In this system, the optical apparatus, such as two layers of mutually orthogonal polarisers, gives a characteristic feature of the defects in its directors $\boldsymbol{n}_{\rm N}$ of (8.4.36) in the planar case formed by patterns called *brushes*, also known as the Schlieren texture [124]. Since we can distinguish four

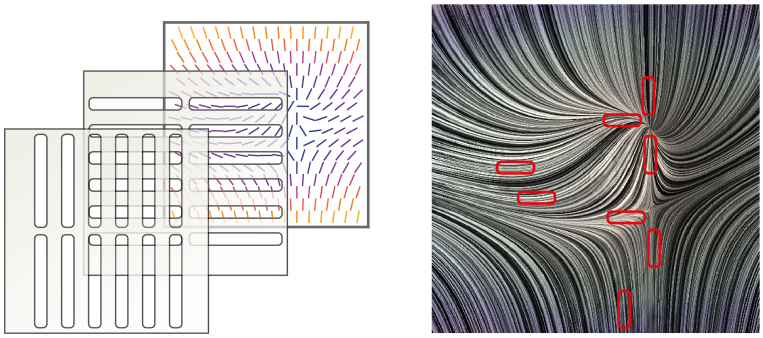

Figure 9.2: The four patterns we can count around a given point are shown in red boxes which are filtered by double-layered polarisers on the model of planar nematic liquid crystals also shown as the vector field.

patterns through double-layered polarisers, we can trace the pattern around the given loop of the planar rotation to count the number of patterns, see Fig. 9.2.

For example, if we count four distinct patterns around the point of interest, this means we can assign a unity to classify the defect occurred around that particular point. This physical measure imposes some difficulties especially if one counts the pattern far away from the defect region which might give different counts around the given loop.

From the mathematical point of view, this counting of the pattern is identical to the winding number defined by (9.2.13), and it is also closely related to the Frank's vector $\boldsymbol{F}$ as the measure of disclination we introduced in terms of the Einstein tensor (7.1.12b)

$$\oint_C \frac{1}{2}\mathring{\omega}_\mu{}^{ab}\epsilon_{ab}{}^c\, dx^\mu = \int_S \frac{1}{2}\mathring{R}^{ab}{}_{\mu\nu}\epsilon_{ab}{}^c\, dx^\mu \wedge dx^\nu = \int_S -\mathring{G}^{\sigma c}\epsilon_{\sigma\mu\nu}\, dx^\mu \wedge dx^\nu = F^c\,, \tag{9.2.19}$$

where $\mathring{\omega}_\mu{}^{ab}$ is the metric compatible spin connection (6.1.2) satisfying $\mathring{\omega}_\mu{}^{ab} = -\mathring{\omega}_\mu{}^{ba}$. In particular, if the defect in the nematic liquid crystals is governed by a fixed uniaxial vector n_i with a planar rotational angle ϕ, from (8.4.14) and (8.4.17) we can write

$$n_i\phi = -\frac{1}{2}\epsilon_{ijk}\phi\, a_{jk} = -\frac{1}{2}\epsilon_{ijk}A_{jk} \tag{9.2.20}$$

where a_{ij} and A_{ij} are antisymmetric 3×3 matrices in the exponential representation $R = e^A$ of $R \in SO(3)$. Then we have, around a simple closed loop C in the plane,

$$\oint_C d(n_i\phi) = n_i \oint_C d\phi = -n_i \oint_C \frac{1}{2}\epsilon_{ijk}dA_{jk} = n_i 2\pi N. \tag{9.2.21}$$

The integer N comes from the vortex field configuration (9.2.15) with the geometrical definition of the winding number in the form of (9.2.13).

Furthermore, if we assign $\partial_\mu A^{jk} = -\mathring{\omega}_\mu{}^{jk}$ into (9.2.19) provided A_{jk} is smooth, we obtain

$$n_i \oint_C d\phi = -n_i \oint_C \frac{1}{2}\epsilon_{ijk}\partial_\mu A^{jk}\, dx^\mu = n_i 2\pi N = F_i\,. \tag{9.2.22}$$

Therefore, the integer N gives us the notion of the winding number at least three different occasions, i) the geometrical integration, ii) the vortex field, iii) the number appears in the Frank's vector as the measure of disclination in this case. Of course, in principle we might have half integers in the vortex field but we would like to restrict ourselves to the integer N. The reason for this becomes apparent when we consider the conserved integer Q in Section 10.

As shown in Fig. 9.3, we can simulate the winding number contribution entirely comes from the vortex field configuration (9.2.15). In particular, in the case of $N = 1$, we can read off four distinct patterns around the centre which gives the winding number one by definition.

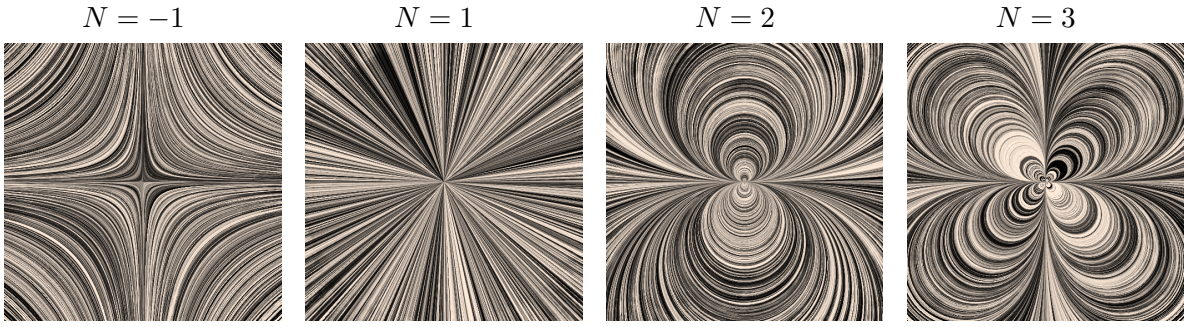

Figure 9.3: Vortex field configurations with various integers N solely using (9.2.15) are shown with the computer generated corresponding defects in the directors.

9.2.2 Conserved current in higher dimensions

We can extend our discussion to the field configuration $\boldsymbol{n}_3 = (n_1, n_2, n_3)$ satisfying $\boldsymbol{n}_3 \cdot \boldsymbol{n}_3 = 1$ in three dimensions, now $\boldsymbol{n}_3$ is on S^2. The current in three dimensions is given by

$$J^\mu = \frac{1}{8\pi}\epsilon^{\mu\nu\rho}\epsilon^{abc} n_a \partial_\nu n_b \partial_\rho n_c \tag{9.2.23}$$

where μ, ν, ρ are spacetime indices in $(2+1)$ dimensions and $a, b, c = 1, 2, 3$ are for the components indices of $\boldsymbol{n}_3 = n_{3i}$. This current is again conserved and its divergence is proportional to the Jacobian matrix similar to (9.2.6). We can compute the J^t component which will give the total charge Q when we integrate it over all space,

$$J^t = \frac{1}{4\pi}\boldsymbol{n}_3 \cdot \left(\frac{\partial \boldsymbol{n}_3}{\partial x} \times \frac{\partial \boldsymbol{n}_3}{\partial y}\right) . \tag{9.2.24}$$

This can be viewed as the volume element of a parallelepiped spanned by $\{\boldsymbol{n}_3, \partial_x \boldsymbol{n}_3, \partial_y \boldsymbol{n}_3\}$. This form of the current is related to the so-called *Mermin-Ho relation* [151] expressing the curl of the velocity in the form of the current (9.2.23) when one considers the director field of the A phase of superfluid helium ^{3}He.

Next, we would like to find an expression for the field configuration in three dimensions, which imposes the winding number N in a natural way, and satisfy the constraint $\boldsymbol{n}_3 \cdot \boldsymbol{n}_3 = 1$. One such an expression comes from the idea that we might regard the non-trivial vortex field $\boldsymbol{n}_{\rm v}$ of (9.2.15) as a projection from the higher dimensional vortex field. This suggests we can simply introduce an additional component in the higher dimensional configuration [152] while we can retain the constraint $\boldsymbol{n}_3 \cdot \boldsymbol{n}_3 = 1$.

This can be done if we combine the non-trivial vortex field $\boldsymbol{n}_{\rm v}$ into the first two component of $\boldsymbol{n}_3$, in such a way that

$$\begin{aligned} \boldsymbol{n}_3 &= (\sin\theta \boldsymbol{n}_{\rm v},\ \cos\theta) \\ &= (\sin\theta\cos N\phi, \sin\theta \sin N\phi, \cos\theta) \ . \end{aligned} \tag{9.2.25}$$

The topological density (another name for the J^t component) for this general field configuration can be obtained simply inserting $\boldsymbol{n}_3$ into (9.2.24)

$$\begin{aligned} J^t &= \frac{1}{4\pi}\det\left(\boldsymbol{n}_3, \frac{\partial \boldsymbol{n}_3}{\partial x}, \frac{\partial \boldsymbol{n}_3}{\partial y}\right) \\ &= -\frac{N}{4\pi}\sin\theta\, \frac{\partial(\phi,\theta)}{\partial(x,y)} \\ &= \frac{N}{4\pi r}\theta' \sin\theta \ , \end{aligned} \tag{9.2.26}$$

where $\theta' = \partial\theta/\partial r$, $r^2 = x^2 + y^2$, and the Jacobian matrix of coordinate changes between the spherical and the Cartesian coordinate system is

$$-N \sin\theta = \frac{\partial(n_1, n_2, n_3)}{\partial(\rho, \phi, \theta)} \ . \tag{9.2.27}$$

Then, the conserved topological charge can be obtained from the integration,

$$\begin{aligned} Q &= \int dxdy \ J^t \\ &= \frac{N}{2} \left[\cos f(0) - \cos f(\infty)\right] \ . \end{aligned} \tag{9.2.28}$$

If we set the radial function to satisfy, $\cos\theta(0) - \cos\theta(\infty) = 2$ or equivalently $\theta(0) - \theta(\infty) = \pi$, we obtain

$$Q = N \ . \tag{9.2.29}$$

The homotopy group in this case is a map from $S^2_{\rm phy}$ to $S^2_{\rm int}$, hence

$$\pi_2(S^2) \cong \mathbb{Z} \ . \tag{9.2.30}$$

For the pure spatial three-dimensional field configuration $\boldsymbol{n}_3 = (n_1, n_2, n_3)$, we can consider the field introduced by Polyakov [153], the **hedgehog field** $\boldsymbol{n}_{\rm h}$ lies on S^2, see Fig. 9.4

$$\boldsymbol{n}_{\rm h} = \frac{1}{r}(x, y, z), \qquad r^2 = x^2 + y^2 + z^2 \ , \tag{9.2.31}$$

corresponding to the $N = 1$ case of the trivial configuration $\boldsymbol{n}_3 = (\sin\theta\cos\phi, \sin\theta\sin\phi, \cos\theta)$, and we will see more of this in Section 9.4.

We can calculate the associated total charge Q, using the divergence theorem to obtain

$$\begin{aligned} \int dxdydz \ \partial_\mu J^\mu &= \int dS_\mu J^\mu \\ &= \frac{1}{8\pi} \int dS_\mu \epsilon^{\mu\nu\rho} \epsilon^{abc} n_a \partial_\nu n_b \partial_\rho n_c \\ &= \frac{1}{4\pi} \int d\boldsymbol{S} \ \boldsymbol{n}_3 \cdot \left(\frac{\partial \boldsymbol{n}_3}{\partial x} \times \frac{\partial \boldsymbol{n}_3}{\partial y} \right) \ . \end{aligned} \tag{9.2.32}$$

In three dimensions the area of S^2 sphere is 4π. This factor exactly cancels out the factor $1/4\pi$. Therefore, the topological density indeed agrees with (9.2.24). And we see that we will obtain the identical total charge Q regardless we integrate J^t from the time-dependent field configuration in $(n+1)$ dimensions over n spatial dimensions, or we integrate the spatial components $\boldsymbol{J}$ from the static field configuration over $(n+1)$ purely spatial total space using the divergence theorem. The latter will give the direct notion of the topological invariant as the degree of mapping of the surface S^2 surrounding the defects on the sphere where the field $\boldsymbol{n}_3$ with the information of winding number N is embedded under the constraint $\boldsymbol{n_3} \cdot \boldsymbol{n_3} = 1$ to yield the homotopy (9.2.30).

Our next task is to construct a field configuration $\boldsymbol{n}_4$ satisfying $\boldsymbol{n}_4 \cdot \boldsymbol{n}_4 = 1$ in four dimensions. This can be done by writing, from our experience of (9.2.25)

$$\boldsymbol{n}_4 = \Big(\sin\omega(r) \boldsymbol{n}_3, \ \cos\omega(r) \Big) \tag{9.2.33}$$

where $\boldsymbol{n}_3$ is defined by (9.2.25) with the integer N firmly embedded. The conserved current, also known as Skyrme's current, is

$$J^\mu = \frac{1}{12\pi^2} \epsilon^{\mu\nu\lambda\rho} \epsilon^{abcd} n_a \partial_\nu n_b \partial_\lambda n_c \partial_\rho n_d \ . \tag{9.2.34}$$

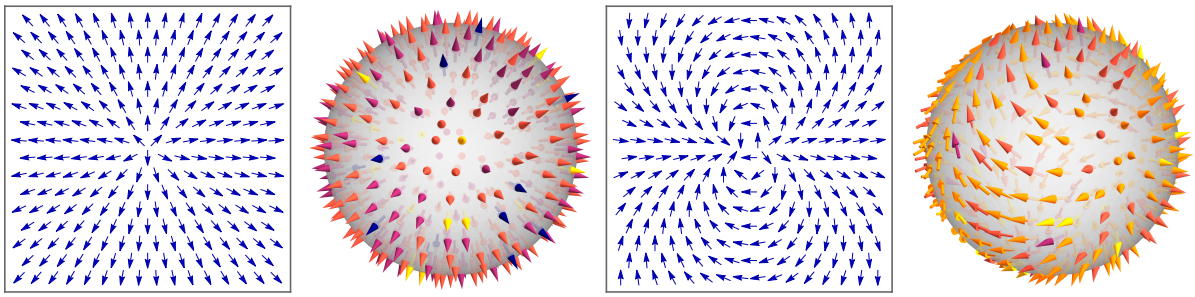

Figure 9.4: Two-dimensional vortex field configurations with various integers N using (9.2.15) and its corresponding $\boldsymbol{n}_3$ fields on S^2 of (9.2.25) are shown where $\boldsymbol{n}_3(N=1)$ is essentially the isotropic director distribution of hedgehog configuration $\boldsymbol{n}_{\rm h}$.

One can compute the topological density by inserting (9.2.33) into (9.2.34)

$$\begin{aligned} J^t &= \frac{N}{2\pi^2}\sin\theta\sin^2\omega(r)\,\frac{\partial(\phi,\theta,\omega(r))}{\partial(x,y,z)} \\ &= -\frac{N}{2\pi^2}\frac{\omega'(r)}{r^2}\sin^2\omega(r)\;, \end{aligned} \tag{9.2.35}$$

where we used the Jacobian matrix, similar to that of (9.2.27)

$$N\sin\theta\sin^2\omega(r) = \frac{\partial(n_1,n_2,n_3,n_4)}{\partial(\rho,\phi,\theta,\omega(r))}\;. \tag{9.2.36}$$

The associated total charge can be obtained

$$Q = \frac{N}{\pi}\left[\omega(0)-\omega(\infty)\right] - \frac{N}{2\pi}\left[\sin 2\omega(0)-\sin 2\omega(\infty)\right]\;. \tag{9.2.37}$$

Now, we notice that the second term on the right-hand side of (9.2.36) may impose the condition against the consideration we discussed in terms of the finite energy requirement. But if we write

$$\sin 2\omega(0)-\sin 2\omega(\infty) = 2\Big[\sin\omega(0)\cos\omega(0)-\sin\omega(\infty)\cos\omega(\infty)\Big]\;,$$

then we can choose the arbitrary radial function $\omega(r)$ in such a way that it removes the possible singularity by putting $\sin\omega(0)=\sin\omega(\infty)=0$. Consequently, the function $\omega(r)$ removes the divergence in the energy when $r\to\infty$. Under these conditions, the problematic terms vanish and the total charge becomes

$$Q = \frac{N}{\pi}[\omega(0)-\omega(\infty)]\;. \tag{9.2.38}$$

In order to ensure the finite integer-valued Q, we further use the identity

$$\sin A-\sin B = 2\sin\left(\frac{A-B}{2}\right)\cos\left(\frac{A+B}{2}\right)\;,$$

so that the condition $\sin\omega(0)=\sin\omega(\infty)=0$ implies that the identical asymptotic condition on the radial function when we derived (9.2.29), $\omega(0)-\omega(\infty)=\pi$. Therefore, the total charge becomes

$$Q = N\;, \tag{9.2.39}$$

as expected, and the homotopy group in this case is a map from $S^3_{\rm phy}$ to $S^3_{\rm int}$ so that

$$\pi_3(S^3) \cong \mathbb{Z} \ . \tag{9.2.40}$$

In deriving the expressions $Q = N$ in (9.2.29) and (9.2.39), we can obtain the identical results but with an additional minus sign. To see this, as noted in [154], let us bring back the stereographic projection space we considered in Section 8.1. The vortex field travels from the south pole to the north pole, or it can travel in the reverse direction on S^2 (or on S^3), as r increases from the origin to infinity on the projective plane or in the reverse order. Then, the total charge Q may acquire a minus sign depending on the choice of the path between the poles, hence $Q = \pm N$. The factor that determines the sign is sometimes called the polarity.

Lastly, we would like to consider the mechanism that lies beneath in evaluating the integrations in various dimensions to assure the integer-valued Q in accordance with the homotopy classification $\pi_n(S^n) \cong \mathbb{Z}$. In general d dimensions, the form of the integration for the charge Q would be

$$\int d^d x \ \partial_\mu J^\mu = \int dS_\mu J^\mu \ . \tag{9.2.41}$$

We can regard the term dS_μ on the right-hand side as an infinitesimal surface element of the hypersurface S^{d-1} embedded by the volume element $d^d x$ of the integration in d dimensions, defined on the left-hand side in the direction of the current J^μ. To see this, for the Euclidean length element x, defined by the strictly positive-definite Euclidean metric tensor, the arbitrary volume element in d dimensions $d^d x$ can be written by

$$d^d x = d\Omega_d \ dx \ x^{d-1} \tag{9.2.42}$$

where $\int d\Omega_d$ is the area of a unit n-sphere S^n in $d = n + 1$ dimensions. This technique is commonly used when one considers the dimensional regularisation in quantum field theory to remove the possible divergences in evaluating the integration [155]. Therefore, we can construct a conserved current in the general d dimensions

$$J^\mu = \frac{1}{n! \int d\Omega_d} \epsilon^{\mu\mu_1\cdots\mu_n} \epsilon^{aa_1\cdots a_n} n_a \partial_{\mu_1} n_{a_1} \cdots \partial_{\mu_n} n_{a_n} \ , \tag{9.2.43}$$

where the factor $n!$ comes from the number of permutations in the indices, and the explicit evaluation of $\int d\Omega_d$ will be given shortly. This will give the topological invariant Q by the integration (9.2.41) with the factor $\int d\Omega_d$ will be canceled out exactly in the integration. In particular, when one considers a static d dimensional problem, the conserved current will take the form

$$J^\mu = \frac{N}{\int d\Omega_d} \frac{\hat{\boldsymbol{r}}}{r^{d-1}} \ , \qquad \boldsymbol{r} = (x_1, \cdots, x_d) \tag{9.2.44}$$

which yields the d-dimensional Dirac delta function,

$$\partial_\mu J^\mu = \frac{N}{\int d\Omega_d} \left(\int d\Omega_d \right) \delta^d(\boldsymbol{r}) \ . \tag{9.2.45}$$

The corresponding field configuration in d dimensions is

$$\boldsymbol{n}_d = (\sin\omega_d(r) \boldsymbol{n}_{d-1}, \ \cos\omega_d(r)) \ , \quad \boldsymbol{n}_2 = \boldsymbol{n}_{\rm v} \ , \quad d \geq 3 \tag{9.2.46}$$

with some angular functions $\omega_d(r)$, satisfying $\boldsymbol{n}_d \cdot \boldsymbol{n}_d = 1$ in $d = n + 1$. The mapping between the field configuration on the sphere $S^n_{\rm phy}$ and the sphere $S^n_{\rm int}$ in the integration (9.2.41) gives precisely the homotopy classification we observed in (9.2.14), (9.2.30) and (9.2.40)

$$\pi_n(S^n) \cong \mathbb{Z} \ . \tag{9.2.47}$$

Nonetheless, the field configuration (9.2.46) is not unique for the purpose of obtaining the topological invariants N. In [156] various forms of J^μ are given, for example, by noting the similarities from the sine-Gordon system which gives a set of distinct Q sectors. Notably, in [157], the form of field configuration $\boldsymbol{n}_3$ is given using an equality based on the lower bound for the finite-energy consideration

$$\partial_\mu \boldsymbol{n}_3 = \pm \epsilon_{\mu\nu} \left(\boldsymbol{n}_3 \times \partial_\nu \boldsymbol{n}_3 \right) \ . \tag{9.2.48}$$

This further yields a conclusion that when the field configuration $\boldsymbol{n}_3$ is projected on the complex plane to form the analytic complex function $w = w_1 + iw_2$, then any such analytic function will give the topological invariants when one writes w in the power expansion of order N. The solution space itself imposes the scale invariance and the translational invariance.

The expression (9.2.42) can be illustrated in simple cases for $d = 2$ and $d = 3$, where the infinitesimal elements to be integrated are expressed as the product of its differential angular elements and radial elements in the polar coordinate system, for example

$$\begin{aligned} d = 2: &\quad dxdy = (d\theta)(rdr) \ , \\ d = 3: &\quad dxdydz = (\sin\theta d\theta d\phi)(r^2 dr) \ . \end{aligned}$$

The factor $\int d\Omega_d$ in general case is given by

$$\int d\Omega_d = \frac{2\pi^{\frac{d}{2}}}{\Gamma\left(\frac{d}{2}\right)} \ . \tag{9.2.49}$$

Using the properties of Gamma function,

$$\Gamma(n+1) = n\Gamma(n), \qquad \text{and} \qquad \Gamma\left(\frac{1}{2} + n\right) = \frac{(2n)!}{4^n n!}\sqrt{\pi} \ ,$$

we can summarise some special cases that frequently appears, as below.

Dimension d	1	2	3	4
$\int d\Omega_d$	2	2π	4π	$2\pi^2$

(9.2.50)

9.3 Topological sectors

In the previous Sections, we started from the conserved current J^μ *a priori* to derive the conserved charge Q in the simple $(1+1)$ dimensions up to the general case of (9.2.43). Unlike the conventionally derived conserved current such as Noether's current, the topological invariants we considered are entirely dependent on the asymptotic boundary conditions, and its conserved invariant property comes from the finite energy requirement from the expression

$$Q \propto \phi(+\infty, t) - \phi(-\infty, t) \ .$$

And we saw explicit field configurations for the associated conserved current in various dimensions, leading to the topological invariants

$$Q = N \ .$$

It becomes evident that our true starting point in developing the argument should be the finite energy requirement rather than the seemingly *ad hoc* construction of the currents J^μ. This

statement can be rephrased that the solution space ϕ should satisfy some finite-valued asymptotic conditions. In this Section, we would like to justify the relation between the topologically invariant total charge and the homotopy classification using a simple case.

Let us start again with the system of a single scalar field $\phi(x,t)$ in two dimensions. We write the Lagrangian by

$$\mathcal{L} = \frac{1}{2}\partial_\mu\phi\partial^\mu\phi - U(\phi) \ , \tag{9.3.1}$$

where the potential $U(\phi)$ might have an integer number of degenerate minima. In particular, the sine-Gordon system of (9.1.18) imposes the infinite number of minima of the system, with the potential $U(\phi) = m^2(1-\cos\phi)$ due to the periodicity in the solution space with the integer N.

If the system possesses a set of degenerate minima, the field (static or time-dependent) must approach a minimum of $U(\phi)$ at every point on spatial infinity for a given t, to retain its finite energy requirement. In this case, as we already imposed in (9.1.5) and (9.1.6), we define formally such asymptotic conditions by

$$\phi(+\infty,t) = \lim_{x\to+\infty}\phi(x,t) \equiv \phi_{+\infty} \ , \qquad \phi(-\infty,t) = \lim_{x\to-\infty}\phi(x,t) \equiv \phi_{-\infty} \ . \tag{9.3.2}$$

And there are two possibilities that either $\phi_{+\infty} = \phi_{-\infty}$ or $\phi_{+\infty} \neq \phi_{-\infty}$ within the finite energy requirement. Then, the field $\phi(x,t)$ will change continuously as the time t varies and the solution space itself is derived from the equation of motion

$$\partial_\mu\partial^\mu\phi = -\frac{\partial U}{\partial\phi} \ . \tag{9.3.3}$$

The trivial solution for this differential equation is again constant vacuum solution $\phi_{\rm vac}$, and if not, it will be a description of the continuous deformation of the system as we saw in Part I. Therefore, in a sense, the non-trivial solution can be regarded as a fluctuation $\phi_{\rm f}$ of the vacuum solution restricted by a finite-energy requirement

$$\phi = \phi_{\rm vac} + \phi_{\rm f} \tag{9.3.4}$$

belongs to each homotopy classification of the solution space, with the asymptotic behaviour that $\phi \to \phi_{\rm vac}$ as seen in the ϕ^4 theory and the sine-Gordon system in Section 9.1.

The continuously deformable condition and the smoothness of the function ϕ suggests that we cannot expect the transition in the configuration of the system have an abrupt change from $\phi_{-\infty}$ to $\phi_{+\infty}$. Hence the transition within the given minima must occur smoothly in such a way that the points of minima remain as the stationary points of $U(\phi)$ within the given class of solution space.

Therefore, there exist a number of regions called **sectors** [40] in the solution space in which the system is allowed to deform continuously around the point of minima while the finite energy requirement is maintained. The sectors are topologically disconnected regions in the solution space, in a sense that fields configuration from one sector cannot be deformed continuously into another without violating the finite energy requirement. But the field configuration in any given sector stays within that sector as time changes.

Hence, this classification of sectors is closely related to the equivalent homotopy classification of the solution space. This is an analogous analysis we made in (7.2.4) in Section 7.2. In particular, if there is only one unique minima, we have only one sector for the solution space and this corresponds to the case of $\phi(+\infty,t) = \phi(-\infty,t)$ which is equivalent to the trivial case $Q = 0$. This is the class $\{0\} \in \pi_1(SO(3))$ we considered in (7.2.4), the equivalent set of configuration that can be continuously deformed uniformly via diffeomorphism.

Let us follow the example given in [40]. If we have the ϕ^4 system of (9.1.7), then the potential is given by

$$U(\phi) = \frac{\lambda}{4}\phi^4 - \frac{\mu^2}{2}\phi^2 \tag{9.3.5}$$

with two minima $\partial U/\partial\phi = 0$ at $\phi = \pm\mu/\sqrt{\lambda}$. Therefore, there are four distinct sectors in this case given by paths along the curve called the *orbits* defined by intervals of these minima,

$$\text{i)}: \left(-\frac{\mu}{\sqrt{\lambda}}, -\frac{\mu}{\sqrt{\lambda}}\right), \quad \text{ii)}: \left(\frac{\mu}{\sqrt{\lambda}}, \frac{\mu}{\sqrt{\lambda}}\right), \quad \text{iii)}: \left(-\frac{\mu}{\sqrt{\lambda}}, \frac{\mu}{\sqrt{\lambda}}\right), \quad \text{iv)}: \left(\frac{\mu}{\sqrt{\lambda}}, -\frac{\mu}{\sqrt{\lambda}}\right), \tag{9.3.6}$$

As shown in Fig. 9.5, there are two physically meaningful orbits, namely type I (i) and ii)) which starts and ends at the same minimum, and type II (iii) and iv)) connecting distinct minimum points among the given set of degenerate minima. Hence we have two distinct types of sectors which are related to the homotopy classification of (9.1.9).

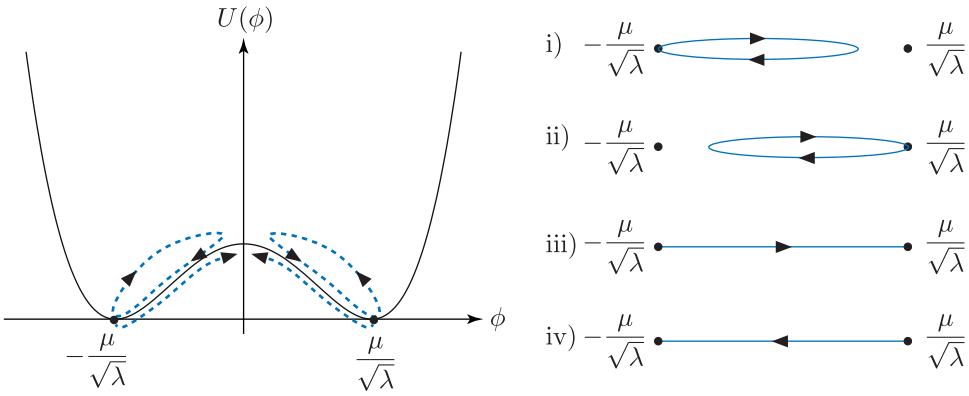

Figure 9.5: The transitions of the field configuration along the orbits (dotted lines) are shown, starting from one of minima and ending either to the same point or the distinct minimum configuration.

Similar conclusion can be made if we consider the sine-Gordon system which gives infinite numbers of types in sectors in analogy with (9.1.20). But we must note that the symmetries we considered in the ϕ^4 theory, the sine-Gordon system, and in the nonlinear $O(N)$ models, all are the global symmetries for the respective Lagrangians. This means, if we have a solution space that possesses a different kinds of symmetry structure, often called the internal or the local symmetry, then our consideration on the sector can break down.

The above discussion can be extended to a general system of n-coupled scalar fields in two dimensions with the Lagrangian

$$\mathcal{L} = \frac{1}{2}\partial_\mu\boldsymbol{\phi}\partial^\mu\boldsymbol{\phi} - U(\boldsymbol{\phi}) \ , \tag{9.3.7}$$

where the n-component scalar field is given by

$$\boldsymbol{\phi}(x,t) = (\phi_1(x,t), \cdots, \phi_n(x,t)) \ .$$

The equations of motion are

$$\partial_\mu\partial^\mu\phi_a = -\frac{\partial U}{\partial\phi_a}, \qquad a = 1, \cdots, n \ . \tag{9.3.8}$$

The requirement that the solution have finite energy leads to the condition that minima of $U(\phi_i)$ must be obtained for some field $\boldsymbol{\phi}$ as $x \to \pm\infty$ in n-dimensional field space, and the sectors can be determined by the intervals defined by those minima.

Now, we must note that there are significant differences from the single field case. In case of the single field, once the smooth continuous deformation starts from one of minima, the transition must terminate at another minima or return to the starting point to lose the kinetic energy. In case of the coupled multi-component field, if $U(\phi_i)$ has a unique minimum the situation is identical to that of the single field case. But if there are degenerate minima, once the transition is initiated from one point towards another point in the n-dimensional ϕ_a-space, the transition can occur along the orbits and return to the starting point without losing all its kinetic energy. Further, if we impose some constraint on the field, such as

$$\boldsymbol{\phi} \cdot \boldsymbol{\phi} = (\phi_1)^2 + \cdots + (\phi_n)^2 = 1 \ , \tag{9.3.9}$$

or a unitary condition for the complex-valued field, the system will remain invariant under the certain internal symmetry, preferably a Lie group, under which the system configuration can be transformed from one into another continuously.

To illustrate this internal symmetry that differs from the global symmetry of the system, consider the real two-component field $\boldsymbol{\phi} = (\phi_1, \phi_2)$ with a potential $U(\phi_1, \phi_2)$ so that the solution space is defined in the $\{\phi_1, \phi_2\}$ plane. Suppose $U(\phi_1, \phi_2)$ has two distinct minima at point A and B on the field plane. And we can see that the possible orbits are given by the similar set of (9.3.6) but the transition can occur through the internal circle through the point A and B to become a periodic orbit which constitutes the internal symmetry. This internal circle is indeed the local symmetry of the system, originated from the internal constraint such as (9.3.9). See Fig. 9.6.

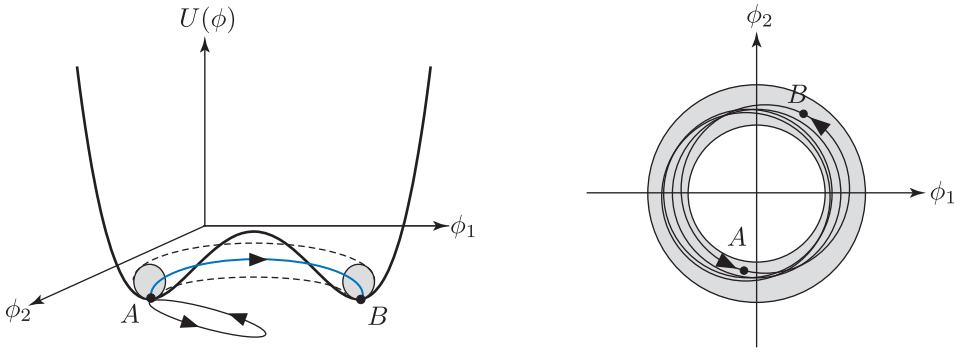

Figure 9.6: The orbit starts and ends at the minimum A and orbits connecting A and B are shown. The orbits can be periodic that eventually lose all its kinetic energy, and terminates its loop at one of minima on the planar solution space.

Now, suppose the Lagrangian and the potential $U(\phi)$ are invariant under some symmetry transformation acting on $\phi(x)$. If $U(\phi)$ had a unique minimum at some $\phi = \phi_0$, then ϕ_0 itself must remain invariant under that transformation. In the case of a set degenerate minima with distinct sectors, the full set of minima is invariant under the symmetry of the Lagrangian of the system (often it is the global symmetry) but each individual minimum can exhibit the local symmetry differs from the original symmetry for the system.

As a simple example, we know that the system (9.3.5), with four topological sectors, has a $U(\phi)$ invariant under $\phi \to -\phi$. But its two minima are not separately invariant but they are transformed into one another under the different symmetry, namely the rotation in phase. This property is also known as the spontaneous symmetry breaking, and this may lead to the existence of the non-trivial topological sectors with a set of degenerate minima of the potential.

In the next Section, we would like to consider another example of the multi-component field $\boldsymbol{\phi} = (\phi_1, \phi_2, \phi_3)$ with the identical form of the potential $U(\boldsymbol{\phi})$ of the ϕ^4 theory. This

configuration is known as the Polyakov's hedgehog field with the solution $\boldsymbol{n}_{\rm h}$ we saw in (9.2.31).

9.4 Polyakov's hedgehog field

In 1974, Polyakov showed [153] that under the weak interaction assumption, the finite range of mass spectrum can be obtained from the Hamiltonian H following the finite energy requirement of the system with the Lagrangian of the higher dimensional ϕ^4 theory in $(1+1)$ dimensions we considered in (9.1.7). For $(3+1)$ dimensions, the Lagrangian is given by

$$\mathcal{L} = \frac{1}{2}\partial_\mu \boldsymbol{\phi}\partial^\mu \boldsymbol{\phi} - U(\boldsymbol{\phi}) \,, \tag{9.4.1}$$

where

$$U(\boldsymbol{\phi}) = -\frac{\mu^2}{2}\boldsymbol{\phi}^2 + \frac{\lambda}{4}\boldsymbol{\phi}^4 \,, \tag{9.4.2}$$

for the three-component field $\boldsymbol{\phi} = (\phi_1, \phi_2, \phi_3)$. The equation of motion identical to (9.3.8), is given by

$$\partial_\mu \partial^\mu \phi_a - \Big(\mu^2 - \lambda(\boldsymbol{\phi}\cdot\boldsymbol{\phi})\Big)\phi_a = 0 \,. \tag{9.4.3}$$

A solution for the static case is given by

$$\phi_a = n_{{\rm h}a}\Theta(r), \qquad n_{{\rm h}a} = \frac{1}{r}(x, y, z) \tag{9.4.4}$$

where $r^2 = x^2 + y^2 + z^2$ and $\boldsymbol{n}_{\rm h} = n_{{\rm h}a}$ for $a = 1, 2, 3$ is the field configuration of (9.2.31). An angular function $\Theta(r)$ satisfies the second-order ordinary differential equation

$$\Theta'' + \frac{2}{r}\Theta' + \left(\mu^2 - \frac{2}{r^2}\right)\Theta - \lambda\Theta^3 = 0 \,. \tag{9.4.5}$$

Apart from the trivial vacuum solutions, i.e. the zeros of the potential $U(\boldsymbol{\phi})$, the non-trivial solution must impose the asymptotic condition that approaches the vacuum solution

$$\Theta(r \to \infty) = \frac{\mu}{\sqrt{\lambda}} \,, \tag{9.4.6}$$

The solution (9.4.4) is called the *hedgehog solution*, as we can see that these are isovectors directed along the radial vector at a given point.

For the rank-two tensor field, also known as the isotensor Higgs field, it is suggested by Polyakov that the solution shall be of the form

$$\phi_{ab} = \left(n_{{\rm h}a}n_{{\rm h}b} - \frac{1}{3}\delta_{ab}\right)\Theta(r) \,, \qquad a, b = 1, 2, 3 \tag{9.4.7}$$

in place of ϕ_a in (9.4.4). We note that this is the identical form of the order parameter $\boldsymbol{Q}$ of (8.4.7) for the nematic liquid crystals we obtained in Section 8.4.

$$Q_{ij} = \left(n_{{\rm N}i}n_{{\rm N}j} - \frac{1}{3}\delta_{ij}\right)\sigma \,, \qquad i, j = 1, 2, 3 \,. \tag{9.4.8}$$

This enters into the energy density function $\mathcal{F}$ of (8.4.3) in the various forms of the invariant. We note that $\Theta(r)$ in (9.4.7) is a function of the position, but σ is a mere constant parameter. This implies, unlike the space S^2 where the nematic liquid crystals with directors $\boldsymbol{n}_{\rm N}$ are identified as the antipodals, we might need higher dimensional space with an additional degree of freedom to harbour the higher-ranked field configuration with some analogous notion of the antipodal identification on that space. It is tempting to promote (9.4.7) to be the order parameter for the micropolar continuum, in line of generalisation of nematic liquid crystals to the micropolar continuum in terms of director fields we saw in Section 8.4. This is the subject we would like to investigate in the next Chapter, followed by formal justification.

Chapter 10

Micropolar continuum and the Skyrme model

A finite energy configuration requires appropriate asymptotic conditions in the total charge Q, for example in (9.2.28) and (9.2.38), to satisfy certain criteria as we observed in the previous Sections with the currents J^μ in various dimensions. We would like to focus on the field configuration $\boldsymbol{n}$ itself constituting such currents J^μ in higher dimensions. This includes the Skyrme model as the spinor system in which the relation between $SU(2)$ and $SO(3)$ signifies its role in various forms of the representation. This further will give us a unique point of view to understand the result we obtained in Part II to connect the deformational measures we used so far.

It is hinted in [35] that the order parameter for the micropolar continua can be taken as $SO(3)$ or $\mathbb{R}P^3$, and in [120] the elements of $R \in SO(3)$ are briefly mentioned as the antipodals on S^3. Using the fibrations between the unit spheres and the real projective space, we would like to generalise the idea that micropolar continua can be regarded as the projective space that contains the nematic liquid crystals as its submanifold followed by the topological and geometrical consideration. This approach is different from that of [142] promoting the micropolar continua as the general case of nematic liquid crystals.

10.1 Rotations of $SO(3)$ and $SU(2)$

An element R of the orthogonal rotation group $SO(3)$, satisfying $R^T R = \mathbb{1}$, can be expressed by the real 3×3 matrix representation we considered in (8.4.20), which is equivalent to (1.2.31)

$$R_{ij} = \cos\Theta \cdot \delta_{ij} + n_{3i} n_{3j}(1 - \cos\Theta) - \epsilon_{ijk} n_{3k} \sin\Theta \ . \tag{10.1.1}$$

This describes the rotation of an angle Θ about the normalised axis

$$\boldsymbol{n}_3 = n_{3i} \qquad \text{satisfying} \qquad \boldsymbol{n}_3 \cdot \boldsymbol{n}_3 = 1 \ . \tag{10.1.2}$$

where $i, j, k = 1, 2, 3$. We are particularly interested in the position-dependent axial configuration. For this purpose, we can choose the axis to be the hedgehog field $\boldsymbol{n}_{\rm h}$ of (9.2.31) or the general field $\boldsymbol{n}_3$ of (9.2.25), which gives the topological invariant N in three dimensions. In particular, when $N = 1$, the hedgehog field is just the static $\boldsymbol{n}_3$ in the usual polar coordinate system

$$\boldsymbol{n}_{\rm h} = (\sin\theta\cos\phi, \sin\theta\sin\phi, \cos\theta) \ , \tag{10.1.3}$$

where $\phi = \arctan(y/x)$ and $\theta = \arctan(\sqrt{x^2 + y^2}/z)$.

An element U of the unitary rotational group $SU(2)$, satisfying $U^\dagger U = I$, can be represented by a complex 2×2 matrix with two complex parameters $a, b \in \mathbb{C}$

$$U = \begin{pmatrix} a & -\bar{b} \\ b & \bar{a} \end{pmatrix} \qquad \text{where} \qquad |a|^2 + |b|^2 = 1 \ . \tag{10.1.4}$$

Since there is a direct isomorphism of $\mathbb{C}^n \cong \mathbb{R}^{2n}$, we can assign a set of four real parameters (n_1, n_2, n_3, n_4) in such a way that $a = n_4 + in_3$ and $b = -n_2 + in_1$. Then (10.1.4) becomes

$$U = \begin{pmatrix} n_4 + in_3 & in_1 + n_2 \\ in_1 - n_2 & n_4 - in_3 \end{pmatrix} = n_4 \cdot I + i(\boldsymbol{n} \cdot \boldsymbol{\sigma}) \ , \tag{10.1.5}$$

where $\boldsymbol{n}_4 = (\boldsymbol{n}, n_4) = (n_1, n_2, n_3, n_4)$ satisfies the condition

$$\boldsymbol{n}_4 \cdot \boldsymbol{n}_4 = 1 \ . \tag{10.1.6}$$

We should not be confused with the first three components $\boldsymbol{n}$ of $\boldsymbol{n}_4$ and $\boldsymbol{n}_3 \in S^2$ satisfying $\boldsymbol{n}_3 \cdot \boldsymbol{n}_3 = 1$ which enters into the representation of (10.1.1) as the normalised axis field in three dimensions. The Pauli matrices $\boldsymbol{\sigma} = (\sigma_1, \sigma_2, \sigma_3)$ in (10.1.5) are the generators of $SU(2)$, defined by

$$\sigma_1 = \begin{pmatrix} 0 & 1 \\ 1 & 0 \end{pmatrix} \ , \qquad \sigma_2 = \begin{pmatrix} 0 & -i \\ i & 0 \end{pmatrix} \ , \qquad \sigma_3 = \begin{pmatrix} 1 & 0 \\ 0 & -1 \end{pmatrix} \ . \tag{10.1.7}$$

It is sometimes convenient to write elements $U \in SU(2)$ and $R \in SO(3)$, respectively,

$$U = e^{i\omega(r)\boldsymbol{n}_3 \cdot \boldsymbol{\sigma}} \quad \text{and} \quad R = e^{i\Theta \boldsymbol{n}_3 \cdot \boldsymbol{J}} \ . \tag{10.1.8}$$

The quantities $\omega(r)$ and Θ are the rotational angles about respective axes. Under these representations, the generators $\boldsymbol{\sigma}$ and $\boldsymbol{J}$ for $SU(2)$ and $SO(3)$, respectively, satisfy commutation relations

$$\left[\frac{\sigma_i}{2}, \frac{\sigma_j}{2}\right] = i\epsilon_{ijk}\frac{\sigma_k}{2} \qquad \text{and} \qquad [J_i, J_j] = i\epsilon_{ijk}J_k \ . \tag{10.1.9}$$

Using the identity for the Pauli matrices,

$$\sigma_i \sigma_j = \delta_{ij} \cdot I + i\epsilon_{ijk}\sigma_k \ , \tag{10.1.10}$$

we can show that $(\boldsymbol{n}_3 \cdot \boldsymbol{\sigma})^2 = I$. This implies that the even power of $(\boldsymbol{n}_3 \cdot \boldsymbol{\sigma})$ is I, and the odd power becomes $(\boldsymbol{n}_3 \cdot \boldsymbol{\sigma})$. Hence, the form of the element $U \in SU(2)$ is indeed,

$$\begin{aligned} e^{i\omega(r)\boldsymbol{n}_3 \cdot \boldsymbol{\sigma}} &= \cos\omega(r) \cdot I + i(\boldsymbol{n}_3 \cdot \boldsymbol{\sigma}) \sin\omega(r) \\ &= n_4 \cdot I + i(\boldsymbol{n} \cdot \boldsymbol{\sigma}) \end{aligned} \tag{10.1.11}$$

where we put $\boldsymbol{n} = \boldsymbol{n}_3 \sin\omega(r)$ and $n_4 = \cos\omega(r)$ for $\boldsymbol{n}_3 \cdot \boldsymbol{n}_3 = \boldsymbol{n}_4 \cdot \boldsymbol{n}_4 = 1$. This is precisely the field configuration $\boldsymbol{n}_4$ of (9.2.33) we used in deriving the topological invariant N by Skyrme's current J^μ of (9.2.34).

$$\boldsymbol{n}_4 = \Big(\sin\omega(r)\boldsymbol{n}_3, \ \cos\omega(r)\Big) \ . \tag{10.1.12}$$

An explicit relation between $R \in SO(3)$ and $U \in SU(2)$ can be explained in many ways, but we would like to take a quaternion for the apparent topological benefit. A quaternion q is defined by

$$q = a + b\boldsymbol{i} + c\boldsymbol{j} + d\boldsymbol{k} \tag{10.1.13}$$

such that $a, b, c, d \in \mathbb{R}$ satisfy

$$a^2 + b^2 + c^2 + d^2 = 1 \qquad \text{and} \qquad \boldsymbol{i}^2 = \boldsymbol{j}^2 = \boldsymbol{k}^2 = -1 \; . \tag{10.1.14}$$

So, it is easy to see that q lives on the sphere S^3, and there is a direct isomorphism between $U \in SU(2)$ of (10.1.5) and the representation of the quaternion. Explicitly, this is

$$q = a \cdot I + (b, c, d) \cdot (\boldsymbol{i}, \boldsymbol{j}, \boldsymbol{k}) \tag{10.1.15}$$

or equivalently, the isomorphism of

$$i\boldsymbol{\sigma} \cong (\boldsymbol{i}, \boldsymbol{j}, \boldsymbol{k}) \; . \tag{10.1.16}$$

In particular, if we have a pure imaginary quaternion there is a one-to-one correspondence between a quaternion and an element of $\mathbb{R}^3$ which transforms under the rotation $SO(3)$. This allows us to take the Pauli matrices $\boldsymbol{\sigma}$ to transform under the rotation, regarding it as a three-component vector acted by the rotation in such a way that

$$\sigma_i = \sigma_j R_{ji} \; .$$

On the other hand, since each Hermitian matrix of the three-component $\boldsymbol{\sigma}$ transforms under $U \in SU(2)$, we must have

$$\sigma_i \longrightarrow U^\dagger \sigma_i U \; .$$

Hence, as introduced in [158], the relation between $U \in SU(2)$ and $R \in SO(3)$ can be written by

$$\sigma_i R_{ij} = U^\dagger \sigma_j U \; . \tag{10.1.17}$$

After applying σ_k on both sides, we take traces using the identity $\mathrm{tr}(\sigma_i \sigma_j) = 2\delta_{ij}$ which can be easily seen from (10.1.10). Then (10.1.17 gives an explicit correspondence between $U \in SU(2)$ and $R \in SO(3)$, used in [159], by

$$R_{ij} = \frac{1}{2} \mathrm{tr} \left(\sigma_i U^\dagger \sigma_j U \right) \; , \tag{10.1.18}$$

where the trace are taken over 2×2 matrices is understood if we write this in components

$$R_{ij} = \frac{1}{2} \left[\sigma^{kl}_{(i)} U^\dagger_{lt} \right]_{kt} \left[\sigma^{tl}_{(j)} U_{lk} \right]_{tk} \; . \tag{10.1.19}$$

Since U and $-U$ will give rise to the identical R, this confirms the two-to-one mapping between $SU(2)$ and $SO(3)$. Straightforward calculation of (10.1.19) by inserting the matrix elements of U of (10.1.5) gives the representation of R_{ij} in terms of (n_i, n_4) for $i, j = 1, 2, 3$

$$R_{ij} = 2n_i n_j - 2\epsilon_{ijk} n_k n_4 + \delta_{ij}(2n_4^2 - 1) \tag{10.1.20}$$

in which, we used the constraint $n_i^2 + n_4^2 = 1$ of (10.1.6), and trace identities

$$\mathrm{tr}\sigma_i = 0, \quad \mathrm{tr}(\sigma_i \sigma_j) = 2\delta_{ij}, \quad \mathrm{tr}(\sigma_i \sigma_j \sigma_k) = 2i\epsilon_{ijk}, \quad \mathrm{tr}(\sigma_i \sigma_j \sigma_s \sigma_t) = \delta_{ij}\delta_{st} - \delta_{is}\delta_{jt} + \delta_{it}\delta_{js} \; .$$

Therefore, we can confirm the well-known correspondence $SU(2) \longrightarrow SO(3)$ stating that $SU(2)$ is a double cover of $SO(3)$

$$SU(2)/\{-I, I\} \cong SO(3) \; .$$

Moreover, if we put

$$n_i = \boldsymbol{n}_3 \sin \frac{\Theta}{2} \qquad \text{and} \qquad n_4 = \cos \frac{\Theta}{2} \; , \tag{10.1.21}$$

into (10.1.20), we will recover the previous representation (10.1.1).

10.2 Spinors

10.2.1 Spin system

A system with **spinors** is characterised by its acquisition of an additional minus sign to its original state after 2π rotational transition, and return to its initial state after a full 4π rotation. This peculiar character of the spinor is observed in many physical systems, notably in the twistor theory by Penrose and Newman [160,161] in which the Dirac's spinors are regarded as a special case. The discussion of the spinor property of spinning particles can be found in [119, 162], and pedagogical yet motivating discussions can be found in [119, 154, 162]. One finds some illustrating explanations of spinors in both macroscopic and microscopic aspects in [163].

It is particularly well-known in particle physics [164, 165] that the spin-1/2 particle takes 4π rotational transition to return to its original state. So let us start with a spin-1/2 particle. It takes one state out of two possible states, namely spin-up $|\uparrow\rangle$ and spin-down $|\downarrow\rangle$. Often it is convention to represent these states by

$$|\uparrow\rangle = \begin{pmatrix} 1 \\ 0 \end{pmatrix} \qquad \text{and} \qquad |\downarrow\rangle = \begin{pmatrix} 0 \\ 1 \end{pmatrix} .$$

Suppose we have a spin-up state aligned with the z-axis with no spin-down component initially. So, we write the initial state by a probability function $P(|\uparrow\rangle, |\downarrow\rangle) = (1, 0)$ which indicates that the probability of finding $|\uparrow\rangle$ distribution is the total space. In this way, we may construct a set of axes to represent orthogonal references with the probability P for the given spin states, with the associated angular variable to express the transition from the initial state. This angular variable is referred as the generalised phase of the state.

After 2π rotation, it will only acquire a minus sign to its original spin state. If we wish to represent this property in a circular motion with the angular variable representing the transforming spin states, we consider the full circle rotation by 4π rather than the usual 2π rotation. See Fig. 10.1.

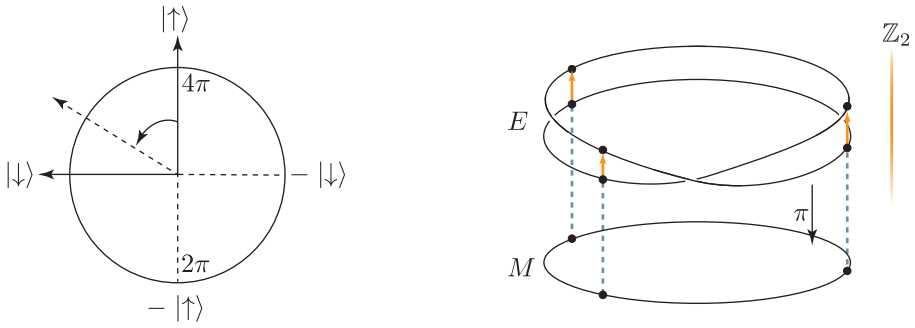

Figure 10.1: A transition of spin states along the 4π full circle is illustrated on the left. The equivalent fibre bundle structure of the Möbius band acted by the element of the order two group $\mathbb{Z}_2 = \{0, 1\}$ implying that the two 2π rotations are required to return to its original configuration in the bundle structure, while it takes only one 2π rotation to return to its initial configuration on the projected base manifold S^1.

So, it is natural to associate the midpoint of this transition of state from zero to 2π rotation, the angle π for which the polarisation of the initial state $|\uparrow\rangle$ vanishes completely, and only the other state $|\downarrow\rangle$ exists occupying the total space $P(|\uparrow\rangle, |\downarrow\rangle) = (0, 1)$. The angle between these transition represents the mixed states of $\alpha\,|\uparrow\rangle + \beta\,|\downarrow\rangle$ for some parameters α, β. Therefore, if we regard a *full circle* as the abstract circle to return a spin-1/2 particle to its original state, it

will take 4π rotation rather than the usual 2π rotation in the physical space.

Angle(phase):	0	π	2π	3π	4π
State:	$\|\uparrow\rangle$	$\|\downarrow\rangle$	$-\|\uparrow\rangle$	$-\|\downarrow\rangle$	$\|\uparrow\rangle$

In Fig. 10.1, a fibre bundle structure $\{S^1, S^1, \mathbb{Z}_2, \pi\}$ is shown describing the particle circling on S^1 becomes the opposite configuration from the original one after 2π rotation in the bundle space. We can regard the bold lines in Fig. 10.1 as the edge of the Möbius band. It will take two such rotations to return to its original configuration. This structure is projected to the base manifold S^1 by a map π with the usual full circle of 2π rotation. Each dot on the base S^1 will have two distinct configurations when the group $\mathbb{Z}_2$ is acted on the fibre bundle. That means, we can associate 2π rotation an element $\{1\}$ and 0 or 4π rotation an element $\{0\}$.

10.2.2 Fibration in the projective space

Now, since we have the correspondences between $SU(2)$ and $SO(3)$, as we saw in the previous Section where each of these are isomorphic to the respective spaces,

$$SU(2) \cong S^3 \qquad \text{and} \qquad SO(3) \cong S^2 \,, \tag{10.2.1}$$

what is left to do next is to establish the explicit relation between S^3 and S^2. Such a relation can be understood by *Hopf fibration* of (8.1.10). In particular the fibration

$$S^1 \hookrightarrow S^3 \to S^2 \tag{10.2.2}$$

gives a unique identification $\mathbb{C}P^1 \cong S^2$ via a fibration

$$S^1 \hookrightarrow S^{2n+1} \to \mathbb{C}P^n \,. \tag{10.2.3}$$

For the $n = 1$ case, we have an isomorphism in terms of the complex projective space

$$\mathbb{C}P^1 \cong S^3/S^1 \cong S^2 \,. \tag{10.2.4}$$

To see this relation more closely, we note that a real-valued field $x = (x_1, \cdots, x_{2n}) \in \mathbb{R}^{2n}$ can be translated into a complex-valued field $z = (z_1, \cdots, z_n) \in \mathbb{C}^n$ by setting

$$z_1 = x_1 + ix_2, \quad z_2 = x_3 + ix_4, \quad \cdots, \quad z_n = x_{2n-1} + ix_{2n} \,.$$

In particular, if we impose a constraint $x_1^2 + \cdots + x_{2n}^2 = 1$ for the real-valued field, then this field configuration lies on S^{2n-1}. For example, if $n = 1$ we only have $z = x_1 + ix_2$ such that $x_1^2 + x_2^2 = 1$. This corresponds to a complex number $z \in \mathbb{C}$ with a modulus 1 on S^1, i.e. $|z| = 1$. If $n = 2$, we have

$$x = (x_1, x_2, x_3, x_4) \in S^3 \qquad \text{and} \qquad \boldsymbol{z} = (z_1, z_2) \in \mathbb{C}^2 \,.$$

So that we may define a complex doublet $\boldsymbol{z} \in \mathbb{C}^2$ which lives on S^3 as the doublet acted by $U \in SU(2)$ of (10.1.5) on the state $|\uparrow\rangle$. For example

$$\boldsymbol{z} = \begin{pmatrix} z_1 \\ z_2 \end{pmatrix} = U\,|\uparrow\rangle = U \begin{pmatrix} 1 \\ 0 \end{pmatrix} = \begin{pmatrix} n_4 + in_3 \\ -n_2 + in_1 \end{pmatrix} \tag{10.2.5}$$

satisfying $n_1^2 + n_2^2 + n_3^2 + n_4^2 = 1$, or equivalently $|z_1|^2 + |z_2|^2 = 1$. Similarly, we can define the action of $U \in SU(2)$ on the spin down state by $\boldsymbol{\omega} = U\,|\downarrow\rangle$.

These particular choice of states in (10.2.5) remove the redundancy in expressing the elements of $U \in SU(2)$ that comes from its unitary property $U^\dagger U = I$. This justifies the field configuration is indeed on S^3 with the constraint (not to be confused with $\boldsymbol{z}\boldsymbol{z}^\dagger$, which is irrelevant in this case)

$$\boldsymbol{z}^\dagger \boldsymbol{z} = 1 \; . \tag{10.2.6}$$

Hence, we can interpret the doublet $\boldsymbol{z}$ as the wavefunction of the spin-1/2 particle, and this field is invariant under the phase transformation,

$$\boldsymbol{z} \longrightarrow e^{i\alpha}\boldsymbol{z} \; . \tag{10.2.7}$$

where $e^{i\alpha} \in U(1) \cong S^1$ as we noted in Fig. 10.1. In other words, the doublet $\boldsymbol{z}$ imposes an internal symmetry $U(1)$ in addition to the originally imposed symmetry on the space $SU(2) \cong S^3$ by the constraint $\boldsymbol{n}_4 \cdot \boldsymbol{n}_4 = 1$. Hence, we can recognise the field configuration $\boldsymbol{z}$ on S^3 must be in the complex projective space $\mathbb{C}P^1$, by taking the quotient space with its internal symmetry $U(1)$. Therefore, it is the fibration (10.2.4).

In case of the real projection space, the fibration is

$$S^0 (= \mathbb{Z}_2) \hookrightarrow S^n \to \mathbb{R}P^n \; , \tag{10.2.8}$$

So that the corresponding quotient space is

$$\mathbb{R}P^3 \cong S^3/\mathbb{Z}_2 \tag{10.2.9}$$

in which we recognise $\mathbb{Z}_2$ the antipodals $\{\boldsymbol{n}, -\boldsymbol{n}\}$ in the real space. Therefore, in the complex projection space (10.2.4) the (complex)antipodals on S^3 are taken to be S^1. We also note that the antipodals in real and complex space are invariant under $SO(2)$ and $U(1)$ respectively,

$$\begin{array}{lll} \text{Quotient space} & \text{Antipodals} & \text{Symmetry group} \\ S^3/S^0 \cong \mathbb{R}P^3 : & \{\boldsymbol{n}, -\boldsymbol{n}\} & SO(2) \\ S^3/S^1 \cong \mathbb{C}P^1 : & \{\boldsymbol{z}, e^{i\alpha}\boldsymbol{z}\} & U(1) \end{array} \tag{10.2.10}$$

in which $SO(2)$ and $U(1)$ are related by the so-called σ-structure introduced by Trautman [109] explaining the appearance of the new gauge fields A_{ij} and its associated gauge invariant field F_{ij} shown by Utiyama [71] in formulating the general local symmetry group $SU(N)$.

10.2.3 Hopf map

The homotopy groups from the fibrations of the real and the complex projective space are given by

$$\pi_2(\mathbb{C}P^1) \cong \pi_2(S^3/S^1) \cong \pi_2(S^2) \cong \mathbb{Z} \tag{10.2.11}$$

and

$$\pi_1(\mathbb{R}P^3) \cong \pi_1(S^3/S^0) \cong \mathbb{Z}_2 \; . \tag{10.2.12}$$

Now, the *Hopf map* H gives an explicit expression for the transformations from the field $\boldsymbol{z} \in S^3$ into the axial field $\boldsymbol{n}_3 \in S^2$ defined by

$$\begin{aligned} &H : S^3 \longrightarrow S^2 \\ &H(\boldsymbol{z}) \longrightarrow \boldsymbol{z}^\dagger \boldsymbol{\sigma} \boldsymbol{z} \end{aligned} \tag{10.2.13}$$

where $\boldsymbol{\sigma}$ are the Pauli matrices. One such coordinate representation of $\mathbb{C}P^1$ is given by the doublet $\boldsymbol{z}$ acted by U of (10.1.5), with its matrix entries are given by $\boldsymbol{n}_4$ of (10.1.12), on the state $|\uparrow\rangle$,

$$\boldsymbol{z} = U\,|\uparrow\rangle = U \begin{pmatrix} 1 \\ 0 \end{pmatrix} = \begin{pmatrix} \cos\omega(r) + i\cos\theta\sin\omega(r) \\ ie^{iN\phi}\sin\theta\sin\omega(r) \end{pmatrix} \; . \tag{10.2.14}$$

It is a straightforward calculation to show that $(\boldsymbol{z}^\dagger \boldsymbol{\sigma} \boldsymbol{z}) \cdot (\boldsymbol{z}^\dagger \boldsymbol{\sigma} \boldsymbol{z}) = 1$, the equivalent constraint of $\boldsymbol{n}_3 \cdot \boldsymbol{n}_3 = 1$ for the normalised axial field on S^2.

Next, we would like to consider the 3-sphere $S^3 \subset \mathbb{R}^4 (\cong \mathbb{C}^2)$ and its projection according to the fibration (10.2.8). We consider a map which induces an element $U \in SU(2)$ from a point

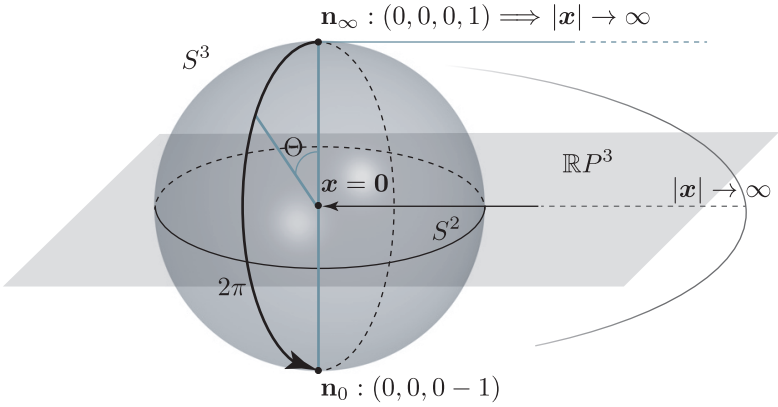

Figure 10.2: The correspondence between S^3 and its projection $\mathbb{R}P^3$ with the asymptotic values of $U \in SU(2)$ acting on the point on S^3 is shown. In particular, the transition from $\boldsymbol{n}_\infty$ to $\boldsymbol{n}_0$ is the phase rotation zero to 2π, expressed by the angular variable Θ on S^3. And this transition is projected on the $\mathbb{R}P^3$ plane by the corresponding transition that brings a point from infinity to the origin.

$\boldsymbol{x} \in \mathbb{R}^3$ where $\boldsymbol{x}$ is not necessarily a normalised vector,

$$\begin{aligned} \boldsymbol{x} \longrightarrow & \ (\boldsymbol{\sigma} \cdot \boldsymbol{x} + i \cdot I)(\boldsymbol{\sigma} \cdot \boldsymbol{x} - i \cdot I)^{-1} \\ = & \frac{1}{1+|\boldsymbol{x}|^2} \begin{pmatrix} x_1^2 + x_2^2 + (i + x_3)^2 & 2(ix_1 + x_2) \\ 2(ix_1 - x_2) & x_1^2 + x_2^2 + (i - x_3)^2 \end{pmatrix} . \end{aligned} \tag{10.2.15}$$

It is easy to check that the 2×2 matrix representation on the right-hand side of (10.2.15) is indeed an element of $U \in SU(2)$ satisfying $U^\dagger U = I$, hence this is a map associating each $\boldsymbol{x} = (x_1, x_2, x_3)$ a unitary matrix of $SU(2)$. The transformation (10.2.15) can be regarded as an inverse map of the stereographic projection from a 3-sphere S^3 onto $\boldsymbol{x}$-space, where the complex unitary 2×2 matrix group $SU(2)$ having the same topology of S^3.

What we can do with this correspondence is that we can restrict the domain $\boldsymbol{x}$-space as the subspace $\mathbb{R}P^3 \subset \mathbb{R}^3$ to construct the correspondence

$$P : \mathbb{R}P^3 \longrightarrow S^3 \ . \tag{10.2.16}$$

And the representation (10.2.15) satisfies the boundary conditions for $U \in SU(2)$,

$$U = \begin{cases} +I & \text{when } |\boldsymbol{x}| \to \infty \\ -I & \text{when } \boldsymbol{x} = 0 \ . \end{cases} \tag{10.2.17}$$

Suppose we set the coordinate of the north pole on S^3 by $\boldsymbol{n}_\infty = (0,0,0,+1)$. This corresponds to the point $|\boldsymbol{x}| \to \infty$ on the projected space $\mathbb{R}P^3$. Now, we apply an element of $U \in SU(2)$ on this state to see the transition by the angular variable Θ as the phase changes from the north pole to the south pole. The south pole is denoted by $\boldsymbol{n}_0$ corresponds to the point $\boldsymbol{x} = 0$ of $\mathbb{R}P^3$ accordingly. But, by the asymptotic conditions (10.2.17), we see that the coordinate of the south pole will be $\boldsymbol{n}_0 = (0,0,0,-1)$. This means the original state from the north pole acquires a minus sign while the phase transition undergoes the 2π rotation on S^3, along the great circle S^2.

The presence of the factor 1/2 that appears in the field configuration for $\boldsymbol{n}_4$ of (10.1.21) may look a bit artificial at first sight, although it is required to recover the representation for $R \in SO(3)$ of (10.1.1) from the representation that does not contain any explicit angular expression (10.1.20). But we now can see, for example through the coordinates for the north pole and the south pole on S^3, it is absolutely required to validate the arguments we developed so far. A different approach in explaining for the origin of this half angle can be found in [114].

The north pole $\boldsymbol{n}_\infty$ and the south pole $\boldsymbol{n}_0$ on S^3 satisfy the following asymptotic conditions, while the transition of the element $U \in SU(2)$ changes $+I \to -I$ as the phase changes from 0 to 2π using (10.2.15),

$$\begin{array}{ccccc} \text{Phase} & SU(2) & S^3 & \mathbb{R}P^3 \\ \hline 0 & +I & \boldsymbol{n}_\infty(0,0,0,+1) & |\boldsymbol{x}| \to \infty \\ 2\pi & -I & \boldsymbol{n}_0\ (0,0,0,-1) & \boldsymbol{x} = 0 \end{array} \tag{10.2.18}$$

For example, if we put a spin state $|\uparrow\rangle$ at the north pole $\boldsymbol{n}_\infty$ on S^3, this will be projected to $|\boldsymbol{x}| \to \infty$ on the $\mathbb{R}P^3$ plane. If we bring this to the point $\boldsymbol{x} = 0$ on the real projective plane, the corresponding state will travel along the great circle on S^3 marking the 2π rotation. In turn, this state will acquire additional minus sign. We summarise the transitions as follows.

$$\begin{array}{rccc} & \boldsymbol{n}_\infty : (0,0,0,+1) & & \boldsymbol{n}_0 : (0,0,0,-1) \\ \hline S^3 : & \boldsymbol{z} = I\,|\uparrow\rangle = +\binom{1}{0} & \longrightarrow & \boldsymbol{z}' = -I\,|\uparrow\rangle = -\binom{1}{0} \\ \mathbb{R}P^3 : & |\boldsymbol{x}| \to \infty & \longrightarrow & \boldsymbol{x} = 0 \end{array} \tag{10.2.19}$$

This establishes the direct link between the state lives on S^3 acted by $SU(2)$, and the state lives on $\mathbb{R}P^3$ acted by $SO(3)$. But what physical system shall we put on S^3 and $\mathbb{R}P^3$ acted upon by these rotations respectively? We would like take such a state on S^3 as the Skyrmion and we will consider the possible candidate for the state living on the projective space $\mathbb{R}P^3$ in the following Sections.

10.3 Skyrmions

In a series of papers [159, 166–169] Skyrme introduced a nonlinear field theory in describing strongly interacting particles. This work has motivated many subsequent studies, and noted some interesting links between baryon numbers (the sum of the proton and neutron numbers) and topological invariants in field theory.

Skyrme defined the field of complex doublet $\boldsymbol{z} \in \mathbb{C}^2$ acted by an element of $U \in SU(2)$ which lies on S^3 [170–172], as we defined in (10.2.5) or (10.2.14)

$$\boldsymbol{z} = \begin{pmatrix} n_4 + in_3 \\ -n_2 + in_1 \end{pmatrix}, \tag{10.3.1}$$

satisfying $n_1^2 + n_2^2 + n_3^2 + n_4^2 = 1$ which we know from the representation (10.1.5)

$$U = n_4 \cdot I + i(\boldsymbol{n} \cdot \boldsymbol{\sigma})\ .$$

The construction of this field comes from the fact that two distinct $SO(3)$ transformations act on the intrinsic elementary particle spin space and isospin space consists with a pion field (π^0, π^+, π^-) independently. Then the property of $SU(2)$ as the double cover of $SO(3)$ is used to contain the complex doublets $\boldsymbol{z}$. Therefore, two independent full circles in each $SO(3)$ for the spin-isospin coupled field means one 4π full circle in $SU(2) \cong S^3$. We note that the operator in the isospin space has nothing to do with the physical spin space. But it acts on the three

states of pion field, and its generators $\boldsymbol{I}$ share the identical group structure with those of the usual generators $\boldsymbol{J}$ of $SO(3)$, such as the commutation relation (10.1.9).

A field $B^a{}_\mu$ is defined as the gradient of pion field $\boldsymbol{z}$, or equivalently the gradient of $U \in SU(2)$ on S^3 by

$$\partial_\mu U = i\sigma^a B^a{}_\mu U \tag{10.3.2}$$

where $a, b, c = 1, 2, 3$ are for the isospin space, μ, ν, ρ for the $(3+1)$-dimensional spacetime indices. We will use $i, j, k = 1, 2, 3$ for the spin space. Then using the identity $\mathrm{tr}(\sigma^a \sigma^b) = 2\delta^{ab}$, one can obtain

$$B^a{}_\mu = \frac{1}{2i}\mathrm{tr}\left(U^\dagger \sigma^a \partial_\mu U\right) \ . \tag{10.3.3}$$

Further, it can be shown that by inserting the representation for the rotation $R \in SO(3)$ of (10.1.20),

$$R_{ab} = 2n_a n_b - 2\epsilon_{abc} n_c n_4 + \delta_{ab}(2n_4^2 - 1)$$

directly into the definition of (10.3.3) using the relation (10.1.18), an equivalent expression of $B^a{}_\mu$ can be obtained by

$$B^a{}_\mu = -\frac{1}{4}\epsilon^{abc} R_{bd} \partial_\mu R_{cd} \ . \tag{10.3.4}$$

Now, let us suppress the index notation for the coordinates $\mu, \nu = 1, 2, 3$ for now. Then we notice that the term on right-hand side $R_{bd}\partial_\mu R_{cd}$ of (10.3.4) is precisely the form of the contortion tensor $K_{b\mu c}$ of (6.2.3), when it is applied by global rotations $Q \in SO(3)$ according to $Q^T K Q$. This gives the relation between $B^a{}_\mu$ field and Nye's tensor (6.2.8) as follows.

$$B^a{}_\mu = \frac{1}{2}\Gamma^a{}_\mu \ . \tag{10.3.5}$$

This relation between two fields gives us a unique identification in what we have discussed extensively in Part II, the compatibility conditions. A Maurer-Cartan form $M = A^{-1}dA$, for A is an element of a Lie matrix group, M satisfies a Maurer-Cartan equation as we briefly mentioned in (6.2.12). Since $B^a{}_\mu$ is in the Maurer-Cartan form by definition, or $i\sigma B = U^\dagger dU$, it must satisfy the Maurer-Cartan equation

$$dB = -B \wedge B \ , \tag{10.3.6}$$

which can be equivalently written

$$\partial_\mu B^a{}_\nu - \partial_\nu B^a{}_\mu + 2\epsilon_{abc} B^b{}_\nu B^c{}_\mu = 0 \ . \tag{10.3.7}$$

After applying $\epsilon^{\nu\mu\sigma}$, we obtain

$$\mathrm{Curl}\, B + 2\mathrm{Cof}\, B = 0 \ .$$

Then, using the definition of the Cof of (4.2.2) and the relation (10.3.5), we recover our compatibility condition for Nye's tensor (6.2.9),

$$\mathrm{Curl}\, \Gamma + \mathrm{Cof}\, \Gamma = 0 \ . \tag{10.3.8}$$

We recall that this is essentially derived from the setting (6.2.4) of vanishing curvature but non-trivial torsion,

$$R^\rho{}_{\sigma\mu\nu} = \partial_\mu K^\rho{}_{\nu\sigma} - \partial_\nu K^\rho{}_{\mu\sigma} + K^\rho{}_{\mu\lambda} K^\lambda{}_{\nu\sigma} - K^\rho{}_{\nu\lambda} K^\lambda{}_{\mu\sigma} \ . \tag{10.3.9}$$

Again this is in the form of the Maurer-Cartan equation, for the contortion tensor $K = R^T dR$ satisfying

$$dK = -K \wedge K \ . \tag{10.3.10}$$

In [168], Skyrme used the explicit field configuration for (10.2.5) in terms of (10.1.21),

$$n_i = \boldsymbol{n}_3 \sin\frac{\Theta}{2} \qquad \text{and} \qquad n_4 = \cos\frac{\Theta}{2} \ , \tag{10.3.11}$$

but with $\boldsymbol{n_3}$ is given by the tetrad field $e^a{}_i$-rotated hedgehog field

$$\boldsymbol{n}_3 = e^a{}_i \boldsymbol{n}_{\rm h} \qquad \text{satisfying} \qquad \boldsymbol{n}_3 \cdot \boldsymbol{n}_3 = 1 \ . \tag{10.3.12}$$

In words, the field configuration $\boldsymbol{n}_3$ is obtained from the $e^a{}_i$-transformed isotropic $\boldsymbol{n}_{\rm h}$ in the spin-isospin system. Moreover, the constraint $\boldsymbol{n}_3 \cdot \boldsymbol{n}_3 = 1$ immediately indicates that the tetrad field $e^a{}_i$ must be an orthogonal matrix, hence it can be regarded as the microrotation $\chi^a{}_\mu$ when we use the polar decomposition (5.1.7) and (6.3.3). And when we insert (10.3.11) into (10.3.3), the explicit expression for $B^a{}_i$ is obtained by

$$B^a{}_i = e^a{}_j \, \frac{1}{2r} \left[(\delta_{ij} - n_{{\rm h}i} n_{{\rm h}j}) \sin\Theta + n_{{\rm h}i} n_{{\rm h}j} \, r\Theta' - \epsilon_{ijk} n_{{\rm h}k} (1 - \cos\Theta) \right] \tag{10.3.13}$$

where B is now a strictly 3×3 matrix, representing the gradient of the spinor field, in terms of three position-dependent hedgehog fields under the constraint $\boldsymbol{n}_{\rm h} \cdot \boldsymbol{n}_{\rm h} = 1$ and an arbitrary radial function Θ.

Skyrmions are field configurations for the quantised invariant number defined by the total charge of integration of the conserved current J^μ of (9.2.34) we saw in Section 9.2. This topological invariant number is regarded as a particle-like quantity, and postulated to be baryon number. In particular, under the configuration (10.3.11), one can obtain the topologically conserved charge $Q = N = 1$. In this case, one proton or one neutron. This is because the field configuration is expressed in terms of the hedgehog field $\boldsymbol{n}_{\rm h}$, which does not contain any vortex field but the trivial one $N = 1$, as we noticed in (9.2.31). In other words, if we use the general spinor configuration such as (10.2.14), we will obtain a non-trivial baryon number N by the integration

$$\begin{aligned} N &= \frac{1}{12\pi^2} \int d^3x \, \epsilon^{t\nu\lambda\rho} \epsilon^{abcd} n_a \partial_\nu n_b \partial_\lambda n_c \partial_\rho n_d \\ &= -\frac{1}{2\pi^2} \int d^3x \, \det B \ . \end{aligned} \tag{10.3.14}$$

Using the relation with Nye's tensor (10.3.5), this can be rewritten by

$$N = -\frac{1}{(4\pi)^2} \int d^3x \, \det \Gamma \ . \tag{10.3.15}$$

Furthermore, after a rather lengthy calculation using the relation with the contortion tensor K of (6.2.8), this becomes

$$N = \frac{1}{96\pi^2} \int d^3x \, {\rm tr} \, (K \wedge K \wedge K) \ . \tag{10.3.16}$$

All three expressions (10.3.14), (10.3.15) and (10.3.16) will give an identical topological invariant integer N, satisfying the finite energy requirement we considered in Section 9.2. The form of integration (10.3.15) has been noted in [145, 173] in the context of Cosserat elasticity.

In particular, (10.3.16) can be derived from a Chern-Simons type action in terms of the contortion tensor, seen as gauge fields [22],

$$S = \frac{1}{4\pi} \int d^3x \, {\rm tr}(K \wedge dK + \frac{2}{3} K \wedge K \wedge K) \ . \tag{10.3.17}$$

Moreover, by varying the action S of (10.3.17) with respect to contortion, one arrives at the equation of motion

$$dK + K \wedge K = 0 \,, \tag{10.3.18}$$

which is again the Maurer-Cartan equation (10.3.10), the vanishing Riemann tensor with nonzero torsion.

When $N = 1$, the expression (10.3.14) manifests [168, 169] that a proton ($N = 1$) cannot decay into the pions ($N = 0$). In other words, the field configuration belongs to the homotopy classification $\{1\}$ cannot continuously deform to be in $\{0\}$ classification. And (10.3.15) or (10.3.16) states that the point defects on $\mathbb{R}P^3$ belongs to the non-trivial class $\{1\}$, emphasising nonzero torsion, differs from $\{0\}$. Both expressions of micropolar continua with nonzero torsion of (10.3.15) and Skyrmions with $Q = 1$ (10.3.14) share the identical geometrical setting of the vanishing Riemann curvature tensor via the identical compatibility condition of the form (10.3.8).

We are ready to find the field configuration that occupies the $\mathbb{R}P^3$ plane. This system is, as already suggested from the relation (10.3.5) and the isomorphism (10.2.9), indeed the micropolar continua. This can be shown by the antipodals on S^3 in analogy with the antipodals on S^2 are for the nematic liquid crystals. Hence this can be viewed that the micropolar continua are the general case of the nematic liquid crystals.

10.4 Micropolar in the projective space

We are now ready to describe the field on the $\mathbb{R}P^3$ plane, the antipodals of S^3 in connection with the micropolar continua. Let us begin with the fibration (8.1.10c) when $n = 3$,

$$S^0 \hookrightarrow S^2 \to \mathbb{R}P^2 \,.$$

This gives rise to the nematic liquid crystals by identifying the antipodals $\boldsymbol{n}_{\rm N} = -\boldsymbol{n}_{\rm N}$ on S^2, as we saw in Section 8.3. The natural extension of this consideration would be the fibration,

$$S^0 \hookrightarrow S^3 \to \mathbb{R}P^3 \,. \tag{10.4.1}$$

This is the central subject of Section 10.2 and in Section 10.3, when we considered various asymptotic conditions. We now know the suitable setting for S^3 is the spinor complex doublet $\boldsymbol{z}$ of (10.2.14) with a natural invariant N is embedded in it. There is one remaining problem in understanding the fibration (10.4.1). This is to interpret the geometrical meaning of *identifying the antipodals* on S^3. In case of S^2, it comes to the realisation quite intuitively by the molecular structure of nematic liquid crystals with the relatively simple property of the director field. We would like to apply similar consideration but with some additional features.

As before, identifying the antipodals will be the statement similar to that of nematic liquid crystals, but we put the antipodals to be two identifiable normalised axial field $\boldsymbol{n}_3$ of (9.2.25)

$$\boldsymbol{n}_3 = (\sin\theta\cos N\phi, \sin\theta\sin N\phi, \cos\theta) \,, \quad \boldsymbol{n}_3 \cdot \boldsymbol{n}_3 = 1 \tag{10.4.2}$$

where the antipodals implies $\boldsymbol{n}_3 = -\boldsymbol{n}_3$ along with the outward-directed rays on S^3. This reduces to the hedgehog field $\boldsymbol{n}_{\rm h}$ if we put $N = 1$. Now, we must have an additional degree of freedom to describe the antipodals on S^3 under the normalisation constraint, and the natural candidate for this is the position-dependent angular variable Θ.

This is precisely the angular variable Θ we considered in (10.3.11) describing the phase rotation of the spinor along the great circle S^2 on S^3, as shown in Fig. 10.2. We can assign the angular variable Θ the rotational angle about the axis taken by the axial field $\boldsymbol{n}_3$ on the

surface of S^3. As shown in Fig. 10.3, suppose a spinor on a point of S^3 undergoes an angular transition along the great circle S^2 with the orientation of the spin by following, for example, left-hand thumb aligned with the axis of rotation initially. Then, through a 2π rotation it will acquire an additional minus sign in the assigned state and we can take these two points on S^3 as the pair of antipodals. We can apply an identical analysis on any set of antipodals on the sphere, separated by a 2π rotation along S^2.

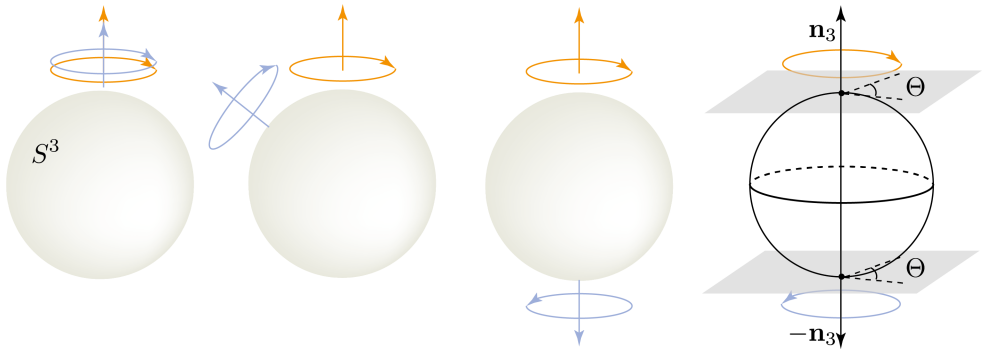

Figure 10.3: Suppose we have started from two identical spin orientations with the same axis. As one spinor configuration undergoes a smooth transition along the great circle, separating from the initial configuration which is kept in the initial state, the spin configuration changes gradually. When the phase reaches its 2π rotation, the spin configuration becomes the complete opposite.

Now, we know that the topological identification of antipodals by means of the fibration and the quotient space $S^3/\{\text{antipodals}\} \cong \mathbb{R}P^3$. On the other hand, the geometrical identification of antipodals is equivalent to the statement that the rotation of $2\pi - \Theta$ about $\boldsymbol{n}_3$ is identifiable to the rotation Θ about $-\boldsymbol{n}_3$ as indicated in Fig. 10.3. This is precise the statement of the rotation $R \in SO(3)$. Therefore, the isomorphism is clearly

$$\mathbb{R}P^3 \cong SO(3) \ . \tag{10.4.3}$$

Consequently, we have

$$S^3/\{\text{antipodals}\} \cong \mathbb{R}P^3 \cong SO(3) \ . \tag{10.4.4}$$

This justifies the identification of antipodals on S^3 both geometrical and topological point of views, and the homotopy classifications we discussed earlier in (7.2.2) and (10.2.12),

$$\pi_1(SO(3)) \cong \pi_1(\mathbb{R}P^3) \cong \mathbb{Z}_2 \ . \tag{10.4.5}$$

Moreover, in the case of nematic liquid crystals, the angular variable (i.e. the phase transition) has been alway $\Theta = \pi$ to be restricted on $S^2 \subset S^3$, see Fig. 10.3. In turn, with the identified antipodals on S^2, we know that this space will be projected to the $\mathbb{R}P^2$ plane constituting the space for the nematic liquid crystals, as we saw in (8.2.1). Hence there has been no need for the angular variable consideration but the identification $\boldsymbol{n}_{\rm N} = -\boldsymbol{n}_{\rm N}$ suffices as the description for the antipodals on S^2. For a set of points on S^3 along a constant latitude, the angular variable must be identical with possibly different set of axial fields $\boldsymbol{n}_3$. In particular, the great circle passes through the equator of S^3 is an equator S^2 with $\Theta = \pi$. Therefore, if a state of configuration for the micropolar continua undergoes the continuous 2π rotational transition on S^3 from the north pole along the great circle, the nematic liquid crystals constitute the set of points on the equator on S^3 during this particular transition, when the micropolar continua are projected on $\mathbb{R}P^3$ plane. See Fig.10.2.

Further, if we consider the element $\overline{R} \in SO(3)$ as the microrotation, then we can conclude the geometrical identification of antipodals are micropolar continua that live on $\mathbb{R}P^3$ governed by the microrotational deformations of an angular function Θ about the position-dependent normalised axis $\boldsymbol{n}_3$ with the nematic liquid crystals are contained in its submanifold.

We can envision the space of axial fields on the sphere, as the space filled with tiny grains rotating independently along with rotational angles about axes determined by parameters $\{\Theta, \boldsymbol{n}_3\}$. Once we identify the antipodals on S^3, these grains are projected to $\mathbb{R}P^3$ constituting the micropolar continua satisfying the boundary conditions we discussed in (10.2.19). Moreover, as we noted in Section 8.4 and Section 7.2, we can regard the microrotation $\overline{R}_{ij}$ as the order parameter in evaluating the energy functionals as we did in Section 2,

$$\frac{\delta V_{\text{total}}}{\delta F} \qquad \text{and} \qquad \frac{\delta V_{\text{total}}}{\delta \overline{R}} \tag{10.4.6}$$

where

$$V = V_{\text{elastic}}(F, \overline{R}) + V_{\text{curvature}}(\overline{R}) + V_{\text{interaction}}(F, \overline{R}) + V_{\text{coupling}}(F, \overline{R}) \ .$$

Since the microrotation $\overline{R}$ can be represented by an angular variable Θ and an axis vector $\boldsymbol{n}_3$, we can take the Q_{ij}, the form of isotensor Higgs field that appears in the Polyakov field (9.4.7), as the order parameter of the micropolar continua but now equipped with the integer N,

$$Q_{ij} = \left(n_{3i} n_{3j} - \frac{1}{3} \delta_{ij} \right) \Theta \ , \qquad i, j = 1, 2, 3 \tag{10.4.7}$$

where $n_{3i} = \boldsymbol{n}_3$ is (9.2.25), the normalised rotational axis with the integer N in three dimensions. This leads us to the following consequences.

1. The equation of motion of (9.4.1) in $(3+1)$ dimension is of the form

$$\partial_\mu \partial^\mu \boldsymbol{Q} = \frac{\partial^2 \boldsymbol{Q}}{\partial t^2} - \nabla^2 \boldsymbol{Q} = -\frac{\partial U}{\partial \boldsymbol{Q}} \tag{10.4.8}$$

   where U is the potential of the given system and ∇^2 is the Laplacian operator. There exists an isomorphism of the order parameters consideration between Q_{ij} of (10.4.7) and the microrotation $\overline{R}_{ij}$ of (10.1.1). Then, after applying the normalisation condition $\boldsymbol{n}_3 \cdot \boldsymbol{n}_3 = 1$ to remove factors of n_{3i} in Q_{ij}, the equation of motion (10.4.8) in $(1+1)$ dimensions is the variation of V_{total} with respect to the microrotation in (10.4.6) with the kinetic term, which is just our dynamic equation of motion for the microrotational angle Θ in $(1+1)$ dimensions given by (2.3.7)

$$\partial_{tt} \Theta - \partial_{\hat{z}\hat{z}} \Theta + \frac{\partial \tilde{U}}{\partial \boldsymbol{Q}} = 0 \ , \tag{10.4.9}$$

   where $\tilde{U}$ is a modified potential accordingly and $\hat{z}$ is the rescaled axis. This observation reinforces the statement that our formulation in deriving the equations of motion is equivalent to the approach from the constitutive equations with order parameter given by (8.4.42) in the free energy formalism. Moreover, the form of the order parameter (10.4.7) in $\mathbb{R}P^3$ for the microcontinuum is the generalised form of the order parameter (8.4.7) for the nematic liquid crystals, both are in traceless and symmetric forms.

2. The 2π rotation will correspond to the maximum energy required in transition of the phase on S^3. On the projective plane $\mathbb{R}P^3$, the maximum energy required will correspond to bring a field configuration from infinity $|\boldsymbol{x}| = \infty$ to the origin $\boldsymbol{x} = 0$. This is the energy difference experienced by a point of continua when it undergoes transition from

a total deformation-free state to its peak deformed configuration, with its maximum microrotational angle before it return to its original configuration, provided the deformation occurs in the elastic regime. Hence, when we consider the static solution of our equation of motion (2.3.17) by putting $t = 0$ and the phase shift $\delta = 0$, the maximum amplitude of the solution is acquired at the origin, see Fig. 2.2.

3. Depending on the form of potential $\tilde{U}$, the equation of motion (10.4.9) can be either the simple ϕ^4 theory, the Klein-Gordon type, the since-Gordon type or more exotic form of equations we saw in solving the chiral case in Chapter 3. Notably these all satisfy the finite energy requirement in the framework of the elasticity leading to the degenerate minima corresponding to the distinct set of topological sectors

$$\Theta(\pm\infty, t) \longrightarrow \Theta_0 \ ,$$

for some fixed vacuum solution Θ_0 which minimises the energy in the given Hamiltonian H. Of course, we can set the trivial angular variable vacuum solution by $\Theta_0 = 0$, the configuration on the north pole of S^3, to be projected to the configuration for $|\boldsymbol{x}| \to \infty$ on $\mathbb{R}P^3$.

4. Since $SU(2)$ is a double cover of $SO(3)$, we can apply the *Lifting Properties* of the fundamental group to classify the various forms of defects such as monopole, vortex, and domain walls, according to (8.1.12). For example

$$\pi_n(S^n) \cong \pi_n(\mathbb{R}P^n) \cong \mathbb{Z}, \qquad n \geq 2 \ , \tag{10.4.10}$$

relating various possible defects in micropolar continua and spinor systems. One of such example is the explicit relation between Skyrmions and Nye's tensor (10.3.5) to describe the vanishing curvature but nonzero torsion on the manifold. In words, Skyrme's field $B^a{}_\mu$ describes the gradient of the pion field through the complex doublet $\boldsymbol{z}$ on S^3 and Nye's tensor describes the defect of the director field $\boldsymbol{\xi}_a$ of the micropolar continua on $\mathbb{R}P^3$. Two deformational descriptions on the different physical systems share the identical homotopic classification (10.4.10), and more explicitly, the analogy can be seen in the integrations such as (10.3.14) and (10.3.16).

We summarise the results we obtained with corresponding homotopy classifications which would be useful to identify the defects in various situations. In particular, once the antipodal points are identified on the sphere S^n, we can write the corresponding projective space. See Table 10.1.

Models	Sphere	Projection	Homotopy
	S^1	$\mathbb{R}P^1$	$\pi_1(\mathbb{R}P^1) \cong \mathbb{Z}$ $\pi_2(\mathbb{R}P^1) \cong \pi_3(\mathbb{R}P^1) \cong \{0\}$
Nematic liquid crystals	S^2	$\mathbb{R}P^2$	$\pi_1(\mathbb{R}P^2) \cong \mathbb{Z}_2$ $\pi_2(\mathbb{R}P^2) \cong \pi_3(\mathbb{R}P^2) \cong \mathbb{Z}$
Micropolar continua	S^3	$\mathbb{R}P^3$	$\pi_1(\mathbb{R}P^3) \cong \mathbb{Z}_2$ $\pi_2(\mathbb{R}P^3) \cong \{0\}$ $\pi_3(\mathbb{R}P^3) \cong \mathbb{Z}$

Table 10.1:

We would like to conclude this Section with one additional remark on the antipodals on S^3. If we are allowed to identify the antipodals, this corresponds to match two opposite rotations,

or to glue together as shown in Fig. 10.3. But now we would like to see this topological identification on the antipodals from a different point of view instead of recognising them as the elements of $\mathbb{R}P^3$. This is indeed identical to the constructing of a Klein bottle in $S^3 \subset \mathbb{R}^4$. It is widely know that the Klein bottle K^3 can be constructed in subspace embedded in $\mathbb{R}^4$ without self-intersection unlike the usual Klein bottle we are familiar with, and K^3 is homeomorphic to the connected sum of two projective planes $\mathbb{R}P^2$ [126, 174].

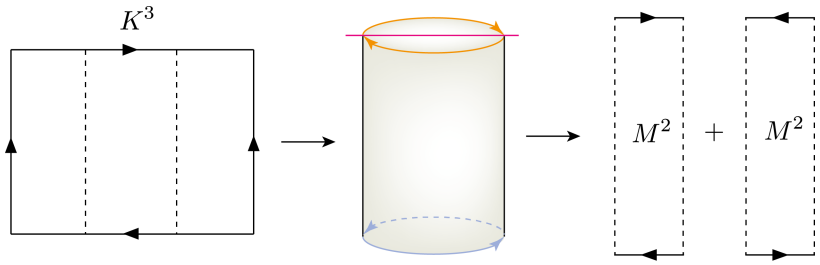

Figure 10.4: A fundamental polygon for the Klein bottle can be constructed in four dimensions without self-intersection. Then it can be divided into two (chiral) Möbius bands.

We note that the construction of the Klein bottle K^3 in $\mathbb{R}^4$ is very similar to identifying the antipodals on S^3 for the $\mathbb{R}P^3$. But this is not by coincidence as we show briefly here. Using the fact that $\mathbb{R}P^2$ is a union of a disk D^2 and a Möbius band M^2 of (8.1.5), and similarly, the projective space $\mathbb{R}P^3$ is a union of S^2 and D^3 using (8.1.3)

$$\mathbb{R}P^3 \cong D^3 \cup \partial D^3 \cong D^3 \cup S^2 \ . \tag{10.4.11}$$

However, the Klein bottle is a union of two Möbius bands as shown in Fig. 10.4. Therefore, identifying the antipodals on the sphere S^2, the relation (10.4.11) becomes the correspondence between the projective space $\mathbb{R}P^3$ and the Klein bottle K^3,

$$\mathbb{R}P^3 \longrightarrow \left(M^2 \cup D^2\right) \cup \left(M^2 \cup D^2\right) \cong \mathbb{R}P^2 * \mathbb{R}P^2 \cong K^3 \tag{10.4.12}$$

in which $*$ is the connected sum along the common disk D^2.

Chapter 11

Conclusions and outlooks

Soliton solutions are obtained in Part I from the variational principle after collecting the most general energy functionals with the set of appropriate coupling moduli. These soliton solutions are descriptions for the coupled system of microscopic and macroscopic deformations both under the achiral and chiral energy considerations. As the chiral solution, we specified the requirements for chiral energy functionals in the higher dimensions by investigating the inversion properties of the individual characteristic deformational measures, such as rotations, translations and deformation gradient tensors. We found that the dislocation density tensor $K = R^T \mathrm{Curl}\, R$ is one of the suitable measures for this purpose among other possible combinations of chiral-inducible energy functionals.

In Part II, we found that the dislocation density tensor played the central role along with the contortion tensor in the manifold where both curvature and torsion are permissible. Within the scope of vanishing curvature, we derived and reinterpreted the compatibility conditions both for vanishing torsion and non-vanishing torsion. The general expression for the Einstein tensor in the Riemann-Cartan manifold gave us a unique opportunity to understand the universal geometrical process to derive various forms of the compatibility conditions. These are widely applicable in micromorphic continua and the Skyrme model we studied in Part III within the framework of the Einstein-Cartan theory.

We also observed there are distinct classifications in the field configurations under the condition of the vanishing curvature by the simple homotopic consideration to obtain two distinct classes such as $\{0\}$ and $\{1\}$. The former defines the diffeomorphic deformational class and the latter is for the non-trivial torsion space which cannot be described by the metric tensor.

In Part III, we considered the criteria for the systems with soliton solutions under the finite energy requirement in connection with the elastic asymptotic conditions. This led us to understand the topological and geometrical origins of the conserved current in the general dimensions in such a way that the integer N, originated from the vortex field in two dimensions, can be embedded to the field configuration in the higher dimensions. This further yields the total charge, in the form of the integration of the current, is again the topologically invariant as integers N in agreement with the finite energy requirement. We found that these conserved topological invariants correspond to the homotopic classification, and conserved charge in the various dimensions and physical models such as the ϕ^4 theory, the Klein-Gordon system, and the sine-Gordon system. These are the topologically stable defects within the given sector determined by the associated charge $Q = N$.

In Part I, we made use of a number of ansatz simplifying the situation to obtain the solutions both analytically and numerically. The ansatz included the same velocities in the microscopic and macroscopic deformational propagations and a fixed microrotational axis. Noting that the general micropolar continua can be occupied by the field of position-dependent axial vectors for

the microrotations in inhomogeneous settings, we derived the conserved currents associated to the topological invariants which can be written in terms of normalised axial field configurations in various dimensions. In particular, to serve the role in the representations of the rotational matrix R_{ij} equipped with the non-trivial vortex field embedded in it.

After establishing a firm relation between the nematic liquid crystals on S^2 and the projective plane $\mathbb{R}P^2$, by identifying the antipodals in its topological and geometrical implications, we briefly considered the role of order parameter in homotopic consideration to re-derive the topological invariants N in the theory of defects such as monopole, vortex and domain wall by tracing the possible defect that can occur in the given order parameter space.

The free energy formulation in terms of order parameter in the classical nematic liquid crystals and in the theory of the micropolar continuum led us to generalise the order parameter of the Higgs isovector in the form of the order parameter that we can use in the micropolar theory. This is consistently applicable to the previously obtained soliton solutions. These are followed by the investigation on the viability of the hedgehog field configuration in three dimensions both for our micropolar model and the Skyrme model supported by the relation between the defect measures of pion fields and Nye's tensor, of which can be written in the identical form of the compatibility condition we obtained in Part II.

The geometrical considerations on S^2 confirms that the nematic liquid crystals can be regarded to be defined on the $\mathbb{R}P^2$ plane with the help of the rather simple assignment of the directors to its molecular nature, by identifying the antipodals on the sphere. As the extension of the identification between S^2 and $\mathbb{R}P^2$, we chose the model on S^3 as the Skyrmions based on the fact that the spin-isospin symmetry of two independently acting $SO(3)$ constitutes the transformation of $SU(2)$. And this consequently yields the realisation that the projective plane $\mathbb{R}P^3$ is for the micropolar continua when we identify the antipodals on S^3. This comes naturally through the Hopf fibration between $SU(2)$ and $SO(3)$. Along with the Hopf fibration, this correspondence links the pion fields as represented by the complex doublet on $\mathbb{C}^2$ and $\boldsymbol{n}_3$ as the axial fields for the microrotations in the projective space. This again enters into the microrotational matrix $\overline{R}_{ij}$ as the components of $\boldsymbol{n}_4$ field, with the topological invariant N and an additional angular variable, to identify that the antipodals on S^3 is the microrotations for the micropolar continua.

We obtained the soliton solutions in Part I and Part II without the specifications of thermodynamic effects, dissipative factors, chemical potentials, electromagnetic interferences or the gravitational attraction to the media. Hence in reality, considering all possible such effects, the soliton solution may lose its characteristic feature of propagating without changing its wave form, not to mention the potential interference from each other when one considers the multi-soliton systems. But if we consider the deformational propagation in a specific physical system such as the continuum consideration in vacuum or a perfect fluid in a low temperature, we might hope to obtain the relevant results we obtained here. For that purpose, we believe the techniques developed in this work to be applicable to certain phases of liquid superfluid helium as good candidates which also possess the spin-orbit symmetry that can be separately represented by $SO(3)$ both in isotropic and anisotropic settings.

Appendix A

Variations of energy functionals

We would like to vary each energy functional using some of identities listed in Notation and Appendix. First, for V_{elastic}, we can expand the expression using the definition of $\|X\|^2 = \langle X, X\rangle = \text{tr}(XX^T)$ and $\text{sym}M = 1/2(M + M^T)$ as

$$\begin{aligned} V_{\text{elastic}}(F,\overline{R}) &= \mu\left\|\text{sym}(\overline{R}^TF - \mathbb{1})\right\|^2 + \frac{\lambda}{2}\left[\text{tr}\left(\text{sym}(\overline{R}^TF - \mathbb{1})\right)\right]^2 \\ &= \left(3\mu + \frac{9}{2}\lambda\right) + \frac{1}{2}\mu\text{tr}\left(\overline{R}^TF\overline{R}^TF\right) + \frac{1}{2}\mu\text{tr}(FF^T) - (2\mu + 3\lambda)\,\text{tr}(\overline{R}^TF) + \frac{\lambda}{2}\left[\text{tr}(\overline{R}^TF)\right]^2 . \end{aligned} \tag{A.0.1}$$

Variation of this is

$$\begin{aligned} \delta V_{\text{elastic}}(F,\overline{R}) = &\left[\mu(\overline{R}F^T\overline{R} + F) - (2\mu + 3\lambda)\overline{R} + \lambda\text{tr}(\overline{R}^TF)\overline{R}\right] : \delta F \\ &+ \left[\mu F\overline{R}^TF - (2\mu + 3\lambda)F + \lambda\text{tr}(\overline{R}^TF)F\right] : \delta\overline{R}. \end{aligned} \tag{A.0.2}$$

If we want to study the dynamical problem, we must take the kinetic term into account in the elastic energy functional

$$V_{\text{elastic,kinetic}} = \frac{1}{2}\rho\|\dot{\varphi}\|^2 , \tag{A.0.3}$$

where ρ is the constant density and φ is the deformation vector. If we vary this term we will obtain

$$\delta V_{\text{elastic,kinetic}} = -\rho\ddot{\varphi}\ \delta\varphi . \tag{A.0.4}$$

But, since $\nabla\varphi = \mathbb{1} + \nabla u$ implies $\delta\varphi = \delta u$ and $\ddot{\varphi} = \ddot{u}$, the variation of the elastic kinetic term can be rewritten as $\delta V_{\text{elastic,kinetic}} = -\rho\ddot{u}\ \delta u$, and the variation of dynamical expression for the elastic energy functional becomes

$$\begin{aligned} \delta V_{\text{elastic}}(F,\overline{R}) = &\left[\mu(\overline{R}F^T\overline{R} + F) - (2\mu + 3\lambda)\overline{R} + \lambda\text{tr}(\overline{R}^TF)\overline{R}\right] : \delta F \\ &+ \left[\mu F\overline{R}^TF - (2\mu + 3\lambda)F + \lambda\text{tr}(\overline{R}^TF)F\right] : \delta\overline{R} + \rho\ddot{u}\ \delta u . \end{aligned} \tag{A.0.5}$$

Similarly, for the curvature functional, we can expand it as

$$\begin{aligned} V_{\text{curvature}}(\overline{R}) = &\frac{(\kappa_1 - \kappa_2)}{2}\text{tr}\left[\overline{R}^T(\text{Curl}\,\overline{R})\overline{R}^T(\text{Curl}\,\overline{R})\right] \\ &+ \frac{(\kappa_1 + \kappa_2)}{2}\text{tr}\left[(\text{Curl}\,\overline{R})^T(\text{Curl}\,\overline{R})\right] - \left(\frac{\kappa_1}{3} - \kappa_3\right)\left(\text{tr}\left[\overline{R}^T(\text{Curl}\,\overline{R})\right]\right)^2 . \end{aligned} \tag{A.0.6}$$

This is a functional dependent only on $\overline{R}$, but the actual variation will involve rather complicated quantities such as $\delta\mathrm{Curl}\,\overline{R}$ multiplied by a tensor. To overcome this problem, we introduce the following identity. Let $A(\overline{R})$ and $B(\overline{R})$ be two matrix valued functions depending on the rotation $\overline{R}$. Then, by a direct calculation, one can show that an identity for any rank-two tensors A and B,

$$\mathrm{tr}(A)B : \delta(\mathrm{Curl}\,\overline{R}) = -\Big[B\big(\mathrm{grad}\,\mathrm{tr}(A)\big)^{\star}\Big] : \delta\overline{R} + \mathrm{tr}(A)\mathrm{Curl}\,B : \delta\overline{R} \tag{A.0.7}$$

where

$$\big(\mathrm{grad}\,\mathrm{tr}(A)\big)^{\star}_{ik} = \epsilon_{ijk}\partial_j \mathrm{tr}(A)\ . \tag{A.0.8}$$

The identity (A.0.7) can be shown if one uses the convention

$$\mathrm{Curl}\,B = \epsilon_{jrs}B_{is,r}e_i \otimes e_j = -B_{,i} \times e_i\ .$$

In particular, if we put $A = \mathbb{1}$ then (A.0.7) reduces to

$$B : \delta(\mathrm{Curl}\,\overline{R}) = \mathrm{Curl}\,B : \delta\overline{R}\ . \tag{A.0.9}$$

And this will play an important role in simplifying the calculation of variation of the energy functionals significantly. For example, the first variational term in (A.0.6) would be

$$\begin{aligned}\delta\Big(\mathrm{tr}\Big[\overline{R}^T(\mathrm{Curl}\,\overline{R})\overline{R}^T(\mathrm{Curl}\,\overline{R})\Big]\Big) &= 2\Big[\overline{R}(\mathrm{Curl}\,\overline{R})^T\overline{R}\Big] : \delta(\mathrm{Curl}\,\overline{R}) + 2(\mathrm{Curl}\,\overline{R})\overline{R}^T(\mathrm{Curl}\,\overline{R}) : \delta\overline{R}\\ &= 2\Big(\mathrm{Curl}\,\Big[\overline{R}(\mathrm{Curl}\,\overline{R})^T\overline{R}\Big] + (\mathrm{Curl}\,\overline{R})\overline{R}^T(\mathrm{Curl}\,\overline{R})\Big) : \delta\overline{R}\ .\end{aligned} \tag{A.0.10}$$

In this way, we find the variation of the curvature term

$$\begin{aligned}\delta V_{\mathrm{curvature}}(\overline{R}) = \Big[&(\kappa_1-\kappa_2)\Big((\mathrm{Curl}\,\overline{R})\overline{R}^T(\mathrm{Curl}\,(\overline{R}))+\mathrm{Curl}\,\Big[\overline{R}(\mathrm{Curl}\,\overline{R})^T\overline{R}\Big]\Big)+(\kappa_1+\kappa_2)\mathrm{Curl}\,\Big[\mathrm{Curl}\,\overline{R}\Big]\\ &-\Big(\frac{\kappa_1}{3}-\kappa_3\Big)\Big(4\mathrm{tr}(\overline{R}^T\mathrm{Curl}\,\overline{R})\mathrm{Curl}\,(\overline{R}) - 2\overline{R}\Big(\mathrm{grad}\,\Big(\mathrm{tr}[\overline{R}^T\mathrm{Curl}\,\overline{R}]\Big)\Big)^{\star}\Big] : \delta\overline{R}\ .\end{aligned} \tag{A.0.11}$$

Again, for the dynamical case, we need to include the kinetic term defined as

$$V_{\mathrm{curvature,kinetic}} = \rho_{\mathrm{rot}}\|\dot{\overline{R}}\|^2 = \rho_{\mathrm{rot}}\mathrm{tr}(\dot{\overline{R}}\,\dot{\overline{R}}^T) \tag{A.0.12}$$

with variational form given by $\delta V_{\mathrm{curvature,kinetic}} = -2\rho_{\mathrm{rot}}\ddot{\overline{R}} : \delta\overline{R}$.
Therefore, the variation of dynamical expression for the curvature energy functional can be written as

$$\begin{aligned}\delta V_{\mathrm{curvature}}(\overline{R}) = \Big[&(\kappa_1-\kappa_2)\Big((\mathrm{Curl}\,\overline{R})\overline{R}^T(\mathrm{Curl}\,(\overline{R}))+\mathrm{Curl}\,\Big[\overline{R}(\mathrm{Curl}\,\overline{R})^T\overline{R}\Big]\Big)+(\kappa_1+\kappa_2)\mathrm{Curl}\,\Big[\mathrm{Curl}\,\overline{R}\Big]\\ -\Big(\frac{\kappa_1}{3}-\kappa_3\Big)&\Big(4\mathrm{tr}(\overline{R}^T\mathrm{Curl}\,\overline{R})\mathrm{Curl}\,(\overline{R}) - 2\overline{R}\Big(\mathrm{grad}\,\Big(\mathrm{tr}[\overline{R}^T\mathrm{Curl}\,\overline{R}]\Big)\Big)^{\star} + 2\rho_{\mathrm{rot}}\ddot{\overline{R}}\Big] : \delta\overline{R}\ .\end{aligned} \tag{A.0.13}$$

For the interaction energy functional, we expand terms dev $\mathrm{sym}(\overline{R}^T\mathrm{Curl}\,\overline{R})$ and dev $\mathrm{sym}(\overline{R}^T F - \mathbb{1})$ to write

$$\begin{aligned}V_{\mathrm{interaction}} = &\Big(\chi_1 - \frac{\chi_3}{3}\Big)\mathrm{tr}(\overline{R}^T\mathrm{Curl}\,\overline{R})\mathrm{tr}(\overline{R}^T F)\\ &+\frac{\chi_3}{2}\Big(\mathrm{tr}\Big[(\mathrm{Curl}\,\overline{R})^T F\Big] + \mathrm{tr}\Big[\overline{R}^T(\mathrm{Curl}\,\overline{R})\overline{R}^T F\Big]\Big)\ .\end{aligned} \tag{A.0.14}$$

The variation of this involves the quantity $\delta\mathrm{Curl}\,\overline{R}$ as in the case of $V_{\mathrm{curvature}}$, so we use the identity (A.0.9) to obtain

$$\begin{aligned}\delta V_{\mathrm{interaction}}(F,\overline{R}) = \Big\{ \Big(\chi_1 - \frac{\chi_3}{3}\Big)\Big(2\mathrm{tr}(\overline{R}^T F)\mathrm{Curl}\,\overline{R} + \mathrm{tr}(\overline{R}^T\mathrm{Curl}\,\overline{R})F - \overline{R}\Big[\mathrm{grad}\,\Big(\mathrm{tr}[\overline{R}^T F]\Big)\Big]^\star\Big) \\ + \frac{\chi_3}{2}\Big(\mathrm{Curl}\,F + (\mathrm{Curl}\,\overline{R})\overline{R}^T F + F\overline{R}^T(\mathrm{Curl}\,\overline{R}) + \mathrm{Curl}\,(\overline{R}F^T\overline{R})\Big)\Big\} : \delta\overline{R} \\ + \Big\{\chi_1\mathrm{tr}(\overline{R}^T\mathrm{Curl}\,\overline{R})\overline{R} + \frac{\chi_3}{2}\Big(\mathrm{Curl}\,\overline{R} + \overline{R}(\mathrm{Curl}\,\overline{R})^T\overline{R}\Big) - \frac{\chi_3}{3}\mathrm{tr}(\overline{R}^T\mathrm{Curl}\,\overline{R})\overline{R}\Big\} : \delta F\ . \quad \text{(A.0.15)}\end{aligned}$$

We write the coupling energy functional as

$$V_{\mathrm{coupling}}(F,\overline{R}) = \mu_c\left\|\overline{R}^T\mathrm{polar}(F) - \mathbb{1}\right\|^2 = 2\mu_c(3 - \mathrm{tr}[\overline{R}^T\mathrm{polar}(F)])\ . \quad \text{(A.0.16)}$$

We note that this depends on $\overline{R}$ and $R = \mathrm{polar}(F)$, hence depends on $\overline{R}$ and F. Therefore, the variation of coupling energy functional is of the form

$$\delta V_{\mathrm{coupling}}(F,\overline{R}) = -2\mu_c R : \delta\overline{R} - 2\mu_c\left[\frac{\partial}{\partial F}\Big(\mathrm{tr}[\overline{R}^T R]\Big)\right] : \delta F\ . \quad \text{(A.0.17)}$$

The term in the brackets in the second term can be written as

$$\frac{\partial}{\partial F}\Big(\mathrm{tr}[\overline{R}^T R]\Big) = \Big(\frac{dR}{dF_{ml}}\Big) : \frac{\partial}{\partial R}\Big[\mathrm{tr}(\overline{R}^T R)\Big] = \Big(\frac{dR}{dF_{ml}}\Big) : \overline{R} = \frac{1}{\det(Y)}\Big[RY(R^T\overline{R} - \overline{R}^T R)Y\Big] \quad \text{(A.0.18)}$$

where $Y = \mathrm{tr}(U)\mathbb{1} - U$. In the first step, we used the chain rule, and in the second and last steps we used the identities given in (A.0.21). Then the variation of the coupling energy becomes

$$\delta V_{\mathrm{coupling}}(F,\overline{R}) = -2\mu_c\overline{R} : \delta\overline{R} - \frac{2\mu_c}{\det(Y)}\Big[RY(R^T\overline{R} - \overline{R}^T R)Y\Big] : \delta F\ . \quad \text{(A.0.19)}$$

Lastly, we vary the chiral energy functional $V_\chi = \chi\mathrm{tr}(\overline{K}^3)$ as follows

$$\begin{aligned}\delta V_\chi &= 3\chi(\overline{K}^2)^T : \delta\overline{K} = 3\chi\Big[(\overline{K}^2)^T_{ij}\delta(\overline{R}^T\mathrm{Curl}\,\overline{R})_{ij}\Big] = 3\chi\Big[(\overline{K}^2)^T_{ij}\Big(\delta\overline{R}_{mi}(\mathrm{Curl}\,\overline{R})_{mj} + \overline{R}_{mi}(\delta\mathrm{Curl}\,\overline{R})_{mj}\Big)\Big] \\ &= 3\chi\Big[(\mathrm{Curl}\,\overline{R})_{mj}(\overline{K}^2)^T_{ij}\delta\overline{R}_{mi} + \overline{R}_{mi}(\overline{K}^2)^T_{ij}(\delta\mathrm{Curl}\,\overline{R})_{mj}\Big] \\ &= 3\chi\Big[(\mathrm{Curl}\,\overline{R})(\overline{K}^2) : \delta\overline{R} + \overline{R}(\overline{K}^2)^T : \delta\mathrm{Curl}\,\overline{R}\Big] = 3\chi\Big[(\mathrm{Curl}\,\overline{R})(\overline{K}^2) : \delta\overline{R} + \mathrm{Curl}\,[\overline{R}(\overline{K}^2)^T] : \delta\overline{R}\Big] \\ &= 3\chi\Big[(\mathrm{Curl}\,\overline{R})(\overline{K}^2) + \mathrm{Curl}\,[\overline{R}(\overline{K}^2)^T]\Big] : \delta\overline{R}\ .\end{aligned} \quad \text{(A.0.20)}$$

We list some useful matrix identities below.

$$\begin{aligned}\frac{\partial}{\partial X}\mathrm{tr}(F(X)) &= [f(X)]^T\ , & \frac{\partial}{\partial X}\mathrm{tr}(X) &= I\ , \\ \frac{\partial}{\partial X}\mathrm{tr}(XA) &= A^T\ , & \frac{\partial}{\partial X}\mathrm{tr}(AXB) &= A^T B^T\ , \\ \frac{d}{dX}(\mathrm{tr}(XX^T)) &= 2X\ , & \frac{d}{dX}(\mathrm{tr}(XA)) &= A^T\ ,\end{aligned} \quad \text{(A.0.21)}$$

and

$$\begin{aligned}\frac{d}{dX}(\mathrm{tr}(AXBX)) &= A^T X^T B^T + B^T X^T A^T\ , \\ \frac{dg(R(F))}{F_{ml}} &= \mathrm{tr}\left[\frac{dR}{dF_{ml}}\left(\frac{dg(R)}{dR}\right)^T\right] = \frac{dR}{dF_{ml}} : \left(\frac{dg(R)}{dR}\right)\ ,\end{aligned} \quad \text{(A.0.22)}$$

where f stands for the scalar derivative of F.

Appendix B

List of homotopy groups

A list of useful homotopy groups and some of its implication, and justification followed by some important theorems.

		π_1	π_2	π_3	π_4	π_5	π_6
$SO(2)$		$\mathbb{Z}$	0	0	0	0	0
$SO(3)$		$\mathbb{Z}_2$	0	$\mathbb{Z}$	$\mathbb{Z}_2$	$\mathbb{Z}_2$	$\mathbb{Z}_{12}$
$SO(4)$		$\mathbb{Z}_2$	0	$\mathbb{Z}+\mathbb{Z}$	$\mathbb{Z}_2+\mathbb{Z}_2$	$\mathbb{Z}_2+\mathbb{Z}_2$	$\mathbb{Z}_{12}+\mathbb{Z}_{12}$
$SO(5)$		$\mathbb{Z}_2$	0	$\mathbb{Z}$	$\mathbb{Z}_2$	$\mathbb{Z}_2$	0
$SO(6)$		$\mathbb{Z}_2$	0	$\mathbb{Z}$	0	$\mathbb{Z}$	0
$SO(n)$	$n>6$	$\mathbb{Z}_2$	0	$\mathbb{Z}$	0	0	0
$U(1)$		$\mathbb{Z}$	0	0	0	0	0
$SU(2)$		0	0	$\mathbb{Z}$	$\mathbb{Z}_2$	$\mathbb{Z}_2$	$\mathbb{Z}_{12}$
$SU(3)$		0	0	$\mathbb{Z}$	0	$\mathbb{Z}$	$\mathbb{Z}_6$
$SU(n)$	$n>3$	0	0	$\mathbb{Z}$	0	$\mathbb{Z}$	0
S^1		$\mathbb{Z}$	0	0	0	0	0
S^2		0	$\mathbb{Z}$	$\mathbb{Z}$	$\mathbb{Z}_2$	$\mathbb{Z}_2$	$\mathbb{Z}_{12}$
S^3		0	0	$\mathbb{Z}$	$\mathbb{Z}_2$	$\mathbb{Z}_2$	$\mathbb{Z}_{12}$
S^4		0	0	0	$\mathbb{Z}$	$\mathbb{Z}_2$	$\mathbb{Z}_2$
$\mathbb{R}P^1$		$\mathbb{Z}$	0	0	0	0	0
$\mathbb{R}P^2$		$\mathbb{Z}_2$	$\mathbb{Z}$	$\mathbb{Z}$	$\mathbb{Z}_2$	$\mathbb{Z}_2$	$\mathbb{Z}_{12}$
$\mathbb{R}P^3$		$\mathbb{Z}_2$	0	$\mathbb{Z}$	$\mathbb{Z}_2$	$\mathbb{Z}_2$	$\mathbb{Z}_{12}$
$\mathbb{R}P^4$		$\mathbb{Z}_2$	0	0	$\mathbb{Z}$	$\mathbb{Z}_2$	$\mathbb{Z}_2$
$\mathbb{C}P^1$		0	$\mathbb{Z}$	$\mathbb{Z}$	$\mathbb{Z}_2$	$\mathbb{Z}_2$	$\mathbb{Z}_{12}$
$\mathbb{C}P^2$		0	$\mathbb{Z}$	0	0	$\mathbb{Z}$	$\mathbb{Z}_2$
$\mathbb{C}P^3$		0	$\mathbb{Z}$	0	0	0	0
$\mathbb{C}P^4$		0	$\mathbb{Z}$	0	0	0	0
$Sp(1)$		0	0	$\mathbb{Z}$	$\mathbb{Z}_2$	$\mathbb{Z}_2$	$\mathbb{Z}_{12}$
$Sp(2)$		0	0	$\mathbb{Z}$	$\mathbb{Z}_2$	$\mathbb{Z}_2$	0
$Sp(3)$		0	0	$\mathbb{Z}$	$\mathbb{Z}_2$	$\mathbb{Z}_2$	0
$Sp(4)$		0	0	$\mathbb{Z}$	$\mathbb{Z}_2$	$\mathbb{Z}_2$	0
G_2		0	0	$\mathbb{Z}$	0	0	$\mathbb{Z}_3$
F_4		0	0	$\mathbb{Z}$	0	0	0
E_6		0	0	$\mathbb{Z}$	0	0	0
E_7		0	0	$\mathbb{Z}$	0	0	0
E_8		0	0	$\mathbb{Z}$	0	0	0

1. Since $\mathrm{Spin}(4) = SU(2) \times SU(2)$ is the universal covering group of $SO(4)$, we have

$$\pi_n(SO(4)) \cong \pi_n(SU(2)) \oplus \pi_n(SU(2)), \qquad n \geq 2 \, .$$

2. There exists a map J called the *J-homomorphism*, introduced in [175]

$$J : \pi_k(SO(n)) \longrightarrow \pi_{k+n}(S^n) \, .$$

It is known that the J-homomorphism is an isomorphism if $k = 1$, and we have

$$\pi_1(SO(n)) \cong \pi_{n+1}(S^n).$$

For example, in [121] it is observed that

$$\begin{aligned} &\pi_1(SO(2)) \cong \pi_3(S^2) \cong \mathbb{Z} \, , \\ &\pi_1(SO(3)) \cong \pi_4(S^3) \cong \pi_4(SU(2)) \cong \pi_4(SO(3)) \cong \mathbb{Z}_2 \, . \end{aligned}$$

3. The *Bott periodicity theorem* states that

$$\pi_k(U(n)) \cong \pi_k(SU(n)) \cong \begin{cases} 0 & \text{if } k \text{ is even} \\ \mathbb{Z} & \text{if } k \text{ is odd} \end{cases} \qquad \text{for } n \geq (k+1)/2$$

$$\pi_k(O(n)) \cong \pi_k(SO(n)) \cong \begin{cases} 0 & \text{if } k = 2,3,5,6 \pmod 8 \\ \mathbb{Z}_2 & \text{if } k = 0,1 \pmod 8 \\ \mathbb{Z} & \text{if } k = 3,7 \pmod 8 \end{cases} \qquad \text{for } n \geq k+2$$

$$\pi_k(Sp(n)) \cong \begin{cases} 0 & \text{if } k = 0,1,2,6 \pmod 8 \\ \mathbb{Z}_2 & \text{if } k = 4,5 \pmod 8 \\ \mathbb{Z} & \text{if } k = 3,7 \pmod 8 \end{cases} \qquad \text{for } n \geq \frac{k-1}{4} \, .$$

4. For the real projective space, we have $\mathbb{R}P^n \cong S^n/\mathbb{Z}_2$ and

$$\pi_n(\mathbb{R}P^m) \cong \begin{cases} 0 & n = 0 \\ \mathbb{Z} & n = 1, m = 1 \\ \mathbb{Z}_2 & n = 1, m \geq 2 \\ \pi_n(S^m) & n \geq 2 \, . \end{cases}$$

5. For the complex projective space, we have $\mathbb{C}P^n \cong S^{2n+1}/S^1$ and

$$\pi_n(\mathbb{C}P^m) \cong \begin{cases} 0 & n = 1 \\ \mathbb{Z} & n = 2 \\ \pi_n(S^{2m+1}) & n \geq 3 \, . \end{cases}$$

6. For tori, we have $T^n = \underbrace{S^1 \times \cdots \times S^1}_{n}$

$$\pi_n(T^m) \cong \begin{cases} \underbrace{\mathbb{Z} \oplus \cdots \oplus \mathbb{Z}}_{m} & n = 1 \\ 0 & n \geq 2 \, . \end{cases}$$

Bibliography

[1] C. G. Böhmer, Y. Lee, and P. Neff. Soliton solutions in geometrically nonlinear Cosserat micropolar elasticity with large deformations. *Wave Motion*, 84:110–124, 2019.

[2] C. G. Böhmer, Y. Lee, and P. Neff. Chirality in the plane. *J. Mech. Phys. Solids*, 134:103753, 2020.

[3] E. Cosserat and F. Cosserat. Théorie des corps déformables. *Librairie Scientifique A*, Hermann et Fils, 1909.

[4] E. Whittaker. *A History of the Theories of Aether and Electricity.* Thomas Nelson and Sons, 1951.

[5] J. L. Ericksen and C. Truesdell. Exact theory of stress and strain in rods and shells. *Arch. Rational Mech. Anal.*, 1:295–323, 1957.

[6] R. A. Toupin. Elastic materials with couple-stresses. *Arch. Rational Mech. Anal.*, 11:385–414, 1962.

[7] J. L. Ericksen. Hydrostatic theory of liquid crystals. *Arch. Rational Mech. Anal.*, 9:379–394, 1962.

[8] A. E. Green. Multipolar continuum mechanics. *Arch. Rational Mech. Anal*, 17:113–147, 1964.

[9] A. C. Eringen and E. S. Suhubi. Nonlinear theory of simple microelastic solids I. *Int. J. Eng. Sci*, 2:189–204, 1964.

[10] R. D. Mindlin. Micro-structure in linear elasticity. *Arch. Rational Mech. Anal.*, 16(1):51–78, 1964.

[11] R. A. Toupin. Theories of elasticity with couple-stress. *Arch. Rational Mech. Anal.*, 17:85–112, 1964.

[12] H. Schaefer. Das Cosserat Kontinuum. *Z. Angew. Math. Mech.*, 47:485–498, 1967.

[13] J. L. Ericksen. Twisting of liquid crystals. *J. Fluid Mech.*, 27:59–64, 1967.

[14] A. C. Eringen and E. S. Suhubi. Nonlinear theory of simple microelastic solids II. *Int. J. Eng. Sci*, 2:389–404, 1964.

[15] A. C. Eringen. *Microcontinuum field theories: I. Foundations and solids.* Springer, 1999.

[16] P. Neff. Existence of minimizers for a finite-strain micromorphic elastic solid. *Proc. Roy. Soc. Edinb. A*, 136:997–1012, 2006.

[17] P. Neff and I. Münch. Curl bounds Grad on SO(3). *ESAIM Control Optim. Calc. Var.*, 14(1):148–159, 2008.

[18] P. Neff. Existence of minimizers in nonlinear elastostatics of micromorphic solids. In D. Iesan, editor, *Encyclopedia of Thermal Stresses*. Springer, Heidelberg, 2013.

[19] P. Neff, I. D. Ghiba, M. Lazar, and A. Madeo. The relaxed linear micromorphic continuum: well-posedness of the static problem and relations to the gauge theory of dislocations. *Q. J. Mech. Appl. Math.*, 68(1):53–84, 2015.

[20] M. Bîrsan and P. Neff. On the dislocation density tensor in the Cosserat theory of elastic shells. In *Advanced Methods of Continuum Mechanics for Materials and Structures*, pages 391–413. Springer, 2016.

[21] C. G. Böhmer, R. J. Downes, and D. Vassiliev. Rotational elasticity. *Q. J. Mechanics Appl. Math.*, 64(4):415–439, 2011.

[22] C. G. Böhmer and Y. N. Obukhov. A gauge-theoretic approach to elasticity with microrotations. *Proc. R. Soc. A*, 468(1391-1407), 2012.

[23] C. G. Böhmer and N. Tamanini. Rotational elasticity and couplings to linear elasticity. *Math. Mech. Solids*, 20(8):959–974, 2013.

[24] S. Bahamonde, C. G. Böhmer, and P. Neff. Geometrically nonlinear Cosserat elasticity in the plane: applications to chirality. *J. Mech. Mater. Struct.*, 12(5):689–710, 2017.

[25] G. A. Maugin and A. Miled. Solitary waves in elastic ferromagnets. *Phys. Rev. B*, 33(7):4830–4842, 1986.

[26] G. A. Maugin and A. Miled. Solitary waves in micropolar elastic crystals. *Int. J. Eng. Sci.*, 24(9):1477–1499, 1986.

[27] A. Fischle, P. Neff, and D. Raabe. The relaxed-polar mechanism of locally optimal Cosserat rotations for an idealized nanoindentation and comparison with 3D-EBSD experiments. *Z. Angew. Math. Phys.*, 68(4):90, 2017.

[28] D. Iesan and L. Nappa. Extremum principles and existence results in micromorphic elasticity. *Int. J. Eng. Sci.*, 39(18):2051–2070, 2001.

[29] S. Forest. Micromorphic approach for gradient elasticity, viscoplasticity, and damage. *J. Eng. Mech.*, 135(3):117–131, 2009.

[30] P. Neff, I. D. Ghiba, A. Madeo, L. Placidi, and G. Rosi. A unifying perspective: the relaxed linear micromorphic continuum. *Cont. Mech. Thermodyn.*, 26:639–681, 2014.

[31] P. Neff, M. Bîrsan, and F. Osterbrink. Existence theorem for geometrically nonlinear Cosserat micropolar model under uniform convexity requirements. *J. Elast.*, 121(1):119–141, 2015.

[32] L. D. Landau and E. M. Lifshitz. *Theory of Elasticity: Vol. 7 of Course of Theoretical Physics*. Elsevier, New York, 1986.

[33] P. B. Burt. Exact, multiple soliton solutions of the double sine Gordon equation. *Proc. R. Soc. Lond. A.*, 359:479–495, 1978.

[34] J. F. Nye. Some geometrical relations in dislocated crystals. *Acta metallurgica*, 1(2):153–162, 1953.

[35] G. Capriz. *Continua with microstructure*, volume 35. Springer-Verlag, New York, 1989.

[36] R. D. Mindlin and H. F. Tiersten. Effects of couple-stresses in linear elasticity. *Arch. Ration. Mech. Anal.*, 11:415–448, 1962.

[37] I. Münch, W. Wagner, and P. Neff. Constitutive modeling and FEM for a nonlinear Cosserat continuum. In *PAMM: Proc. Appl. Math. Mech*, volume 6, pages 499–500, 2006.

[38] P. Neff. The Cosserat couple modulus for continuous solids is zero viz the linearized Cauchy-stress tensor is symmetric. *ZAMM-Z. Angew. Math. Mech.*, 86(11):892–912, 2006.

[39] C. G. Böhmer, P. Neff, and B. Seymenoglu. Soliton-like solutions based on geometrically nonlinear Cosserat micropolar elasticity. *Wave Motion*, 60:158–165, 2016.

[40] R. Rajaraman. *Solitons and instantons*. North-Holland, Netherlands, 1982.

[41] S. W. Smith. Chiral toxicology: it's the same thing... only different. *Toxicol. Sci.*, 110(1):4–30, 2009.

[42] R. S. Lakes and R. L. Benedict. Noncentrosymmetry in micropolar elasticity. *Int. J. Eng. Sci.*, 20(10):1161–1167, 1982.

[43] A. Spadoni and M. Ruzzene. Elasto-static micropolar behavior of a chiral auxetic lattice. *J. Mech. Phys. Solids*, 60(1):156–171, 2012.

[44] X. N. Liu, G. L. Huang, and G. K. Hu. Chiral effect in plane isotropic micropolar elasticity and its application to chiral lattices. *J. Mech. Phys. Solids*, 60(11):1907–1921, 2012.

[45] R. S. Lakes. Elastic and viscoelastic behavior of chiral materials. *Int. J. Mech. Sci.*, 43(7):1579–1589, 2001.

[46] S. A. Papanicolopulos. Chirality in isotropic linear gradient elasticity. *Int. J. Solids Struct.*, 48(5):745–752, 2011.

[47] K. J. Cheverton and M. F. Beatty. Extension, torsion and expansion of an incompressible, hemitropic Cosserat circular cylinder. *J. Elast.*, 11(2):207–227, 1981.

[48] X. N. Liu, G. L. Huang, and G. K. Hu. Analytical formulation of a discrete chiral elastic metamaterial model. In *Health Monitoring of Structural and Biological Systems 2012*, volume 8348, pages 834–823. International Society for Optics and Photonics, 2012.

[49] X. N. Liu and G. K. Hu. Elastic metamaterials making use of chirality: a review. *Strojniški vestnik-J. Mech. Eng.*, 62(7-8):403–418, 2016.

[50] Y. Chen, X. Liu, and G. Hu. Micropolar modeling of planar orthotropic rectangular chiral lattices. *Comptes Rendus Mécanique*, 342(5):273–283, 2014.

[51] V. A. Fedotov, P. L. Mladyonov, S. L. Prosvirnin, A. V. Rogacheva, Y. Chen, and N. I. Zheludev. Asymmetric propagation of electromagnetic waves through a planar chiral structure. *Phys. Rev. Lett.*, 97(16):167401, 2006.

[52] A. Papakostas, A. Potts, D. M. Bagnall, S. L. Prosvirnin, H. J. Coles, and N. I. Zheludev. Optical manifestations of planar chirality. *Phys. Rev. Lett.*, 90(10):107404, 2003.

[53] W. Zhang, A. Potts, and D. M. Bagnall. Giant optical activity in dielectric planar metamaterials with two-dimensional chirality. *J. Opt. A*, 8(10):878, 2006.

[54] X. Ma, C. Huang, M. Pu, Y. Wang, Z. Zhao, C. Wang, and X. Luo. Dual-band asymmetry chiral metamaterial based on planar spiral structure. *Appl. Phys. Lett.*, 101(16):161901, 2012.

[55] Z. Li, M. Gokkavas, and E. Ozbay. Manipulation of asymmetric transmission in planar chiral nanostructures by anisotropic loss. *Adv. Opt. Mater.*, 1(7):482–488, 2013.

[56] O. Arteaga, J. Sancho-Parramon, S. Nichols, B. M. Maoz, A. Canillas, S. Bosch, G. Markovich, and B. Kahr. Relation between 2d/3d chirality and the appearance of chiroptical effects in real nanostructures. *Opt. Express*, 24(3):2242–2252, 2016.

[57] D. Prall and R. S. Lakes. Properties of a chiral honeycomb with a Poisson's ratio of 1. *Int. J. Mech. Sci.*, 39(3):305–314, 1997.

[58] Y. Chen, X. N. Liu, G. Hu, and Q. Sunand Q. Zheng. Micropolar continuum modelling of bi-dimensional tetrachiral lattices. *Proc. R. Soc. Lond. A*, 470(2165):20130734, 2014.

[59] W. Zhang, R. Neville, D. Zhang, F. Scarpa, L. Wang, and R. Lakes. The two-dimensional elasticity of a chiral hinge lattice metamaterial. *Int. J. Solids Struct.*, 141:254–263, 2018.

[60] R. Raval. Chiral expression from molecular assemblies at metal surfaces: insights from surface science techniques. *Chem. Soc. Rev.*, 38(3):707–721, 2009.

[61] F. Chiadini, V. Fiumara, T. G. Mackay, A. Scaglione, and A. Lakhtakia. Left/right asymmetry in Dyakonov-Tamm-wave propagation guided by a topological insulator and a structurally chiral material. *J. Opt.*, 18(11):115101, 2016.

[62] D. Ieşan. Thermoelastic deformation of reinforced chiral cylinders. *Acta Mechanica*, 228, 07 2017.

[63] W. Wu, D. Qi, H. Liao, G. Qian, L. Geng, Y. Niu, and J. Liang. Deformation mechanism of innovative 3d chiral metamaterials. *Sci. Rep.*, 8(1):12575, 2018.

[64] H. Joumaa and M. Ostoja-Starzewski. Stress and couple-stress invariance in non-centrosymmetric micropolar planar elasticity. *Proc. R. Soc. Lond. A*, 467(2134):2896–2911, 2011.

[65] I. Münch and P. Neff. Rotational invariance conditions in elasticity, gradient elasticity and its connection to isotropy. *Math. Mech. Solids*, 23(1):3–42, 2018.

[66] K. Kondo. On the analytical and physical foundations of the theory of dislocations and yielding by the differential geometry of continua. *Int. J. Engng. Sci.*, 2(3):219–251, 1964.

[67] R. deWit. Relation between Dislocations and Disclinations. *J. Appl. Phys.*, 42(9):3304–3308, 1971.

[68] M. Kléman. Relationship between Burgers circuit, Volterra process and homotopy groups. *Journal de Physique Lettres*, 38(10):199–202, 1977.

[69] M. Kléman. Defects in liquid crystals. *Rep. Prog. Phys.*, 52(5):555–654, May 1989.

[70] C. N. Yang and R. L. Mills. Conservation of isotopic spin and isotopic gauge invariance. *Phys. Rev.*, 96(1):191, 1954.

[71] R. Utiyama. Invariant theoretical interpretation of interaction. *Phys. Rev.*, 101(5):1597, 1956.

[72] T. W. B. Kibble. Lorentz invariance and the gravitational field. *J. Math. Phys.*, 2(2):212–221, 1961.

[73] S. Deser and B. Zumino. Consistent supergravity. *Phys. Lett. B*, 62(3):335–337, 1976.

[74] F. W. Hehl, P. Von Der Heyde, G. D. Kerlick, and J. M. Nester. General Relativity with Spin and Torsion: Foundations and Prospects. *Rev. Mod. Phys.*, 48:393–416, 1976.

[75] S. Hojman, M. Rosenbaum, M. P. Ryan, and L. C. Shepley. Gauge invariance, minimal coupling, and torsion. *Phys. Rev. D*, 17(12):3141, 1978.

[76] A. H. Cottrell and B. A. Bilby. Dislocation theory of yielding and strain ageing of iron. *Proc. Phys. Soc. A*, 62(1):49, 1949.

[77] E. Kröner. Allgemeine kontinuumstheorie der versetzungen und eigenspannungen. *Arch. Rational Mech. Anal.*, 4(1):273, 1959.

[78] W. Noll. A mathematical theory of the mechanical behavior of continuous media. *Arch. Rational Mech. Anal.*, 2(1):197–226, 1958.

[79] B. A. Bilby. Geometry and continuum mechanics. In *Mechanics of Generalized Continua*, pages 180–199. Springer, 1968.

[80] H. Kleinert. Gravity as a Theory of Defects in a Crystal with Only Second Gradient Elasticity. *Ann. Phys.*, 499(2):117–119, 1987.

[81] M. O. Katanaev and I. V. Volovich. Theory of defects in solids and three-dimensional gravity. *Ann. Phys.*, 216(1):1–28, 1992.

[82] F. W. Hehl and Y. N. Obukhov. Élie Cartan's torsion in geometry and in field theory, an essay. *Annales Fond. Broglie*, 32:157–194, 2007.

[83] A. Yavari and A. Goriely. Riemann-Cartan geometry of nonlinear dislocation mechanics. *Arch. Rational Mech. Anal.*, 205(1):59–118, 2012.

[84] A. Yavari and A. Goriely. Riemann-Cartan geometry of nonlinear disclination mechanics. *Math. Mech. Solids*, 18(1):91–102, 2013.

[85] H. I. Arcos and J. G. Pereira. Torsion gravity: a reappraisal. *Int. J. Mod. Phys. D*, 13(10):2193–2240, 2004.

[86] C. G. Böhmer and R. J. Downes. From continuum mechanics to general relativity. *Int. J. Mod. Phys. D*, 23(12):1442015, 2014.

[87] R. Aldrovandi and J. G. Pereira. *Teleparallel Gravity: An Introduction*, volume 173. Springer, Dordrecht Heidelberg New York London, 2013.

[88] M. Lazar and F. W. Hehl. Cartan's spiral staircase in physics and, in particular, in the gauge theory of dislocations. *Found. Phys.*, 40(9-10):1298–1325, 2010.

[89] H. Kleinert. New gauge symmetry in gravity and the evanescent role of torsion. In *Proceedings Of The Conference In Honour Of Murray Gell-Mann's 80th Birthday*, pages 174–185. World Scientific, 2011.

[90] M. Blagojević and F. W. Hehl. *Gauge Theories of Gravitation: A Reader with Commentaries*. Imperial Collge Press, 2013.

[91] H. Kleinert and J. Zaanen. Nematic world crystal model of gravity explaining absence of torsion in spacetime. *Phys. Lett. A*, 324(5-6):361–365, 2004.

[92] A. J. Beekman, J. Nissinen, K. Wu, K. Liu, R. Slager, Z. Nussinov, V. Cvetkovic, and J. Zaanen. Dual gauge field theory of quantum liquid crystals in two dimensions. *Phys. Rep.*, 683:1–110, 2017.

[93] J. Nissinen. Emergent Spacetime and Gravitational Nieh-Yan Anomaly in Chiral $p + ip$ Weyl Superfluids and Superconductors. *Phys. Rev. Lett.*, 124(11):117002, 2020.

[94] I. Peshkov, E. Romenski, and M. Dumbser. Continuum mechanics with torsion. *Continuum Mech. Thermodyn.*, 31(5):1517–1541, 2019.

[95] J. Nissinen and G. E. Volovik. Tetrads in solids: from elasticity theory to topological quantum Hall systems and Weyl fermions. *J. Exp. Theor. Phys.*, 127(5):948–957, 2018.

[96] J. Nissinen and G. E. Volovik. Elasticity tetrads, mixed axial-gravitational anomalies, and (3+1)-d quantum Hall effect. *Phys. Rev. Research*, 1(023007), September 2019.

[97] A. D. Sakharov. Vacuum quantum fluctuations in curved space and the theory of gravitation. *Soviet Physics Uspekhi*, 34(5):394, 1991.

[98] B. A. Bilby, R. Bullough, and E. Smith. Continuous distributions of dislocations: a new application of the methods of non-Riemannian geometry. *Proc. R. Soc. Lond. A*, 231(1185):263–273, 1955.

[99] K. Kondo. Non-Riemannian and Finslerian approaches to the theory of yielding. *Int. J. Engng. Sci.*, 1(1):71–88, 1963.

[100] S. K. Godunov and E. I. Romenskii. Nonstationary equations of nonlinear elasticity theory in Eulerian coordinates. *J. Appl. Mech. Tech. Phys.*, 13(6):868–884, 1972.

[101] E. Kröner. Continuum theory of defects, in Physics of defects (Les Houches, Session 35), ed. R. Balian et al. North-Holland, Amsterdam, 1980.

[102] H. Kleinert. *Gauge Fields in Condensed Matter Vol. 2: Stresses and Defects (Differential Geometry, Crystal Melting)*. World Scientific, Singapore, 1989.

[103] S. K. Godunov and E. Romenskii. *Elements of continuum mechanics and conservation laws*. Kluwer Academic/Plenum Publishers, New York, 2003.

[104] C. G. Böhmer and Y. Lee. Compatibility conditions of continua using Riemann-Cartan geometry. *Math. Mech. Solids*, 2020.

[105] C. Vallée. Compatibility equations for large deformations. *Int. J. Eng. Sci*, 30(12):1753–1757, 1992.

[106] P. G. Ciarlet, L. Gratie, O. Iosifescu, C. Mardare, and C. Vallée. Another approach to the fundamental theorem of Riemannian geometry in $\mathbb{R}^3$, by way of rotation fields. *J. Math. Pures. Appl.*, 87(3):237–252, 2007.

[107] H. Poincaré. *Sur les propriétés des fonctions définies par les équations aux différences partielles*. Number 432. Gauthier-Villars, 1879.

[108] D. G. B. Edelen. A new look at the compatability problem of elasticity theory. *Int. J. Engng. Sci.*, 28(1):23–27, 1990.

[109] A. Trautman. Fibre bundles associated with space-time. *Rep. Math. Phys.*, 1(1):29–62, 1970.

[110] J. Lankeit, P. Neff, and F. Osterbrink. Integrability conditions between the first and second Cosserat deformation tensor in geometrically nonlinear micropolar models and existence of minimizers. *Z. Angew. Math. Mech.*, 68(1):11, 2016.

[111] H. Kleinert. Towards a unified field theory of defects and stresses. *Lettere al Nuovo Cimento*, 35(2):41–45, 1982.

[112] J. A. Schouten. *Ricci-Calculus*. Springer, Berlin, Heidelberg, 1954.

[113] R. M. Wald. *General relativity*. University of Chicago press, Chicago, 1984.

[114] C. W. Misner, K. S. Thorne, and J. A. Wheeler. *Gravitation*. W. H. Freeman and Company, New York, 1999.

[115] R. deWit. Theory of disclinations: II. Continuous and discrete disclinations in anisotropic elasticity. *J. Res. Natl. Bur. Stand. A Phys. Chem.*, 77(1):49, 1973.

[116] M. Nakahara. *Geometry, topology and physics*. IOP Publishing, Bristol and Philadelphia, 2003.

[117] R. deWit. Theory of disclinations: II. Continuous and discrete disclinations in isotropic elasticity. *J. Res. Nat. Stand. Sec. A*, 77A(1):49, Jan 1973.

[118] P. G. Ciarlet. An introduction to differential geometry with applications to elasticity. *J. Elast.*, 78(1-3):1–125, 2005.

[119] D. Finkelstein. Kinks. *J. Math. Phys.*, 7(7):1218–1225, 1966.

[120] R. Shankar. Applications of topology to the study of ordered systems. *Journal de Physique*, 38(11):1405–1412, 1977.

[121] M. Nakahara. Toy-Skyrmions in Superfluid 3He-A. *Prog. Theor. Phys.*, 77(5):1011–1013, 1987.

[122] M. V. Kurik and O. D. Lavrentovich. Defects in liquid crystals: homotopy theory and experimental studies. *Physics-Uspekhi*, 31(3):196–224, 1988.

[123] M. Kleman and O. D. Lavrentovich. Topological point defects in nematic liquid crystals. *Philos. Mag.*, 86(25-26):4117–4137, 2006.

[124] G. P. Alexander, B. G. Chen, E. A. Matsumoto, and R. D. Kamien. Disclination Loops, Hedgehogs, and All That. *Rev. Mod. Phys.*, 84(2):497, 2012.

[125] Y. Lee. Micropolar continua as projective space of Skyrmions. *arXiv preprint arXiv:2106.08926*, 2021.

[126] A. Hatcher. *Algebraic Topology*. Cambridge University Press, 2002.

[127] K. Iwasawa. On some types of topological groups. *Ann. Math.*, pages 507–558, 1949.

[128] L. J. Boya, J. F. Cariñena, and J. Mateos. Homotopy and solitons. *Fortschritte der Physik*, 26(3):175–214, 1978.

[129] N. D. Mermin. The topological theory of defects in ordered media. *Rev. Mod. Phys.*, 51(3):591, 1979.

[130] J. P. Sethna. Order parameters, broken symmetry, and topology. *arXiv preprint cond-mat/9204009*, 1992.

[131] A. Unzicker. *Topological defects in an elastic medium: A valid model particle physics.* Structured media, Proc. Int. Symp, in memory of E. Kröner, Poznań, ed. B. T. Maruszewski, September 16-21 2001. page 293-311, House Poznań Univ. of Technology, 2002.

[132] A. Randono and T. L. Hughes. Torsional monopoles and torqued geometries in gravity and condensed matter. *Phys. Rev. Lett.*, 106(16):161102, 2011.

[133] G. Toulouse and M. Kléman. Principles of a classification of defects in ordered media. *J. Physique Lett.*, 37(6):149–151, 1976.

[134] C. W. Oseen. The theory of liquid crystals. *Trans. Faraday Soc.*, 29:883–899, 1933.

[135] F. C. Frank. I. liquid crystals. on the theory of liquid crystals. *Discuss. Faraday Soc.*, 25:19–28, 1958.

[136] J. L. Ericksen. Inequalities in liquid crystal theory. *Phys. Fluids*, 9(6):1205–1207, 1966.

[137] F. M. Leslie. Some thermal effects in cholesteric liquid crystals. *Proc. R. Soc. Lond. A*, 307(1490):359–372, 1968.

[138] J. L. Ericksen. Continuum theory of liquid crystals of nematic type. *Molecular crystals and liquid crystals*, 7(1):153–164, 1969.

[139] P. De Gennes. *The physics of liquid crystals.* Oxford University Press, 1974.

[140] P. M. Chaikinand and T. C. Lubensky. *Principles of condensed matter physics.* Cambridge University Press, Cambridge, 1995.

[141] D. C. Wright and N. D. Mermin. Crystalline liquids: the blue phases. *Rev. Mod. Phys.*, 61(2):385, 1989.

[142] A. C. Eringen. An assessment of director and micropolar theories of liquid crystals. *Int. J. Eng. Sci*, 31(4):605–616, 1993.

[143] B. C. Hall. *Lie groups, Lie algebras, and representations: An Elementary Introduction*, volume 222. Springer, 2003.

[144] M. C. Cross. A generalized Ginzburg-Landau approach to the superfluidity of helium 3. *J. Low. Temp. Phys.*, 21(5-6):525–534, 1975.

[145] H.-R. Trebin. Elastic energies of a directional medium. *J. Phys.*, 42(11):1573–1576, 1981.

[146] Cz. Rymarz. More about the relations between the Ericksen-Leslie-Parodi and Eringen-Lee theories of nematic liquid crystals. *Int. J. Eng. Sci.*, 28(1):11–21, 1990.

[147] A. C. Eringen. Micropolar theory of liquid crystals. In *Liquid crystals and ordered fluids*, pages 443–474. Springer, 1978.

[148] V. G. Makhankov, Y. P. Rybakov, and V. I. Sanyuk. *The Skyrme Model: Fundamentals Methods Applications*. Springer-Verlag, Berlin Heidelberg, 1993.

[149] S. Coleman. *Aspects of symmetry: selected Erice lectures*. Cambridge University Press, 1988.

[150] J. Arafune, P. G. O. Freund, and C. J. Goebel. Topology of Higgs fields. *J. Math. Phys.*, 16(2):433–437, 1975.

[151] N. D. Mermin and T. L. Ho. Circulation and angular momentum in the a phase of superfluid helium-3. *Phys. Rev. Lett.*, 36(11):594, 1976.

[152] E. J. Weinberg and A. H. Guth. Nonexistence of spherically symmetric monopoles with multiple magnetic charge. *Phys. Rev. D*, 14(6):1660, 1976.

[153] A. M. Polyakov. Particle spectrum in the quantum field theory. *JETP Lett.*, 20:194–195, 1974.

[154] F. Wilczek and A. Zee. Linking Numbers, Spin, and Statistics of Solitons. *Phys. Rev. Lett.*, 51(25):2250–2252, 1983.

[155] M. E. Peskin and D. V. Schroeder. *An introduction to Quantum Field Theory*. Perseus Books, Cambridge, Massachusetts, 1995.

[156] L. D. Faddeev. Some comments on the many-dimensional solitons. *Lett. Math. Phys.*, 1(4):289–293, 1976.

[157] A. A. Belavin and A. M. Polyakov. Metastable states of two-dimensional isotropic ferromagnets. *JETP Lett.*, 22(10):245–248, 1975.

[158] A. P. Balachandran. Solitons in 3He-B. *Nucl. Phys. B*, 271(3-4):227–252, 1986.

[159] T. H. R. Skyrme. A unified field theory of mesons and baryons. *Nucl. Phys.*, 31:556–569, 1962.

[160] R. Penrose. A spinor approach to general relativity. *Ann. Phys.*, 10(2):171–201, 1960.

[161] E. Newman and R. Penrose. An approach to gravitational radiation by a method of spin coefficients. *J. Math. Phys.*, 3(3):566–578, 1962.

[162] D. Finkelstein and J. Rubinstein. Connection between Spin, Statistics, and Kinks. *J. Math. Phys.*, 9(11):1762–1779, Nov 1968.

[163] H. J. Bernstein and A. V. Phillips. Fiber bundles and quantum theory. *Scientific American*, 245(1):122–137, 1981.

[164] H. J. Bernstein. Spin precession during interferometry of fermions and the phase factor associated with rotations through 2π radians. *Phys. Rev. Lett.*, 18(24):1102, 1967.

[165] Y. Aharonov and L. Susskind. Observability of the sign change of spinors under 2π rotations. *Phys. Rev.*, 158(5):1237, 1967.

[166] T. H. R. Skyrme. A non-linear theory of strong interactions. *Proc. R. Soc. Lond. A*, 247(260), 1958.

[167] T. H. R. Skyrme. A unified model of K- and π-mesons. *Proc. Roy. Soc. Lond. A*, 252(1269), 1959.

[168] T. H. R. Skyrme. A non-linear field theory. *Proc. Roy. Soc. Lond. A*, 260:127–138, 1961.

[169] T. H. R. Skyrme. Particle states of a quantized meson field. *Proc. Roy. Soc. Lond. A*, 262(1309):237–245, 1961.

[170] N. S. Manton and P. J. Ruback. Skyrmions in flat space and curved space. *Phy. Lett. B*, 181(1-2):137–140, 1986.

[171] N. S. Manton. Geometry of Skyrmions. *Commun. Math. Phys.*, 111(3):469–478, 1987.

[172] M. F. Atiyah and N. S. Manton. Skyrmions from instantons. *Phys. Lett. B*, 222(3-4):438–442, 1989.

[173] H.-R. Trebin. The topology of non-uniform media in condensed matter physics. *Adv. Phys.*, 31(3):195–254, 1982.

[174] J. R. Munkres. *Topology*. Prentice Hall, Inc, Upper Saddle River, 2000.

[175] G. W. Whitehead. *Elements of homotopy theory*, volume 61. Springer Science & Business Media, 2012.